# Conformal invariance and universality of the dimer model

Russkikh, Marianna

Université de Genève
l'École Normale Supérieure (Paris)

Professeur Stanislav Smirnov
Professeur Dmitry Chelkak

# Conformal Invariance and Universality of the Dimer Model

THÈSE

Présentée à la Faculté des Sciences de l'Université de Genève
pour obtenir le grade de Docteur ès Sciences, mention Mathématiques

par

**Marianna RUSSKIKH**
de
St. Petersburg (Russia)

Thèse N°5344

GENÈVE
Atelier d'impression ReproMail
2019

UNIVERSITÉ
DE GENÈVE

FACULTÉ DES SCIENCES

# DOCTORAT ÈS SCIENCES, MENTION MATHEMATIQUES

## Thèse de Madame Marianna RUSSKIKH

intitulée :

## «Conformal Invariance and Universality of the Dimer Model»

La Faculté des sciences, sur le préavis de Monsieur S. SMIRNOV, professeur ordinaire et directeur de thèse (Section de mathématiques), Monsieur D. CHELKAK, professeur et codirecteur de thèse (Département de mathématiques et applications, Ecole Normale Supérieure, Paris, France), Monsieur H. DUMINIL-COPIN, professeur ordinaire (Section de mathématiques), Monsieur C. BOUTILLIER, professeur (Laboratoire de Probabilités, Statistiques et Modélisation, Sorbonne Université, Jussieu (Paris) France), autorise l'impression de la présente thèse, sans exprimer d'opinion sur les propositions qui y sont énoncées.

Genève, le 20 mai 2019

**Thèse - 5344 -**

**Le Doyen**

N.B. - La thèse doit porter la déclaration précédente et remplir les conditions énumérées dans les "Informations relatives aux thèses de doctorat à l'Université de Genève".

# Abstract

This thesis is dedicated to the study of the conformal invariance and the universality of the dimer model on planar bipartite graphs.

**Dimer model.** The dimer model is one of the best-known models of statistical physics, first introduced to model a diatomic gas. A dimer covering (or perfect matching) of a graph is a subset of edges that covers every vertex exactly once. The *planar dimer model* is the study of random perfect matchings of a planar graph. Several other statistical models, like the Ising model and the spanning tree model (tied to planar networks), can be regarded as a dimer model by subdividing the underlying graph.

Uniform dimer model is an exactly solvable model, meaning that many quantities in the model have exact expressions. Most notably, Kasteleyn [40] showed that the number of dimer configurations can be evaluated as the determinant of a signed adjacency matrix. On the square and honeycomb lattices, dimer configurations can also be interpreted as interlacing particle arrays related to Schur processes [8, 12, 13, 39, 66]. However, the availability of such formulae does not make the analysis of the dimer model trivial, since it is extremely sensitive to boundary conditions. Indeed, the macroscopic behavior of many interesting functionals of the dimer model, such as the *Thurston height function*, may have vastly different average behavior, depending on the boundary conditions. To study the height function, we use the classical approach of Kenyon [41] based on the Kasteleyn theory of the dimer model on planar graphs. Using this approach, Kenyon [41, 42] has established the conformal invariance of the limiting distribution of the height function in the case of Temperleyan discretizations, discrete domains on the square lattice with special boundary conditions. In the thesis, we extended Kenyon's result for more general classes of approximations on the square lattice.

**Double-dimer model.** A double-dimer configuration is a superposition of two independent dimer coverings. Alternatively, one can think about a set of simple loops and double edges and an additional simple path (an interface) for a special type of boundary conditions. Perhaps the biggest conjecture in the double-dimer model is that an interface defined by a configuration converges to a conformally invariant random curve $SLE(4)$ (Schramm-Loewner evolution). In [72] Schramm proved that all conformally invariant random curves satisfying domain Markov property can be described by a one-parameter family of random curves $SLE(\kappa)$. In [57] a strategy of proving the convergence of the interface using an observable was introduced. An observable is a function on edges, vertices or faces of the discrete domain that satisfies particular local relations (e.g. discrete Cauchy-Riemann equations) and that has a strong connection with the interface when the latter grows step by step. If such an observable has a conformally invariant limit satisfying domain Markov property, one can deduce convergence towards $SLE(\kappa)$ (with $\kappa$ determined by the model). The main issue with applying this strategy in the double-

dimer model is the Markov property: even in a well-behaved initial domain, analysing the growing curves requires working with a sufficiently general class of approximations, not only Temperleyan domains. In the thesis, we introduced a construction of the discrete integral of two discrete holomorphic functions and showed that one of the observables in the double-dimer model on the square lattice can be interpreted as such a discrete integral. Using this construction, we obtain scaling limit results for double-dimer height function in the case of more general classes of approximations on the square lattice.

**Universality.** Yet another direction of research in the dimer model is the universality (which means that the scaling limit is independent of the shape of the lattice) of the planar dimer model. In physical and mathematical literature it is widely believed that the macroscopic properties of the model do not depend on the microscopic structure. The main problem here is to find a certain "nice" embedding of the dimer planar graph. Such an embedding should be strongly connected to the model and it should admit a nice discretization of the Cauchy–Riemann operator. In the thesis, we establish a correspondence between dimer models on a bipartite graph and circle patterns with the combinatorics of that graph. We describe how to construct a circle pattern embedding of a dimer planar graph using its Kasteleyn weights. This embedding is the generalization of the isoradial embedding [21, 46, 61, 58] and it is closely related to the T-graph embedding [52]. We also introduce the definition of discrete holomorphicity on such an embedding. We focus on understanding the link between these functions and actual continuous holomorphic functions to study holomorphic observables of the dimer model.

This thesis contains results obtained by the author in [68, 69], results of joint project with R. Kenyon, W. Lam, and S. Ramassamy [47] and some results of joint project (work in progress) with D. Chelkak and B. Laslier [20]. The thesis is organized as follows. Chapters 2 and 3 devoted to results obtained in [68]. Chapter 4 contains results of [69]. The material provided in Chapter 5 closely follows [47]. Finally, Chapter 6 contains some results of [20].

# Résumé

Cette thèse est dédiée à l'étude de l'invariance conforme et de l'universalité du modèle de dimères sur les graphes planaires bipartis.

**Modèle de dimères.** Le modèle de dimères, introduit initialement comme modèle d'un gaz diatomique, est un des modèles les plus connus de la physique statistique. Un pavage par dimères (ou association idéale) d'un graphe est un sous-ensemble d'arêtes qui recouvre chaque sommet exactement une fois. Le modèle de dimères planaire est l'étude de pavages aléatoires par dimères d'un graphe planaire. Un certain nombre d'autres modèles de physique statistique, comme le modèle d'Ising et le modèle de l'arbre couvrant (associé aux réseaux planaires), peuvent être vus comme comme un modèle de dimères en subdivisant le graphe sous-jacent.

Le modèle de dimères uniformes est un modèle exactement soluble au sens que beaucoup de quantités dans le modèle admettent des formules exactes. Notamment, Kasteleyn [40] a montré que le nombre de configurations de dimères peut être exprimé comme un déterminant d'un matrice d'adjacence signée. Sur les réseaux carré et hexagonal les configurations de dimères peuvent être interprétées comme des ensembles de particules entrelacées liés au processus de Schur [8, 12, 13, 39, 66]. Toutefois ces formules ne rendent pas trivial l'analyse du modèle de dimères car celui-ci est très sensible aux conditions au bord. En effet, le comportement macroscopique d'un grand nombre de fonctionnelles intéressantes, comme la fonction de hauteur de Thurston, peut être très différent suivant les conditions au bord. Pour étudier la fonction de hauteur nous avons adopté l'approche classique de Kenyon [41] reposant sur la théorie de Kasteleyn des modèles de dimères sur graphes planaires. En utilisant cette approche, Kenyon [41, 42] a établi l'invariance conforme de la loi limite de la fonction de hauteur dans le cas des discrétisations temperleyennes, c'est à dire des domaines discrets sur un réseau carré avec des conditions au bord spéciales. Dans cette thèse nous avons étendu le résultat de Kenyon à des classes plus générales d'approximations sur réseau carré.

**Modèle de doubles dimères.** Une configuration de doubles dimères est une superposition de deux pavages par dimères indépendants. On peut la voir également comme un ensemble de boucles simples, d'arêtes doubles et un chemin simple (interface) supplémentaire pour un type particulier de conditions au bord. Sans doute la plus importante conjecture dans le modèle de doubles dimères est que l'interface définie par une configuration converge vers une courbe aléatoire conformément invariante, plus précisément vers $SLE(4)$ (évolution de Schramm-Loewner). Dans [72] Schramm a prouvé que toutes les courbes aléatoires conformément invariantes satisfaisant la propriété de Markov domaniale peuvent être décrites par une famille à un paramètre de courbes aléatoires $SLE(\kappa)$. Dans [57] a été introduite une stratégie de preuve pour la convergence de l'interface en utilisant une observable. Une observable est une fonction sur les arêtes, le sommets

ou les faces du domaine discret qui satisfait des relations locales particulières (comme les équations de Cauchy-Riemann discrètes) et qui est fortement reliée à l'interface qu'on fait croître pas à pas. Si une telle observable à une limite conformément invariante et satisfaisant la propriété de Markov domaniale, on peut en déduire la convergence de l'interface vers $SLE(\kappa)$ ($\kappa$ étant déterminé par le modèle). L'obstacle principal pour appliquer cette stratégie dans le cas du modèle de doubles dimères est la propriété de Markov : même si le domaine initial est convenable, l'analyse de la croissance des courbes nécessite de travailler avec une classe suffisamment générale d'approximations, et pas seulement des domaines temperleyens. Dans cette thèse nous avons introduit une construction de l'intégrale de contour discrète de deux fonctions holomorphes discrètes et montré que l'une des observables dans le modèle de doubles dimères sur un réseau carré peut être interprétée comme une telle intégrale discrète. En utilisant cette construction, nous obtenons des résultats sur la limite d'échelle de la fonction de hauteur de doubles dimères dans le cas de classes plus générales d'approximations sur réseau carré.

**Universalité.** Encore une autre direction de recherche dans le modèle de dimères est l'universalité (ceux qui signifie que la limite d'échelle est indépendante de la forme du réseau) du modèle de dimères planaire. Dans la littérature physique et mathématique il est généralement considéré que les propriétés macroscopiques du modèle ne dépendent pas de la structure microscopique. Ici le problème principal est de trouver un certain plongement "gentil" du graphe de dimères planaire. Un tel plongement doit être fortement relié au modèle et il doit admettre une belle discrétisation de l'opérateur de Cauchy-Riemann. Dans cette thèse nous établissons une correspondance entre les modèles de dimères sur un graphe biparti et des configurations de cercles à travers la combinatoire de ce graphe. Nous décrivons comment construire un plongement par configuration de cercles d'un graphe de dimères planaire en utilisant ses poids de Kasteleyn. Ce plongement est une généralisation du plongement isoradial [21, 46, 61, 58] et est étroitement lié au plongement de T-graphe [52]. On se focalise sur la compréhension du lien entre ces fonctions et les vraies fonctions continues holomorphes afin d'étudier les observables holomorphes du modèle de dimères.

Cette thèse contient des résultats obtenus par l'auteur dans [68, 69], des résultats d'un projet commun avec R. Kenyon, W. Lam, and S. Ramassamy [47] et quelques résultats d'un projet commun (en cours) avec D. Chelkak et B. Laslier [20]. Cette thèse est organisée de manière suivante. Les chapitres 2 et 3 sont dédiés aux résultats obtenus dans [68]. Le chapitre 4 contient les résultats de [69]. Le contenu du chapitre 5 suit de près [47]. Enfin, le chapitre 6 contient quelques résultats de [20].

# Acknowledgments

First of all I would like to thank my advisors, Prof. Stanislav Smirnov and Prof. Dmitry Chelkak for their help, care, and support during all these years, and for introducing me to this beautiful subject. I am grateful to Stanislav Smirnov for being a fantastic thesis advisor, for his enthusiasm and optimism, his brilliant ideas, all his support and encouragement. I would like to thank Dmitry Chelkak for his magnificent guidance, for numerous fruitful discussions and strong motivation; I am very grateful for the time and effort that he invested, especially in the beginning when it was much needed. I was extremely lucky to have these two wonderful people not only as academical advisors but also as life mentors. Their sense of humour and fascinating life stories made working on my Ph.D. an even more memorable experience.

I am also grateful to Prof. Sergey Kislyakov, who directed my first steps in mathematical research.

My mathematical journey has been marked by many people. Without being exhaustive, I would particularly like to thank David Cimasoni, Hugo Duminil-Copin, Clément Hongler, Konstantin Izyurov, Ioan Manolescu, Wendelin Werner, Alexei Borodin, Vadim Gorin and Richard Kenyon, all of whom influenced my academic life in their own way. I was fortunate to work with Rick who gave me a lot of insights into the dimer model.

My growth as a researcher has been greatly enhanced by fruitful collaborations with many fantastic people of whom I would like to particularly mention Nathanael Berestycki, Benoit Laslier, Wai Yeung Lam, and Sanjay Ramassamy.

I would also like to express my gratitude to Cédric Boutillier and Hugo Duminil-Copin for kindly agreeing to be on the jury.

The experience of doing a Ph.D. would not have been so much fun without all the people I met during my scientific visits: Adrien Kassel, Marcin Lis, Titus Lupu (whom I also thank for his help with translating the abstract in French), Dražen Petrović and Alexey Bufetov, thanks to all of them for their support and friendship.

Thanks to my colleagues and friends at the University of Geneva who made these five years pleasant. It was a great pleasure to collaborate with people at the probability working group in Geneva. I would like to thank my officemates Dmitry Krachun and Daria Smirnova for eventful evenings spent together in our office, intense debates over different scientific and non-scientific topics, their help and support.

Thanks to my mother and my niece for their support.

Finally, I am very grateful to my friends Mikhail Basok and Maria Podkopaeva for all their help.

# Contents

# Chapter 1

# Introduction

## 1.1 Main results

The dimer model is at the heart of one of the most fascinating and rapidly growing research areas of the last 20 years: the conformal invariance of two-dimensional critical models of statistical physics. More precisely, the limiting objects of many "combinatorial" models, defined in terms of an underlying lattice approximating a planar domain, have been found to be conformally invariant — i.e. possessing the (continuous) symmetries of conformal transformations. Over the past 20 years, this kind of results have been obtained for several important models (such as the dimer model, site percolation on the triangular lattice, uniform spanning trees, loop-erased random walk, and the Ising model) in the works of D. Chelkak, H. Duminil-Copin, R. Kenyon, G. Lawler, O. Schramm, S. Smirnov, W. Werner and others (see, for instance, [16, 41, 42, 57, 78, 79]).

The dimer model is one of the best known models of statistical physics, first introduced to model a gas of diatomic molecules [32]. Several other two-dimensional statistical models, including the Ising model and the spanning tree model, can be regarded as special cases of the dimer model by subdividing the underlying graph [26, 51]. Under the name "perfect matchings", it prominently appears in theoretical computer science and combinatorics.

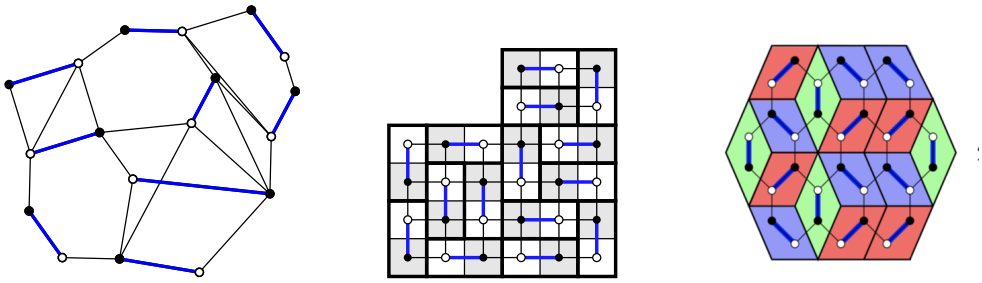

Figure 1.1: A dimer cover of a planar bipartite graph is a set of edges with the property: every vertex is contained in exactly one edge of the set. On a square lattice / honeycomb lattice it can be viewed as a tiling of a domain on the dual lattice by dominos / lozenges.

A dimer covering (or perfect matching) of a graph is a subset of edges that covers every vertex exactly once. The *bipartite planar dimer model* is the study of random dimer coverings of a bipartite planar graph. Our prototipical examples are the dimer model on $\mathbb{Z}^2$ and on the honeycomb graph. Natural parameters for the dimer model, defining the underlying probability measure, are *face weights*, which are positive real

parameters on the bounded faces of the graph [35]. The dimer model is a classical statistical mechanical model, and can be analyzed using determinantal methods: partition functions and correlation kernels are computed by determinants of associated matrices defined from the weighted graph [44].

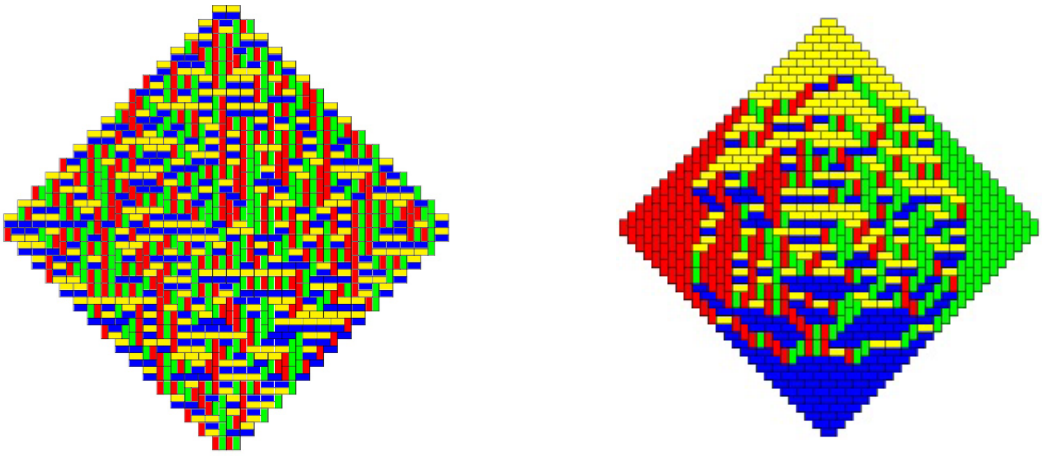

(a) Liquid case

(b) Non-liquid case

Figure 1.2: Random domino tilings of two Aztec diamonds with different boundary conditions. Dominos are coloured with respect to the chessboard colouring of the square lattice.

In the case of subgraphs of the square lattice, the dimer model is equivalent to random tiling of a domain on the dual lattice by dominos $2 \times 1$. The main question in the dimer model is: What does a generic domino tiling look like? The two pictures in Figure 1.2 clearly display some very different behaviors. The first picture appears homogeneous, while in the second, the densities of the tiles of a given orientation vary throughout the region. The dimer model in a given domain can have both "frozen" (non-liquid regime), in which one orientation and parity dominates, and "chaotic" (liquid regime) pieces, where all dominoes are roughly equivalent. The behavior of the boundary between them in the scaling limit was described by Kenyon and Okounkov [48] in terms of a variational problem for the complex Burgers equation. We are focused on the liquid case, as the non-liquid regime requires somewhat different methods [7, 10, 11, 24, 65].

### 1.1.1 Boundary conditions in the Dimer model

> The effect of boundary conditions is, however, not entirely trivial and will be discussed in more detail in a subsequent paper.
>
> P. W. Kasteleyn, 1961

For planar graphs, Kasteleyn [40] showed that the partition function of the dimer model can be evaluated as the determinant of a weighted, signed adjacency matrix whose rows indexed by the white vertices and columns indexed by the black vertices, called the *Kasteleyn matrix*. The local statistics for the uniform measure on dimer configurations

can be computed using the inverse Kasteleyn matrix, see [44]. The latter can be viewed as a two-point function, called the *coupling function* [41]. The coupling function is a complex-valued discrete holomorphic function. As such, its real and imaginary parts are discrete harmonic, and the study of the local statistics of random tilings can be reduced to the study of the convergence of discrete harmonic functions. Let us start with the case of the *uniform* dimer model on *the square lattice*.

### Temperleyan domain

The classical situation in which boundary conditions of the coupling function can be easily described is *Temperleyan* discretizations, see Fig. 1.10. In the Temperleyan case, the real part of the coupling function has Dirichlet boundary conditions. Kenyon [41, 42] used this approach to prove the conformal invariance of the limiting distribution of the height function in the case of Temperleyan discretizations. More precisely, in [41] Kenyon showed that the limit of the expected height function is a harmonic function with boundary values depending on the direction (the argument of the tangent vector) of the boundary. In [42] Kenyon proved that, in the case of Temperleyan discretizations, the fluctuations of the height function converge (as the mesh size tends to zero) to the Gaussian Free Field [75] on $\Omega$ with Dirichlet boundary conditions.

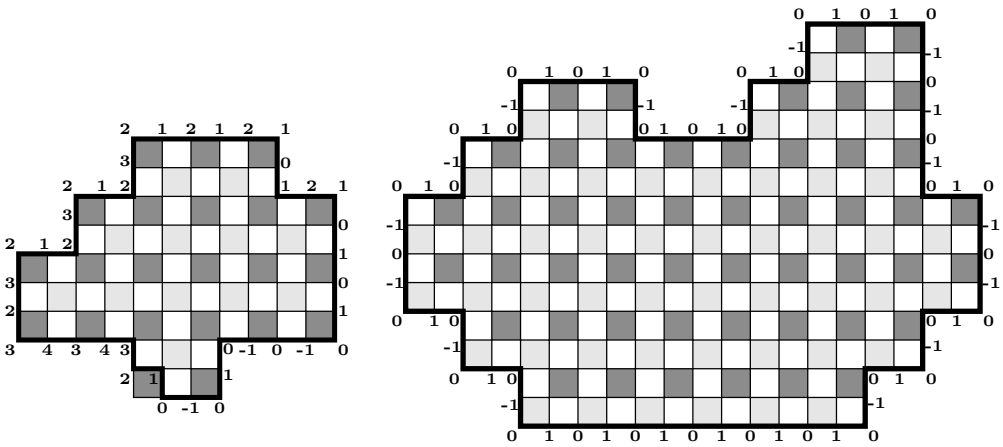

Figure 1.3: **Left:** A Temperleyan domain. The difference of the height function at two boundary vertices is related to the amount of the winding of the boundary (the number of left turns minus the number of right turns) between them. **Right:** An even domain: the boundary height function is almost trivial, it varies between three values.

In [68] we extended Kenyon's result to a class of *Piecewise Temperleyan* discretizations, domains which correspond to mixed Dirichlet and Neumann boundary conditions for the real part of the coupling function (see Fig. 1.11).

**Theorem 1.1.1** ([68])**.** *Let $\Omega^\delta$ be a sequence of discrete $2k$-black-piecewise Temperleyan domains of mesh size $\delta$ approximating a continuous domain $\Omega$. Suppose that each $\Omega^\delta$ admits a domino tiling. Assume that white square $v_0^\delta$ of the domain $\Omega^\delta$ tends to the point $v_0$ of the domain $\Omega$. Then the coupling function $\frac{1}{\delta}C_{\Omega^\delta}(\cdot, v_0^\delta)$ converges uniformly on*

*compact subsets of* $\Omega \setminus v_0$ *to a continuous holomorphic function* $f$ *with a singularity at* $v_0$*, as* $\delta$ *tends to* 0*.*

For a more precise statement, see Theorem 3.3.1 and Theorem 3.2.5.

It is known that all moments of the scaling limit of the height function can be written in terms of the scaling limit of the coupling function, see [42]. Thus, adopting the proof of [42, Theorem 1.1], we obtain the convergence of the dimer height function to the Gaussian Free Field in the setup of Theorem 1.1.1. More precisely, we have the following result.

**Corollary 1.1.2** ([68])**.** *Let* $\Omega$ *be a Jordan domain with smooth boundary in* $\mathbb{R}^2$*. Let* $\Omega^\delta$ *be a black-piecewise Temperleyan domain approximating* $\Omega$*. Let* $h^\delta$ *be the height function of* $\Omega^\delta$*. Then* $h^\delta - \mathbb{E}h^\delta$ *converges weakly in distribution to the Gaussian Free Field on* $\Omega$ *with Dirichlet boundary conditions, as* $\delta$ *tends to* 0*.*

As it was shown in [42] it is enough to compute all the limit moments of the fluctuations $h^\delta - \mathbb{E}h^\delta$ of the height function to prove that their limit is the Gaussian Free Field. The main tool to compute these moments is the coupling function. The scaling limit of the coupling function is very sensible to the boundary conditions, in particular the limits of the coupling function in the Temperleyan case and the piecewise Temperleyan case are different. However all the limits of $h^\delta - \mathbb{E}h^\delta$ turns out to be the same.

For more general discretizations, with domains that are not necessarily Temperleyan, the large-scale behavior of the expectation of the height function and its fluctuations is much more complicated, see [24, 48, 50, 65]. In particular, the exact nature of fluctuations is not established yet.

### Even domain

Note that the height function on the boundary does not depend on a domino tiling, and is completely determined by the shape of the boundary. In a Temperleyan domain the boundary values of the height function are related to the winding of the boundary, see Fig 1.10. Kenyon has shown [42], that the fluctuations of the height function on Temperleyan discretizations of a planar domain converge in the scaling limit (as the mesh size tends to zero) to the Gaussian Free Field with Dirichlet boundary conditions. This result has been extended for piecewise Temperleyan discretizations in [68]. The latter discrete domains correspond to mixed Dirichlet and Neumann boundary conditions for the real part of the coupling function, with prescribed number of changes between them.

However, it seems that the most natural discretizations are given by *even* domains, domains with all edges of even length (e.g., see a discussion in [41, Section 8]). Such a domain obviously always has domino tilings. Furthermore, the boundary height function in this case is almost trivial, see Fig 1.3. Unfortunately, in this case the boundary conditions for the coupling function are much less transparent, so that the following question is still open.

**Open problem ([41]).** *Prove that the fluctuations of the height function on even discretizations of a planar domain converge in the scaling limit (as the mesh size tends to zero) to the Gaussian Free Field with Dirichlet boundary conditions.*

In particular, Temperleyan discretizations are never even domains and, more generally, situations when an even domain can be treated as a piecewise Temperleyan one are very rare.

In this thesis, we introduce a special subclass of even discretizations. We call this type of domains *hedgehog domains*, see Fig. 1.3, a formal definition is given in Section 4.1.1. The class of hedgehog discretizations contains *two-step Aztec diamonds* (see [23, Fig. 4]), which is one of the Aztec diamond-type shapes considered in [23]. Compared to the class of (piecewise) Temperlyan discretizations, the class of hedgehog discretizations is of a very different nature. In particular,

$$\{\text{(piecewise) Temperlyan discretizations}\} \cap \{\text{Hedgehog discretizations}\} = \varnothing.$$

The most conceptual difference between (piecewise) Temperlyan and hedgehog domains lies in boundary conditions satisfied by the coupling function. In the Temperleyan case the coupling function $\frac{1}{\delta}C_{\Omega^\delta}(\cdot, v_0^\delta)$ satisfies $\mathrm{Re}[C_{\Omega^\delta}(\cdot, v_0^\delta)] = 0$ on the boundary, see [41]. In the piecewise Temperleyn [68] case one deals with mixed $\mathrm{Re}[C_{\Omega^\delta}(\cdot, v_0^\delta)] = 0$ / $\mathrm{Im}[C_{\Omega^\delta}(\cdot, v_0^\delta)] = 0$ boundary conditions with the number of changes prescribed in advance. In sharp contrast, hedgehog domains give rise to Riemann-type boundary conditions of the coupling function, see Section 4.2.1. This is consistent with the fact that scaling limits of the coupling function in the Temperlyan [41] and piecewise Temperlyan [68] cases are different, though being different from each other they have the same conformal covariance $(0, 1)$, while the scaling limit of the coupling function in the case of hedgehog approximations has conformal covariance $(\frac{1}{2}, \frac{1}{2})$, see Theorem 4.2.5 and Proposition 4.1.9.

We prove the convergence of the fluctuations of the height function to the Gaussian Free Field in the case of hedgehog discretizations. Our result is based on the following convergence theorem for the dimer coupling function.

**Theorem 1.1.3** ([69]). *Let $\Omega^\delta$ be a sequence of discrete hedgehog domains of mesh size $\delta$ approximating a simply connected domain $\Omega$. Let $v_0^\delta$ approximate a point $v \in \Omega$. Then, $\frac{1}{\delta}C_{\Omega^\delta}(\cdot, v_0^\delta)$ converges uniformly on compact subsets of $\Omega \setminus \{v\}$ to a continuous holomorphic function satisfying Riemann-type boundary conditions*

$$\mathrm{Im}[f(z)\sqrt{n(z)}] = 0, \quad z \in \partial\Omega,$$

*where $n(z)$ is the outer normal to the boundary at $z$.*

For a more precise statement, see Theorem 4.2.5. In particular, note that we *do not* assume that the boundary $\partial\Omega$ is smooth. The main advantage of hedgehog-type discretizations is that the primitive of the square of s-holomorphic version of the coupling function is constant at (a half of) boundary vertices, see Proposition 4.2.1. This allows to obtain, after slight modification, Riemann boundary conditions for the coupling function on a discrete level, see Proposition 4.2.2, and to use discrete complex analysis techniques originally developed in the Ising model context [78].

Due to [42] the dimer height function converges to the Gaussian Free Field in the setup of Theorem 1.1.3.

**Corollary 1.1.4** ([69]). *Let $\Omega$ be a bounded simply connected domain in $\mathbb{C}$, whose boundary $\partial\Omega$ contains a straight segment. Let $\Omega^\delta$ be a hedgehog domain approximating $\Omega$. Let $h^\delta$ be the height function of $\Omega^\delta$. Then $h^\delta - \mathbb{E}h^\delta$ converges weakly in distribution to the Gaussian Free Field on $\Omega$ with Dirichlet boundary conditions, as $\delta$ tends to 0.*

The existence of a straight part of the boundary is a technical condition, which we use in the proof. However, we believe that it can be relaxed.

### 1.1.2 Double-dimer model

In this section we describe main results obtained in this thesis for the uniform double-dimer model on the square lattice.

A double-dimer configuration is a union of two dimer coverings, or equivalently a set of even-length simple loops and double edges with the property that every vertex is the endpoint of exactly two edges, see Fig. 1.4.

Note that there are two ways to obtain a given loop (on the dual graph). This can be interpreted as a choice of the orientation of the loop, see Fig. 1.4. Thus, the double-dimer model can be represented as a random covering of the dual graph by the oriented loops and double edges [64]. The height function in the double-dimer model, which is the difference of height functions for two dimer configurations, has a simple geometric representation: if we cross a loop, then the height function changes by $+1$ or $-1$, depending on the orientation of the loop.

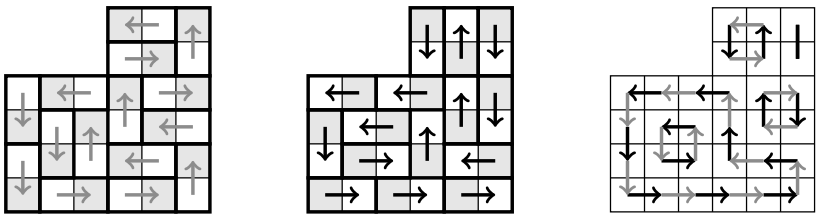

Figure 1.4: Two different domino tilings of the same domain can be combined into the collection of loops and double edges. Orienting the edges of the first covering from white to black, and the edges of the second one from black to white, one gets an orientation of resulting loops.

There is a prediction that the loop ensemble of the double-dimer model converges to the conformal loop ensemble $CLE(4)$, see [74, 76]. In the case of discretizations by Temperleyan domains Kenyon [45] and Dubedat [28] obtained results confirming this prediction. The loop ensemble $CLE(4)$ is a conformally invariant object. It corresponds to level lines of the Gaussian Free Field. There is a gap of $\pm 2\lambda = \pm\sqrt{\pi/2}$ between the values of the Gaussian Free Field on the interior and the exterior side of each $CLE(4)$ loop [73, 84]. This is similar to loops in the double-dimer model outlining the discontinuities of the double-dimer height function, the gap being $\pm 1$.

**Open problem.** *Prove that the loop ensemble of the double-dimer model converges to the conformal loop ensemble $CLE(4)$.*

We will consider coverings of a pair of domains that differ by two squares, see Fig. 1.5. In this case, in addition to a collection of loops and double edges, the resulting composition of the coverings contains an interface (a simple path between these two squares). It is expected that the interface converges to a conformally invariant random curve $SLE(4)$ as the mesh size tends to zero, see [71].

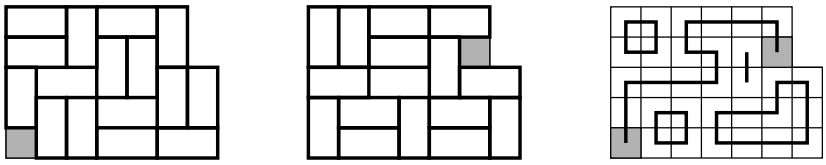

Figure 1.5: Left: the coverings of the domains that differ on two squares. Right: the interface between these two squares and the collection of loops and double edges is the result of the composition of the coverings.

**Open problem.** *Prove that the interface of the double-dimer model converges to the conformally invariant random curve* $SLE(4)$.

The coupling function plays an important role in the proof of convergence of height functions. In [68] we showed that in the double-dimer model the coupling function $C_{\text{dbl-d}(u,v)}$ has a factorization into a product of two discrete holomorphic functions $F(u)$ and $G(v)$. We described the construction of the discrete integral of this product of two discrete holomorphic functions. This construction is close to the construction of the discrete primitive of the square of the s-holomorphic function [22, 77, 78]. Then for any discrete domain, the expectation of the height function of the double-dimer model can be interpreted as an integral of two discrete holomorphic functions. Due to Kenyon [41], for the single-dimer model, the expectation of the height function is harmonic in the limit for approximations by Temperleyan domains. In [68] using the factorization of the double-dimer coupling function we showed that the expectation of the double-dimer height function is harmonic already on the discrete level.

**Theorem 1.1.5** ([68])**.** *The expectation of the double-dimer height function on a Temperleyan domain is exactly discrete harmonic.*

We also prove the convergence of average height functions in the double-dimer model to the harmonic measure for the discretizations by polygonal domains.

**Theorem 1.1.6** ([68])**.** *Let* $\Omega$ *be a polygon with* $n$ *sides parallel to the axes. Let* $u_0$ *and* $v_0$ *be points on straight parts of the boundary of* $\Omega$*. Suppose that a sequence of discrete* $n$*-gons* $\Omega^\delta$ *on a grid with mesh size* $\delta$ *approximates the polygon* $\Omega$ *in a proper way, and that each polygon* $\Omega^\delta$ *has at least one domino tiling. Let black and white squares* $u_0^\delta$ *and* $v_0^\delta$ *of domain* $\Omega^\delta$ *tend to boundary points* $u_0$ *and* $v_0$ *of the domain* $\Omega$*. Let* $h^\delta$ *be the height function of a uniform double-dimer configuration on* $\Omega$*. Then* $\mathbb{E}h^\delta$ *converges to the harmonic measure* $\mathrm{hm}_\Omega(\,\cdot\,,(u_0v_0))$ *of the boundary arc* $(u_0v_0)$ *on the domain* $\Omega$*.*

In the case of hedgehog approximations the functions $F$ and $G$ solve the discrete Riemann boundary value problems described in Section 4.1.3. This allows us to prove the following theorem.

**Theorem 1.1.7** ([69])**.** *Let* $\Omega$ *be a bounded simply connected domain. Let* $u_0$ *and* $v_0$ *be points on straight parts of the boundary of* $\Omega$*. Suppose that a sequence of discrete hedgehog domains* $\Omega^\delta$ *on a grid with mesh size* $\delta$ *approximates the domain* $\Omega$*. Let black and white squares* $u_0^\delta$ *and* $v_0^\delta$ *of the domain* $\Omega^\delta$ *tend to boundary points* $u_0$ *and* $v_0$ *of the domain* $\Omega$*. Finally, let* $h^\delta$ *be the height function of a uniform double-dimer configuration on* $\Omega$*. Then*

$\mathbb{E}h^\delta$ *converges to the harmonic measure* $\mathrm{hm}_\Omega(\,\cdot\,,(u_0v_0))$ *of the boundary arc* $(u_0v_0)$ *on the domain* $\Omega$.

### 1.1.3 Embeddings of the dimer graphs

Now, let us think about the dimer model on a general *weighted* bipartite planar graph $\mathcal{G}$, with bipartition $(W,B)$.

Finding good embedding of graphs, and in particular the operation of scaling it provides, is at the heart of what is arguably one of the biggest questions of statistical mechanics, namely, universality. Indeed, this is the belief that if we consider discrete models of statistical mechanics and rescale them appropriately, we should see continuous objects in the limit which do not depend on local details of the model. In particular, these limits should not depend on the underlying graph and in dimension two they should be conformally invariant.

The main tool for establishing convergence of critical $2D$ lattice models to conformally invariant scaling limits is a discrete version of complex analysis and potential theory in the complex plane. There are no "canonical" discretizations of Laplace and Cauchy-Riemann operators, the most studied ones are for the square grid. One of the main questions in the context of the universality and conformal invariance of a critical $2D$ lattice model is to find an embedding which geometrically encodes the weights of the model and that admits "nice" discretizations of Laplace and Cauchy-Riemann operators.

#### Kasteleyn matrix as a discrete Cauchy–Riemann operator

The Kasteleyn matrix $K$ can be seen as a discrete $\bar\partial$-operator $K:\mathbb{C}^B\to\mathbb{C}^W$. Then one can define discrete holomorphic functions on a bipartite dimer graph as follows:

**Definition 1.1.8.** *A function* $F^\bullet: B\to\mathbb{C}$ *is discrete holomorphic at* $w\in W$ *if*

$$[\bar\partial F^\bullet](w):=\sum_{b\sim w}F^\bullet(b)\cdot K(w,b)=[F^\bullet K](w)=0;$$

It is easy to see, that for a fixed $w_0\in W$ the function $K^{-1}(\,\cdot\,,w_0)$ is a discrete holomorphic function with a simple pole at $w_0$.

#### Isoradial graph

A rhombic lattice was introduced by Duffin [29] as a large family of graphs, where discretizations of Laplace and Cauchy-Riemann operators can be defined similarly to that for the square lattice. They reappeared recently as isoradial graphs in the work of Mercat and Kenyon, as a family of graphs where certain $2D$ statistical mechanical models preserve some integrability.

The planar graph embedded in $\mathbb{C}$ is called *isoradial* if each face is inscribed into a circle of a common radius $\delta$. Also, one can think about $\delta$ as a mesh size of the isoradial graph. If all circle centers are inside the corresponding faces, then one can naturally embed the dual graph in $\mathbb{C}$ isoradially with the same $\delta$. The name rhombic lattice is due to the fact that all quadrilateral faces of the graph on the union of the vertex set and set of dual vertices of the initial graph are rhombi with sides of length $\delta$, see Fig. 1.6.

A lot of planar graphs admit isoradial embeddings. It was shown by Kenyon and Schlenker that in fact, there are only three topological obstructions for a graph not to have an isoradial embedding [53]. However, the choice of weights of the model is given by the geometry of the isoradial embedding.

The class of isoradial graphs is one of the largest known classes of graphs where classical complex analysis results have discrete analogs. Chelkak and Smirnov provided a "toolbox" of discrete versions of continuous results sufficient to perform a passage to the scaling limit, see [21]. Discrete complex analysis allows to obtain results for two-dimensional lattice models on isoradial graphs, notably the Ising [61, 22] and dimer [46, 25, 27, 58] models. In [68] we proved the convergence of the coupling function in the case of isoradial piecewise Temperleyan approximations, see Appendix A.

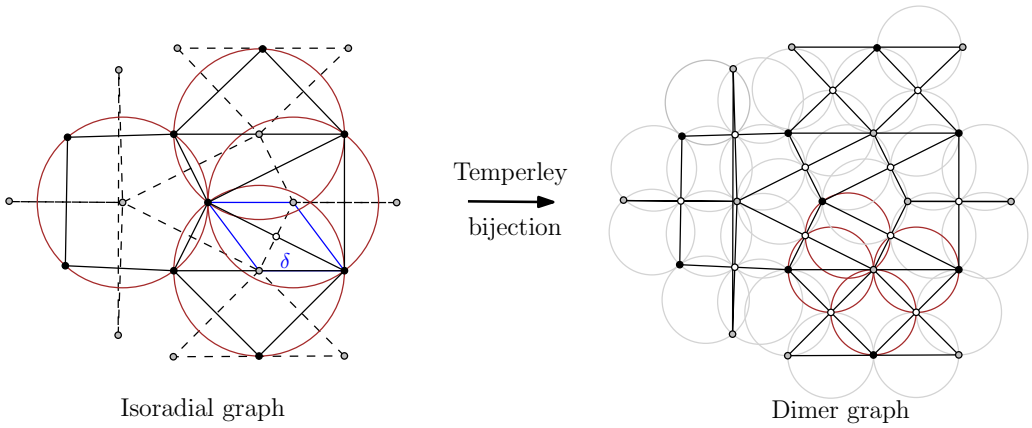


Figure 1.6: A construction of dimer graph on isoradial graphs via Temperley bijection.

Isoradial dimer model was introduced by Kenyon [46]. To define an isoradial dimer graph, such that the Kasteleyn matrix can be viewed as a discretization (as in [21]) of the Cauchy-Riemann operator, one should use Temperley's bijection. In [80] Temperley described a bijection between spanning trees of the $m \times n$ grid and perfect matchings in the $(2m+1) \times (2n+1)$ rectangular grid with a corner removed. Propp [67] and, independently, Burton and Pemantle [14] generalized this bijection to map spanning trees of general undirected unweighted planar graphs to perfect matchings of a related graph. This bijection was extended to the directed weighted case in [51].

Let $G^\delta$ be an isoradial graph. A dimer configuration in this setup is a perfect matching of the bipartite graph $G_D$. The vertex set of $G_D$ obtained as a superposition of $G^\delta$ and $G^\delta_*$ (two types of black vertices) and rhombi centers (white vertices), and there is an edge between black and white vertices if the black vertex and corresponding rhombus are adjacent (see Fig. 1.6). Note that $G_D$ is an isoradial graph, where each face is inscribed into a circle of radius $\frac{\delta}{2}$. The class of isoradial dimer graphs can be considered as a generalisation of the square lattice. However, some natural planar graphs, such as the honeycomb lattice, are not isoradial dimer graphs for all isoradial dimer graphs have only faces of degree four. Also, the choice of weights is given by the geometry of the isoradial dimer embedding. Therefore, in the context of universality of the dimer model on weighted planar graphs, a wider class of embeddings should be sought.

### Dimers and T-graphs

The construction of a T-graph was introduced by Kenyon and Sheffield in [52]. Starting from a T-graph one can define a bipartite graph, whose black vertices are the open line segments $L_i$ and whose white vertices are the faces of the T-graph. A white vertex is adjacent to a black vertex if the corresponding face contains a portion of the corresponding segment as its boundary. Using a T-graph one can define in a natural geometric way complex Kasteleyn signs on this bipartite graph. Any planar bipartite graph with real-valued Kasteleyn weights can be embedded as a T-graph corresponding to this bipartite graph. Complex-valued Kasteleyn weights defined using this T-graph are gauge equivalent to the initial ones.

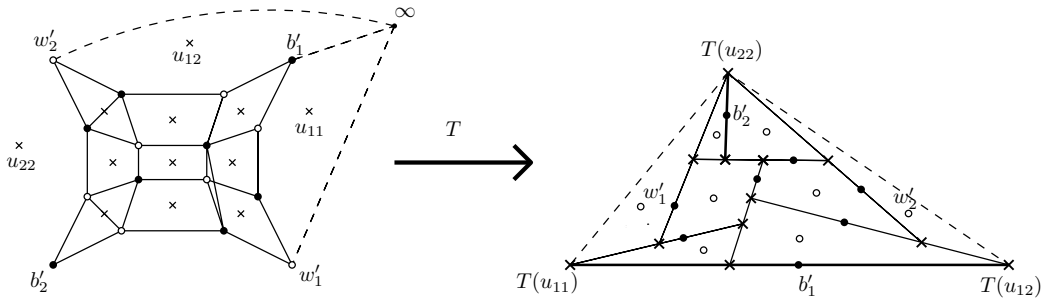


Figure 1.7: A construction of a T-graph.

Associating to a T-graph $G_{\text{T-graph}}$ a Markov chain, as described in [43], allows one to consider a natural random walk on $G_{\text{T-graph}}$ and to define discrete harmonic functions (coordinate functions) on $G_{\text{T-graph}}$. The central limit theorem proved in [56] provides an information about convergence of discrete harmonic functions to its continuous counterparts. However, an estimate on the discrete derivative of such functions as well as quantitative bounds on the speed of convergence are not proven. This disallow one to use a classical strategy to show the conformal invariance of the dimer model.

The construction of a T-graph was used by Berestycki, Laslier and Ray in [5] to show the convergence of the fluctuations of the dimer height function to the Gaussian free field in the case of lozenge tilings with flat boundary conditions. The approach appearing in this paper relies more on properties of the limiting objects in the continuum rather than exact computations at the microscopic level. This approach uses a bijection of the dimer model with uniform spanning trees which makes it arduous to work with non-Temperleyan-type boundary conditions. This strategy does not work, for example, in the case of hedgehog approximations.

### S-embeddings

In [15] Chelkak introduced a new class of embeddings of general weighted planar graphs based on s-holomorphic spinors. He introduced approximations of Laplace and Cauchy-Riemann operators on s-embeddings and showed a priori regularity of discrete holomorphic functions. It allowed him to obtain the following result:

**Theorem 1.1.9** (Chelkak, 2018)**.** *The convergence of critical FK-Ising interfaces to SLE(16/3) holds for all bi-periodic weighted graphs.*

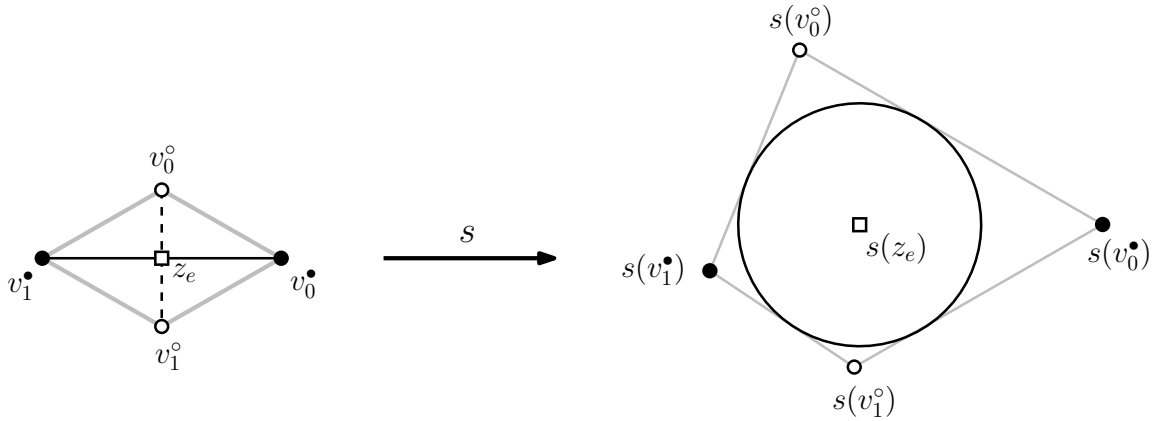


Figure 1.8: S-embedding. Points $s(v_0^\bullet)$, $s(v_0^\circ)$, $s(v_1^\bullet)$ and $s(v_1^\circ)$ form a tangential quadrilateral with incenter $s(z_e)$.

An s-embedding of a planar graph $G$ is an embedding $s$ defined on each vertex, dual vertex and edge midpoint of $G$ with the following property: For any edge $e$ in $G$, if $v_0^\bullet$ and $v_1^\bullet$ (resp. $v_0^\circ$ and $v_1^\circ$) denote the endpoints of $e$ (resp. of the edge dual to $e$) and $z_e$ denotes the midpoint of $e$ as on Figure 1.8, then $s(v_0^\bullet)$, $s(v_0^\circ)$, $s(v_1^\bullet)$ and $s(v_1^\circ)$ form a tangential quadrilateral with incenter $s(v_e)$, meaning that there exists a circle centered at $s(z_e)$ and tangential to the four sides of the quadrilateral.

It was shown in [47] that an s-embedding of $G$ provides an embedding (t-embedding) of $G_D^*$ into $\mathbb{C}$, where $G_D$ is a dimer graph obtained from $G$ using Dubedat's bijection [26], see Section 5.4.

### Circle patterns and t-embeddings

We generalise the above constructions for a weighted planar bipartite graphs. We introduce a fairly new type of embeddings called t-embeddings or circle patterns (depending on whether one looks at the primal or dual graph). The purpose of Chapters 5 and 6 is to introduce the definitions and justify why t-embeddings or circle-patterns are "nice" embeddings to study the dimer model.

**Geometric properties.** In Chapter 5 we establish a correspondence between the dimer model on a bipartite graph and a circle pattern with the combinatorics of that graph, which holds for graphs that are either planar or embedded on the torus.

Natural parameters for the dimer model, defining the underlying probability measure, are face weights, which are positive real parameters on the bounded faces of the graph [35]. A question raised in [35] concerns relating the parameters (the face weights of the dimer model) to some geometric property of the underlying graph or embedding. We associate to a face-weighted bipartite planar graph a *circle pattern*: a realization of the graph in $\mathbb{C}$ with cyclic faces where all vertices of a face lie on a circle. Our circle patterns are not necessarily embedded. An *embedded circle pattern* is a more restrictive object, when the realization is an actual embedding of the graph. This realization has the following important features:

1. Face weights are given by certain length biratios.

2. The construction generalizes the isoradial case.

3. Local rearrangements of the graph, called *urban renewals* or *spider moves* or *cluster mutations*, correspond to applications of the Miquel six-circles theorem for the underlying circle pattern.

4. Planar resistor networks can be subdivided into bipartite planar graphs with face weights. Our construction of circle patterns is compatible with harmonic embeddings of the network.

5. The (ferromagnetic) Ising model on a planar graph can be associated with dimers on a related bipartite planar graph. Our construction is compatible with the s-embedding of the associated Ising model [15, 59].

The circle patterns arising under this correspondence are those with bipartite graph and with an *embedded dual*, where the dual graph is the graph of circle centers. Having embedded dual does not imply that the primal pattern is embedded, although the set of circle patterns with embedded dual includes all embedded circle patterns in which each face contains the center.

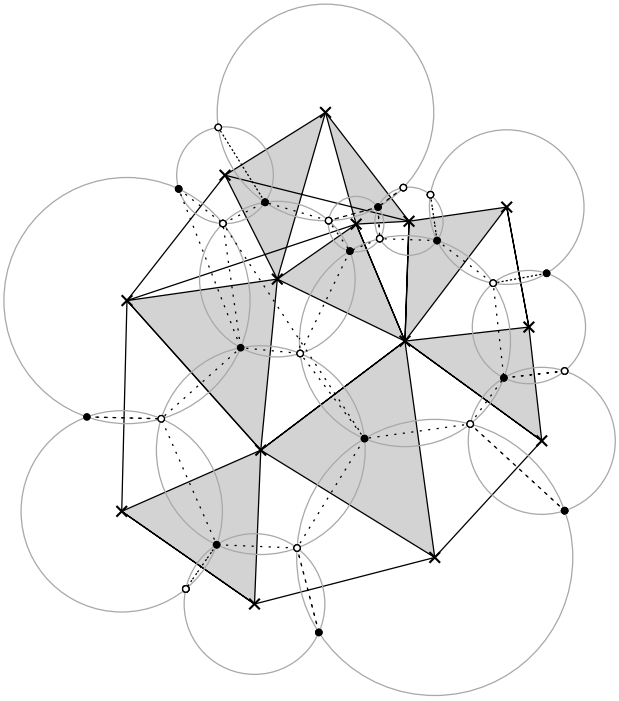

Figure 1.9: A circle pattern.

**T-holomorphicity.** Circle center realizations are also considered in Chapter 6 under the name of t-embeddings with an emphasis on the convergence of discrete holomorphic functions to continuous ones in the small mesh size limit, i.e., when the circle radii tend to zero.

We are interested in a form of *large scale conformal structure* of the graph, as seen from the dimer model. We will show that t-embeddings can match this conformal structure at large scale, in the sense that one can define a notion of discrete holomorphicity using the geometry which is simultaneously relevant to the dimer model and close at large scale to continuous holomorphicity.

We will show that one can define on t-embeddings a notion of discrete t-holomorphic function. In fact, any t-holomorphic function is in the kernel of the Kasteleyn matrix. So, on the one hand, it is related to the dimer model while on the other hand, under natural conditions on the t-embedding, any scaling limit of discrete t-holomorphic function will be a continuous holomorphic function. In addition to this definition and the basic properties of these functions, in [20] we prove a-priori estimates such as Harnack inequality on these discrete holomorphic functions. These tools should be useful when studying their scaling limits, in particular, we believe that using this result it can be essentially enough to show that $\mathrm{Cov}(H^\delta(x), H^\delta(y))$ stays bounded independently of the size of the graph to deduce that the height function $H^\delta$ converges to the Gaussian free field.

## 1.2 Definitions and basic facts of the dimer model on the square lattice

In this section we deal with uniform random coverings of a subgraphs of the square lattice. That is, those chosen from the distribution in which all dimer configurations are equally weighted.

### 1.2.1 Height function and Temperleyan domain

Consider a checkerboard tiling of a discrete domain $\Omega$ with unit squares. We will use grey color for the black squares in our figures. Sometimes for convenience we will distinguish between two types of black squares, in this case in the figures black squares in even rows will be represented by a light grey and those in odd rows will be dark grey (see Fig. 1.3). A domain where all corner squares are dark grey is called an *odd Temperleyan domain*. To obtain the *Temperleyan domain* one removes one dark grey square adjacent to the boundary from an odd Temperleyan domain.

W. P. Thurston [82] defines the *height function* $h$ (which is a real-valued function on the vertices of $\Omega$) as follows. Fix a vertex $z_0$ and set $h(z_0) = 0$. For every other vertex $z$ in the tiling, take an edge-path $\gamma$ from $z_0$ to $z$. The height along $\gamma$ changes by $\pm\frac{1}{4}$ if the traversed edge does not cross a domino from the tiling or by $\mp\frac{3}{4}$ otherwise: if the traversed edge has a black square on its left then the height increases by $\frac{1}{4}$ or decreases by $\frac{3}{4}$; if it has a white square on its left then it decreases by $\frac{1}{4}$ or increases by $\frac{3}{4}$, see Fig. 1.10. Note that for a simply connected domain, the height is independent of the choice of $\gamma$. The height function in the double-dimer model is defined as the difference of the height functions of the two corresponding dimer coverings.

### 1.2.2 Kasteleyn weights and discrete holomorphic functions

Let $G$ be a bipartite graph with $n$ black and $n$ white vertices. A *Kasteleyn matrix* $K_G$ is an $n \times n$ weighted adjacency matrix whose rows index the black vertices and columns index the white vertices. Let us denote by $\tau(u, v)$ an element of this matrix, where $u$ and $v$ are adjacent black and white vertices. For finite planar bipartite graphs Kasteleyn [40] proved that if the edge-weights are Kasteleyn, i.e. the alternating product of the weights along any simple face of degree $p$ is equal to $(-1)^{(p+2)/2}$, then the absolute value of the determinant of the Kasteleyn matrix is equal to the number of perfect matchings of the graph.

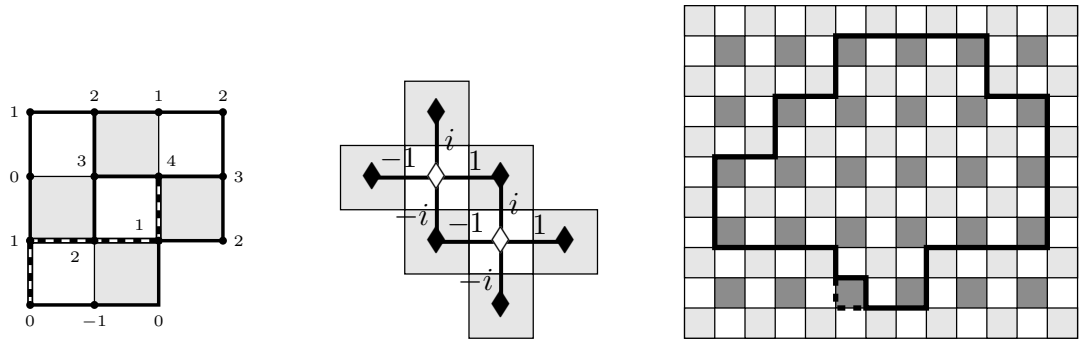


Figure 1.10: **Left:** a domino tiling of a domain; an edge-path $\gamma$ from $z_0$ to $z$ and the height along this path: $h^\delta(z_0) = 0$, $h^\delta(z) = 4$. **Center:** Weights of the Kasteleyn matrix $K_\Omega$ on the square lattice (proposed by Kenyon in [41]): at each white vertex the four edge weights going counterclockwise from the right-going edge are 1, $i$, $-1$, $-i$ respectively. **Right:** A Temperleyan domain.

Kenyon showed how to compute local statistics for the uniform measure on dimer configurations on a planar graph, using the inverse of the Kasteleyn matrix. Let $E$ be a finite collection of disjoint edges of $\Omega$. Let $\mu$ be the uniform probability measure on perfect matchings of $\Omega$. Let $b_1, \dots, b_k$ and $w_1, \dots, w_k$ be the black and white vertices of the edges belonging to $E$ correspondingly.

**Theorem 1.2.1** ([44]). *The $\mu$-probability that the set $E$ occurs in a perfect matching is given by $|\det(K_E^{-1})|$, where $K_E^{-1}$ is the submatrix of $K_\Omega^{-1}$ whose rows are indexed by $b_1, \dots, b_k$ and columns are indexed by $w_1, \dots, w_k$. More precisely, the probability is $c \cdot (-1)^{\sum p_i + q_j} \cdot a_E \cdot \det(K_E^{-1})$, where $p_i, q_i$ is the index of $b_i$, resp. $w_i$, in a fixed ordering of the vertices, $c = \pm 1$ is a constant depending only on that ordering, and $a_E$ is the product of the edge weights of the edges $E$.*

For a given planar graph $G$, there are many ways to choose the edge-weights satisfying the Kasteleyn condition. Let us fix the following ones, which were proposed by Kenyon in [41]: put $\tau(e) = \pm 1$ for horizontal edges and $\tau(e) = \pm i$ if $e$ is a vertical edge, see Fig. 1.10. It is easy to check that these weights are Kasteleyn weights.

Let $\Omega$ be a discrete domain on a square lattice that has at least one domino tiling. Let $K_\Omega$ be a Kasteleyn matrix of this domain. Let us denote by $C_\Omega(u, v)$ the elements of the inverse matrix $K_\Omega^{-1}$, where $u$ and $v$ are black and white squares of $\Omega$. The main advantage of choosing Kasteleyn weights as shown in Fig. 1.10 is the following: with this choice of weights the function $C_\Omega(u, v)$ is discrete holomorphic on the domain. Thus its limiting behavior can be studied using the methods of discrete complex analysis, see [41]. Following [41], we call $C_\Omega(u, v)$ the *coupling function*.

Let $F$ be a function defined on the set of black squares of the domain $\Omega$. Recall that the function $F$ is called *discrete holomorphic* on $\Omega$ if for any white square $v \in \Omega$ it satisfies a discrete analogue of the Cauchy-Riemann equation (see Fig. 1.12), and at the same time the values of the function $F$ on the set of light grey squares are real, while on the set of dark grey squares they are purely imaginary. Note that the real and imaginary parts of a holomorphic function are harmonic functions. It is also true on a

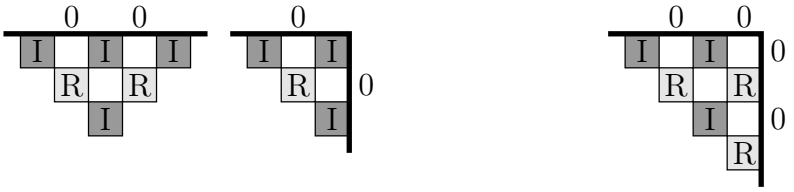


Figure 1.11: The coupling function $C(u, v_0)$ with fixed $v_0$ is real on the set of light grey squares, and it is pure imaginary on the set of dark grey squares. On the left pictures the coupling function restricted to the light grey squares satisfies the Dirichlet boundary conditions, and the coupling function restricted to the dark grey squares obeys Neumann boundary conditions. The picture on the right corresponds to mixed Dirichlet and Neumann boundary conditions for the coupling function.


$$F(c) - F(a) = -i \cdot (F(d) - F(b)) \qquad [\Delta F](u) = \tfrac{1}{4} \sum_{s=1}^{4} (F(u_s) - F(u))$$

Figure 1.12: Left: Discrete Cauchy-Riemann equation. Right: Discrete leap-frog Laplacian on the light grey lattice. The function $F$ is called discrete harmonic at $u$ if $[\Delta F](u) = 0$.

discrete level: consider the discrete Cauchy-Riemann equations at four white neighbours of a black square $u$, then it is easy to show that $F(u) = \frac{1}{4} \sum_{i=1}^{4} F(u_i)$. Therefore the *discrete leap-frog Laplacian* of $F$ at $u$ equals zero (see. Fig. 1.12). In other words, real and imaginary parts of discrete holomorphic functions are discrete harmonic functions.

The coupling function $C_\Omega(u, v) = K_\Omega^{-1}(u, v)$ can be extended to be zero on all boundary black squares, see Fig. 1.11. We know that $K_\Omega^{-1} \cdot K_\Omega = I$, which is equivalent to the following relation:

$$1 \cdot C_\Omega(v + 1, v_0) - 1 \cdot C_\Omega(v - 1, v_0) + i \cdot C_\Omega(v + i, v_0) - i \cdot C_\Omega(v - i, v_0) = \mathbb{1}_{\{v = v_0\}}. \quad (2.1)$$

Note that this relation is the discrete Cauchy-Riemann equation for the coupling function $C_\Omega(\cdot, v_0)$, so for any white square $v_0 \in \Omega$ the function $C_\Omega(u, v_0)$ considered as a function of $u \in \Omega$ is discrete holomorphic on $\Omega \setminus \{v_0\}$, for more details see [41]. Therefore, the restriction of $C_\Omega(u, v_0)$ to one type of black squares is a discrete harmonic function everywhere except the two squares adjacent to $v_0$.

In addition, the function $C_\Omega(u, v)$ satisfies the following property:

- ▷ if $u$ and $v$ are adjacent squares, then $|C_\Omega(u, v)|$ is equal to the probability that the domino $[uv]$ is contained in a random domino tiling of $\Omega$, see [41],
- ▷ moreover, all the joint probabilities to see a collection of dominos $\{[u_k v_k]\}_{k=1}^{n}$ in a random domino tiling of $\Omega$, can be expressed via $C_\Omega$ as $n \times n$ determinants.

For Temperleyan domains, each of the two discrete harmonic components of the function $C_\Omega(u, v_0)$ has the following boundary conditions: the restriction of the coupling function to the light grey squares (see Fig. 1.11), satisfies the Dirichlet boundary conditions, and coupling function restricted to the dark grey squares obeys Neumann boundary conditions.

### 1.2.3 Even/Odd double dimers

A double-dimer configuration is the union of two dimer coverings. We will consider coverings of a pair of domains $\Omega_1$, $\Omega_2$ that differ by two squares, i.e. $|\Omega_1 \triangle \Omega_2| = 2$. Note that there are two different situations depending on whether $\Omega := \Omega_1 \cup \Omega_2$ contains an odd or an even number of squares. In the *odd* case, assume that $\Omega$ has one more black square than white squares. Then the domains $\Omega_1$ and $\Omega_2$ are obtained from $\Omega$ by removing black squares $u_1$ and $u_2$ adjacent to the boundary (see Fig. 1.14). In the *even* case, let $\Omega_1 = \Omega$ and $\Omega_2$ be obtained from $\Omega$ by removing black and white squares $u_0$ and $v_0$, which are adjacent to the boundary. One can modify a domain in the odd case to reduce it to the even case, see Fig. 2.3 and Remark 2.3.1.

Let us define the *double-dimer coupling function* on $\Omega = \Omega_1 \cup \Omega_2$ as the difference of the two dimer coupling functions on domains $\Omega_1$ and $\Omega_2$

$$C_{\text{dbl-d},\Omega}(u, v) := C_{\Omega_1}(u, v) - C_{\Omega_2}(u, v).$$

Recall that the absolute value of the coupling function is the probability that the corresponding domino is contained in a random tiling, and the determinant of the Kasteleyn matrix is equal to the number of domino tilings of our domain, so, $|C_{\Omega\setminus\{u_0,v_0\}}(u, v)| = \left|\frac{\det(K_{\Omega\setminus\{u_0,v_0,u,v\}})}{\det(K_{\Omega\setminus\{u_0,v_0\}})}\right|$. Note that

$$\frac{\det(K_{\Omega\setminus\{u_0,v_0\}})}{\det(K_\Omega)} = \pm K_\Omega^{-1}(u_0, v_0) \quad \text{and} \quad \frac{\det(K_{\Omega\setminus\{u,v\}})}{\det(K_\Omega)} = \pm K_\Omega^{-1}(u, v),$$

and also

$$\frac{\det(K_{\Omega\setminus\{u_0,v_0,u,v\}})}{\det(K_\Omega)} = \pm \det \begin{pmatrix} K_\Omega^{-1}(u_0, v_0) & K_\Omega^{-1}(u_0, v) \\ K_\Omega^{-1}(u, v_0) & K_\Omega^{-1}(u, v) \end{pmatrix}.$$

Therefore,

$$C_{\text{dbl-d},\Omega}(u, v) = C_\Omega(u, v) - C_{\Omega\setminus\{u_0,v_0\}}(u, v) = \pm \frac{K_\Omega^{-1}(u_0, v) \cdot K_\Omega^{-1}(u, v_0)}{K_\Omega^{-1}(u_0, v_0)}.$$

Recall that for a fixed $v_0$ the function $K_\Omega^{-1}(u, v_0)$ is a discrete holomorphic function of $u$. Let us denote it by $F_{v_0}(u)$ and similarly let us define a function $G_{u_0}(v) := K_\Omega^{-1}(u_0, v)$. So, we obtain

$$C_{\text{dbl-d},\Omega}(u, v) = const_{u_0,v_0} \cdot F_{v_0}(u) \cdot G_{u_0}(v),$$

where $const_{u_0,v_0} = \pm 1/K_\Omega^{-1}(u_0, v_0)$.

Below we discuss the above factorization of the double-dimer coupling function from the viewpoint of discrete holomorphic solutions to appropriate boundary value problems, the framework which we use later to prove the main convergence theorems.

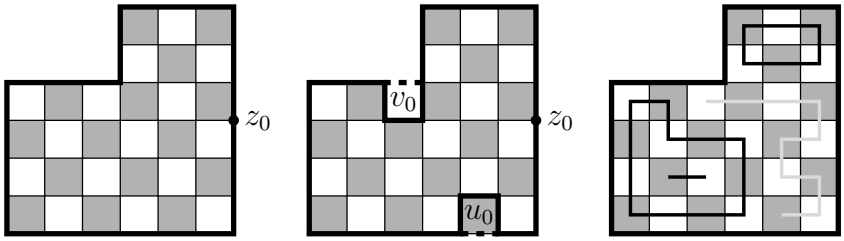


Figure 1.13: *Even case.* The vertex $z_0$ is the vertex on the boundary where $h_1(z_0) = h_2(z_0) = h(z_0) = 0$. The squares $u_0$ and $v_0$ are the difference between the domains $\Omega_1 = \Omega$ and $\Omega_2 = \Omega \setminus \{u_0, v_0\}$. On the right: an example of the interface (grey) from $u_0$ to $v_0$ and the set of loops and double edges in $\Omega$.

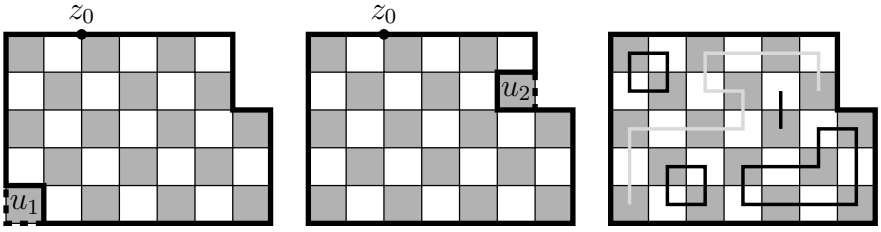


Figure 1.14: *Odd case.* The vertex $z_0$ is the vertex on the boundary where $h_1(z_0) = h_2(z_0) = h(z_0) = 0$. The squares $u_1$ and $u_2$ are the difference between the domains $\Omega_1 = \Omega \setminus \{u_1\}$ and $\Omega_2 = \Omega \setminus \{u_2\}$. On the right: an example of the interface (grey) from $u_1$ to $u_2$ and the set of loops and double edges in $\Omega$.

### 1.2.4 Notation

Put $\lambda = e^{i\frac{\pi}{4}}$ and $\bar{\lambda} = e^{-i\frac{\pi}{4}}$. Consider a checkerboard tiling $\mathbb{C}^\delta$ of $\mathbb{C}$ with squares, each square has side $\delta$ and centered at a lattice point of

$$\left\{\left(\frac{\delta n}{\sqrt{2}}, \frac{\delta m}{\sqrt{2}}\right) \mid n, m \in \mathbb{Z}; n+m \in 2\mathbb{Z}\right\}$$

(see Fig. 1.15). The pair $(n, m)$ is called the coordinates of a point on this lattice. Let $\Omega^\delta$ be a simply connected discrete domain composed of a finite number of squares of $\mathbb{C}^\delta$ bounded by a disjoint simple closed lattice path. Let $\mathcal{V}^\delta$ be the vertex set of $\Omega^\delta$. We will denote the set of black squares by $\blacklozenge^\delta$ and the set of white squares of $\Omega^\delta$ by $\lozenge^\delta$. Thus, $\Omega^\delta = \blacklozenge^\delta \sqcup \lozenge^\delta$. Let the coordinates of a square be the coordinates of its center. Then we can define the sets $\blacklozenge^\delta_0$ and $\blacklozenge^\delta_1$ of black squares of $\Omega^\delta$ and the sets $\lozenge^\delta_0$ and $\lozenge^\delta_1$ of white squares by the following properties:

($\blacklozenge^\delta_0$) both coordinates are even and the sum of coordinates is divisible by 4;

($\blacklozenge^\delta_1$) both coordinates are even and the sum of coordinates is not divisible by 4;

($\lozenge^\delta_0$) both coordinates are odd and the sum of coordinates is not divisible by 4;

($\lozenge^\delta_1$) both coordinates are odd and the sum of coordinates is divisible by 4.

Define $\partial\mathcal{V}^\delta$ to be the set of vertices on the boundary. Let $\partial\Omega^\delta$ be the set of faces adjacent to $\Omega^\delta$ but not in $\Omega^\delta$. Let $\partial\blacklozenge^\delta$ and $\partial\lozenge^\delta$ be the sets of black and white faces of $\partial\Omega^\delta$ correspondingly. Let $\partial_{\text{int}}\Omega^\delta$ be the set of interior faces that have a common edge with boundary of $\Omega^\delta$. Similarly define sets $\partial_{\text{int}}\blacklozenge^\delta$ and $\partial_{\text{int}}\lozenge^\delta$ ($\partial_{\text{int}}\Omega^\delta = \partial_{\text{int}}\blacklozenge^\delta \sqcup \partial_{\text{int}}\lozenge^\delta$). Let $\operatorname{Int}\Omega^\delta = \Omega^\delta \setminus \partial_{\text{int}}\Omega^\delta$. Let us denote by $\overline{\Omega}^\delta$ the set $\Omega^\delta \sqcup \partial\Omega^\delta$, define also sets $\bar{\blacklozenge}^\delta$ and $\bar{\lozenge}^\delta$, to be exact: $\bar{\blacklozenge}^\delta = \blacklozenge^\delta \sqcup \partial\blacklozenge^\delta$ and $\bar{\lozenge}^\delta = \lozenge^\delta \sqcup \partial\lozenge^\delta$. In the same way we define the sets $\partial\blacklozenge^\delta_{0,1}$, $\partial\lozenge^\delta_{0,1}$, $\partial_{\text{int}}\blacklozenge^\delta_{0,1}$, $\partial_{\text{int}}\lozenge^\delta_{0,1}$, $\operatorname{Int}\blacklozenge^\delta_{0,1}$, $\operatorname{Int}\lozenge^\delta_{0,1}$, $\bar{\blacklozenge}^\delta_{0,1}$ and $\bar{\lozenge}^\delta_{0,1}$.

We say that a discrete domain $\Omega^\delta$ approximates a simply connected domain $\Omega$ if $\Omega^\delta \to \Omega$ in the sense of Carathéodory, see [21, Section 3.2].

Let $F^\delta : \bar{\blacklozenge}^\delta \to \mathbb{C}$ be a function. The following definition is similar to [21, 46, 61]. Let us define discrete operators $\partial^\delta \colon \mathbb{C}^{\blacklozenge^\delta} \to \mathbb{C}^{\lozenge^\delta}$ and $\bar{\partial}^\delta \colon \mathbb{C}^{\blacklozenge^\delta} \to \mathbb{C}^{\lozenge^\delta}$ by the formulas:

$$[\partial^\delta F^\delta](v) = \frac{1}{2}\left(\frac{F^\delta(v+\delta\lambda) - F^\delta(v-\delta\lambda)}{2\delta\lambda} + \frac{F^\delta(v+\delta\bar{\lambda}) - F^\delta(v-\delta\bar{\lambda})}{2\delta\bar{\lambda}}\right),$$

$$[\bar{\partial}^\delta F^\delta](v) = \frac{1}{2}\left(\frac{F^\delta(v+\delta\lambda) - F^\delta(v-\delta\lambda)}{2\delta\bar{\lambda}} + \frac{F^\delta(v+\delta\bar{\lambda}) - F^\delta(v-\delta\bar{\lambda})}{2\delta\lambda}\right),$$

where $v \in \lozenge^\delta$. Note that, If $[\bar{\partial}^\delta F^\delta](v) = 0$, then the two terms involved in the definition of $[\partial F^\delta]$ are equal to each other.

We can similarly define these operators for a function $G^\delta \colon \bar{\lozenge}^\delta \to \mathbb{C}$.

**Definition 1.2.2.** *A function $F^\delta \colon \bar{\blacklozenge}^\delta \to \mathbb{C}$ is called discrete holomorphic in $\Omega^\delta$ if $[\bar{\partial}^\delta F^\delta](v) = 0$ for all $v \in \lozenge^\delta$. Also, we always assume that $F^\delta$ is real on $\bar{\blacklozenge}^\delta_0$ and purely imaginary on $\bar{\blacklozenge}^\delta_1$.*

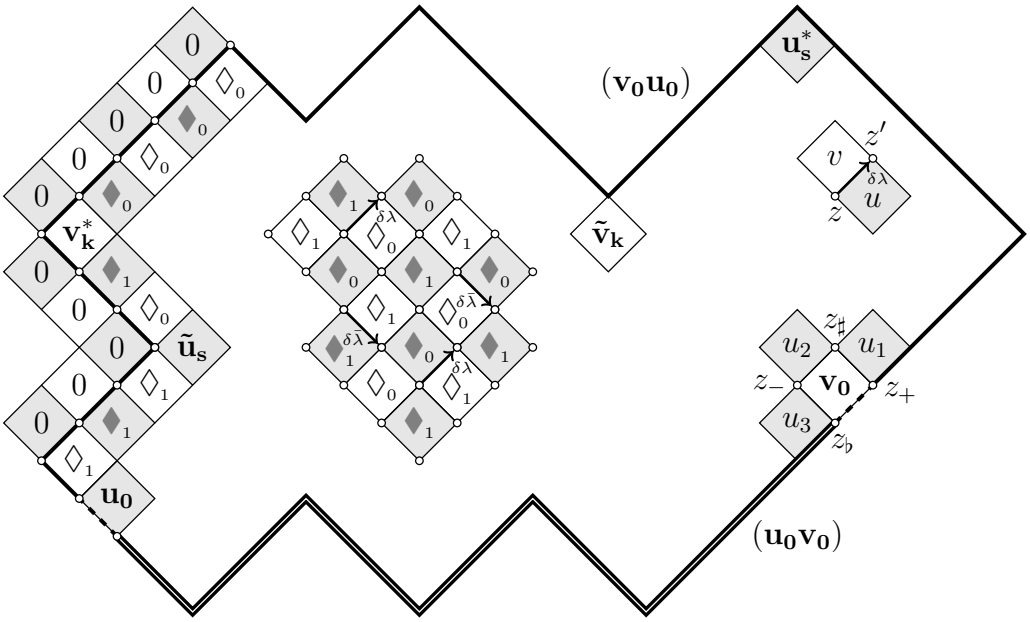


Figure 1.15: The domain $\Omega^\delta$, the sets $\blacklozenge^\delta$ and $\diamondsuit^\delta$ of this domain and the set $\mathcal{V}^\delta$ is the vertex set of $\Omega^\delta$, the squares $u_0 \in \partial_{\text{int}}\blacklozenge_0$ and $v_0 \in \partial_{\text{int}}\diamondsuit_0$, and the elements of the sets of square corners $\{u_s^*\}_{s=1}^{m+1}$, $\{v_k^*\}_{k=1}^{n+1}$, $\{\tilde{u}_s\}_{s=1}^{m-1}$ and $\{\tilde{v}_k\}_{k=1}^{n-1}$. We call a corner of $\Omega^\delta$ a convex corner if the interior angle is $\pi/2$, and concave if the interior angle is $3\pi/2$. A corner is called white if there is a white square in the corner, and black if there is a black square in this corner. The discrete holomorphic function $F^\delta$ is real on $\bar{\blacklozenge}_0^\delta$ and purely imaginary on $\bar{\blacklozenge}_1^\delta$; the discrete holomorphic function $G^\delta$ belongs to $\lambda\mathbb{R}$ on $\bar{\diamondsuit}_0^\delta$ and belongs to $\bar{\lambda}\mathbb{R}$ on $\bar{\diamondsuit}_1^\delta$. The discrete primitive $H^\delta$ is defined on vertices and is purely real: it is easy to check that in all possible positions (according to the types of the squares) the difference of values of function $H^\delta$ at two adjacent vertices is real. For all $u \in \partial\blacklozenge^\delta$, either $\text{Re}[F^\delta(u)] = 0$ or $\text{Im}[F^\delta(u)] = 0$; for all $v \in \partial\diamondsuit^\delta$, either $\text{Re}[\bar{\lambda}G^\delta(v)] = 0$ or $\text{Re}[\lambda G^\delta(v)] = 0$. The function $F^\delta$ (resp., $G^\delta$) changes boundary conditions only at white (resp., black) corners of $\Omega^\delta$. Let $(u_0v_0)$ be a part of the boundary starting at the middle of the boundary side of the square $u_0$ and going to the middle of the boundary side of square $v_0$ in the positive direction. Note that two segments of the boundary $(u_0v_0)$ and $(v_0u_0)$ form the whole boundary. The function $H^\delta$ is a constant on $(u_0v_0)$ and $(v_0u_0)$. The difference of the values on these segments is nonzero: $H^\delta(z_\flat) - H^\delta(z_+) = 4i\delta^2 G^\delta(v_0)[\bar{\partial}^\delta F^\delta](v_0)$.

*A function $G^\delta\colon \bar{\diamondsuit}^\delta \to \mathbb{C}$ is called discrete holomorphic in $\Omega^\delta$ if $[\bar\partial^\delta G^\delta](u) = 0$ for all $u \in \blacklozenge^\delta$.Also, we always assume that $G^\delta$ is belong to $\lambda\mathbb{R}$ (resp., $\bar\lambda\mathbb{R}$) on $\bar{\diamondsuit}_0^\delta$ (resp., on $\bar{\diamondsuit}_1^\delta$).*

**Remark 1.2.3.** *If a function $F^\delta\colon \bar{\blacklozenge}^\delta \to \mathbb{C}$ is discrete holomorphic in $\Omega^\delta$ then the function $[i\cdot\partial^\delta F^\delta]\colon \diamondsuit^\delta \to \mathbb{C}$ is discrete holomorphic in $\Omega^\delta \setminus \partial_{\rm int}\Omega^\delta$. Similarly, if $G^\delta\colon \bar{\diamondsuit}^\delta \to \mathbb{C}$ is discrete holomorphic in $\Omega^\delta$ then $\partial^\delta G^\delta\colon \blacklozenge^\delta \to \mathbb{C}$ is discrete holomorphic in $\Omega^\delta \setminus \partial_{\rm int}\Omega^\delta$.*

Define the discrete Laplacian of $F^\delta$ by

$$\Delta^\delta F^\delta(u) = \frac{F^\delta(u+2\delta\lambda) + F^\delta(u+2\delta\bar\lambda) + F^\delta(u-2\delta\lambda) + F^\delta(u-2\delta\bar\lambda) - 4F^\delta(u)}{4\delta^2},$$

where $u \in \blacklozenge^\delta$. Note that $\Delta^\delta F^\delta(u) = 4[\partial^\delta\bar\partial^\delta F^\delta](u) = 4[\bar\partial^\delta\partial^\delta F^\delta](u)$, the factorisation was noted in [21, 46, 61].

A function $F^\delta\colon \bar{\blacklozenge}^\delta \to \mathbb{C}$ (resp., $G^\delta\colon \bar{\diamondsuit}^\delta \to \mathbb{C}$) is called *discrete harmonic* in $\Omega^\delta$ if it satisfies $\Delta^\delta F^\delta(u) = 0$ for all $u \in \blacklozenge^\delta$ (resp., $\Delta^\delta G^\delta(v) = 0$ for all $v \in \diamondsuit^\delta$).

It is easy to see that discrete harmonic functions satisfy the maximum principle:

$$\max_{u\in\Omega^\delta} F^\delta(u) = \max_{u\in\partial\Omega^\delta} F^\delta(u).$$

Let us divide the set vertex $\mathcal{V}^\delta$ into three sets $\mathcal{V}^\delta_\circ$ , $\mathcal{V}^\delta_\bullet$ and $\mathcal{V}^\delta_\diamond$ as it shown on Fig. 1.15. The notion of s-holomorphicity, which is a version of discrete holomorphicity, was introduced in [77, 78].

**Definition 1.2.4.** A function $F^\delta_{\text{s-hol}}\colon \mathcal{V}^\delta_\diamond \to \mathbb{C}$ is called *s-holomorphic* on $\mathcal{V}^\delta_\diamond$ if for each pair of vertices $z_1, z_2 \in \mathcal{V}^\delta_\diamond$ of the same square $a \in \Omega^\delta$

$$\mathrm{Proj}_{\tau(a)}[F^\delta_{\text{s-hol}}(z_1)] = \mathrm{Proj}_{\tau(a)}[F^\delta_{\text{s-hol}}(z_2)],$$

where $\mathrm{Proj}_{\tau(a)}[z] = \tau(a)\cdot \mathrm{Re}\left[z\cdot\overline{\tau(a)}\right]$ and $\tau(a)$ is 1, $i$, $\lambda$ or $\bar\lambda$ if the square $a$ is a square of type $\blacklozenge^\delta_0$, $\blacklozenge^\delta_1$, $\diamondsuit^\delta_0$ or $\diamondsuit^\delta_1$ correspondingly.

**Remark 1.2.5.** *An s-holomorphic function $F^\delta_{\text{s-hol}}\colon \mathcal{V}^\delta_\diamond \to \mathbb{C}$ can be extended to the faces of $\overline{\Omega}^\delta$. For any $a \in \overline{\Omega}^\delta$*

$$F^\delta_{\text{s-hol}}(a) := \mathrm{Proj}_{\tau(a)}[F^\delta_{\text{s-hol}}(z)],$$

*where $z \in \mathcal{V}^\delta_\diamond$ is a vertex of the square $a$.*

From now onwards, we will think that s-holomorphic functions are defined on the set $\mathcal{V}^\delta_\diamond \sqcup \overline{\Omega}^\delta$ rather than on the set $\mathcal{V}^\delta_\diamond$ only.

**Remark 1.2.6.** *There is a bijection between s-holomorphic functions on $\mathcal{V}^\delta_\diamond \sqcup \overline{\Omega}^\delta$ and holomorphic functions on $\bar{\blacklozenge}^\delta$:*

*1. Let a function $F^\delta_{\text{s-hol}}$ be s-holomorphic. It is easy to check that $\mathrm{Proj}_{\tau(\cdot)}[F^\delta_{\text{s-hol}}]|_{\bar{\blacklozenge}^\delta}$ is holomorphic;*

*2. Let $F^\delta\colon \bar{\blacklozenge}^\delta \to \mathbb{C}$ be a discrete holomorphic function. Let $F^\delta_{\text{s-hol}}$ be a function defined as follows:*

$$\begin{cases} F^\delta_{\text{s-hol}}(u) = F^\delta(u) & \text{if } u \in \blacklozenge^\delta; \\ F^\delta_{\text{s-hol}}(z) = F^\delta(u_{\scriptscriptstyle R}) + F^\delta(u_{\scriptscriptstyle I}) & \text{if } z \in \mathcal{V}^\delta_\diamond; \\ F^\delta_{\text{s-hol}}(v_\lambda) = \frac{\lambda}{\sqrt{2}} \cdot (F^\delta(u_{\scriptscriptstyle R}) - iF^\delta(u_{\scriptscriptstyle I})) & \text{if } v_\lambda \in \diamondsuit^\delta_0; \\ F^\delta_{\text{s-hol}}(v_{\bar\lambda}) = \frac{\bar\lambda}{\sqrt{2}} \cdot (F^\delta(u_{\scriptscriptstyle R}) + iF^\delta(u_{\scriptscriptstyle I})) & \text{if } v_{\bar\lambda} \in \diamondsuit^\delta_1, \end{cases}$$

*where $z \in \mathcal{V}^\delta_\diamond$ and $u_{\scriptscriptstyle I}, v_{\bar\lambda}, u_{\scriptscriptstyle R}, v_\lambda$ are squares of types $\blacklozenge^\delta_1$, $\diamondsuit^\delta_1$, $\blacklozenge^\delta_0$ and $\diamondsuit^\delta_0$ adjacent to the vertex $z$ (see Fig. 2.2). Discrete holomorphicity of $F^\delta$ guarantees that the function $F^\delta_{\text{s-hol}}$ is well defined. Note that*

$$\frac{\lambda}{\sqrt{2}} \cdot (F^\delta(u_{\scriptscriptstyle R}) - iF^\delta(u_{\scriptscriptstyle I})) = \text{Proj}_\lambda[F^\delta(u_{\scriptscriptstyle R}) + F^\delta(u_{\scriptscriptstyle I})],$$

$$\frac{\bar\lambda}{\sqrt{2}} \cdot (F^\delta(u_{\scriptscriptstyle R}) + iF^\delta(u_{\scriptscriptstyle I})) = \text{Proj}_{\bar\lambda}[F^\delta(u_{\scriptscriptstyle R}) + F^\delta(u_{\scriptscriptstyle I})].$$

*Therefore the function $F^\delta_{\text{s-hol}}$ is s-holomorphic on $\mathcal{V}^\delta_\diamond \sqcup \overline{\Omega}^\delta$.*

Let us similarly define an s-holomorphic function $G^\delta_{\text{s-hol}}$:

$$\begin{cases} G^\delta_{\text{s-hol}}(v) = G^\delta(v) & \text{if } v \in \diamondsuit^\delta; \\ G^\delta_{\text{s-hol}}(z) = G^\delta(v_\lambda) + G^\delta(v_{\bar\lambda}) & \text{if } z \in \mathcal{V}^\delta_\diamond; \\ G^\delta_{\text{s-hol}}(u_{\text{R}}) = \frac{1}{\sqrt{2}} \left(\bar\lambda G^\delta(v_\lambda) + \lambda G^\delta(v_{\bar\lambda})\right) & \text{if } u_{\text{R}} \in \blacklozenge^\delta_0; \\ G^\delta_{\text{s-hol}}(u_{\text{I}}) = \frac{i}{\sqrt{2}} \cdot \left(\bar\lambda G^\delta(v_\lambda) - \lambda G^\delta(v_{\bar\lambda})\right) & \text{if } u_{\text{I}} \in \blacklozenge^\delta_1, \end{cases}$$

where $z \in \mathcal{V}^\delta_\diamond$ and $u_{\text{I}}, v_{\bar\lambda}, u_{\text{R}}, v_\lambda$ are squares of types $\blacklozenge^\delta_1$, $\diamondsuit^\delta_1$, $\blacklozenge^\delta_0$ and $\diamondsuit^\delta_0$ adjacent to the vertex $z$.

## 1.3 Dimer model on planar bipartite graphs

In this section we deal with a dimer model on general bipartite planar graphs. We will assume our graphs are always connected. A graph is *nondegenerate* (for the dimer model) if it has dimer covers, and each edge occurs in some dimer cover.

### 1.3.1 Kasteleyn weights

If $\nu : E \to \mathbb{R}_{>0}$ is a positive weight function on edges, we associate a weight $\nu(m) = \prod_{e\in m} \nu(e)$ to a dimer cover which is the product of its edge weights. We can also associate to this data a probability measure $\mu$ on the set $M$ of dimer covers, giving a dimer cover $m$ a probability $\frac{1}{Z}\nu(m)$, where $Z = \sum_{m\in M} \nu(m)$ is a normalizing constant, called the *partition function.*

Two weight functions $\nu_1, \nu_2$ are said to be *gauge equivalent* if there is a function $F : V \to \mathbb{R}$ such that for any edge $vw$, $\nu_1(vw) = F(v)F(w)\nu_2(vw)$. Gauge equivalent weights define the same probability measure $\mu$. For a planar bipartite graph, two weight functions are gauge equivalent if and only if their *face weights* are equal, where the face weight of a face with vertices $w_1, b_1, \ldots, w_k, b_k$ is

$$X = \frac{\nu(w_1b_1)\ldots\nu(w_kb_k)}{\nu(b_1w_2)\ldots\nu(b_kw_1)}. \tag{3.2}$$

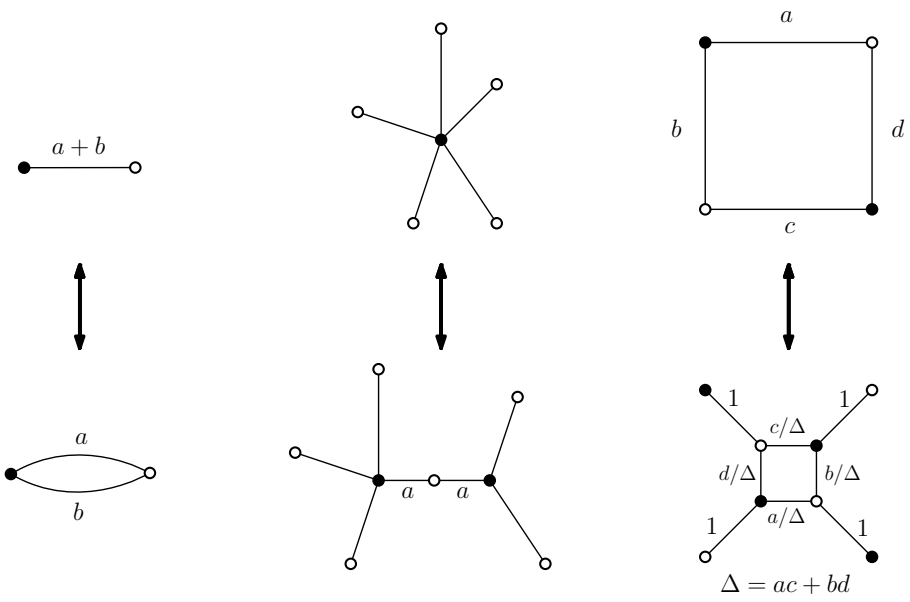


Figure 1.16: Elementary transformations preserving the dimer measure $\mu$. **Left:** Replacing parallel edges with weights $a, b$ by a single edge with weight $a+b$; **center:** contracting a degree 2 vertex whose edge have equal weights; **right:** the spider move, with weights transformed as indicated.

If $\mathcal{G}$ is a planar bipartite graph which has dimer covers, a *Kasteleyn matrix* is a signed, weighted adjacency matrix, with rows indexing the white vertices and columns indexing the black vertices, with $K(w, b) = 0$ if $w$ and $b$ are not adjacent, and $K(w, b) = \pm\nu(w, b)$ otherwise, where the signs are chosen so that the product of signs around a face is $(-1)^{k+1}$ for a face of degree $2k$. Kasteleyn [40] showed that the determinant of a Kasteleyn matrix is the weighted sum of dimer covers:

$$|\det K| = Z = \sum_{m \in M} \nu(m).$$

Different choices of signs satisfying the Kasteleyn condition correspond to multiplying $K$ on the right and/or left by diagonal matrices with $\pm 1$ on the diagonals. Different choices of gauge correspond to multiplying $K$ on the right and left by diagonal matrices with positive diagonal entries (see e.g. [35]). We call two matrices *gauge equivalent* if they are related by these two operations: multiplication on the right and left by diagonal matrices with real nonzero diagonal entries. Note that in terms of any (gauge equivalent) Kasteleyn matrix we can recover the face weights via the formula

$$X = (-1)^{k+1} \frac{K(w_1, b_1) \dots K(w_k, b_k)}{K(w_2, b_1) K(w_3, b_2) \dots K(w_1, b_k)}. \tag{3.3}$$

In some circumstances it is convenient to take complex signs $e^{i\theta}$ in the Kasteleyn matrix, rather than just $\pm 1$; in that case the required condition on the signs is that the quantity $X$ in (3.3) is positive, see [64]. This generalization will be used below.

Certain elementary transformations of $\mathcal{G}$ preserve the measure $\mu$; see Figure 1.16.

### 1.3.2 Height function

A flow, or 1-form, is a function $\omega$ on oriented edges of $\mathcal{G}$ which is antisymmetric under changing orientation: $\omega(e) = -\omega(-e)$. The divergence $\mathrm{div}_\omega$ of a flow $\omega$ is a function on vertices defined by $\mathrm{div}_\omega(v) = \sum_{v' \sim v} \omega(vv')$. Given a divergence-free flow $\tilde{\omega}$ and a fixed face $f_0$, one can define a function $H_{\tilde{\omega}}$ on all faces of $\mathcal{G}$ as follows: $H_{\tilde{\omega}}(f_0) = 0$, and for any other face $f$, $H_{\tilde{\omega}}(f)$ is the net flow crossing (from left to right) a path in the dual graph from $f_0$ to $f$. The fact that the flow is divergence-free means that $H_{\tilde{\omega}}(f)$ does not depend on the path from $f_0$ to $f$.

Given a dimer cover $M$ of a bipartite graph, there is a naturally associated flow $\omega_M$: it has value 1 on each edge covered by a dimer, when the edge is oriented from its white vertex to its black vertex. Other edges have flow 0. This flow has divergence $\mathrm{div}_\omega M = \pm 1$ at white, respectively black vertices.

Let us define the height function for a dimer cover $M$. Fix a flow $\omega_0$ with divergence 1 at white vertices and divergence $-1$ at black vertices (for example, $\omega_0$ might come from a fixed dimer cover). Then the difference $\omega_M - \omega_0$ is a divergence-free flow. Let $H_M := H_{(\omega_M - \omega_0)}$ be the corresponding function on faces of $\mathcal{G}$. Then $H_M$ is the height function of $M$. Note that if $M_1$, $M_2$ are two dimer coverings then $H_{M_1} - H_{M_1}$ does not depend on the choice of $\omega_0$.

For the square lattice a natural choice of $\omega_0$ is the flow with value $1/4$ on each edge (oriented from white to black).

# Chapter 2

# The primitive of the product of two discrete holomorphic functions

## 2.1 The primitive of the product of two discrete holomorphic functions

In this chapter we will define the discrete primitive of the product of two discrete holomorphic functions. This definition is close to the definition of the discrete primitive of the square of the s-holomorphic function [22, 77]. Also, there is a straightforward generalization of this construction on isoradial graphs, see Appendix A.

**Definition 2.1.1.** *Let $F^\delta\colon \bar{\blacklozenge}^\delta \to \mathbb{C}$ and $G^\delta\colon \bar{\lozenge}^\delta \to \mathbb{C}$ be discrete holomorphic functions. Let us define a discrete primitive $H^\delta\colon \mathcal{V}^\delta \to \mathbb{R}$ by the equality*

$$H^\delta(z') - H^\delta(z) = (z' - z)F^\delta(u)G^\delta(v), \tag{1.1}$$

*where $u$, $v$ are adjacent black and white squares (correspondingly); and $z$, $z'$ are their common vertices, see Fig. 1.15.*

**Remark 2.1.2.** *It is easy to see that, if $\Omega^\delta$ is simply connected, then $H^\delta$ is well defined (see Fig. 2.1).*


Figure 2.1: Left: The discrete holomorphic condition $[\bar\partial^\delta F^\delta](v) = 0$ guarantees that $(H^\delta(z_\flat) - H^\delta(z_-)) + (H^\delta(z_+) - H^\delta(z_\flat)) + (H^\delta(z_\sharp) - H^\delta(z_+)) + (H^\delta(z_-) - H^\delta(z_\sharp)) = 0$. Right: The discrete leap-frog Laplacian of $H^\delta$ is defined by (1.2). The function $H^\delta$ has no saddle points: a value at an interior vertex cannot be strictly greater than values at two of its neighbouring vertices and strictly smaller than values at two other neighbouring vertices at the same time.

Let us define the discrete leap-frog Laplacian of $H^\delta$ at $z \in \mathrm{Int}\mathcal{V}^\delta$ by

$$[\Delta^\delta H^\delta](z) = \frac{1}{4\delta^2} \sum_{z'_s \sim z} (H^\delta(z'_s) - H^\delta(z)), \tag{1.2}$$

where $s \in \{1,2,3,4\}$, and $z'_s$ are defined as shown in Fig. 2.1.

**Proposition 2.1.3.** *Let $u_-$, $u_+$, $v_\sharp$, $v_\flat$, $z$ be as shown in Fig. 2.1, then*

$$\begin{aligned}[\Delta^\delta H^\delta](z) = \delta \cdot (&\lambda[\partial^\delta F^\delta](v_\sharp)[\partial^\delta G^\delta](u_-) - \bar\lambda[\partial^\delta F^\delta](v_\sharp)[\partial^\delta G^\delta](u_+) \\ &+\bar\lambda[\partial^\delta F^\delta](v_\flat)[\partial^\delta G^\delta](u_-) - \lambda[\partial^\delta F^\delta](v_\flat)[\partial^\delta G^\delta](u_+)).\end{aligned} \tag{1.3}$$

*Proof.* Note that

$$\begin{aligned}4\delta^2[\Delta^\delta H^\delta](z) =&\delta\lambda[F^\delta(u_-) + 2\delta\lambda[\partial^\delta F^\delta](v_\sharp)] \cdot [G^\delta(v_\flat) + 2\delta\lambda[\partial^\delta G^\delta](u_+)] + \delta\lambda F^\delta(u_+)G^\delta(v_\sharp) \\ &-\delta\bar\lambda[F^\delta(u_+) - 2\delta\bar\lambda[\partial^\delta F^\delta](v_\sharp)] \cdot [G^\delta(v_\flat) - 2\delta\bar\lambda[\partial^\delta G^\delta](u_-)] - \delta\bar\lambda F^\delta(u_-)G^\delta(v_\sharp) \\ &-\delta\lambda[F^\delta(u_+) - 2\delta\lambda[\partial^\delta F^\delta](v_\flat)] \cdot [G^\delta(v_\sharp) - 2\delta\lambda[\partial^\delta G^\delta](u_-)] - \delta\lambda F^\delta(u_-)G^\delta(v_\flat) \\ &+\delta\bar\lambda[F^\delta(u_-) + 2\delta\bar\lambda[\partial^\delta F^\delta](v_\flat)] \cdot [G^\delta(v_\sharp) + 2\delta\bar\lambda[\partial^\delta G^\delta](u_+)] + \delta\bar\lambda F^\delta(u_+)G^\delta(v_\flat).\end{aligned}$$

One can rewrite the above formula in the following form

$$\begin{aligned}&F^\delta(u_-) \cdot \underbrace{[\delta\lambda G^\delta(v_\flat) + 2\delta^2\lambda^2[\partial^\delta G^\delta](u_+) - \delta\bar\lambda G^\delta(v_\sharp) - \delta\lambda G^\delta(v_\flat) + \delta\bar\lambda G^\delta(v_\sharp) + 2\delta^2\bar\lambda^2[\partial^\delta G^\delta](u_+)]}_{=0} \\ &+F^\delta(u_+) \cdot \underbrace{[\delta\lambda G^\delta(v_\sharp) + 2\delta^2\lambda^2[\partial^\delta G^\delta](u_-) - \delta\bar\lambda G^\delta(v_\flat) - \delta\lambda G^\delta(v_\sharp) + \delta\bar\lambda G^\delta(v_\flat) + 2\delta^2\bar\lambda^2[\partial^\delta G^\delta](u_-)]}_{=0} \\ &+G^\delta(v_\flat) \cdot \underbrace{[2\delta^2\bar\lambda^2[\partial^\delta F^\delta](v_\sharp) + 2\delta^2\lambda^2[\partial^\delta F^\delta](v_\sharp)]}_{=0} + G^\delta(v_\sharp) \cdot \underbrace{[2\delta^2\bar\lambda^2[\partial^\delta F^\delta](v_\flat) + 2\delta^2\lambda^2[\partial^\delta F^\delta](v_\flat)]}_{=0} \\ &+4 \cdot [\delta^3\lambda^3[\partial^\delta F^\delta](v_\sharp)[\partial^\delta G^\delta](u_+) - \delta^3\bar\lambda^3[\partial^\delta F^\delta](v_\sharp)[\partial^\delta G^\delta](u_-) \\ &-\delta^3\lambda^3[\partial^\delta F^\delta](v_\flat)[\partial^\delta G^\delta](u_-) + \delta^3\bar\lambda^3[\partial^\delta F^\delta](v_\flat)[\partial^\delta G^\delta](u_+)].\end{aligned}$$

Finally, note that $\bar\lambda^3 = -\lambda$ and $\lambda^3 = -\bar\lambda$. □

**Proposition 2.1.4.** *The function $H^\delta$ has no local maxima or minima. Moreover, a value at an interior vertex cannot be strictly greater than values at two of its neighbouring vertices and strictly smaller than values at two other neighbouring vertices at the same time.*

*Proof.* It is enough to show that the product of all the differences is non-positive (see Fig. 2.1):

$$\begin{aligned}&(H^\delta(z) - H^\delta(z_1)) \cdot (H^\delta(z) - H^\delta(z_2)) \cdot (H^\delta(z) - H^\delta(z_3)) \cdot (H^\delta(z) - H^\delta(z_4)) \\ =&(-\delta\lambda)F^\delta(u_+)G^\delta(v_\sharp) \cdot \delta\bar\lambda G^\delta(v_\sharp)F^\delta(u_-) \cdot \delta\lambda F^\delta(u_-)G^\delta(v_\flat) \cdot (-\delta\bar\lambda)G^\delta(v_\flat)F^\delta(u_+) \\ =&\delta^4 \cdot (F^\delta(u_+) \cdot G^\delta(v_\sharp) \cdot F^\delta(u_-) \cdot G^\delta(v_\flat))^2 \le 0,\end{aligned}$$

since $F^\delta(u_+) \cdot F^\delta(u_-) \in i\mathbb{R}$ and $G^\delta(v_\sharp) \cdot G^\delta(v_\flat) \in \mathbb{R}$. □

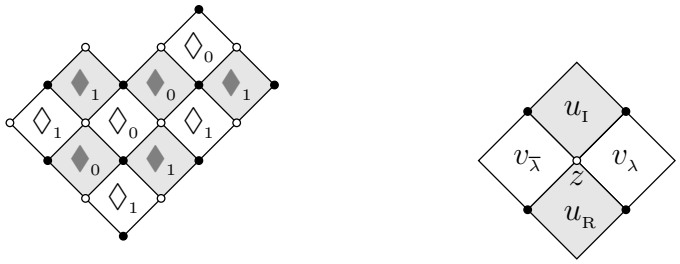


Figure 2.2: Left: the set $\mathcal{V}_\circ$ (white vertices), the set $\mathcal{V}_\bullet$ (black vertices). So, $\mathcal{V} = \mathcal{V}_\circ \sqcup \mathcal{V}_\bullet$. Right: adjacent to the vertex $z \in \mathcal{V}_\circ$ squares $u_{\mathrm{I}}, v_{\overline{\lambda}}, u_{\mathrm{R}}, v_\lambda$. S-holomorphic functions defined on $\mathcal{V}_\circ$ and its projections defined on $\Diamond \sqcup \blacklozenge$.

**Remark 2.1.5.** *1. The function $H^\delta$ satisfies the maximum principle:*

$$\max_{z\in\mathcal{V}^\delta} H^\delta(z) = \max_{z\in\partial\mathcal{V}^\delta} H^\delta(z).$$

*2. Also, it is easy to see that $H^\delta$ satisfies the following non-linear equation:*

$$(H^\delta(z) - H^\delta(z_1)) \cdot (H^\delta(z) - H^\delta(z_3)) + (H^\delta(z) - H^\delta(z_2)) \cdot (H^\delta(z) - H^\delta(z_4)) = 0,$$

*where $z$, $z_1$, $z_2$, $z_3$, $z_4$ are defined as shown in Fig. 2.1.*

It is worth noting that Definition 2.1.1 coincides with the definition of a primitive of the product of two s-holomorphic functions used in [78]. To see this let us divide the vertex set $\mathcal{V}$ into two sets $\mathcal{V}_\circ$ and $\mathcal{V}_\bullet$ as it shown on Fig. 2.2. On the set $\mathcal{V}_\bullet$ the function $H_{\text{s-hol}}$ defined below as a discrete integral of the product of two discrete s-holomorphic functions coincides with the function $H$ defined above.

Let $F_{\text{s-hol}}$ (resp., $G_{\text{s-hol}}$) be s-holomorphic extension (defined as in Remark 1.2.6) of discrete holomorphic function $F\colon \bar{\blacklozenge} \to \mathbb{C}$ (resp., $G\colon \bar{\Diamond} \to \mathbb{C}$) defined above. Let $H_{\text{s-hol}}\colon \mathcal{V}_\bullet \to \mathbb{R}$ be a function defined by the equality

$$H_{\text{s-hol}}(z_2^\bullet) - H_{\text{s-hol}}(z_1^\bullet) = F_{\text{s-hol}}(a) \cdot G_{\text{s-hol}}(a) \cdot (z_2^\bullet - z_1^\bullet),$$

where $z_1^\bullet$, $z_2^\bullet$ are two black vertices of the same square $a$. It is easy to check that

$$H_{\text{s-hol}}(z_2^\bullet) - H_{\text{s-hol}}(z_1^\bullet) = (H(z_2^\bullet) - H(z^\circ)) + (H(z^\circ) - H(z_1^\bullet)),$$

where $z^\circ$ is one of two white vertices of the square $a$. Note that the function $H_{\text{s-hol}}(\cdot)$ is defined up to an additive constant. One can choose the additive constant such that the function $H_{\text{s-hol}}$ coincides with the function $H|_{\mathcal{V}_\bullet}$.

## 2.2 The expectation of the double dimer height function

In the rest of this chapter, we will use the square lattice with mesh size 1 rather than $\delta$. For the simplicity of notations we will not write the index $\delta$. (Later, in section 3.1, we are going to use notations without index for continuous objects.) We prove that the function $H$ defined by formula (1.1) with an appropriate choice of functions $F$ and $G$ described above is the expectation of the height function for double dimers up to a multiplicative constant.

**Lemma 2.2.1.** 1. *Let a domain $\Omega$ admit a domino tiling. Suppose that a discrete holomorphic function $F\colon \bar{\blacklozenge} \to \mathbb{C}$ vanishes on $\partial\blacklozenge$. Then $F$ is identically zero.*

2. *Let $\Omega$ be a domain which contains $m$ white squares and $m+1$ black squares. Let the domain have a domino tiling after removing one black square from $\partial_{\text{int}}\blacklozenge$. Then there exists a nontrivial discrete holomorphic function $F\colon \bar{\blacklozenge} \to \mathbb{C}$, which is equal to zero on $\partial\blacklozenge$. Such a function $F$ is unique up to a multiplicative constant. Moreover $F(u) \neq 0$ for all black squares $u \in \partial_{\text{int}}\blacklozenge$ such that $\Omega \setminus u$ admits a domino tiling.*

*Proof.* 1. Consider a system of linear equations with variables that correspond to values of $F$ in the black faces, and each equation means that the function $F$ is holomorphic in some white face. The number of variables is equal to the number of black faces, and the number of equations is equal to the number of white faces. So we have a linear system with a square matrix, the same linear system as (2.1) but with a vanishing right hand side. To prove that this system has only a trivial solution it is enough to show that the determinant of the matrix is not equal to zero. Note that the absolute value of the determinant is equal to the number of the domino tilings of $\Omega$, since the matrix is the Kasteleyn matrix of $\Omega$. Hence, if the domain has a domino tiling then the determinant is not zero. Therefore $F \equiv 0$.

2. We can consider a system of linear equations in the same way as described above. Note that in this case the number of variables is one more then the number of equations. Hence the system has a non-trivial solution. Let $F$ have the values which correspond to this solution. Let $u'$ be a square in $\partial_{\text{int}}\blacklozenge$ and let the domain $\Omega \setminus u'$ have a domino tiling. Let $F$ be equal to zero at $u'$. Note that the function $F$ satisfies the conditions of the first part of the lemma, therefore $F \equiv 0$ on $\Omega$. We obtain a contradiction with a non-triviality of the solution of our system. Similarly to the proof of the first part of the lemma we can show that there is the unique discrete holomorphic function $F$ such that $F(u') = 1$. □

**Corollary 2.2.2.** *Let a domain $\Omega$ contain the same number of black and white squares, and let $\Omega$ admit a domino tiling. Fix a black square $u_0 \in \partial_{\text{int}}\blacklozenge_0$ and a white square $v_0 \in \partial_{\text{int}}\diamondsuit_0$ such that the domain $\Omega \setminus \{u_0, v_0\}$ admits a domino tiling. Then the following holds:*

1. *There exists the unique function $F\colon \bar{\blacklozenge} \to \mathbb{C}$ such that $F|_{\partial\blacklozenge} = 0$ and $F$ is discrete holomorphic everywhere in $\diamondsuit$ except at the face $v_0$ where one has $[\bar{\partial}F](v_0) = \lambda$. Moreover, $F(u_0) \neq 0$.*

2. *Similarly, there exists the unique function $G : \bar{\diamondsuit} \to \mathbb{C}$ such that $G|_{\partial\diamondsuit} = 0$ and $G$ is discrete holomorphic everywhere in $\blacklozenge$ except at the face $u_0$ where one has $[\bar{\partial}G](u_0) = i$. Moreover, $G(v_0) \neq 0$.*

*Proof.* Due to Lemma 2.2.1 the function $F$ on $\Omega \setminus v_0$ is unique up to a multiplicative constant. Moreover, $F(u_0) \neq 0$ since the domain $\Omega \setminus \{u_0, v_0\}$ admits a domino tiling. Therefore, $[\bar{\partial}F](v_0) \neq 0$ (otherwise $F$ is identically zero due to Lemma 2.2.1). Finally, the condition $[\bar{\partial}F](v_0) = \lambda$ defined the function $F$ uniquely. □

In the setup of Corollary 2.2.2, we construct the function $H$ defined on the vertex set of the domain $\Omega \setminus \{u_0, v_0\}$ as described in Section 2. So, the formula (1.1) holds for all square edges of the domain $\Omega$ except boundary edges of the squares $u_0$, $v_0$. Note that if $u_0$ and $v_0$ are not corner squares of the domain $\Omega$, then the vertex set of the domain $\Omega \setminus \{u_0, v_0\}$ and the vertex set of the domain $\Omega$ are the same. Define $\partial\Omega = (u_0v_0) \cup (v_0u_0)$,

see Fig. 1.15. Note that the product $F \cdot G$ along each boundary square edge equals zero, since $F|_{\partial\blacklozenge} = 0$ and $G|_{\partial\diamondsuit} = 0$. Therefore $H$ is constant on each of boundary segments. Recall that $H$ is defined up to an additive constant, which can be chosen so that $H|_{(v_0u_0)} \equiv 0$.

**Lemma 2.2.3.** *The value of the function $H$ on the boundary segment $(u_0v_0)$ equals*

$$H|_{(u_0v_0)} = 4iG(v_0)[\bar\partial F](v_0) = -4iF(u_0)[\bar\partial G](u_0) \neq 0.$$

*Proof.* Consider the difference between the values of the function $H$ in boundary vertices of the square $v_0$:

$$\begin{aligned}(H(z_\flat) - H(z_+)) &= (H(z_\sharp) - H(z_+)) + (H(z_-) - H(z_\sharp)) + (H(z_\flat) - H(z_-))\\ &= G(v_0)(-\bar\lambda F(u_1) - \lambda F(u_2) + \bar\lambda F(u_3))\\ &= 4iG(v_0)[\bar\partial F](v_0),\end{aligned}$$

where $u_1$, $u_2$, $u_3$, $z_+$, $z_-$, $z_\sharp$, $z_\flat$ and $v_0$ are defined as shown in Fig. 1.15.

The second expression for $H|_{(u_0v_0)}$ can be obtained in a similar way. Finally, $H|_{(u_0v_0)} \neq 0$ since $G(v_0) \neq 0$. □

Recall that we can think about the inverse Kasteleyn matrix $C_\Omega(u, v)$ as a function of two variables $u \in \blacklozenge$ and $v \in \diamondsuit$. If $v \in \diamondsuit_0$, then $C_\Omega(u, v)$ is a discrete holomorphic function of $u$, with a simple pole at $v$:

$$4\bar\lambda\bar\partial[C_\Omega(u, v)](v) = C_\Omega(v + \lambda, v) - C_\Omega(v - \lambda, v) + iC_\Omega(v + \bar\lambda, v) - iC_\Omega(v - \bar\lambda, v) = 1,$$

since the product of the Kasteleyn matrix and the inverse Kasteleyn matrix is equal to the identity matrix.

Let functions $F$ and $G$ be constructed as in Corollary 2.2.2. Let $\Omega' = \Omega \setminus \{u_0, v_0\}$. Recall that $C_{\text{dbl-d},\Omega}(u, v) = C_\Omega(u, v) - C_{\Omega'}(u, v)$.

**Proposition 2.2.4** (factorization of the double-dimer coupling function)**.** *Let $u \in \blacklozenge$ and $v \in \diamondsuit$, then the following identity holds*

$$C_{\text{dbl-d},\Omega}(u, v) = \text{const} \cdot F(u)G(v),$$

*where* $\text{const} = \frac{1}{4G(v_0)}$.

*Proof.* For a fixed $\widetilde v \in \diamondsuit$, consider $C_\Omega(u, \widetilde v) - C_{\Omega'}(u, \widetilde v)$ as a function of $u$. This function is holomorphic at all faces in $\diamondsuit \setminus v_0$. Moreover $\bar\partial[(C_\Omega - C_{\Omega'})(u, \widetilde v)](v_0) \neq 0$, since otherwise the function $C_\Omega(u, \widetilde v) - C_{\Omega'}(u, \widetilde v)$ is discrete holomorphic everywhere in $\Omega$ and vanishes on the boundary and then $C_\Omega(u, \widetilde v) - C_{\Omega'}(u, \widetilde v) \equiv 0$ from Lemma 2.2.1. Hence, for fixed $\widetilde v \in \diamondsuit$ this difference is equal to $F(u)$ up to a multiplicative constant. So,

$$C_\Omega(u, \widetilde v) - C_{\Omega'}(u, \widetilde v) = k_1 \cdot F(u),$$

where $k_1$ depends on $\widetilde v$.

Similarly, for a fixed $\widetilde u \in \blacklozenge$, consider $C_\Omega(\widetilde u, v) - C_{\Omega'}(\widetilde u, v)$ as a function of $v$. We obtain that $C_\Omega(\widetilde u, v) - C_{\Omega'}(\widetilde u, v) = k_2 \cdot \lambda G(v)$, where $k_2$ depends on $\widetilde u$.

Therefore

$$C_\Omega(u,v) - C_{\Omega'}(u,v) = \text{const} \cdot F(u)G(v).$$

Consider $C_\Omega(u,v_0) - C_{\Omega'}(u,v_0)$ as a function of $u$. Note that

$$C_{\Omega'}(u,v_0) \equiv 0.$$

Hence

$$C_\Omega(u,v_0) = \text{const} \cdot F(u)G(v_0).$$

Recall that

$$4\bar{\partial}[C_\Omega(u,v_0)](v_0) = \lambda.$$

Thus, const $= \frac{1}{4G(v_0)}$. □

**Corollary 2.2.5.** *Let $h$ be the height function in the double-dimer model on the vertices of the domain $\Omega$. Then for all $z \in \mathcal{V}$ the following equality holds*

$$\mathbb{E}[h(z)] = H(z) \cdot H|^{-1}_{(u_0v_0)},$$

*where the value $H|_{(u_0v_0)}$ is given in Lemma 2.2.3.*

*Proof.* Let $h_\Omega$ and $h'_\Omega$ be height functions in the dimer model on domains $\Omega$ and $\Omega'$, i.e. $h = h_\Omega - h'_\Omega$. Recall that the probability that there is a domino $[uv]$ in the domino tiling of $\Omega$ is equal to $|C_\Omega(u,v)|$. It is easy to see, that

$$\mathbb{E}[h_\Omega(z_1) - h_\Omega(z_2)] = \tfrac{3}{4} \cdot \mathbb{P}[uv] + (-\tfrac{1}{4}) \cdot (1 - \mathbb{P}[uv]),$$

where $u$, $v$ are adjacent squares; and $z_1$, $z_2$ are their common vertices. Therefore,

$$\mathbb{E}[h_\Omega(z_1) - h_\Omega(z_2)] = \mathbb{P}[uv] - \tfrac{1}{4} = |C_\Omega(u,v)| - \tfrac{1}{4}.$$

Similarly, $\mathbb{E}[h_{\Omega'}(z_1) - h_{\Omega'}(z_2)] = |C_{\Omega'}(u,v)| - \frac{1}{4}$.
So, $\mathbb{E}[h(z_1) - h(z_2)] = |C_\Omega(u,v)| - |C_{\Omega'}(u,v)|$.

Note that for $u_1$, $u_2$, $u_3$, $u_4$ and $v$ defined as shown on Fig. 2.1 the following equality holds:

$$\begin{aligned} 1 &= \mathbb{P}[u_1v] + \mathbb{P}[u_2v] + \mathbb{P}[u_3v] + \mathbb{P}[u_4v] \\ &= |C_\Omega(u_1,v)| + |C_\Omega(u_2,v)| + |C_\Omega(u_3,v)| + |C_\Omega(u_4,v)|. \end{aligned}$$

Moreover,

$$C_\Omega(u_2,v) + iC_\Omega(u_3,v) - C_\Omega(u_4,v) - iC_\Omega(u_1,v) = 1,$$

since the product of the Kasteleyn matrix and the inverse Kasteleyn matrix is equal to the identity matrix. Therefore

$$|C_\Omega(u,v)| - |C_{\Omega'}(u,v)| = \tau(uv) \cdot (C_\Omega(u,v) - C_{\Omega'}(u,v)),$$

where $\tau(uv)$ is the Kasteleyn weight of the edge $(uv)$. To complete the proof it is enough to apply Proposition 2.2.4. □

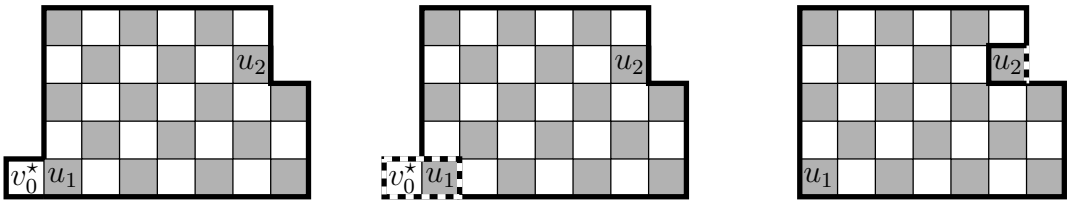


Figure 2.3: Left: $\Omega^\star = \Omega \cup \{v_0^\star\}$. Center: $\Omega_1^\star = \Omega_1 \cup \{v_0^\star, u_1\}$. Note that each domino covering of the domain $\Omega_1^\star$ has domino $[v_0^\star u_1]$. Therefore there is a bijection between the sets of domino coverings of domains $\Omega_1$ and $\Omega_1^\star$. Right: $\Omega_2^\star = \Omega_2$.

## 2.3 Proof of Theorem 1.1.5

We call a discrete domain an *odd Temperleyan domain* if all its corner squares are of type $\blacklozenge_0$. Recall that to obtain a Temperleyan domain one should remove a square of type $\blacklozenge_0$ from the set $\partial_{\text{int}}\blacklozenge$ from an odd Temperleyan domain, see Fig. 1.3. A Temperleyan domain always admits a domino tiling.

We need to adjust the notation from the previous section to this setup. Corollary 2.2.2 is stated for the case of the domain containing the same number of black and white squares. If we consider a discrete domain in which the number of black squares is greater by one than the number of white squares (see Fig. 1.14), then we have some differences in definitions of functions $F$ and $G$. Fix two black squares $u_1, u_2 \in \partial_{\text{int}}\blacklozenge$ in such a way, that after removing one of them the resulting domain admits a domino tiling. Let $u_1 \in \blacklozenge_0$.

1. There exists the unique function $F\colon \bar{\blacklozenge} \to \mathbb{C}$ such that $F|_{\partial\blacklozenge} = 0$, $F(u_1) = 1$ and $F$ is discrete holomorphic everywhere in $\lozenge$.

2. There exists the unique function $G : \bar{\lozenge} \to \mathbb{C}$ such that $G|_{\partial\lozenge} = 0$ and $G$ is discrete holomorphic everywhere in $\blacklozenge$ except at faces $u_1$, $u_2$ and one has $[\bar{\partial}G](u_2) = i$.

The existence and the uniqueness of functions $F$ and $G$ follow from Lemma 2.2.1.

*Proof of Theorem 1.1.5.* Let $\Omega$ be an odd Temperleyan domain. Note that Proposition 2.2.4 and Corollary 2.2.5 are still true in odd case. So, it is enough to show that $H$ is a discrete leap-frog harmonic function. This follows directly from Proposition 2.1.3. In this case $F$ is a discrete holomorphic function at all white squares of $\Omega$. So, its imaginary part is a discrete harmonic function with zero boundary conditions. Therefore $\mathrm{Im}F$ is identically zero, and thus the real part of $F$ is a constant. Hence, $\partial F$ is identically zero. □

Let $v_0^\star$ be a white square on $\partial\Omega$ adjacent to $u_1$. Let us define domains $\Omega^\star$, $\Omega_1^\star$ and $\Omega_2^\star$ as it shown on Fig. 2.3. Let $u_0^\star = u_2$. Then there are unique functions $F^\star$ and $G^\star$ satisfying Corollary 2.2.2 on the domain $\Omega^\star$ with marked squares $v_0^\star$ and $u_0^\star$.

**Remark 2.3.1.** *It is easy to check that the functions $F$ (resp., $G$) defined above equals $F^\star$ (resp., $G^\star$) on $\Omega$. Hence there is no difference between odd and even cases in terms of functions $F$ and $G$.*

# Chapter 3

# Piecewise Temperleyan domains

## 3.1 Double-dimer height function in polygonal domains

From now onwards, we will use the square lattice with mesh size $\delta$ rather than 1. Let $\Omega$ be a polygon in $\mathbb{C}$ with sides parallel to vectors $\lambda$ and $\bar{\lambda}$. For each sufficiently small $\delta > 0$, let $\Omega^\delta$ be a discrete polygon approximating $\Omega$ on the square lattice with mesh size $\delta$.

Let us define functions $F^\delta$ and $G^\delta$ similarly to the previous section:

1. The function $F^\delta$ is discrete holomorphic everywhere in $\diamondsuit^\delta$ except at the face $v_0^\delta$ where one has $[\bar{\partial}^\delta F^\delta](v_0^\delta) = \frac{\lambda}{\delta^2}$.

2. Similarly, the function $G^\delta$ is discrete holomorphic everywhere in $\blacklozenge^\delta$ except at the face $u_0^\delta$ where one has $[\bar{\partial}^\delta G^\delta](u_0^\delta) = \frac{i}{\delta^2}$.

Our goal is to prove the convergence of the functions $H^\delta$ defined by the formula (1.1). Recall that this definition can be thought of as "$H^\delta = \int^\delta \mathrm{Re}[F^\delta G^\delta dz]$". We will prove that the functions $F^\delta$ and $G^\delta$ converge individually.

To prove the convergence of the functions $F^\delta$ we will consider approximations by domains $\Omega^\delta$ with fixed colour type of the corners. We will describe this classification below. The limits of the functions $F^\delta$ and $G^\delta$ depend on the type of the corners. At the same time the limit of the functions $H^\delta$ does not depend on the type of the corners.

We will call a corner of $\Omega^\delta$ a *convex* corner if the interior angle is $\pi/2$, and *concave* if the interior angle is $3\pi/2$. A corner is called *white* if there is a white square in the corner, and *black* if there is a black square in this corner, see Fig. 1.15.

**Lemma 3.1.1.** *If a simply connected domain $\Omega^\delta$ contains the same number of black and white squares then*

$$\#\{\textit{white convex corners}\} = \#\{\textit{white concave corners}\} + 2,$$

$$\#\{\textit{black convex corners}\} = \#\{\textit{black concave corners}\} + 2.$$

*Proof.* Note that $\pi\cdot(\#\{\textit{corners}\}-2) = \frac{\pi}{2}\cdot\#\{\textit{convex corners}\}+\frac{3\pi}{2}\cdot\#\{\textit{concave corners}\}$, hence

$$\#\{\textit{convex corners}\} = \#\{\textit{concave corners}\} + 4.$$

Recall that the height along the boundary changes by $\pm\frac{1}{4}$: if an edge has a black square on its left then the height increases by $\frac{1}{4}$; if it has a white square on its left then

the height decreases by $\frac{1}{4}$. Along each straight segment of the boundary of the domain the height function varies between two values. This pair increases (resp., decreases) by $\frac{1}{4}$ if the boundary turns left along black (resp., white) convex square, and decreases (resp., increases) by $\frac{1}{4}$ if it turns right along black (resp., white) concave square. Then

$$\#\{\textit{white convex corners}\} + \#\{\textit{black concave corners}\} = \\ \#\{\textit{white concave corners}\} + \#\{\textit{black convex corners}\},$$

since the height function on the boundary is well defined if the domain contains the same number of black and white squares (this is easily proved by induction on the number of black squares, starting from the case of a $2 \times 1$ rectangle). □

Let $\Omega^\delta$ admit a domino tiling. Let $u_0^\delta$ and $v_0^\delta$ be black and white squares in $\partial_{\text{int}}\Omega^\delta$ placed away from the corners of $\Omega^\delta$ in such a way that the domain $\Omega^\delta \setminus \{u_0^\delta, v_0^\delta\}$ admits a domino tiling. Let $\{\tilde{v}_k^\delta\}_{k=1}^{n-1}$ be the set of white squares located in the concave white corners of the domain $\Omega^\delta$, and let $\{v_k^{*\delta}\}_{k=1}^{n+1}$ be the set of white squares located in the convex white corners of the domain $\Omega^\delta$, see Fig. 1.15. Recall that the cardinality of the latter set is greater by two than the cardinality of the former due to Lemma 3.1.1. Similarly, let $\{\tilde{u}_s^\delta\}_{s=1}^{m-1}$ be the set of black squares located in the concave black corners of the domain $\Omega^\delta$, and let $\{u_s^{*\delta}\}_{s=1}^{m+1}$ be the set of black squares located in the convex black corners of the domain $\Omega^\delta$ (see Fig. 1.15).

### 3.1.1 Discrete boundary value problem for the functions $F$ and $G$

Note that for all $u^\delta \in \partial\blacklozenge^\delta$ one has $F^\delta(u^\delta) = 0$, which can be thought of as a zero Dirichlet boundary conditions either for $\mathrm{Re}[F^\delta]$ or for $\mathrm{Im}[F^\delta]$. Similarly, for all $v^\delta \in \partial\diamondsuit^\delta$, either $\mathrm{Re}[\bar{\lambda}G^\delta]$ or $\mathrm{Re}[\lambda G^\delta]$ has zero Dirichlet boundary conditions.

**Remark 3.1.2.** *The function $F^\delta$ (resp., $G^\delta$) changes boundary conditions only at white (resp., black) corners of $\Omega^\delta$.*

A function on a discrete domain $\Omega^\delta$ is called *semibounded by its boundary values* in a subdomain $U^\delta \subset \Omega^\delta$ if either the maximum or the minimum of this function in $U^\delta$ is attained on the boundary of $U^\delta$. A function on a discrete domain $\Omega^\delta$ is called *bounded by its boundary values* in a subdomain $U^\delta \subset \Omega^\delta$ if both, the maximum and the minimum of this function in $U^\delta$, are attained on $\partial U^\delta$.

**Lemma 3.1.3.** *The function $F^\delta|_{\blacklozenge_0^\delta}$ is bounded by its boundary values in neighbourhoods of white convex corners and semibounded by its boundary values in neighbourhoods of white concave corners.*

*Proof.* Note that the function $F^\delta|_{\blacklozenge_0^\delta}$ is discrete harmonic in $\blacklozenge_0^\delta$, except at the squares of type $\blacklozenge_0^\delta$ adjacent to $\{\tilde{v}_k^\delta\}$ and $v_0^\delta$, where $\{\tilde{v}_k^\delta\}$ is the set of white squares in the white concave corners. In particular, the function $F^\delta$ is bounded by its boundary values in vicinities of white convex corners $\{v_k^{*\delta}\}$, see Fig. 3.1.

Let us consider a neighbourhood of a corner $\tilde{v}_k^\delta$. Note that in this neighbourhood the function $F^\delta|_{\blacklozenge_0^\delta}$ is discrete harmonic everywhere except at the unique black square of type $\blacklozenge_0^\delta$ adjacent to $\tilde{v}_k^\delta$. Note that at this square either the maximum or the minimum of $F^\delta$ can be reached, thus $F^\delta|_{\blacklozenge_0^\delta}$ is semi-bounded near $\tilde{v}_k^\delta$. □

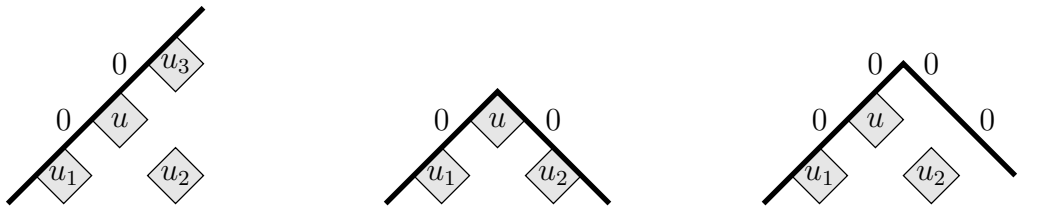


$F^\delta(u) = \frac{F^\delta(u_1)+F^\delta(u_2)+F^\delta(u_3)}{3}$ $\quad$ $F^\delta(u) = \frac{F^\delta(u_1)+F^\delta(u_2)}{2}$ $\quad$ $F^\delta(u) = \frac{F^\delta(u_1)+F^\delta(u_2)}{3}$

Figure 3.1: Discrete harmonicity of the function $F^\delta$ together with the boundary conditions implies the following equations for $u \in \partial_{\text{int}}\Omega^\delta$, see also Fig. 1.11.

### 3.1.2 The continuous analogue of the functions $F^\delta$ and $G^\delta$

In this section we will describe the continuous analogue of the functions $F^\delta$ and $G^\delta$. Also, we will show that the primitive of their product is the harmonic measure.

**Proposition 3.1.4.** *Let $\Omega$ be a simply connected Jordan domain. Let $v_0$ be a boundary point which lies on a straight segment of the boundary of $\Omega$, and this segment goes to the direction $\lambda$. Let $\{v_k^*\}_{k=1}^{n+1} \cup \{\tilde{v}_k\}_{k=1}^{n-1}$ be a set of marked points on $\partial\Omega \setminus \{v_0\}$. Then there exists the unique holomorphic function $f_\Omega$ on $\Omega$ such that:*

- ▷ *$f_\Omega(z) = \frac{\lambda}{z-v_0} + O(1)$ in a vicinity of the point $v_0$;*
- ▷ *$f_\Omega$ is bounded in vicinities of the points $v_k^*$;*
- ▷ *$f_\Omega$ is semi-bounded (either from above or from below) in vicinities of the points $\tilde{v}_k$;*
- ▷ *along each boundary arc between marked points $\{v_k^*\}_{k=1}^{n+1} \cup \{\tilde{v}_k\}_{k=1}^{n-1}$, one has either $\operatorname{Re}[f_\Omega] = 0$ or $\operatorname{Im}[f_\Omega] = 0$;*
- ▷ *aforementioned boundary conditions change at all marked points $\tilde{v}_k$ and $v_s^*$.*

*Proof.* Let $\phi$ be a conformal mapping of the domain $\Omega$ onto the upper half plane $\mathbb{H}$ such that none of the marked points and $v_0$ is mapped onto infinity. Then $f_\mathbb{H} := f_\Omega \circ \phi^{-1}$ is a holomorphic function on $\mathbb{H}$, which satisfies the following conditions:

1. $f_\mathbb{H}(w) = \frac{\lambda\cdot\phi'(v_0)}{w-\phi(v_0)} + O(1)$ in a vicinity of the point $\phi(v_0)$;
2. $f_\mathbb{H}$ is bounded in vicinities of the points $\phi(v_k^*)$;
3. $f_\mathbb{H}$ is semi-bounded (either from above or from below) in vicinities of the points $\phi(\tilde{v}_k)$;
4. $f_\mathbb{H}$ is bounded at infinity;
5. on each segment of the real line between the points of the set $\{\phi(\tilde{v}_k)\}_{k=1}^{n-1} \cup \{\phi(v_k^*)\}_{k=1}^{n+1}$ one has either $\operatorname{Re}[f_\mathbb{H}] = 0$ or $\operatorname{Im}[f_\mathbb{H}] = 0$;

6. the function $f_{\mathbb{H}}$ changes the boundary conditions at all points $\phi(\tilde{v}_k)$ and $\phi(v_k^*)$, and only at these points.

For a given $k$ let us add a constant to $\phi$ so that $\phi(\tilde{v}_k) = 0$. Let us consider a function $f_{\mathbb{H}}(w^2)$ in a vicinity of zero. The boundary conditions (5), (6) of the function $f_{\mathbb{H}}(w^2)$ allow one to extend this function to a punctured vicinity of 0 by the Schwarz reflection principle.

Let us show that $f_{\mathbb{H}}(w^2) = O(1/w)$ as $w \to 0$. Great Picard's Theorem together with the semi-boundedness condition (3) implies that $f_{\mathbb{H}}(w^2)$ cannot have an essential singularity at zero. So, the function $f_{\mathbb{H}}(w^2)$ either is regular or has a pole at zero. This pole must be simple due to (3), and hence $f_{\mathbb{H}}(w) = O\big((w - \phi(\tilde{v}_k))^{-\frac{1}{2}}\big)$ in a vicinity of $\tilde{v}_k$.

Similarly, conditions (2), (5) and (6) imply that $f_{\mathbb{H}}(w) = O\big((w-\phi(v_k^*))^{\frac{1}{2}}\big)$ in a vicinity of each of the points $v_k^*$

Consider a function

$$f_{\mathbb{H}}(w) \cdot (w - \phi(v_0)) \cdot \prod_{k=1}^{n-1} (w - \phi(\tilde{v}_k))^{\frac{1}{2}} \cdot \prod_{k=1}^{n+1} (w - \phi(v_k^*))^{-\frac{1}{2}},$$

which can be extended to a bounded function in the whole plane by the Schwarz reflection principle. Hence it is a constant, and

$$f_{\mathbb{H}}(w) = \frac{c_\phi}{w - \phi(v_0)} \cdot \prod_{k=1}^{n+1} (w - \phi(v_k^*))^{\frac{1}{2}} \cdot \prod_{k=1}^{n-1} (w - \phi(\tilde{v}_k))^{-\frac{1}{2}},$$

where the real constant $c_\phi$ can be determined from the condition (1).

Since $f_{\mathbb{H}} = f \circ \phi^{-1}$, we obtain

$$f_\Omega(z) = \frac{c_\phi}{(\phi(z) - \phi(v_0))} \cdot \prod_{k=1}^{n+1} (\phi(z) - \phi(v_k^*))^{\frac{1}{2}} \cdot \prod_{k=1}^{n-1} (\phi(z) - \phi(\tilde{v}_k))^{-\frac{1}{2}}, \tag{1.1}$$

where $c_\phi$ is a real constant that depends on $\phi$. □

**Remark 3.1.5.** *The previous proposition also holds if $v_0$ is an inner point of $\Omega$. In this case*

$$f_\Omega(z) = c_\phi \cdot \left( \frac{1}{\phi(z) - \phi(v_0)} - \frac{1}{\phi(z) - \overline{\phi(v_0)}} \right) \cdot \prod_{k=1}^{n+1} (\phi(z) - \phi(v_k^*))^{\frac{1}{2}} \cdot \prod_{k=1}^{n-1} (\phi(z) - \phi(\tilde{v}_k))^{-\frac{1}{2}}.$$

Similarly, for the set of boundary points $\{\tilde{u}_k\}_{s=1}^{m-1} \cup \{u_k^*\}_{s=1}^{m+1}$ and the point $u_0$ on a straight segment of the boundary of $\Omega$ parallel to vector $\overline{\lambda}$, there exists the unique holomorphic function $g$, which satisfies conditions analogous to conditions from Proposition 3.1.4:

- ▷ $g_\Omega(z) = \frac{i}{z-u_0} + O(1)$ in a vicinity of the point $u_0$;
- ▷ $g_\Omega$ is bounded in vicinities of the points $u_k^*$;
- ▷ $g_\Omega$ is semi-bounded in vicinities of the points $\tilde{u}_k$;

- ▷ along each boundary segment between boundary points of the set $\{u_k^*\}_{k=1}^{m+1} \cup \{\tilde{u}_k\}_{k=1}^{m-1}$, one has either $\mathrm{Re}[\bar{\lambda} g_\Omega] = 0$ or $\mathrm{Re}[\lambda g_\Omega] = 0$;
- ▷ aforementioned boundary conditions of the function $g_\Omega$ change at all points $\tilde{u}_k$ and $u_s^*$.

This function is written as follows

$$g_\Omega(z) = \frac{\lambda \widetilde{c_\phi}}{(\phi(z) - \phi(u_0))} \cdot \prod_{k=1}^{m+1} (\phi(z) - \phi(u_k^*))^{\frac{1}{2}} \cdot \prod_{k=1}^{m-1} (\phi(z) - \phi(\tilde{u}_k))^{-\frac{1}{2}}, \tag{1.2}$$

where $\widetilde{c_\phi}$ is a real constant that depends on $\phi$.

It is worth noting that the product of the functions $f_\Omega(z)$ and $g_\Omega(z)$ defined by (1.1) and (1.2) , respectively, does not depend on the colours of corners of $\Omega$ (while each of $f_\Omega(z)$, $g_\Omega(z)$ does depend on these colours).

**Proposition 3.1.6.** *Let $\Omega$ be a polygon in $\mathbb{C}$ with sides parallel to vectors $\lambda$ and $\bar{\lambda}$. Let $v_0$ and $u_0$ be the points on the straight part of the boundary of the polygon $\Omega$. Let $\{v_k^*\}_{k=1}^{n+1} \cup \{u_s^*\}_{s=1}^{m+1}$ be the set of vertices of the convex corners of the polygon $\Omega$, and $\{\tilde{v}_k\}_{k=1}^{n-1} \cup \{\tilde{u}_s\}_{s=1}^{m-1}$ be the set of vertices of the concave corners of the polygon $\Omega$. Assume that the boundary arc $(u_0 v_0)$ contains* 0.

*Let functions $f_\Omega$ and $g_\Omega$ be defined as in Proposition* 3.1.4*, then the function*

$$\int_0^w \mathrm{Re}[f_\Omega(z) g_\Omega(z) dz]$$

*is proportional to the harmonic measure* $\mathrm{hm}_\Omega(w, (v_0 u_0))$ *in the domain $\Omega$.*

*Proof.* Let us consider the product of functions $f_\Omega(z)$ and $g_\Omega(z)$. It equals

$$f_\Omega(z) \cdot g_\Omega(z) = \frac{\lambda c_\phi \widetilde{c_\phi}}{(\phi(z) - \phi(v_0)) \cdot (\phi(z) - \phi(u_0))} \times$$
$$\prod_{k=1}^{n+1} (\phi(z) - \phi(v_k^*))^{\frac{1}{2}} \cdot \prod_{k=1}^{n-1} (\phi(z) - \phi(\tilde{v}_k))^{-\frac{1}{2}} \cdot \prod_{k=1}^{m+1} (\phi(z) - \phi(u_k^*))^{\frac{1}{2}} \cdot \prod_{k=1}^{m-1} (\phi(z) - \phi(\tilde{u}_k))^{-\frac{1}{2}}.$$

Let $\psi(w)$ be a conformal transformation of the upper half-plane onto the interior of a simple polygon $\Omega$, the inverse mapping to $\phi$. The Schwarz–Christoffel mapping theorem implies that

$$\psi'(w) = \lambda c_\psi \cdot \prod_{k=1}^{n-1} (w - \phi(\tilde{v}_k))^{\frac{1}{2}} \cdot \prod_{k=1}^{m-1} (w - \phi(\tilde{u}_k))^{\frac{1}{2}} \cdot \prod_{k=1}^{n+1} (w - \phi(v_k^*))^{-\frac{1}{2}} \cdot \prod_{k=1}^{m+1} (w - \phi(u_k^*))^{-\frac{1}{2}},$$

where $c_\psi$ is a real constant.

Note that $\phi$ is the inverse mapping to $\psi$, so $\frac{1}{\psi'(\phi(z))} = \phi'(z)$.

Therefore

$$f(z) \cdot g(z) = \frac{\lambda c_\phi \widetilde{c_\phi} \lambda c_\psi \cdot \phi'(z)}{(\phi(z) - \phi(v_0))(\phi(z) - \phi(u_0))} = \frac{i c_\phi \widetilde{c_\phi} c_\psi}{\phi(v_0) - \phi(u_0)} \cdot \left( \log \frac{(\phi(z) - \phi(v_0))}{(\phi(z) - \phi(u_0))} \right)',$$

hence $\int \mathrm{Re}[f g dz]$ is proportional to $\frac{1}{\pi} \mathrm{Im} \log \left( \frac{(\phi(z) - \phi(v_0))}{(\phi(z) - \phi(u_0))} \right)$ which is the harmonic measure of $(v_0 u_0)$. □

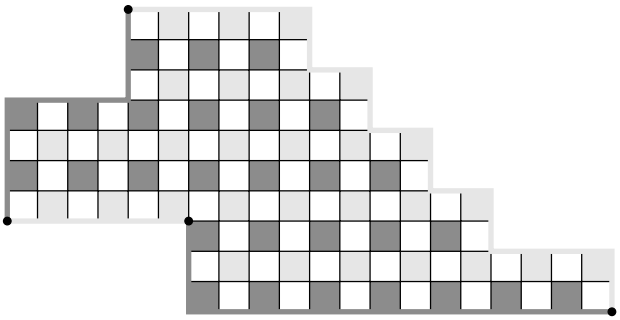

Figure 3.2: A 4-black-piecewise Temperleyan domain.

Now to complete the proof of Theorem 1.1.6 it is enough to prove convergence of functions $F^\delta$ and $G^\delta$. In Section 3.2 we will prove a more general result: the convergence of $F^\delta$ for approximations by black-piecewise Temperleyan domains. This special type of discrete domains is defined below in Section 3.2.1. Similarly, one can show the convergence of $G^\delta$ for approximations by white-piecewise Temperleyan domains. In the setup of Proposition 3.1.6 the polygonal approximations $\Omega^\delta$ are $2n$-black-piecewise Temperleyan and $2m$-white-piecewise Temperleyan domains at the same time.

## 3.2 Convergence of $F^\delta$ in black-piecewise Temperleyan domains

### 3.2.1 Black-piecewise Temperleyan domains

Let us fix a natural number $n$. A discrete domain is called a *$2n$-black-piecewise Temperleyan domain* if it is a domain with $n+1$ convex white corners and $n-1$ concave white corners. Consider a segment of the boundary between two neighbouring white corners; we will call such a segment a *black Temperleyan segment*. Note that all black squares on this part of the boundary are of the same type: either they all are of type $\blacklozenge_0^\delta$ or all of type $\blacklozenge_1^\delta$ (see Fig. 3.2).

Let $\Omega$ be a bounded, simply connected Jordan domain with a piecewise-smooth boundary and $2n$ boundary marked points $v_1^*, \dots, v_{n+1}^*, \tilde{v}_1, \dots, \tilde{v}_{n-1}$. For sufficiently small $\delta$,we say that a $2n$-black-piecewise Temperleyan domain $\Omega^\delta$ approximates $\Omega$ if the boundaries of the $2n$-black-piecewise Temperleyan domain are within $O(\delta)$ of the boundaries of $\Omega$, and if furthermore, all convex white corners $v_k^{*\delta}$ are within $O(\delta)$ of the set of marked points $v_k^*$ and all concave white corners $\tilde{v}_j^\delta$ are within $O(\delta)$ of the set of marked points $\tilde{v}_j$.

### 3.2.2 Proof of the convergence

Let $u^\delta$ be a square on the square lattice with mesh size $\delta$. By $B_r^\delta(u^\delta)$ we denote the set of squares on this lattice such that the distance from them to $u^\delta$ is less then or equal to $r$. Let $\partial B_r^\delta(u^\delta)$ be the set of boundary squares of the set $B_r^\delta(u^\delta)$.

Consider a discrete domain $\Omega^\delta$. Let $E^\delta$ be a subset of the set $\partial\Omega^\delta$. Let $\mathrm{hm}_{\Omega^\delta}(x^\delta, E^\delta)$ be a discrete harmonic function in $\Omega^\delta$ such that it is equal to $\chi_{E^\delta}$ on the boundary of $\Omega^\delta$, where $\chi_{E^\delta}$ is the characteristic function of the set $E^\delta$. The function $\mathrm{hm}_{\Omega^\delta}(x^\delta, E^\delta)$ is called the harmonic measure. Note that the harmonic measure is a probabilistic measure for any fixed $x^\delta \in \Omega^\delta$. Note also that the value of $\mathrm{hm}_{\Omega^\delta}(x^\delta, E^\delta)$ equals to the probability that a simple random walk starting at $x$ first hits the boundary of the domain $\Omega^\delta$ on the

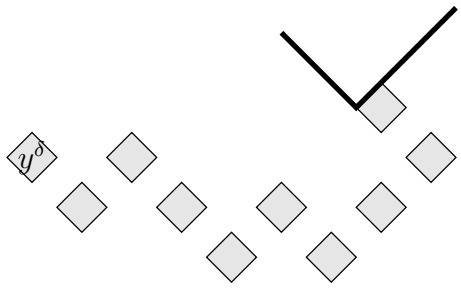


Figure 3.3: A path on the set $\blacklozenge_0^\delta$ from the square $y^\delta$ to the square adjacent to $\tilde{v}_k^\delta$.

set $E^\delta$.

Let $F^\delta_{\mathrm{harm}}$ be a discrete harmonic function in $\Omega^\delta$ defined on the set $\Omega^\delta \cup \partial\Omega^\delta$. Then it is easy to see that

$$F^\delta_{\mathrm{harm}}(x^\delta) = \sum_{y^\delta \in \partial\Omega^\delta} F^\delta_{\mathrm{harm}}(y^\delta) \cdot \mathrm{hm}_{\Omega^\delta}(x^\delta, \{y^\delta\}).$$

**Remark 3.2.1.** *From now on we assume that $\delta > 0$ and $r > 0$ are chosen so that the discrete punctured vicinity $B^\delta_r(\tilde{v}^\delta_k) \setminus \{\tilde{v}^\delta_k\}$ contains neither $v^\delta_0$ nor white corner squares of $\Omega^\delta$ for all $k \in \{1, \dots, n-1\}$.*

**Lemma 3.2.2.** *Let $x^\delta$ be a black square in the middle of one of the arcs of the set $\partial B^\delta_r(\tilde{v}^\delta_k) \cap \blacklozenge^\delta_0$. Let $y^\delta \in \blacklozenge^\delta_0$ be a black square on the boundary of $B^\delta_{r/2}(\tilde{v}^\delta_k)$. Let $\gamma^\delta$ be a path on the set $\blacklozenge^\delta_0$ starting in $y^\delta$ and ending at the black square of $\blacklozenge^\delta_0$ adjacent to $\tilde{v}^\delta_k$ (see Fig. 3.3). Let $\mathrm{hm}^\delta(x^\delta, \gamma^\delta)$ be the harmonic measure on $B^\delta_{2r}(\tilde{v}^\delta_k) \cap \blacklozenge^\delta_0 \setminus \gamma^\delta$. Then there exists a constant $\widetilde{c} > 0$ that does not depend on $\delta$ such that for all $y^\delta \in \blacklozenge^\delta_0 \cap \partial B^\delta_{r/2}$, one has*

$$\mathrm{hm}^\delta(x^\delta, \gamma^\delta) \geq \widetilde{c} = \widetilde{c}\,(\Omega) > 0.$$

For a more general statement see [21, Lemma 3.14].

*Proof.* Let us consider two gray discrete domains of width $\frac{r}{l}$, where $l$ is a large enough positive number, see Fig. 3.4. Let these domains contain $x^\delta$ and cross the boundary of $\Omega^\delta$. The probability that a random walk on a square lattice with mesh size $2\delta$ travels all the way from $x^\delta$ to the boundary of $\Omega^\delta$ inside the gray domain is uniformly bounded away from zero [21, Fig. 3B], for each of the two domains.

Note that the path $\gamma^\delta$ necessarily intersects at least one of the gray domains. The probability of the event that a random walk travels all the way from $x^\delta$ to the boundary of $\Omega^\delta$ inside this gray domain is less then $\mathrm{hm}^\delta(x^\delta, \gamma^\delta)$. □

**Lemma 3.2.3.** *Let $M^\delta_t(r) = \max\limits_{u^\delta \in \Omega^\delta_{r,t}} |F^\delta(u^\delta)|$, where*

$$\Omega^\delta_{r,t} = \Omega^\delta \setminus \left( \bigcup_{k=1}^{n-1} B^\delta_r(\tilde{v}^\delta_k) \cup B^\delta_t(v^\delta_0) \right).$$

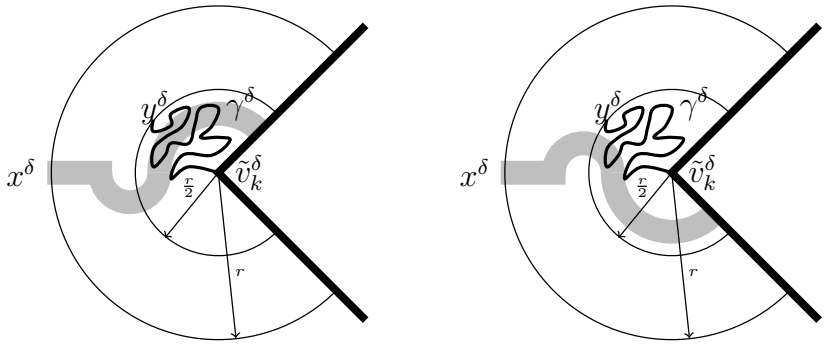


Figure 3.4: The probability that a random walk on a square lattice with mesh size $2\delta$ travels all the way from $x^\delta$ to the boundary of $\Omega^\delta$ inside the gray domain is bounded away from zero uniformly in $\delta$.

*Then for some fixed $t > 0$ small enough and for any sufficiently small fixed $r > 0$, as $\delta \to 0$ we have*

$$M_t^\delta\left(\frac{r}{2}\right) \le \frac{4}{\widetilde{c}} \cdot M_t^\delta(r),$$

*where $\widetilde{c}$ is the absolute constant from Lemma* 3.2.2.

*Proof.* Note that it is enough to prove that

$$\max_{u^\delta \in \Omega^\delta \cap \partial B^\delta_{r/2}(\tilde{v}_k^\delta)} |\mathrm{Re} F^\delta(u^\delta)| \le \frac{2}{\widetilde{c}} \cdot M_t^\delta(r),$$

for all $k \in \{1, \dots, n-1\}$, since similarly the same inequality holds for $\mathrm{Im} F^\delta$.

Let $y^\delta$ be the square in $\Omega^\delta \cap \partial B^\delta_{r/2}(\tilde{v}_k^\delta)$ such that

$$|\mathrm{Re} F^\delta(y^\delta)| = \max_{u^\delta \in \Omega^\delta \cap \partial B^\delta_{r/2}(\tilde{v}_k^\delta)} |\mathrm{Re} F^\delta(u^\delta)|.$$

Without loss of generality we may assume that $\mathrm{Re} F^\delta(y^\delta) > 0$. Note that $\mathrm{Re} F^\delta$ is a discrete harmonic function, and hence there exists a path $\gamma^\delta$ on the set $\blacklozenge_0^\delta$ from $y^\delta$ to the boundary of the domain $\Omega^\delta \cap B_r^\delta(\tilde{v}_k^\delta)$ or to the square adjacent to $\tilde{v}_k^\delta$ along which the absolute value of the function $\mathrm{Re} F^\delta$ increases, since discrete harmonic functions satisfy the maximum principle. If the path $\gamma^\delta$ ends on the boundary of the domain $\Omega^\delta \cap B_r^\delta(\tilde{v}_k^\delta)$, then

$$\max_{u^\delta \in \Omega^\delta \cap \partial B^\delta_{r/2}(\tilde{v}_k^\delta)} |\mathrm{Re} F^\delta(u^\delta)| \le \max_{u^\delta \in \Omega^\delta \cap \partial B^\delta_{r}(\tilde{v}_k^\delta)} |\mathrm{Re} F^\delta(u^\delta)|.$$

Assume that $\gamma^\delta$ ends at the square adjacent to $\tilde{v}_k^\delta$. Let $\mathrm{hm}^\delta(\cdot, \gamma^\delta)$ be the harmonic measure in the domain $B^\delta_{2r}(\tilde{v}_k^\delta) \cap \blacklozenge_0^\delta \setminus \gamma^\delta$. Due to Lemma 3.2.2 there exists a black square $x^\delta \in \blacklozenge_0^\delta$ on the boundary of $B_r^\delta(\tilde{v}_k^\delta)$ such that $\mathrm{hm}^\delta(x^\delta, \gamma^\delta) \ge \widetilde{c} > 0$. Note that

$$M_t^\delta(r) \ge \mathrm{Re} F^\delta(x^\delta) \ge \mathrm{Re} F^\delta(y^\delta) \cdot \mathrm{hm}^\delta(x^\delta, \gamma^\delta) - M_t^\delta(r) \cdot (1 - \mathrm{hm}^\delta(x^\delta, \gamma^\delta)).$$

Hence,

$$2M_t^\delta(r) \ge \mathrm{hm}^\delta(x^\delta, \gamma^\delta) \cdot \mathrm{Re} F^\delta(y) \ge \widetilde{c} \cdot \mathrm{Re} F^\delta(y^\delta).$$

To complete the proof, recall that we assumed $\mathrm{Re}F^\delta(y^\delta) = \max_{u^\delta \in \Omega^\delta \cap \partial B^\delta_{r/2}(\tilde{v}^\delta_k)} |\mathrm{Re}F^\delta(u^\delta)|$. □

Let $F^\delta_{\mathbb{C},v^\delta_0}$ be the unique discrete holomorphic function on the whole plane $\mathbb{C}^\delta \setminus \{v^\delta_0\}$ tending to zero at infinity and such that $[\bar\partial^\delta F^\delta_{\mathbb{C},v^\delta_0}](v^\delta_0) = \frac{\lambda}{\delta^2}$, see [21, Theorem 2.21]. Note that $\mathrm{Re}F^\delta_{\mathbb{C},v^\delta_0}$ and $\mathrm{Im}F^\delta_{\mathbb{C},v^\delta_0}$ are discrete harmonic everywhere except two squares adjacent to $v^\delta_0$. It is well known that $F^\delta_{\mathbb{C}(z),v^\delta_0}$ is asymptotically equal $\frac{1}{2\pi}\cdot\frac{\lambda}{z-v_0}$ as $\delta \downarrow 0$. We need to introduce a similar function $F^\delta_{\mathbb{H},v^\delta_0}$ on a half-plane $\mathbb{H}^\delta$, where $\partial\mathbb{H}^\delta$ goes to the direction $\lambda$ and $v^\delta_0 \in \partial_{\mathrm{int}}\mathbb{H}^\delta \cap \diamondsuit^\delta_0$. The imaginary part of $F^\delta_{\mathbb{H},v^\delta_0}$ equals zero on the boundary, and $[\bar\partial^\delta F^\delta_{\mathbb{H},v^\delta_0}](v^\delta_0) = \frac{\lambda}{\delta^2}$. There is the unique discrete holomorphic function with these two properties that tends to zero at infinity.

Let us consider the sum $F^\delta_{\mathbb{C},v^\delta_0} + F^\delta_{\mathbb{C},v^\delta_0+2\bar\lambda\delta}$, where by $v^\delta_0 + 2\bar\lambda\delta$ we denote a white square at distance $\delta$ from the square $v^\delta_0$ that does not belong to $\mathbb{H}^\delta$. This sum tends to zero at infinity, since both $F^\delta_{\mathbb{C},v^\delta_0}$ and $F^\delta_{\mathbb{C},v^\delta_0+2\bar\lambda\delta}$ tend to zero at the infinity. Note that $F^\delta_{\mathbb{C},v^\delta_0+2\bar\lambda\delta}$ is discrete holomorphic on $\mathbb{H}^\delta$, therefore $F^\delta_{\mathbb{C},v^\delta_0} + F^\delta_{\mathbb{C},v^\delta_0+2\bar\lambda\delta}$ is holomorphic on $\mathbb{H}^\delta \setminus \{v^\delta_0\}$ and $[\bar\partial^\delta(F^\delta_{\mathbb{C},v^\delta_0} + F^\delta_{\mathbb{C},v^\delta_0+2\bar\lambda\delta})](v^\delta_0) = \frac{\lambda}{\delta^2}$. Finally, note that

$$\mathrm{Im}F^\delta_{\mathbb{C},v^\delta_0}(u) = G^\delta(u, v^\delta_0 + \bar\lambda\delta) - G^\delta(u, v^\delta_0 - \bar\lambda\delta),$$

where $G^\delta(u,u')$ is the classical Green's function on $\mathbb{C}^\delta \cap \blacklozenge^\delta_1$ satisfies $\Delta^\delta G^\delta(u,u') = \mathbb{1}_{u=u'}\cdot\frac{1}{2\delta^3}$. The Green's function is symmetric, therefore $\mathrm{Im}[F^\delta_{\mathbb{C},v^\delta_0} + F^\delta_{\mathbb{C},v^\delta_0+2\bar\lambda\delta}]$ vanishes on $\partial\mathbb{H}^\delta$. As a consequence we have $F^\delta_{\mathbb{H}}(u) = F^\delta_{\mathbb{C},v^\delta_0} + F^\delta_{\mathbb{C},v^\delta_0+2\bar\lambda\delta}$.

**Corollary 3.2.4.** *Let*

$$M^\delta_*(r) = \max_{u\in\Omega^\delta_{r,0}} |F^\delta(u) - F^\delta_{\mathbb{H}}(u)|.$$

*Then, for all sufficiently small $\delta$, one has*

$$M^\delta_*\left(\frac{r}{2}\right) \le \frac{4}{\widetilde{c}}\cdot M^\delta_*(r) + C_*,$$

*where $C_*$ is an absolute constant and $\widetilde{c}$ is the constant from Lemma* 3.2.2.

*Proof.* Note that $F^\delta_{\mathbb{H}}$ is uniformly bounded away from $v^\delta_0$ and vanishes on $\partial\mathbb{H}^\delta$, hence $F^\delta - F^\delta_{\mathbb{H}}$ is uniformly bounded on $\partial\Omega^\delta$. Moreover, function $F^\delta - F^\delta_{\mathbb{H}}$ is discrete holomorphic on $\Omega^\delta$, in particular it is discrete holomorphic on $B^\delta_t(v^\delta_0)\cap\Omega^\delta$ and vanishes on $\partial\Omega^\delta \cap B^\delta_t(v^\delta_0)$. Therefore the statement of Lemma 3.2.3 is valid for $F^\delta - F^\delta_{\mathbb{H}}$ and $t = 0$. □

We are now in the position to prove the convergence of $F^\delta$. Note that $F^\delta$ can be thought of as defined in polygonal representation of $\Omega^\delta$ by some standard continuation procedure, linear on edges and multilinear inside faces. Then we have the following

**Theorem 3.2.5.** *Let $\Omega^\delta$ be a sequence of discrete $2k$-black-piecewise Temperleyan domains of mesh size $\delta$ approximating a continuous domain $\Omega$. Suppose that each $\Omega^\delta$ admits a domino tiling. Let the sets of white corner squares $\{v^{*\delta}_k\}_{k=1}^{n+1}$ and $\{\tilde v^\delta_k\}_{k=1}^{n-1}$ approximate the sets of boundary points $\{v^*_k\}_{k=1}^{n+1}$ and $\{\tilde v_k\}_{k=1}^{n-1}$ correspondingly, and let $v^\delta_0$ approximate*

*a boundary point $v_0$, which lies on a straight segment of the boundary of $\Omega$. Then $F^\delta$ converges uniformly on compact subsets of $\Omega$ to a continuous holomorphic function $f_\Omega$, where $f_\Omega$ is defined as in Proposition* 3.1.4.

In the following proof we use the idea described in [18] (proof of Theorem 2.16).

*Proof. First case*: suppose that for each fixed positive $r$ the function $M^\delta_*(r)$ remains bounded, as $\delta \to 0$. Corollary 3.2.4 implies that discrete holomorphic functions $F^\delta - F^\delta_{\mathbb{H}}$ are uniformly bounded, and therefore equicontinuous due to Harnack principle on compact subsets of $\Omega$. Thus, due to the Arzelà–Ascoli theorem, the family $F^\delta - F^\delta_{\mathbb{H}}$ is precompact and hence converges along a subsequence to some holomorphic function $\widetilde{f}$ uniformly on compact subsets of $\Omega$. Note that $F^\delta_{\mathbb{H}} \rightrightarrows f_{\mathbb{H}} = \frac{1}{\pi} \cdot \frac{\lambda}{z - v_0}$ as $\delta \to 0$, uniformly on compacts. Let $f_\Omega := \widetilde{f} - f_{\mathbb{H}}$, then $F^\delta \rightrightarrows f_\Omega$, i.e. $\mathrm{Re}F^\delta \rightrightarrows \mathrm{Re}f_\Omega$ and $\mathrm{Im}F^\delta \rightrightarrows \mathrm{Im}f_\Omega$, uniformly on compacts. Since a discrete solution of Dirichlet problem converges to its continuous counterpart up to the boundary [21, Section 3.3], the boundary conditions for the functions $F^\delta$ yield the same boundary conditions for their limit. Thus, the function $f_\Omega$ solves the boundary value problem described in Proposition 3.1.4, therefore it is determined uniquely. This implies that all convergent subsequences of the family $\{F^\delta\}$ have the same limit and thus the whole family converges to $f_\Omega$.

*Second case*: suppose that $M^\delta_*(r)$ tends to infinity along a subsequence as $\delta \to 0$ for some $r > 0$. Let us show that this is impossible. Consider a discrete holomorphic function $\widetilde{F}^\delta_* := \frac{F^\delta - F^\delta_{\mathbb{H}}}{M^\delta_*(r)}$. Using the same arguments as above, we can show that the family $\widetilde{F}^\delta_*$ converges to some holomorphic function $f_*$. Note that the limit is bounded near $v_0$, since $F^\delta - F^\delta_{\mathbb{H}}$ is discrete holomorphic and bounded near $v^\delta_0$. Also, note that $\frac{F^\delta_{\mathbb{H}}}{M^\delta_*(r)}$ tends to zero away from $v_0$. Therefore, as in the previous case, the limit satisfies all boundary conditions described in Proposition 3.1.4 except the first one: the behaviour near the point $v_0$. The only function satisfying these properties is zero.

Suppose that there exists a sequence of squares $u^\delta_{\text{inner}}$ converging to $u_{\text{inner}} \in \Omega$ such that

$$\mathrm{Re}\widetilde{F}^\delta_*(u^\delta_{\text{inner}}) > \text{const}_\Omega > 0. \tag{2.1}$$

Then we have $f_*(u_{\text{inner}}) > 0$, which contradicts the fact that $f_*$ vanishes on $\Omega$, and therefore the second case is impossible.

To complete the proof let us show the existence of the sequence $\{u^\delta_{\text{inner}}\}$. Let $u^\delta_{\max}$ be chosen so that $1 = \sup\limits_{u^\delta \in \Omega^\delta_{r,0}} |\widetilde{F}^\delta_*(u^\delta)| = |\widetilde{F}^\delta_*(u^\delta_{\max})|$. Assume that $u^\delta_{\max} \in \blacklozenge^\delta_0$, i.e. $|\widetilde{F}^\delta_*(u^\delta_{\max})| = |\mathrm{Re}\widetilde{F}^\delta_*(u^\delta_{\max})|$. Without loss of generality we may assume that $\mathrm{Re}\widetilde{F}^\delta_*(u^\delta_{\max}) > 0$. Let $u^\delta_{\max} \to u_{\max} \in \overline{\Omega}_r$ as $\delta \to 0$, where $\Omega_r = \Omega \setminus \left( \bigcup\limits_{k=1}^{n-1} B_r(\tilde{v}_k) \right)$. The discrete maximum principle implies that $u_{\max} \in \bigcup\limits_{k=1}^{n-1} \partial B_r(\tilde{v}_k)$. Note that $\mathrm{Re}\widetilde{F}^\delta_*$ is a discrete harmonic function, and hence there exists a path $\gamma^\delta$ on the set $\blacklozenge^\delta_0$ from $u^\delta_{\max}$ to the boundary of the domain $\Omega^\delta$ or to the square adjacent to $\tilde{v}^\delta_k$ along which the absolute value of the function $\mathrm{Re}\widetilde{F}^\delta_*$ increases. The boundary conditions together with the fact that the limit function vanishes imply that $\gamma^\delta$ goes along a subarc $N^\delta_k \subset \partial\Omega^\delta$ where $\mathrm{Re}F^\delta$ has Neumann boundary condition and ends at the square adjacent to $\tilde{v}^\delta_k$.

Assume that $B_r(\tilde{v}_k) \cap \Omega$ is connected, the other case is treated similarly. Denote by $U^\delta$ the discrete subdomain of $B_r^\delta(\tilde{v}_k^\delta) \cap \Omega^\delta$ that is bounded by the subarc of $\partial\Omega^\delta$ where $\mathrm{Re}F^\delta$ has Dirichlet boundary condition, the path $\gamma^\delta \cap \Omega^\delta$ and the arc $\partial B_r^\delta(\tilde{v}_k^\delta) \cap \Omega^\delta$. Note that $U^\delta$ converges to $B_r(\tilde{v}_k) \cap \Omega$.

The absolute value of $\mathrm{Re}\widetilde{F}_*^\delta$ is bounded by $\epsilon_\delta$ away from the pieces of the boundary of $\Omega^\delta$ where $\mathrm{Re}F^\delta$ has Neumann boundary conditions. Note that the function $\mathrm{Re}\widetilde{F}_*^\delta$ is semi-bounded in a vicinity of the point $\tilde{v}_k^\delta$, therefore near the boundary $\mathrm{Re}\widetilde{F}_*^\delta > -c$, where $c > 0$ is a constant. Let $u_{\text{inner}}^\delta \in U^\delta$ be a black square in the middle of one of the arcs of the set $\partial B_{r/2}^\delta(\tilde{v}_k^\delta) \cap \blacklozenge_0^\delta$. Then

$$\mathrm{Re}\widetilde{F}_*^\delta(u^\delta) \geq -\epsilon_\delta \cdot 1 + (-c) \cdot \mathrm{hm}_{U^\delta}(u^\delta, (\widetilde{\epsilon}_\delta\text{-vicinity of } N_k^\delta) \cap (\partial B_r^\delta(\tilde{v}_k^\delta) \cap \Omega^\delta)) + 1 \cdot \mathrm{hm}_{U^\delta}(u^\delta, \gamma^\delta \cap \partial U^\delta).$$

Due to Lemma 3.2.2 we have $\mathrm{hm}_{U^\delta}(u_{\text{inner}}^\delta, \gamma^\delta \cap \partial U^\delta) > \mathrm{const}(U) > 0$. Note that $\epsilon_\delta$ tends to zero as $\delta \to 0$. Also, $\mathrm{hm}_{U^\delta}(u_{\text{inner}}^\delta, (\widetilde{\epsilon}_\delta\text{-vicinity of } N_k^\delta) \cap (\partial B_r^\delta(\tilde{v}_k^\delta) \cap \Omega^\delta))$ tends to zero as $\delta \to 0$. Hence we construct a sequence of squares $u_{\text{inner}}^\delta$ converging to $u_{\text{inner}} \in \Omega$ such that (2.1) holds. □

**Remark 3.2.6.** *Let in the setup of Theorem 3.2.5 the squares $v_0^\delta$ approximate an inner point $v_0$ of the domain $\Omega$, instead of a boundary one. Then $F^\delta$ converges uniformly on compact subsets of $\Omega \setminus v_0$ to a continuous holomorphic function $f_\Omega$, where $f_\Omega$ is defined as in Remark* 3.1.5.

## 3.3 Single dimer model and the Gaussian Free Field

In [42] Kenyon proved that the scaling limit of the height function in the dimer model on Temperleyan domains is the Gaussian Free Field. Our goal in this section is to prove Corollary 1.1.2, i.e. to show that the same scaling limit appears for approximations by a more general class of discrete domains which we call *black-piecewise Temperleyan* domains. Also, in Appendix we will show that the same holds for *isoradial black-piecewise Temperleyan* graphs.

### 3.3.1 Boundary conditions for the coupling function

For a fixed $v' \in \diamondsuit_0$, the function $C_\Omega(u, v')$ is discrete holomorphic as a function of $u$, with a simple pole at $v'$:

$$\begin{cases} C_\Omega(\cdot, v')|_{\partial\blacklozenge} = 0, \\ C_\Omega(\cdot, v')|_{\blacklozenge_0} \in \mathbb{R}, \quad C_\Omega(\cdot, v')|_{\blacklozenge_1} \in i\mathbb{R}, \\ \bar{\partial}[C_\Omega(\cdot, v')](v) = 0, \quad \forall v \in \diamondsuit, v \neq v' \\ \bar{\partial}[C_\Omega(\cdot, v')](v') = \frac{1}{4\lambda}. \end{cases}$$

Therefore in a $2n$-black-piecewise Temperleyan domain, for a fixed $v' \in \diamondsuit$, the boundary conditions of the coupling function $C_\Omega(u, v')$ as a function of $u$ change at all white corners, and there are $2n$ parts of the boundary with either $\mathrm{Re}[C_\Omega(\cdot, v')] = 0$ or $\mathrm{Im}[C_\Omega(\cdot, v')] = 0$.

In other words, a black-piecewise Temperleyan domain corresponds to mixed Dirichlet and Neumann boundary conditions for the discrete harmonic components of the coupling function. Recall that in a Temperleyan domain we have a simple boundary conditions, namely, $\mathrm{Im}[C_\Omega(u, v')] = 0$ for all boundary squares $u$, in other words $\mathrm{Im}[C_\Omega(u, v')]$ as a function of $u$ has Dirichlet boundary conditions.

### 3.3.2 Asymptotic values of the coupling function

Following [41], we define two functions $f_0(z_1, z_2)$ and $f_1(z_1, z_2)$. For a fixed $z_2$,

- ▷ the function $f_0(z_1, z_2)$ is analytic as a function of $z_1$, has a simple pole of residue $1/\pi$ at $z_1 = z_2$, and no other poles on $\overline{\Omega}$;
- ▷ $f_0(\cdot, z_2)$ is bounded in the vicinity of the points $v_s^*$;
- ▷ the function $f_0(\cdot, z_2)$ is semi-bounded in the vicinity of the points $\tilde{v}_k$;
- ▷ on each segment into which points from the set $\{\tilde{v}_k\}_{k=1}^{n-1} \cup \{v_s^*\}_{s=1}^{n+1}$ split the boundary, we have either $\mathrm{Re}[f_0(\cdot, z_2)] = 0$ or $\mathrm{Im}[f_0(\cdot, z_2)] = 0$;
- ▷ the boundary conditions of the function $f_0(\cdot, z_2)$ change at all points $\tilde{v}_k$, $v_s^*$.

The function $f_1(z_1, z_2)$ has the same definition, except for a difference in the boundary conditions: if on a segment between two points from the set $\{\tilde{v}_k\}_{k=1}^{n-1} \cup \{v_s^*\}_{s=1}^{n+1}$ we have $\mathrm{Re}[f_0(\cdot, z_2)] = 0$ (or $\mathrm{Im}[f_0(\cdot, z_2)] = 0$), then on that segment $\mathrm{Im}[f_1(\cdot, z_2)] = 0$ (or $\mathrm{Re}[f_1(\cdot, z_2)] = 0$). The existence and uniqueness of such functions can be shown using the technique described in Section 3, see Remark 3.1.5. In particular, we can write these functions in the following way

$$f_0(z, w) = \prod_{k=1}^{n+1} (z - v_k^*)^{\frac{1}{2}} \cdot \prod_{k=1}^{n-1} (z - \tilde{v}_k)^{-\frac{1}{2}} \cdot \left( \frac{s(w)}{z - w} + \frac{\overline{s(w)}}{z - \overline{w}} \right),$$

$$f_1(z, w) = \prod_{k=1}^{n+1} (z - v_k^*)^{\frac{1}{2}} \cdot \prod_{k=1}^{n-1} (z - \tilde{v}_k)^{-\frac{1}{2}} \cdot \left( \frac{s(w)}{z - w} - \frac{\overline{s(w)}}{z - \overline{w}} \right),$$

where

$$s(w) = \prod_{k=1}^{n+1} (w - v_k^*)^{-\frac{1}{2}} \cdot \prod_{k=1}^{n-1} (w - \tilde{v}_k)^{\frac{1}{2}}. \tag{3.2}$$

**Theorem 3.3.1.** *Let $\Omega$ be a bounded, simply connected domain in $\mathbb{C}$ with $k$ marked points. Assume that a sequence of discrete $k$-black-piecewise Temperleyan domains $\Omega^\delta$ on a grid with mesh size $\delta$ approximates the domain $\Omega$, and each domain $\Omega^\delta$ has at least one domino tiling. Let a sequence of white squares $v^\delta$ approximates a point $v \in \Omega$. Then the coupling function $\frac{1}{\delta} C_{\Omega^\delta}(u, v)$ satisfies the following asymptotics:*
*for $v^\delta \in \diamondsuit_0$*

$$\frac{1}{\delta} C_{\Omega^\delta}(u, v^\delta) - \frac{2}{\lambda} \cdot F^\delta_{\mathbb{C}, v^\delta}(u) = f_0(u, v) - \frac{1}{\pi(u - v)} + o(1);$$

*if $v^\delta \in \diamondsuit_1$, then*

$$\frac{1}{\delta} C_{\Omega^\delta}(u, v^\delta) - \frac{2}{\lambda} \cdot F^\delta_{\mathbb{C}, v^\delta}(u) = f_1(u, v) - \frac{1}{\pi(u - v)} + o(1),$$

*where $F^\delta_{\mathbb{C}, v^\delta}(u)$ is defined in Section 3.2.2.*

*Proof.* Recall that $F^\delta_{\mathbb{C}(z), v_0^\delta}$ is asymptotically equal $\frac{1}{2\pi} \cdot \frac{\lambda}{z - v_0}$ as $\delta \downarrow 0$. Now, to obtain the result one can use the techniques described in Section 3.2.2. More precisely, the first asymptotic can be obtained exactly from the proof of Theorem 3.2.5, see Remark 3.2.6. The second one can be obtained similarly. □

### 3.3.3 Sketch of the proof of Corollary 1.1.2

This section contains the sketch of the proof of Corollary 1.1.2. In [42] Kenyon proved convergence of the height function on Temperleyan domains to the Gaussian free field. To obtain the same result for black-piecewise Temperleyan domains it is enough to show that the limits of moments of height function in Temperleyan case and black-piecewise Temperleyan case are the same. Essentially the novel part of the argument is in (3.3), then Lemma 3.3.3 implies Corollary 3.3.4, and the rest of the argument is exactly as in [42, Theorem 1.1].

Similarly to [41] one can obtain the following result for black-piecewise Temperleyan approximations. Let $f_+(z,w) = f_0(z,w) + f_1(z,w)$ and $f_-(z,w) = f_0(z,w) - f_1(z,w)$.

**Proposition 3.3.2.** *Let $\gamma_1, \dots, \gamma_m$ be a collection of pairwise disjoint paths running from the boundary of $\Omega$ to $z_1, \dots, z_m$ respectively. Let $h(z_i)$ denote the height function at a point in black-piecewise Temperleyan domain $\Omega^\delta$ lying within $O(\delta)$ of $z_i$. Then*

$$\lim_{\delta \to o} \mathbb{E}[(h(z_1) - \mathbb{E}[h(z_1)]) \cdot \ldots \cdot (h(z_m) - \mathbb{E}[h(z_m)])] \; = \\ \sum_{\epsilon_1, \dots, \epsilon_m \in \{-1,1\}} \epsilon_1 \cdots \epsilon_m \int_{\gamma_1} \cdots \int_{\gamma_m} \det_{i,j \in [1,m]} (F_{\epsilon_i, \epsilon_j}(z_i, z_j)) \, dz_1^{(\epsilon_1)} \cdots dz_m^{(\epsilon_m)},$$

*where $dz_j^{(1)} = dz_j$ and $dz_j^{(-1)} = d\overline{z_j}$, and*

$$F_{\epsilon_i,\epsilon_j}(z_i,z_j) = \begin{cases} 0 & i = j \\ f_+(z_i,z_j) & (\epsilon_i,\epsilon_j) = (1,1) \\ f_-(z_i,z_j) & (\epsilon_i,\epsilon_j) = (-1,1) \\ \overline{f_-(z_i,z_j)} & (\epsilon_i,\epsilon_j) = (1,-1) \\ \overline{f_+(z_i,z_j)} & (\epsilon_i,\epsilon_j) = (-1,-1). \end{cases}$$

*Proof.* See the proof of [41, Proposition 20]. □

Recall that in the Temperleyan case [41] one has $f_+(z,w) = \frac{2}{z-w}$ and $f_-(z,w) = \frac{2}{z-\overline{w}}$. In the black-piecewise Temperleyan case we have

$$\begin{cases} f_-(z,w) = \frac{2}{z-\overline{w}} \cdot \frac{\overline{s(w)}}{s(z)} \\ f_+(z,w) = \frac{2}{z-w} \cdot \frac{s(w)}{s(z)} \end{cases} \tag{3.3}$$

where the function $s(w)$ is defined by (3.2).

One can easily check that the following lemma holds:

**Lemma 3.3.3.** *Let $\epsilon_1, \dots, \epsilon_m \in \{-1, 1\}$. Let us define function $S_{\epsilon_i,\epsilon_j}(z,w)$ as follows:*

$$S_{\epsilon_i,\epsilon_j}(z,w) = \begin{cases} 0 & i = j \\ s(w)/s(z) & (\epsilon_i,\epsilon_j) = (1,1) \\ \overline{s(w)}/s(z) & (\epsilon_i,\epsilon_j) = (-1,1) \\ s(w)/\overline{s(z)} & (\epsilon_i,\epsilon_j) = (1,-1) \\ \overline{s(w)}/\overline{s(z)} & (\epsilon_i,\epsilon_j) = (-1,-1). \end{cases}$$

*Then*

$$S_{\epsilon_{\alpha(1)},\epsilon_1}(z_{\alpha(1)},z_1)\cdot\ldots\cdot S_{\epsilon_{\alpha(m)},\epsilon_m}(z_{\alpha(m)},z_m)=\begin{cases}1 & \alpha(i)\neq i \quad \forall i\in\{1,2,\ldots,m\}\\ 0 & otherwise,\end{cases}$$

*where $\alpha$ is a permutation of the set $\{1,2,\ldots,m\}$.*

**Corollary 3.3.4.** *The limits of moments of the height function in the Temperleyan case and the black-piecewise Temperleyan case are the same.*

In [42] Kenyon showed that:

**Proposition 3.3.5.** *Let $\Omega$ be a Jordan domain with smooth boundary. Let $z_1,\ldots,z_m$ (with $m$ even) be distinct points of $\Omega$. Let $\Omega^\delta$ be a Temperleyan approximation of $\Omega$ and $h_{\Omega^\delta}$ be the height function of a uniform domino tiling in the domain $\Omega^\delta$. Then*

$$\lim_{\delta\to o}\mathbb{E}[(h_{\Omega^\delta}(z_1)-\mathbb{E}[h_{\Omega^\delta}(z_1)])\cdot\ldots\cdot(h_{\Omega^\delta}(z_m)-\mathbb{E}[h_{\Omega^\delta}(z_m)])] = \left(-\frac{16}{\pi}\right)^{m/2}\sum_{pairings\,\alpha} g_D(z_{\alpha(1)},z_{\alpha(2)})\cdot\ldots\cdot g_D(z_{\alpha(m-1)},z_{\alpha(m)}),$$

*where $g_D$ is the Green function with Dirichlet boundary conditions on $\Omega$.*

*Proof.* See the proof of [42, Proposition 3.2]. □

By Corollary 3.3.4 this proposition holds for black-piecewise Temperleyan domains as well. And the following lemma completes the proof of Corollary 1.1.2.

**Lemma 3.3.6** ([6])**.** *A sequence of multidimensional random variables whose moments converge to the moments of a Gaussian, converges itself to a Gaussian.*

# Chapter 4

# Hedgehog domains

In this chapter we assume that $\Omega^\delta$ is a simply connected discrete domain formed by a finite number of squares of $\mathbb{C}^\delta$ (the boundary doesn't required to be a disjoint simple closed lattice path).

## 4.1 The boundary value problem for s-holomorphic functions

In this section we introduce *hedgehog domains*. We study the specific discrete boundary value problem of Riemann type on hedgehog domains.

### 4.1.1 Hedgehog domains

Let us divide the set vertex $\mathcal{V}^\delta$ into three sets $\mathcal{V}^\delta_\circ$ , $\mathcal{V}^\delta_\bullet$ and $\mathcal{V}^\delta_\diamond$ as is shown on Fig. 4.1. Let $\partial\mathcal{V}^\delta_\circ$, $\partial\mathcal{V}^\delta_\bullet$ and $\partial\mathcal{V}^\delta_\diamond$ be the sets of white, black and dimond vertices of $\partial\mathcal{V}^\delta$ correspondingly. Let $\tilde\partial\mathcal{V}^\delta$ be the set of vertices adjacent to $\partial\Omega^\delta$ but not in $\partial\mathcal{V}^\delta$. In the same way we define the sets $\tilde\partial\mathcal{V}^\delta_\circ$, $\tilde\partial\mathcal{V}^\delta_\bullet$, $\tilde\partial\mathcal{V}^\delta_\diamond$.

To define a hedgehog domain let us define a *dashed square lattice* (see Fig. 4.1), a lattice where each square has side $2\sqrt{2}\delta$ and centered at a lattice point of

$$\left\{\left(\frac{4\delta n+1}{\sqrt{2}},\frac{4\delta m+1}{\sqrt{2}}\right)\,|\,n,m\in\mathbb{Z}\right\}.$$

**Definition 4.1.1.** *A discrete simply connected domain $\Omega^\delta$ is called a hedgehog domain if it is composed of a finite number of squares $2\delta\times 2\delta$ with vertices in $\mathcal{V}^\delta_\circ$ and each such square has either zero or two consecutive edges on the boundary of $\Omega^\delta$. Equivalently, one can take an arbitrary simply-connected union of $2\sqrt{2}\delta\times 2\sqrt{2}\delta$ squares of the dashed square lattice and add $2\delta\times 2\delta$ right triangles to each of its boundary edges, see Fig. 3.*

**Remark 4.1.2.** *Note that the boundary of a hedgehog domain need not be a simple curve.*

Let us divide the set $\partial_{\rm int}\Omega^\delta$ of a hedgehog domain into four sets $\partial^+_{\rm int}\Omega^\delta$, $\partial^-_{\rm int}\Omega^\delta$, $\partial^\sharp_{\rm int}\Omega^\delta$ and $\partial^\flat_{\rm int}\Omega^\delta$: note that each $\delta\times\delta$ square $a\in\partial_{\rm int}\Omega^\delta$ belongs to exactly one square $2\delta\times 2\delta$ with vertices in $\mathcal{V}_\circ$ touching the boundary, if north-east and south-east (resp., N-W and S-W; N-W and N-E; S-W and S-E) sides of this $2\delta\times 2\delta$ square belong to the boundary of $\Omega^\delta$, then $a\in\partial^+_{\rm int}\Omega^\delta$ (resp., $a\in\partial^-_{\rm int}\Omega^\delta$; $a\in\partial^\sharp_{\rm int}\Omega^\delta$; $a\in\partial^\flat_{\rm int}\Omega^\delta$). In the same way as above we define the sets $\partial^+_{\rm int}\blacklozenge^\delta_{0,1}$, $\partial^+_{\rm int}\lozenge^\delta_{0,1}$, $\partial^-_{\rm int}\blacklozenge^\delta_{0,1}$, $\partial^-_{\rm int}\lozenge^\delta_{0,1}$, $\partial^\flat_{\rm int}\blacklozenge^\delta_{0,1}$, $\partial^\flat_{\rm int}\lozenge^\delta_{0,1}$, $\partial^\sharp_{\rm int}\blacklozenge^\delta_{0,1}$ and $\partial^\sharp_{\rm int}\lozenge^\delta_{0,1}$, see Fig. 4.1. Note that the sets $\partial\mathcal{V}^\delta_\bullet$, $\tilde\partial\mathcal{V}^\delta_\circ$, $\partial^+_{\rm int}\blacklozenge^\delta_1$, $\partial^-_{\rm int}\blacklozenge^\delta_0$, $\partial^\sharp_{\rm int}\lozenge^\delta_0$ and $\partial^\flat_{\rm int}\lozenge^\delta_1$ of hedgehog domain $\Omega^\delta$ are empty.

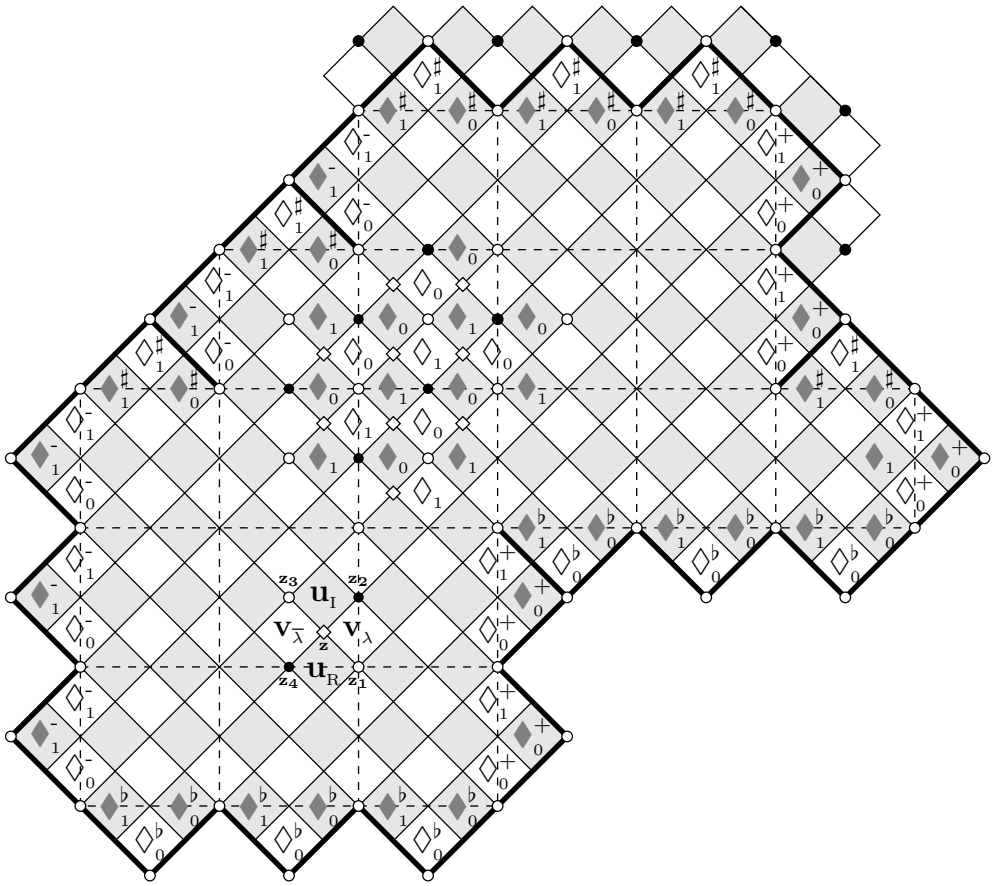


Figure 4.1: A hedgehog domain $\Omega^\delta$ with the boundary (thick line) and portions of the sets $\blacklozenge^\delta$ and $\diamondsuit^\delta$. A portion of faces of $\partial\Omega^\delta$. The vertex set $\mathcal{V}^\delta = \mathcal{V}^\delta_\circ \sqcup \mathcal{V}^\delta_\bullet \sqcup \mathcal{V}^\delta_\diamond$ of $\Omega^\delta$ consists of white vertices ($\mathcal{V}^\delta_\circ$), black vertices ($\mathcal{V}^\delta_\bullet$) and "diamond" ones ($\mathcal{V}^\delta_\diamond$). The boundary vertex set $\partial\mathcal{V}^\delta_\circ$ (white vertices on the thick line) and a portion of the set $\tilde{\partial}\mathcal{V}^\delta_\bullet$. S-holomorphic functions are defined on $\mathcal{V}^\delta_\diamond$, and their projections on $\diamondsuit^\delta \sqcup \blacklozenge^\delta$. Given a vertex $z \in \mathcal{V}^\delta_\diamond$, we denote the neighbouring squares by $u_{\text{I}} \in \blacklozenge^\delta_1, v_{\bar\lambda} \in \diamondsuit^\delta_1, u_{\text{R}} \in \blacklozenge^\delta_0$ and $v_\lambda \in \diamondsuit^\delta_0$. The set $\partial_{\text{int}}\Omega^\delta$ is composed of subsets $\partial^+_{\text{int}}\Omega^\delta$, $\partial^-_{\text{int}}\Omega^\delta$, $\partial^\sharp_{\text{int}}\Omega^\delta$ and $\partial^\flat_{\text{int}}\Omega^\delta$.

### 4.1.2 Riemann boundary value problem for s-holomorphic functions

Fermionic observables in the Ising model are s-holomorphic functions with Riemann-type boundary conditions [18, 19, 22, 36, 77, 78]. In Section 4.2 we show that the dimer coupling function on hedgehog domains can be considered as an s-holomorphic function satisfying Riemann boundary conditions.

**Definition 4.1.3.** *Let $\Omega^\delta$ be a hedgehog domain. Let $v_0 \in \mathrm{Int}\diamondsuit_\circ^\delta$. We say that $F^\delta_{\text{s-hol}}$ solves the discrete Riemann boundary value problem* $\mathbf{RBVP}(\mathbf{\Omega^\delta, v_0})$ *if*

$$\begin{cases} F^\delta_{\text{s-hol}} \text{ is s-holomorphic on } (\overline{\Omega}^\delta \setminus \{v_0\}) \sqcup \mathcal{V}^\delta_\diamond; \\ [\bar\partial F^\delta_{\text{s-hol}}](v_0) = \frac{\lambda}{4\delta^2}; \\ \mathrm{Im}[F^\delta_{\text{s-hol}}(z) \cdot \sqrt{(n(z))}] = 0, \quad z \in \partial\mathcal{V}^\delta_\diamond. \end{cases}$$

### 4.1.3 The primitive of the square of the s-holomorphic function

This definition was introduced by Smirnov in [77]. The primitive of the square of the s-holomorphic function is a crucial tool for the analysis of fermionic observables in the Ising model via boundary value problems for s-holomorphic functions [77, 78, 22]. We use this approach to study the scaling limit of the dimer coupling function.

**Definition 4.1.4.** *Let a function $F^\delta_{\text{s-hol}}$ be s-holomorphic. Let us define a function $H^\delta\colon \mathcal{V}^\delta_\bullet \sqcup \mathcal{V}^\delta_\circ \to \mathbb{R}$ by the equality*

$$H^\delta_\bullet(z_2) - H^\delta_\circ(z_1) = (F^\delta_{\text{s-hol}}(a))^2 \cdot (z_2 - z_1), \tag{1.1}$$

*where $H^\delta_\bullet$ (resp., $H^\delta_\circ$) is a restriction of the function $H^\delta$ to the set $\mathcal{V}^\delta_\bullet$ (resp., $\mathcal{V}^\delta_\circ$), and $z_1 \in \mathcal{V}^\delta_\circ$, $z_2 \in \mathcal{V}^\delta_\bullet$ are two vertices of the same square $a$. Note that the function $H^\delta$ can be viewed as the primitive of the real part of the square of the s-holomorphic function $F^\delta_{\text{s-hol}}$, see [22, Proposition 3.6].*

**Remark 4.1.5.** *1. The primitive $H^\delta$ is defined up to an additive constant.*

*2. S-holomorphicity of the function $F^\delta_{\text{s-hol}}$ guarantees that*

$$(H^\delta(z_1) - H^\delta(z_2)) + (H^\delta(z_4) - H^\delta(z_1)) + (H^\delta(z_3) - H^\delta(z_4)) + (H^\delta(z_2) - H^\delta(z_3)) = 0,$$

*since $|F^\delta_{\text{s-hol}}(z)|^2 = (F^\delta_{\text{s-hol}}(u_{\scriptscriptstyle R}))^2 - (F^\delta_{\text{s-hol}}(u_{\scriptscriptstyle I}))^2 = i((F^\delta_{\text{s-hol}}(v_{\bar\lambda}))^2 - (F^\delta_{\text{s-hol}}(v_\lambda))^2)$, where vertices $z, z_1, z_2, z_3, z_4$ and squares $u_{\scriptscriptstyle I}, v_{\bar\lambda}, u_{\scriptscriptstyle R}, v_\lambda$ are as shown on Fig. 4.1. Therefore, if $\Omega^\delta$ is simply connected, then $H^\delta$ is well defined.*

Recall that $\tilde\partial\mathcal{V}^\delta_\bullet$ of hedgehog domain $\Omega^\delta$ is the set of black vertices of squares of the set $\partial\Omega^\delta$, see Fig. 4.3. Let us define the discrete *leap-frog Laplacian* of $H^\delta_\circ$ by

$$[\Delta^\delta_\circ H^\delta_\circ](z) = \frac{1}{4\delta^2}\sum_{w\sim z}(H^\delta_\circ(w) - H^\delta_\circ(z)), \quad z \in \mathrm{Int}\mathcal{V}^\delta_\circ, \tag{1.2}$$

where the sum is over the four neighbours $w \in \mathcal{V}^\delta_\circ$ of $z$. Similarly, one can define the slightly modified discrete leap-frog Laplacian of $H^\delta_\bullet$ by

$$[\Delta^\delta_\bullet H^\delta_\bullet](z) = \frac{1}{c_z\delta^2}\sum_{w\sim z} c_{zw}(H^\delta_\bullet(w) - H^\delta_\bullet(z)), \quad z \in \mathrm{Int}\mathcal{V}^\delta_\bullet, \tag{1.3}$$

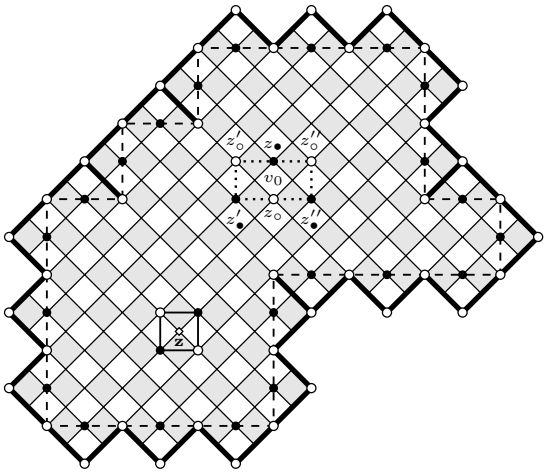


Figure 4.2: Boundary contour around $\mathrm{Int}\mathcal{V}_\diamond^\delta$ (dashed): s-holomorphicity together with Riemann boundary conditions imply that at two consecutive white vertices on the boundary contour the values of $H^\delta$ coincide; contour around $z_\diamond \in \mathrm{Int}\mathcal{V}_\diamond^\delta$ (full); contour around $v_0$ (dotted).

where $c_z = \sum_{w\sim z} c_{zw}$, and $c_{zw}$ equals 1 for inner edges and $2(\sqrt{2}-1)$ for the boundary edges, see Fig. 4.3. For the reason of this "boundary modification" of $\Delta_\bullet^\delta$, see [22, Section 3.6].

Let $F_{\text{s-hol}}^\delta$ be an s-holomorphic function solving a discrete boundary value problem $\mathrm{RBVP}(\Omega^\delta, v_0)$. Let $H^\delta$ be the primitive of the square of $F_{\text{s-hol}}^\delta$ defined by (1.1). Note that $F_{\text{s-hol}}^\delta$ is not defined at $v_0$. Hence, we need to check that the definition of $H^\delta$ is consistent around $v_0$. Given a discrete path $\gamma = (z_1, ..., z_n)$ with vertices in $\mathcal{V}_\bullet^\delta \cup \mathcal{V}_\circ^\delta$ and a function $F_{\text{s-hol}}^\delta$ on faces, we define

$$\int_\gamma (F_{\text{s-hol}}^\delta)^2\, dz = \sum_{i=1}^{n-1} (F_{\text{s-hol}}^\delta(a_{i,i+1}))^2 (z_{i+1} - z_i),$$

where $z_i, z_{i+1} \in \mathcal{V}_\bullet^\delta \cup \mathcal{V}_\circ^\delta$ are two vertices of the same square $a_{i,i+1}$. We similarly define contour integrals around sets of vertices of type $\mathcal{V}_\diamond^\delta$. Remark 4.1.5 implies that for each $z_\diamond \in \mathrm{Int}\mathcal{V}_\diamond^\delta$ non-adjacent to the face $v_0$ one has $\oint_{z_\diamond} (F_{\text{s-hol}}^\delta)^2\, dz = 0$. Moreover, since $F_{\text{s-hol}}^\delta$ satisfies Riemann boundary conditions, the contour integral along the boundary contour is zero, see Fig. 4.2. Note that

$$\oint_{v_0} (F_{\text{s-hol}}^\delta)^2\, dz = \oint_{\mathrm{Int}\mathcal{V}_\diamond^\delta} (F_{\text{s-hol}}^\delta)^2\, dz,$$

where the contour around $v_0$ is as shown on Fig. 4.2. Therefore, $H^\delta$ is well defined. Then due to [22] we have the following proposition.

**Proposition 4.1.6.** *Let $z_\circ \in \mathcal{V}_\circ^\delta$ and $z_\bullet \in \mathcal{V}_\bullet^\delta$ be vertices of the square $v_0$. The function $H^\delta$ satisfies the following properties:*

- ▷ *if $z$ and $z'$ are two vertices of the same square, then $H_\circ^\delta(z) \geq H_\bullet^\delta(z')$;*

▷ $H^\delta$ *satisfies Dirichlet boundary conditions:* $H^\delta_\circ(z) = 0$ *for any* $z \in \partial\mathcal{V}^\delta_\circ$, *and* $H^\delta_\bullet(z') = 0$ *for any* $z' \in \tilde{\partial}\mathcal{V}^\delta_\bullet$;

▷ $H^\delta_\bullet$ *has a "nonpositive inner normal derivative", i.e.* $H^\delta_\bullet(w) \le 0$ *for any vertex* $w \in \mathcal{V}^\delta_\bullet$ *adjacent to a boundary vertex;*

▷ $H^\delta_\circ$ *is leap-frog subharmonic on* $\mathcal{V}^\delta_\circ \setminus \{z_\circ\}$, *while* $H^\delta_\bullet$ *is leap-frog superharmonic on* $\mathcal{V}^\delta_\bullet \setminus \{z_\bullet\}$.

*Proof.* All the statements follow directly from [22, Section 3.3]. □

**Remark 4.1.7.** *The function* $H^\delta$ *satisfies the maximum principle: if* $\widetilde{\mathcal{V}}^\delta \subset \mathcal{V}^\delta$ *does not contain* $z_\circ$ *(respectively* $z_\bullet$*), then*

$$\max_{z\in\widetilde{\mathcal{V}}^\delta} H^\delta(z) = \max_{z\in\partial\widetilde{\mathcal{V}}^\delta} H^\delta_\circ(z) \quad (\textit{respectively } \min_{z\in\widetilde{\mathcal{V}}^\delta} H^\delta(z) = \min_{z\in\partial\widetilde{\mathcal{V}}^\delta} H^\delta_\bullet(z)).$$

**Proposition 4.1.8.** *A discrete Riemann boundary value problem* $\mathrm{RBVP}(\Omega^\delta, v_0)$ *has a unique solution.*

*Proof.* The existence of such a function will be shown in Section 4.2.1. Let us prove that the solution is unique. Let $F^\delta_1$ and $F^\delta_2$ be two different solutions. Then $F^\delta_1 - F^\delta_2$ is s-holomorphic on $\overline{\Omega}^\delta \sqcup \mathcal{V}^\delta_\diamond$ and $\mathrm{Im}[(F^\delta_1 - F^\delta_2)(z)\cdot\sqrt{(n(z))}] = 0, \quad z \in \partial\mathcal{V}^\delta_\diamond$. Hence one can define the primitive of the square of the difference. The maximum principle for the primitive tells us that such a primitive is identically zero. Therefore $F^\delta_1 - F^\delta_2$ is identically zero. □

### 4.1.4 The continuous analogue of the functions $F^\delta_{\text{s-hol}}$ and $H^\delta$

In this section we describe the continuous analogue of the functions $F^\delta_{\text{s-hol}}$ and $H^\delta$. Also, we give a characterisation of the holomorphic solution of the Riemann-type boundary value problem in terms of the primitive of its square.

**Proposition 4.1.9.** *Let* $\Omega$ *be a bounded simply connected domain with smooth boundary, and* $v$ *be a point in the interior of* $\Omega$. *Then for any* $\lambda \in \mathbb{C}$ *there exists a unique holomorphic function* $f^v_\Omega$ *such that:*

*(f1)* $f^v_\Omega(z) = \frac{1}{2\pi}\cdot\frac{\lambda}{z-v} + O(1)$ *in a vicinity of the point* $v$;

*(f2)* $\mathrm{Im}[f^v_\Omega(z)\sqrt{(n(z))}] = 0, \quad z \in \partial\Omega$.

*Proof.* Let $\phi$ be a conformal mapping of the domain $\Omega$ onto the unit disk $\mathbb{D}$ such that $v$ is mapped onto 0 and $\phi'(v) > 0$. Note that if $f^0_{\mathbb{D}}$ is a solution in the unit disk with singularity at zero, then

$$f^v_\Omega(z) := f^0_{\mathbb{D}}(\phi(z))\cdot(\phi'(z))^{\frac{1}{2}}\cdot(\phi'(v))^{\frac{1}{2}} \tag{1.4}$$

solves our boundary value problem. It is easy to check that $f^0_{\mathbb{D}}(z) = \frac{1}{2\pi}(\frac{\lambda}{z} + \bar{\lambda})$.

Let $f_1$ and $f_2$ be two different solutions. Let $z(t)$ be the natural parametrization of $\partial\Omega$. Note that the difference $f_1 - f_2$ is holomorphic on $\Omega$, then

$$0 = \int_{\partial\Omega} (f_1 - f_2)^2(z)\, dz = \int_{\partial\Omega} (f_1 - f_2)^2(z(t)) \cdot in(z(t))\, dt.$$

The boundary conditions imply that $(f_1 - f_2)^2(z(t)) \cdot n(z(t)) \geq 0$. So, $f_1 - f_2 = 0$ on the boundary of $\Omega$. Thus, $f_1 = f_2$ in $\Omega$. □

The previous proposition also holds if $v$ is a boundary point of $\Omega$.

**Lemma 4.1.10.** *Let $\Omega$ be a bounded simply connected domain with smooth boundary, and $v \in \partial\Omega$. Then there exists a unique holomorphic function $f_\Omega^v$ such that:*

*(F1)* $f_\Omega^v(z) = \frac{1}{2\pi} \cdot \frac{i\sqrt{n(v)}}{z-v} + O(1)$ *in a vicinity of the point $v$;*

*(F2)* $\operatorname{Im}[f_\Omega^v(z)\sqrt{(n(z))}] = 0, \quad z \in \partial\Omega \setminus \{v\}$.

*Proof.* The uniqueness of the solution can be proven using the same arguments as in Proposition 4.1.9. To construct $f_\Omega^v$, consider a holomorphic map $\phi$ of $\Omega$ onto $\mathbb{D}$ such that $\phi(v) = n(v)$ and hence $\phi'(v) > 0$. As in Proposition 4.1.9, we can define

$$f_\Omega^v(z) := f_{\mathbb{D}}^{\phi(v)}(\phi(z)) \cdot (\phi'(z))^{\frac{1}{2}} \cdot (\phi'(v))^{\frac{1}{2}}, \tag{1.5}$$

where the function $f_{\mathbb{D}}^w(z) = \frac{i\sqrt{w}}{2\pi\cdot(z-w)}$ solves a similar boundary value problem in $\mathbb{D}$. □

Due to [18, Section 3.3.2] one can give a characterisation of the holomorphic solution of the boundary value problem (f1)–(f2) in terms of the primitive of its square. This characterisation will be used in the proof of Theorem 4.2.5 dedicated to one of the main convergence results.

**Proposition 4.1.11.** *Let $\Omega$ be a simply connected domain, and $v$ be a point in the interior of $\Omega$. Let a holomorphic function $f$ solve the boundary value problem described in Proposition 4.1.9 (or $f$ is defined by (1.4), if $\Omega$ is not smooth). Define two harmonic functions*

$$h := \int Re[f^2(z)\, dz] \quad \text{and} \quad h_\star := \int Re\left[\left(f(z) - \frac{1}{2\pi} \cdot \frac{\lambda}{z-v}\right)^2 dz\right].$$

*Then the following holds:*

*(h1) $h$ satisfies Dirichlet boundary conditions, since $h$ is defined up to an additive constant, we can assume that $h \equiv 0$ on $\partial\Omega$;*

*(h2) $\partial_n h \geq 0$ (outer normal derivative is nonnegative);*

*(h3) $h_\star$ is bounded in a vicinity of $v$.*

*Moreover, if $h$ and $h_\star$ satisfy all these conditions, then $f$ coincides with the solution $f_\Omega^v$ defined in Proposition 4.1.9.*

*Proof.* The property (f2) is equivalent to (h1) and (h2). Property (f1) is equivalent to (h3). □

In this section we show that a slightly modified s-holomorphic version of the coupling function satisfies Riemann-type boundary conditions on hedgehog domains. We then prove the convergence of the coupling function.

### 4.2.1 Coupling function as s-holomorphic function

We can think of the inverse Kasteleyn matrix $\frac{1}{\delta}C_{\Omega^\delta}(u,v)$ as a function of two variables $u \in \blacklozenge^\delta$ and $v \in \diamondsuit^\delta$. If $v \in \diamondsuit_0^\delta$, then $\frac{1}{\delta}C_{\Omega^\delta}(u,v)$ is a discrete holomorphic function of $u$, with a simple pole at $v$:

$$4\delta\bar{\lambda}\bar{\partial}[C_{\Omega^\delta}(\,\cdot\,,v)](v) = C_{\Omega^\delta}(v+\delta\lambda,v) - C_{\Omega^\delta}(v-\delta\lambda,v) + iC_{\Omega^\delta}(v-\delta\bar{\lambda},v) - iC_{\Omega^\delta}(v+\delta\bar{\lambda},v) = 1,$$

since the product of the Kasteleyn matrix and the inverse Kasteleyn matrix is equal to the identity matrix. For more details see [41, 68]. Note that the coupling function as a function of $u$ can be extended to be zero on $\partial\blacklozenge^\delta$, so that the above equation makes sense.

Let $\Omega^\delta$ be a hedgehog domain. Fix a white square $v_0 \in \mathrm{Int}\diamondsuit_0^\delta$. Let us define a function $\check{F}^\delta\colon \bar{\blacklozenge}^\delta \to \mathbb{C}$ by $\check{F}^\delta(u) := \frac{1}{\delta}C_{\Omega^\delta}(u,v_0)$. Note that $\check{F}^\delta$ is a discrete holomorphic everywhere in $\diamondsuit^\delta$ except at the face $v_0$ where one has $[\bar{\partial}^\delta \check{F}^\delta](v_0) = \frac{\lambda}{\delta^2}$. Therefore one can define an s-holomorphic function $\check{F}^\delta_{\text{s-hol}}$ on the set $(\overline{\Omega}^\delta \smallsetminus \{v_0\}) \sqcup \mathcal{V}_\diamond^\delta$ as described in Remark 1.2.6.

Let us divide the set $\partial\mathcal{V}_\circ^\delta$ into two sets $\partial\check{\mathcal{V}}_\circ^\delta$ and $\partial\hat{\mathcal{V}}_\circ^\delta$, where $\partial\check{\mathcal{V}}_\circ^\delta$ are vertices of the dashed lattice and $\partial\mathcal{V}_\circ^\delta = \partial\check{\mathcal{V}}_\circ^\delta \sqcup \partial\hat{\mathcal{V}}_\circ^\delta$.

**Proposition 4.2.1.** *Let $\check{H}^\delta$ be the primitive of the square of $\check{F}^\delta_{\text{s-hol}}$ defined by (1.1). Then $\check{H}^\delta$ satisfies Dirichlet boundary conditions on the set $\partial\check{\mathcal{V}}_\circ^\delta$: $\check{H}^\delta(z) = 0$ for any $z \in \partial\check{\mathcal{V}}_\circ^\delta$.*

*Proof.* Let $u_{\text{I}}, u_{\text{R}}, v_\lambda, v_{\bar{\lambda}}, z, z_1, z_2, \check{z}, \check{z}'$ be as shown on Fig. 4.3 and $v_\lambda \neq v_0$. Note that on the upper boundary

$$-C_{\Omega^\delta}(u_{\text{I}},v_0) + iC_{\Omega^\delta}(u_{\text{R}},v_0) = 0,$$

since the product of the Kasteleyn matrix and the inverse Kasteleyn matrix is equal to the identity matrix. Therefore $i\check{F}^\delta_{\text{s-hol}}(u_{\text{I}}) = -\check{F}^\delta_{\text{s-hol}}(u_{\text{R}})$, then by (1.1) we obtain that

$$\check{H}^\delta(\check{z}) - \check{H}^\delta(\check{z}') = (\check{H}^\delta(\check{z}) - \check{H}^\delta(z)) + (\check{H}^\delta(z) - \check{H}^\delta(\check{z}')) = -(\check{F}^\delta_{\text{s-hol}}(u_{\text{I}}))^2 - (\check{F}^\delta_{\text{s-hol}}(u_{\text{R}}))^2 = 0,$$

on the upper boundary. Similarly, one can check that $i\check{F}^\delta_{\text{s-hol}}(u_{\text{I}}) = \check{F}^\delta_{\text{s-hol}}(u_{\text{R}})$ and $\check{H}^\delta(\check{z}) - \check{H}^\delta(\check{z}') = 0$ on the lower boundary.

Recall that $\check{H}^\delta$ is defined up to an additive constant, which can be chosen so that $\check{H}^\delta(z) = 0$ for any $z \in \partial\check{\mathcal{V}}_\circ^\delta$, therefore to finish the proof it is enough to check that $\check{H}^\delta(\check{z}) = \check{H}^\delta(\check{z}')$ on the right and left boundaries.

On the right boundary $\check{F}^\delta_{\text{s-hol}}(z_1) = \check{F}^\delta_{\text{s-hol}}(z_2) = \check{F}^\delta_{\text{s-hol}}(u_{\text{R}})$. Therefore, on the right boundary,

$$i\check{F}^\delta_{\text{s-hol}}(v_{\bar{\lambda}}) = i\mathrm{Proj}_{\bar{\lambda}}[F^\delta_{\text{s-hol}}(z_1)] = \mathrm{Proj}_\lambda[F^\delta_{\text{s-hol}}(z_2)] = \check{F}^\delta_{\text{s-hol}}(v_\lambda).$$

Analogously, one can check that $i\check{F}^\delta_{\text{s-hol}}(v_{\bar{\lambda}}) = -\check{F}^\delta_{\text{s-hol}}(v_\lambda)$ on the left boundary. Hence $\check{H}^\delta(\,\cdot\,)$ is a constant on $\partial\check{\mathcal{V}}_\circ^\delta$. □

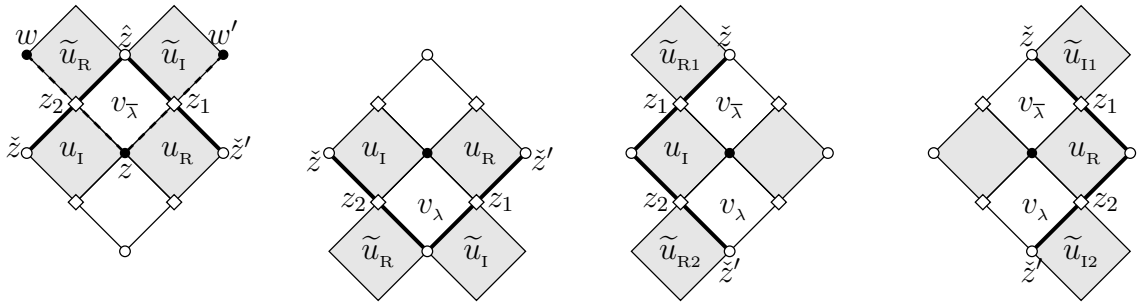


Figure 4.3: **First**: upper boundary; black vertices $w, w' \in \tilde{\partial}\mathcal{V}^\delta_\bullet$; boundary weights of the leap-frog Laplacian $\Delta^\delta_\bullet$: $c_{zw} = c_{zw'} = 2(\sqrt{2}-1)$; **Second**: lower boundary. **Third**: left boundary. **Fourth**: right boundary.

The above proposition does not hold for the whole $\partial\mathcal{V}^\delta_\circ$. Let $u_{\mathrm{R}}, v_{\overline{\lambda}}, z, \hat{z}, \check{z}'$ be as shown on Fig. 4.3. Then on the upper boundary one has

$$\check{H}^\delta(\hat{z}) - \check{H}^\delta(\check{z}') = (\check{H}^\delta(\hat{z}) - \check{H}^\delta(z)) + (\check{H}^\delta(z) - \check{H}^\delta(\check{z}')) = i(\check{F}^\delta_{\text{s-hol}}(v_{\overline{\lambda}}))^2 - (\check{F}^\delta_{\text{s-hol}}(u_{\mathrm{R}}))^2.$$

Note that in this case $\check{F}^\delta_{\text{s-hol}}(v_{\overline{\lambda}}) = \frac{\lambda}{\sqrt{2}}\check{F}^\delta_{\text{s-hol}}(u_{\mathrm{R}})$. Therefore, $\check{H}^\delta(\hat{z}) - \check{H}^\delta(\check{z}') \neq 0$.

One can modify the s-holomorphic version $\check{F}^\delta_{\text{s-hol}}$ of the normalised coupling function on hedgehog domain, in such a way that the primitive of its square vanishes *everywhere* on $\partial\mathcal{V}^\delta_\circ$. In other words, one can define an s-holomorphic function $F^\delta_{\text{s-hol}}(\cdot)$, which satisfies Riemann-type boundary conditions everywhere on $\partial\mathcal{V}^\delta_\diamond$ and coincides with $\frac{1}{\delta}C_{\Omega^\delta}(\cdot, v_0)$ on the set $\mathrm{Int}\blacklozenge^\delta$. Such a modification is possible since the values $\check{F}^\delta_{\text{s-hol}}(z_1), \check{F}^\delta_{\text{s-hol}}(z_2)$ near a given vertex $z_\circ \in \partial\hat{\mathcal{V}}^\delta_\circ$ are subject to only three real equations from Definition 1.2.4, which leave one degree of freedom to adjust the value $H^\delta(z_\circ)$.

Let $F^\delta_{\text{s-hol}}$ be an s-holomorphic function defined on $(\overline{\Omega}^\delta \smallsetminus \{v_0\}) \sqcup \mathcal{V}^\delta$ coinciding with $\check{F}^\delta_{\text{s-hol}}$ on the set $(\Omega^\delta \smallsetminus (\{v_0\} \cup \partial^+_{\text{int}}\blacklozenge^\delta_0 \cup \partial^-_{\text{int}}\blacklozenge^\delta_1 \cup \partial^\flat_{\text{int}}\lozenge^\delta_0 \cup \partial^\sharp_{\text{int}}\lozenge^\delta_1)) \sqcup (\mathcal{V}^\delta_\diamond \smallsetminus \partial\mathcal{V}^\delta_\diamond)$, i.e.:

$$\begin{cases} F^\delta_{\text{s-hol}}(u) = \check{F}^\delta_{\text{s-hol}}(u) & \text{if } u \in \blacklozenge^\delta \smallsetminus (\partial^+_{\text{int}}\blacklozenge^\delta_0 \cup \partial^-_{\text{int}}\blacklozenge^\delta_1); \\ F^\delta_{\text{s-hol}}(v) = \check{F}^\delta_{\text{s-hol}}(v) & \text{if } v \in \lozenge^\delta \smallsetminus (\{v_0\} \cup \partial^\flat_{\text{int}}\lozenge^\delta_0 \cup \partial^\sharp_{\text{int}}\lozenge^\delta_1); \\ F^\delta_{\text{s-hol}}(z) = \check{F}^\delta_{\text{s-hol}}(z) & \text{if } z \in \mathcal{V}^\delta_\diamond \smallsetminus \partial\mathcal{V}^\delta_\diamond. \end{cases}$$

We define the function $F^\delta_{\text{s-hol}}$ on $(\partial\Omega^\delta \cup \partial^+_{\text{int}}\blacklozenge^\delta_0 \cup \partial^-_{\text{int}}\blacklozenge^\delta_1 \cup \partial^\flat_{\text{int}}\lozenge^\delta_0 \cup \partial^\sharp_{\text{int}}\lozenge^\delta_1) \sqcup \partial\mathcal{V}^\delta_\diamond$ as follows, see Fig. 4.3 for the notation:

$$\text{Upper boundary} \begin{cases} F^\delta_{\text{s-hol}}(\widetilde{u}_{\mathrm{I}}) & := i(1-\sqrt{2})\check{F}^\delta_{\text{s-hol}}(u_{\mathrm{R}}); \\ F^\delta_{\text{s-hol}}(\widetilde{u}_{\mathrm{R}}) & := -(1-\sqrt{2})\check{F}^\delta_{\text{s-hol}}(u_{\mathrm{R}}); \\ F^\delta_{\text{s-hol}}(v_{\overline{\lambda}}) & := \overline{\lambda}\check{F}^\delta_{\text{s-hol}}(u_{\mathrm{R}}); \\ F^\delta_{\text{s-hol}}(z_1) & := \check{F}^\delta_{\text{s-hol}}(u_{\mathrm{R}}) + \check{F}^\delta_{\text{s-hol}}(\widetilde{u}_{\mathrm{I}}); \\ F^\delta_{\text{s-hol}}(z_2) & := \check{F}^\delta_{\text{s-hol}}(\widetilde{u}_{\mathrm{R}}) + \check{F}^\delta_{\text{s-hol}}(u_{\mathrm{I}}); \end{cases}$$

$$\text{Lower boundary}\begin{cases} F^\delta_{\text{s-hol}}(\widetilde{u}_{\text{I}}) & := i(\sqrt{2}-1)\check{F}^\delta_{\text{s-hol}}(u_{\text{R}});\\ F^\delta_{\text{s-hol}}(\widetilde{u}_{\text{R}}) & := (\sqrt{2}-1)\check{F}^\delta_{\text{s-hol}}(u_{\text{R}});\\ F^\delta_{\text{s-hol}}(v_\lambda) & := \lambda\check{F}^\delta_{\text{s-hol}}(u_{\text{R}});\\ F^\delta_{\text{s-hol}}(z_1) & := \check{F}^\delta_{\text{s-hol}}(u_{\text{R}})+\check{F}^\delta_{\text{s-hol}}(\widetilde{u}_{\text{I}});\\ F^\delta_{\text{s-hol}}(z_2) & := \check{F}^\delta_{\text{s-hol}}(\widetilde{u}_{\text{R}})+\check{F}^\delta_{\text{s-hol}}(u_{\text{I}}); \end{cases}$$

$$\text{Left boundary}\begin{cases} F^\delta_{\text{s-hol}}(\widetilde{u}_{\text{R1}}) & := (\sqrt{2}-1)\lambda\check{F}^\delta_{\text{s-hol}}(v_{\overline{\lambda}});\\ F^\delta_{\text{s-hol}}(\widetilde{u}_{\text{R2}}) & := (1-\sqrt{2})\lambda\check{F}^\delta_{\text{s-hol}}(v_{\overline{\lambda}});\\ F^\delta_{\text{s-hol}}(u_{\text{I}}) & := -i\lambda\check{F}^\delta_{\text{s-hol}}(v_{\overline{\lambda}});\\ F^\delta_{\text{s-hol}}(z_1) & := \check{F}^\delta_{\text{s-hol}}(\widetilde{u}_{\text{R1}})+\check{F}^\delta_{\text{s-hol}}(u_{\text{I}});\\ F^\delta_{\text{s-hol}}(z_2) & := \check{F}^\delta_{\text{s-hol}}(\widetilde{u}_{\text{R2}})+\check{F}^\delta_{\text{s-hol}}(u_{\text{I}}); \end{cases}$$

$$\text{Right boundary}\begin{cases} F^\delta_{\text{s-hol}}(\widetilde{u}_{\text{I1}}) & := i(1-\sqrt{2})\lambda\check{F}^\delta_{\text{s-hol}}(v_{\overline{\lambda}});\\ F^\delta_{\text{s-hol}}(\widetilde{u}_{\text{I2}}) & := i(\sqrt{2}-1)\lambda\check{F}^\delta_{\text{s-hol}}(v_{\overline{\lambda}});\\ F^\delta_{\text{s-hol}}(u_{\text{R}}) & := \lambda\check{F}^\delta_{\text{s-hol}}(v_{\overline{\lambda}});\\ F^\delta_{\text{s-hol}}(z_1) & := \check{F}^\delta_{\text{s-hol}}(\widetilde{u}_{\text{I1}})+\check{F}^\delta_{\text{s-hol}}(u_{\text{R}});\\ F^\delta_{\text{s-hol}}(z_2) & := \check{F}^\delta_{\text{s-hol}}(\widetilde{u}_{\text{I2}})+\check{F}^\delta_{\text{s-hol}}(u_{\text{R}}). \end{cases}$$

**Proposition 4.2.2.** *The function $F^\delta_{\text{s-hol}}$ is s-holomorphic on $(\overline{\Omega}^\delta \setminus \{v_0\}) \sqcup \mathcal{V}^\delta_\diamond$ with $[\bar\partial F^\delta_{\text{s-hol}}](v_0) = \frac{\lambda}{4\delta^2}$. Moreover, it satisfies Riemann-type boundary conditions, i.e. for any $z \in \partial\mathcal{V}^\delta_\diamond$ one has*

$$\operatorname{Im}[F^\delta_{\text{s-hol}}(z)\cdot\sqrt{(n(z))}] = 0.$$

*Proof.* Let us check that $F^\delta_{\text{s-hol}}$ is s-holomorphic on the upper boundary. Note that, for the above definition of the function $F^\delta_{\text{s-hol}}$ the following holds:

$$\operatorname{Proj}_{\overline{\lambda}}[F^\delta_{\text{s-hol}}(z_1)] = \operatorname{Proj}_{\overline{\lambda}}[F^\delta_{\text{s-hol}}(z_2)] = F^\delta_{\text{s-hol}}(v_{\overline{\lambda}}),$$

$$\operatorname{Proj}_{i}[F^\delta_{\text{s-hol}}(z_1)] = F^\delta_{\text{s-hol}}(u_{\text{I}}),$$
$$\operatorname{Proj}_{1}[F^\delta_{\text{s-hol}}(z_1)] = F^\delta_{\text{s-hol}}(\widetilde{u}_{\text{R}}),$$
$$\operatorname{Proj}_{i}[F^\delta_{\text{s-hol}}(z_2)] = F^\delta_{\text{s-hol}}(\widetilde{u}_{\text{I}}),$$
$$\operatorname{Proj}_{1}[F^\delta_{\text{s-hol}}(z_2)] = F^\delta_{\text{s-hol}}(u_{\text{R}}),$$

where $z_1, z_2, v_{\overline{\lambda}}, u_{\text{R}}, u_{\text{I}}, \widetilde{u}_{\text{R}}, \widetilde{u}_{\text{R}}$ are on the upper boundary as shown on Fig. 4.3. The cases of lower, right and left boundaries can be checked similarly. Therefore, $F^\delta_{\text{s-hol}}$ is s-holomorphic on $(\overline{\Omega}^\delta \setminus \{v_0\}) \sqcup \mathcal{V}^\delta_\diamond$.

We now check that $F^\delta_{\text{s-hol}}$ satisfies Riemann-type boundary conditions on the left boundary. Note that by the above definition

$$F^\delta_{\text{s-hol}}(z_1) = F^\delta_{\text{s-hol}}(\widetilde{u}_{\text{R1}}) + F^\delta_{\text{s-hol}}(u_{\text{I}}) = (\sqrt{2}-1)\lambda F^\delta_{\text{s-hol}}(v_{\overline{\lambda}}) + F^\delta_{\text{s-hol}}(u_{\text{I}}),$$

$$F^\delta_{\text{s-hol}}(z_2) = F^\delta_{\text{s-hol}}(\widetilde{u}_{\text{R2}}) + F^\delta_{\text{s-hol}}(u_{\text{I}}) = (1-\sqrt{2})\lambda F^\delta_{\text{s-hol}}(v_{\overline{\lambda}}) + F^\delta_{\text{s-hol}}(u_{\text{I}}),$$

where $z_1, z_2, v_{\overline{\lambda}}, u_{\text{I}}, \widetilde{u}_{\text{R1}}, \widetilde{u}_{\text{R2}}$ are on the left boundary as shown on Fig. 4.3. Therefore,

$$F^\delta_{\text{s-hol}}(z_1) = (\sqrt{2}-1)\lambda F^\delta_{\text{s-hol}}(v_{\overline{\lambda}}) - i\lambda F^\delta_{\text{s-hol}}(v_{\overline{\lambda}}) = \sqrt{2}\lambda F^\delta_{\text{s-hol}}(v_{\overline{\lambda}})(1-\lambda),$$

$$F^{\delta}_{\text{s-hol}}(z_2) = (1-\sqrt{2})\lambda F^{\delta}_{\text{s-hol}}(v_{\bar\lambda}) - i\lambda F^{\delta}_{\text{s-hol}}(v_{\bar\lambda}) = \sqrt{2}\lambda F^{\delta}_{\text{s-hol}}(v_{\bar\lambda})(\bar\lambda - 1),$$

since $F^{\delta}_{\text{s-hol}}(u_{\text{I}}) = -i\lambda F^{\delta}_{\text{s-hol}}(v_{\bar\lambda})$. Note that $(1-\lambda)\cdot\sqrt{(n(z_1))} \in \mathbb{R}$, $(\bar\lambda - 1)\cdot\sqrt{(n(z_2))} \in \mathbb{R}$ on the left boundary and $\lambda F^{\delta}_{\text{s-hol}}(v_{\bar\lambda}) \in \mathbb{R}$. Therefore, for any $z \in \partial\mathcal{V}^{\delta}_{\diamond}$ on the left boundary we obtain $\operatorname{Im}[F^{\delta}_{\text{s-hol}}(z)\cdot\sqrt{(n(z))}] = 0$. The cases of upper, lower and right boundaries can be checked similarly.

To finish the proof note that $[\bar\partial F^{\delta}_{\text{s-hol}}](v_0) = [\bar\partial F^{\delta}](v_0) = \frac{\lambda}{4\delta^2}$. □

Riemann boundary conditions of the coupling function imply the following local relations for the domino probabilities in hedgehog domains. These relations are not satisfied for general even domains.

**Corollary 4.2.3.** *Let $\mathbb{P}[u,v]$ be the probability that the domino $[uv]$ is contained in a random domino tiling of $\Omega^{\delta}$, where $u \in \blacklozenge$ and $v \in \lozenge$. Then for a hedgehog domain $\Omega^{\delta}$ the following holds*
*for $a \in \operatorname{Int}\lozenge$*

$$\mathbb{P}[a-\delta\lambda, a] + \mathbb{P}[a-\delta\bar\lambda, a] = \mathbb{P}[a+\delta\lambda, a] + \mathbb{P}[a+\delta\bar\lambda, a] = \frac{1}{2},$$

*for $a \in \operatorname{Int}\blacklozenge$*

$$\mathbb{P}[a, a+\delta\lambda] + \mathbb{P}[a, a-\delta\bar\lambda] = \mathbb{P}[a, a-\delta\lambda] + \mathbb{P}[a, a+\delta\bar\lambda] = \frac{1}{2}.$$

*Proof.* We check the statement for $a \in \operatorname{Int}\lozenge_0$. Let $v_0 = a$. Recall that $|C_{\Omega^{\delta}}(u,v)| = \mathbb{P}[u,v]$ for adjacent $u \in \blacklozenge$ and $v \in \lozenge$, therefore,

$$|C_{\Omega^{\delta}}(v+\delta\lambda, v)| + |C_{\Omega^{\delta}}(v-\delta\lambda, v)| + |C_{\Omega^{\delta}}(v-\delta\bar\lambda, v)| + |C_{\Omega^{\delta}}(v+\delta\bar\lambda, v)| = 1.$$

On the other hand,

$$C_{\Omega^{\delta}}(v+\delta\lambda, v) - C_{\Omega^{\delta}}(v-\delta\lambda, v) + iC_{\Omega^{\delta}}(v-\delta\bar\lambda, v) - iC_{\Omega^{\delta}}(v+\delta\bar\lambda, v) = 1.$$

Hence,

$$\begin{aligned}
\mathbb{P}[v_0+\delta\lambda, v_0] &= C_{\Omega^{\delta}}(v_0+\delta\lambda, v_0) = \delta F^{\delta}_{\text{s-hol}}(v_0+\delta\lambda),\\
\mathbb{P}[v_0-\delta\lambda, v_0] &= -C_{\Omega^{\delta}}(v_0-\delta\lambda, v_0) = -\delta F^{\delta}_{\text{s-hol}}(v_0-\delta\lambda),\\
\mathbb{P}[v_0+\delta\bar\lambda, v_0] &= -iC_{\Omega^{\delta}}(v_0+\delta\bar\lambda, v_0) = -i\delta F^{\delta}_{\text{s-hol}}(v_0+\delta\bar\lambda),\\
\mathbb{P}[v_0-\delta\bar\lambda, v_0] &= iC_{\Omega^{\delta}}(v_0-\delta\bar\lambda, v_0) = i\delta F^{\delta}_{\text{s-hol}}(v_0-\delta\bar\lambda).
\end{aligned}$$

In Section 4.1.3 we showed that the primitive $H^{\delta}$ of the square of the solution $F^{\delta}_{\text{s-hol}}$ of a discrete boundary value problem $\operatorname{RBVP}(\Omega^{\delta}, v_0)$ defined by (1.1) is well-defined, therefore, for $z_{\bullet}$, $z'_{\bullet}$, $z''_{\bullet}$, $z_{\circ}$, $z'_{\circ}$, $z''_{\circ}$ and $v_0$ as shown on Fig. 4.2

$$\begin{aligned}
0 =&(H(z_{\bullet}) - H(z'_{\circ})) + (H(z'_{\circ}) - H(z'_{\bullet})) + (H(z'_{\bullet}) - H(z_{\circ}))+\\
&(H(z_{\circ}) - H(z''_{\bullet})) + (H(z''_{\bullet}) - H(z''_{\circ})) + (H(z''_{\circ}) - H(z_{\bullet})) =\\
&i\delta\left(\tfrac{\lambda}{\sqrt{2}}\left(F^{\delta}_{\text{s-hol}}(v_0-\delta\lambda) - iF^{\delta}_{\text{s-hol}}(v_0-\delta\bar\lambda)\right)\right)^2 - i\delta\left(\tfrac{\lambda}{\sqrt{2}}\left(F^{\delta}_{\text{s-hol}}(v_0+\delta\lambda) - iF^{\delta}_{\text{s-hol}}(v_0+\delta\bar\lambda)\right)\right)^2\\
&= -\tfrac{1}{2}\left(F^{\delta}_{\text{s-hol}}(v_0+\delta\lambda) - iF^{\delta}_{\text{s-hol}}(v_0+\delta\bar\lambda) + F^{\delta}_{\text{s-hol}}(v_0-\delta\lambda) - iF^{\delta}_{\text{s-hol}}(v_0-\delta\bar\lambda)\right) =\\
&\tfrac{1}{2\delta}\left(\left(\mathbb{P}[v_0-\delta\lambda, v_0] + \mathbb{P}[v_0-\delta\bar\lambda, v_0]\right) - \left(\mathbb{P}[v_0+\delta\lambda, v_0] + \mathbb{P}[v_0+\delta\bar\lambda, v_0]\right)\right).
\end{aligned}$$

To obtain the result for $a \in \operatorname{Int}\lozenge_1$ rotate $\Omega^{\delta}$ by $\pi$ and note that $\lozenge_0$ and $\lozenge_1$ change the roles. For $a \in \operatorname{Int}\blacklozenge_{1,2}$ rotate $\Omega^{\delta}$ by $\frac{\pi}{2}$ and $\frac{3\pi}{2}$. □

### 4.2.2 Proof of the convergence

Let $F^{\delta}_{\text{s-hol}}$ solve the discrete Riemann boundary value problem RBVP$(\Omega^{\delta}, v_0)$. In this section we prove the convergence of $F^{\delta}_{\text{s-hol}}$ to its continuous counterpart.

Let $F^{\delta}_{\mathbb{C},v_0^{\delta}}$ be the unique discrete s-holomorphic function on the whole plane $\mathbb{C}^{\delta} \setminus \{v_0^{\delta}\}$ tending to zero at infinity and such that $[\bar{\partial}^{\delta} F^{\delta}_{\mathbb{C},v_0^{\delta}}](v_0^{\delta}) = \frac{\lambda}{4\delta^2}$. The function $F^{\delta}_{\mathbb{C}(z),v_0^{\delta}}$ is asymptotically equal to $\frac{1}{2\pi} \cdot \frac{\lambda}{z-v_0}$ as $\delta \downarrow 0$, see [21, Theorem 2.21]. Let us define a discrete primitive $H^{\delta}_{\star} \colon \mathcal{V}^{\delta}_{\bullet} \sqcup \mathcal{V}^{\delta}_{\circ} \to \mathbb{R}$ of the difference $F^{\delta}_{\text{s-hol}} - F^{\delta}_{\mathbb{C},v_0^{\delta}}$ in the same way as above:

$$H^{\delta}_{\star}(z_2) - H^{\delta}_{\star}(z_1) = [F^{\delta}_{\text{s-hol}} - F^{\delta}_{\mathbb{C},v_0^{\delta}}]^2(a) \cdot (z_2 - z_1), \tag{2.6}$$

where $z_1 \in \mathcal{V}^{\delta}_{\circ}$, $z_2 \in \mathcal{V}^{\delta}_{\bullet}$ are two vertices of the same square $a$.

**Remark 4.2.4.** *The difference $F^{\delta}_{\text{s-hol}} - F^{\delta}_{\mathbb{C},v_0^{\delta}}$ is s-holomorphic everywhere on $\mathcal{V}^{\delta}_{\diamond} \sqcup \overline{\Omega}^{\delta}$, therefore the function $H^{\delta}_{\star}$ is leap-frog subharmonic on $\mathcal{V}^{\delta}_{\circ}$ and it is leap-frog superharmonic on $\mathcal{V}^{\delta}_{\bullet}$.*

The following convergence theorem for s-holomorphic functions is a straightforward analogue of [36, Theorem 1.8]. Alternatively, one can use ideas described in the proof of [17, Theorem 5.5] or ideas from the proof of [18, Theorem 2.16].

**Theorem 4.2.5.** *Let $\Omega^{\delta}$ be a sequence of discrete hedgehog domains of mesh size $\delta$ approximating a simply connected domain $\Omega$. Let $v_0^{\delta}$ approximate an inner point $v \in \Omega$. Then $F^{\delta}_{\text{s-hol}}$ converges uniformly on compact subsets of $\Omega \setminus \{v\}$ to a continuous holomorphic function $f^{v}_{\Omega}$, where $f^{v}_{\Omega}$ is defined as in Proposition* 4.1.9 *(or is defined by (1.4), if $\Omega$ is not smooth).*

The proof is done following the ideas described in [18] and using results described in [22].

*Proof.* Let $u^{\delta}$ be a square on the square lattice with mesh size $\delta$. We denote by $B^{\delta}_{r}(u^{\delta})$ the set of squares and vertices on this lattice such that the distance from them to $u^{\delta}$ is less than or equal to $r$. Let $\partial B^{\delta}_{r}(u^{\delta})$ be the set of boundary squares and vertices of the set $B^{\delta}_{r}(u^{\delta})$.

Let $\Omega^{\delta}_{r} = (\Omega^{\delta} \sqcup \mathcal{V}^{\delta}) \setminus B^{\delta}_{r}(v_0^{\delta})$. Let $M^{\delta}(r) = \max\limits_{z^{\delta} \in \Omega^{\delta}_{r}} |H^{\delta}(z^{\delta})|$.

*1. Assume that for each fixed positive $r$ the function $M^{\delta}(r)$ is bounded, as $\delta \to 0$.*

Theorem 3.12 in [22] implies that the functions $F^{\delta}_{\text{s-hol}}$ are uniformly bounded and therefore equicontinuous on $\Omega^{\delta}_{r}$. Thus, due to the Arzelà–Ascoli theorem, the family $F^{\delta}_{\text{s-hol}}$ is precompact and hence converges along a subsequence to some holomorphic function $\widetilde{f}$ and $H^{\delta}$ converges to $\widetilde{h} := \operatorname{Re} \int \widetilde{f}^2$ uniformly on compact subsets of $\Omega \setminus \{v\}$. Let us show that $\widetilde{f} = f^{v}_{\Omega}$. It is enough to check that $\widetilde{f}$ satisfies properties (h1) – (h3). Then the uniqueness of a solution of the boundary value problem (f1) – (f2) implies that $\widetilde{f}$ coincides with the function $f^{v}_{\Omega}$.

Discrete Dirichlet boundary conditions together with the maximum principle for $H^{\delta}$ implies $\widetilde{h} \equiv 0$ on $\partial\Omega$, which gives us (h1). It follows from [22, Remark 6.3] that we also

have (h2). The fact that $F^{\delta}_{\mathbb{C}(z),v_0^\delta}$ is asymptotically equal to $\frac{1}{2\pi}\cdot\frac{\lambda}{z-v_0}$ implies that $H^\delta_\star$ converges to a harmonic function $\widetilde{h}_\star := \operatorname{Re}\int\left(\widetilde{f}(z)-\frac{1}{2\pi}\cdot\frac{\lambda}{z-v}\right)^2 dz$. Remark 4.2.4 gives us that $\widetilde{h}_\star$ is bounded in a vicinity of $v$. Hence $\widetilde{f}$ satisfies properties (h1) – (h3), so $\widetilde{f}=f^v_\Omega$.

*2. Now, suppose that, for some $r>0$, $M^\delta(r)$ tends to infinity along a subsequence as $\delta\to 0$.*

Let us show that this is impossible. Consider renormalized functions $\widetilde{F}^\delta := \frac{F^\delta_{\text{s-hol}}}{\sqrt{M^\delta(r)}}$ and $\widetilde{H}^\delta := \frac{H^\delta}{M^\delta(r)}$. Using the same arguments as above, we can show that the family $\widetilde{F}^\delta$ converges to some holomorphic function $\widetilde{f}$ and $\widetilde{H}^\delta$ converges to the harmonic function $\widetilde{h}=\operatorname{Re}\int\widetilde{f}^2$ on compact subsets of $\Omega\smallsetminus B_r(v)$.

Suppose that $\widetilde{h}$ cannot be identically zero. Then for any $0<r'<r$ there exists $C(r',r)$ independent of $\delta$, such that $M^\delta(r')\le C(r',r)\cdot M^\delta(r)$. Therefore we may assume that $\widetilde{H}^\delta$ converges to $\widetilde{h}$ uniformly on each $\Omega_{r'}=\Omega\smallsetminus B_{r'}(v)$. Arguing as above, we see that $\widetilde{h}$ is harmonic and satisfies properties (h1) – (h2). Moreover, since $\frac{F^\delta_{\mathbb{C},v_0^\delta}}{\sqrt{M^\delta(r)}}$ tends to zero (as $\delta\to 0$), the limit of $\widetilde{H}^\delta_\star$ coincides with $\widetilde{h}$. Therefore $\widetilde{h}$ is bounded in a vicinity of $v$, satisfies Dirichlet boundary conditions $h\equiv 0$ on $\partial\Omega$ and has a nonnegative outer normal derivative. This contradicts the maximum principle, if it is not identically zero.

*3. To complete the proof it remains to show that none of the subsequential limits of $\widetilde{H}^\delta$ is identically zero.*

Suppose that $\widetilde{H}^\delta$ converges to zero uniformly on compact subsets of $\Omega\smallsetminus B_r(v)$. Let $z^\delta_{\max}$ be chosen so that $1=\sup\limits_{z^\delta\in\Omega^\delta_r}|\widetilde{H}^\delta(z^\delta)|=|\widetilde{H}^\delta(z^\delta_{\max})|$. Since $\widetilde{H}^\delta$ vanishes on the boundary, the discrete maximum principle implies that $z_{\max}\in\partial B^\delta_r(v^\delta_0)$.

Consider the function $\frac{H^\delta_\star}{M^\delta(r)}$. Note that it tends to zero on compact subsets of $\Omega\smallsetminus B_r(v)$. Therefore the maximum principle together with Remark 4.2.4 implies that $\frac{H^\delta_\star}{M^\delta(r)}$ tends to zero in the neighbourhood of $\partial B_r(v)$. Hence, each of the functions $\frac{F^\delta_{\text{s-hol}}-F^\delta_{\mathbb{C},v_0^\delta}}{\sqrt{M^\delta(r)}}$, $\frac{F^\delta_{\text{s-hol}}}{\sqrt{M^\delta(r)}}$ and $\frac{H^\delta}{M^\delta(r)}$ tends to zero uniformly in the neighbourhood of $\partial B_r(v)$. In particular, we have $1=|\widetilde{H}^\delta(z^\delta_{\max})|\to 0$, which is a contradiction. □

To show the convergence of the fluctuations of the height function we need to show the convergence of the coupling function up to a straight horizontal boundary segment. To prove Theorem 1.1.7 we also need a version of Theorem 4.2.5 for the boundary vertex $v$. In order to obtain these results we need to introduce discrete Schwarz reflection principle for hedgehog-type straight boundary. We also need to introduce an analog of the function $F^\delta_{\mathbb{C},v_0^\delta}(u)$ in the upper half-plane.

**Lemma 4.2.6** (discrete Schwarz reflection principle)**.** *Let $F^\delta_{\mathbb{H}}:\blacklozenge\to\mathbb{C}$ be a discrete holomorphic on the upper half plane $\mathbb{H}^\delta$, such that $\operatorname{Im}F^\delta_{\mathbb{H}}(u)=0$ on the real axis, see*

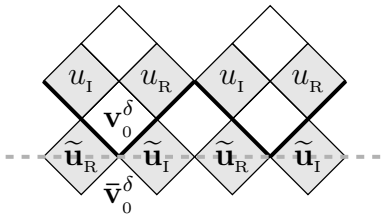


Figure 4.4: The upper half plane $\mathbb{H}^\delta$ and its boundary (solid line). The real axis (dashed). On the real axis $\mathrm{Im}F^\delta_{\mathbb{H}}(u) = F^\delta_{\mathbb{H}}(\widetilde{u}_I) = 0$. The function $F^\delta_{\mathbb{H},v_0^\delta}$ equals zero on the boundary, and $[\bar\partial^\delta F^\delta_{\mathbb{H},v_0^\delta}](v_0^\delta) = \frac{\lambda}{\delta^2}$, $\bar v_0^\delta = v_0^\delta - i\sqrt{2}\delta$.

*Fig. 4.4. Then the function $F^\delta_{\mathbb{C}}$ defined by*

$$\begin{cases} F^\delta_{\mathbb{C}}(u) := F^\delta_{\mathbb{H}}(u) & \text{if } u \in \mathbb{H}^\delta \\ F^\delta_{\mathbb{C}}(u) := \overline{F^\delta_{\mathbb{H}}(\bar u)} & \text{if } u \in \mathbb{C}^\delta \setminus \mathbb{H}^\delta \end{cases}$$

*is discrete holomorphic on the whole plane $\mathbb{C}^\delta$, where squares $u$ and $\bar u$ are symmetric with respect to the real axis.*

*Proof.* Note that on the upper half plane $\bar\partial^\delta F^\delta_{\mathbb{C}} = \bar\partial^\delta F^\delta_{\mathbb{H}} = 0$. Therefore we need to check that $[\bar\partial^\delta F^\delta_{\mathbb{C}}](\bar v) = 0$ for all $v \in \mathbb{H}^\delta$:

$$[\bar\partial^\delta F^\delta_{\mathbb{C}}](\bar v) = \frac{1}{2}\left(\frac{F^\delta_{\mathbb{C}}(\bar v + \delta\lambda) - F^\delta_{\mathbb{C}}(\bar v - \delta\lambda)}{2\delta\bar\lambda} + \frac{F^\delta_{\mathbb{C}}(\bar v + \delta\bar\lambda) - F^\delta_{\mathbb{C}}(\bar v - \delta\bar\lambda)}{2\delta\lambda}\right) =$$
$$\frac{1}{2}\left(\frac{\overline{F^\delta_{\mathbb{H}}(v + \delta\bar\lambda)} - \overline{F^\delta_{\mathbb{H}}(v - \delta\bar\lambda)}}{2\delta\bar\lambda} + \frac{\overline{F^\delta_{\mathbb{H}}(v + \delta\lambda)} - \overline{F^\delta_{\mathbb{H}}(v - \delta\lambda)}}{2\delta\lambda}\right) = \overline{[\bar\partial^\delta F^\delta_{\mathbb{H}}](v)} = 0.$$

To complete the proof, note that for $u$ on the real axis $\overline{F^\delta_{\mathbb{H}}(u)} = F^\delta_{\mathbb{H}}(u)$. □

Let us introduce a function $F^\delta_{\mathbb{H},v_0^\delta} : \blacklozenge \to \mathbb{C}$ on the half-plane $\mathbb{H}^\delta$. The function $F^\delta_{\mathbb{H},v_0^\delta}$ equals zero on the boundary, and $[\bar\partial^\delta F^\delta_{\mathbb{H},v_0^\delta}](v_0^\delta) = \frac{\lambda}{\delta^2}$. Let $F_1^\delta$ and $F_2^\delta$ be two different discrete holomorphic functions that satisfy these two properties and tend to zero at infinity. Then the difference $F_1^\delta - F_2^\delta$ is discrete holomorphic everywhere in $\mathbb{H}^\delta$, vanishes on the boundary and tends to zero at infinity. Therefore $F_1^\delta - F_2^\delta \equiv 0$. Thus, there is a unique such discrete holomorphic function $F^\delta_{\mathbb{H},v_0^\delta}$.

Let us consider the sum $F^\delta_{\mathbb{C},v_0^\delta} + F^\delta_{\mathbb{C},v_0^\delta - i\sqrt{2}\delta}$, where by $v_0^\delta - i\sqrt{2}\delta$ we denote a white square symmetric to $v_0^\delta$ with respect to the real axis that does not belong to $\mathbb{H}^\delta$, see Fig. 4.4. This sum tends to zero at infinity, since both $F^\delta_{\mathbb{C},v_0^\delta}$ and $F^\delta_{\mathbb{C},v_0^\delta - i\sqrt{2}\delta}$ tend to zero at the infinity. Note that $F^\delta_{\mathbb{C},v_0^\delta - i\sqrt{2}\delta}$ is discrete holomorphic on $\mathbb{H}^\delta$, therefore $F^\delta_{\mathbb{C},v_0^\delta} + F^\delta_{\mathbb{C},v_0^\delta - i\sqrt{2}\delta}$ is holomorphic on $\mathbb{H}^\delta \setminus \{v_0^\delta\}$ and $[\bar\partial^\delta(F^\delta_{\mathbb{C},v_0^\delta} + F^\delta_{\mathbb{C},v_0^\delta - i\sqrt{2}\delta})](v_0^\delta) = \frac{\lambda}{\delta^2}$. Finally, note that

$$\mathrm{Im}F^\delta_{\mathbb{C},v_0^\delta}(u) = G^\delta(u, v_0^\delta + \bar\lambda\delta) - G^\delta(u, v_0^\delta - \bar\lambda\delta),$$

where $G^\delta(u,u')$ is the classical Green's function on $\mathbb{C}^\delta \cap \blacklozenge^\delta_1$ satisfying $\Delta^\delta G^\delta(u,u') = \mathbb{1}_{u=u'} \cdot \frac{1}{2\delta^3}$. The Green's function is symmetric, therefore $\mathrm{Im}[F^\delta_{\mathbb{C},v_0^\delta} + F^\delta_{\mathbb{C},v_0^\delta - i\sqrt{2}\delta}]$ vanishes

on $\partial\mathbb{H}^\delta$. Similarly the real part of $F^\delta_{\mathbb{H},v_0^\delta}$ vanishes on the boundary. As a consequence we have $F^\delta_{\mathbb{H},v_0^\delta}(u) = F^\delta_{\mathbb{C},v_0^\delta}(u) + F^\delta_{\mathbb{C},v_0^\delta - i\sqrt{2}\delta}(u)$ for all $u \in \blacklozenge \cap \mathbb{H}^\delta$.

We will call a part of the boundary of hedgehog domain $\Omega^\delta$ *a right vertical straight part of the boundary* if all inner boundary squares along this part belong to the set $\partial^+_{\text{int}}\Omega^\delta$. Similarly one can define *left vertical*, *upper horizontal* and *lower horizontal* straight parts of the boundary of hedgehog domain.

**Proposition 4.2.7.** *1. Let $J$ be an open straight horizontal (or vertical) segment of the boundary of $\Omega$. Then the uniform convergence in Theorem 4.2.5 holds on compact subsets of $(\Omega \cup J) \setminus \{v\}$.*

*2. Let in the setup of Theorem 4.2.5 the square $v_0^\delta$ on a horizontal part of the boundary of $\Omega^\delta$ approximate a boundary point $v$, which lies on a straight horizontal segment of the boundary of $\Omega$. Then $F^\delta_{\text{s-hol}}$ converges uniformly on compact subsets of $\Omega \setminus \{v\}$ to a continuous holomorphic function $f^v_\Omega$, where $f^v_\Omega$ is defined as in Lemma* 4.1.10 *(or is defined by (1.5), if $\Omega$ is not smooth).*

*Proof.* Reflect $\Omega^\delta$ across the lower horizontal straight part of the boundary to get a domain $\mho_\delta$. Glue domains $\Omega^\delta$ and $\mho_\delta$ together, note that the resulting domain is a hedgehog domain. The discrete holomorphic function $\check{F}^\delta_{\text{s-hol}}|_{\blacklozenge^\delta}$ which is zero on the lower horizontal straight part of $\partial\Omega^\delta$ extends to a discrete holomorphic function on this glued domain by discrete Schwarz reflection principle, see Lemma 4.2.6. Then one can define a function $F^\delta_{\text{s-hol}}$ on the glued hedgehog domain as above. The argument of Theorem 4.2.5 can then be applied in this case, with $F^\delta_{\mathbb{C},v_0^\delta}$ replaced by $F^\delta_{\mathbb{H},v_0^\delta}$. □

## 4.3 Dimers on hedgehog domains and the Gaussian Free Field

In [42] Kenyon proved that the scaling limit of the height function in the dimer model on Temperleyan domains is the Gaussian Free Field. In Section 3.3 it is proven, that the same scaling limit appears for approximations by piecewise Temperleyan domains. Our goal in this section is to show that the same holds for approximations by hedgehog domains.

### 4.3.1 Asymptotic values of the coupling function

Following [41], we define two functions $f_0(z_1, z_2)$ and $f_1(z_1, z_2)$. For a fixed $z_2$,

- ▷ the function $f_0(z_1, z_2)$ is analytic as a function of $z_1$, has a simple pole of residue $1/2\pi$ at $z_1 = z_2$, and no other poles on $\Omega$;
- ▷ $f_0(z, z_2)||\frac{1}{\sqrt{(n(z))}}, \quad z \in \partial\Omega.$

The function $f_1(z_1, z_2)$ has the same definition, except for a difference in the boundary conditions: $f_1(z, z_2)||\frac{i}{\sqrt{(n(z))}}, \quad z \in \partial\Omega$. The existence and uniqueness of such functions can be shown using the technique described in Section 4.1.4, see Proposition 4.1.9. In particular, we can write these functions on the upper half plane in the following way:

$$f_0(z, w) = \frac{1}{2\pi} \cdot \left( \frac{1}{z - w} + \frac{i}{z - \overline{w}} \right),$$

$$f_1(z,w) = \frac{1}{2\pi} \cdot \left( \frac{1}{z-w} - \frac{i}{z-\overline{w}} \right).$$

**Theorem 4.3.1.** *Let $\Omega$ be a simply connected domain in $\mathbb{C}$. Assume that a sequence of discrete hedgehog domains $\Omega^\delta$ of mesh sizes $\delta$ approximates the domain $\Omega$. Let a sequence of white squares $v^\delta$ approximates a point $v \in \Omega$. Then the coupling function $\frac{1}{\delta} C_{\Omega^\delta}(u,v)$ satisfies the following asymptotics:*
*for $v^\delta \in \diamondsuit_0^\delta$*

$$\frac{1}{\delta} C_{\Omega^\delta}(u, v^\delta) - \bar{\lambda} \cdot F^\delta_{\mathbb{C}, v^\delta}(u) = f_0(u,v) - \frac{1}{2\pi(u-v)} + o(1);$$

*if $v^\delta \in \diamondsuit_1^\delta$, then*

$$\frac{1}{\delta} C_{\Omega^\delta}(u, v^\delta) - \bar{\lambda} \cdot F^\delta_{\mathbb{C}, v^\delta}(u) = f_1(u,v) - \frac{1}{2\pi(u-v)} + o(1),$$

*where $F^\delta_{\mathbb{C}, v^\delta}(u)$ is defined in Section 4.2.2.*

*Proof.* Recall that $F^\delta_{\mathbb{C}(z), v_0^\delta}$ is asymptotically equal to $\frac{1}{2\pi} \cdot \frac{\lambda}{z - v_0}$ as $\delta \downarrow 0$. Recall that the function $F^\delta_{\text{s-hol}}(\cdot)$ coincides with $\frac{1}{\delta} C_{\Omega^\delta}(\cdot, v_0)$ on the set $\text{Int}\blacklozenge^\delta \cup \partial^\flat_{\text{int}} \blacklozenge^\delta \cup \partial^\sharp_{\text{int}} \blacklozenge^\delta$. Now, to obtain the first asymptotic one can use Theorem 4.2.5. The second one can be obtained similarly. To see this note that for $v^\delta \in \diamondsuit_1^\delta$ the function $\frac{i}{\delta} C_{\Omega^\delta}(\,\cdot\,, v^\delta)$ is discrete holomorphic everywhere in $\diamondsuit^\delta \setminus v^\delta$ with $[\bar{\partial}^\delta \frac{i}{\delta} C_{\Omega^\delta}(\,\cdot\,, v^\delta)](v^\delta) = \frac{i\lambda}{\delta^2}$ and satisfies the same boundary conditions as $\frac{1}{\delta} C_{\Omega^\delta}(\,\cdot\,, v^\delta)$ for $v^\delta \in \diamondsuit_0^\delta$. □

### 4.3.2 Convergence to GFF

To obtain the convergence of the height function on hedgehog domains to the Gaussian free field it is enough to show that the limits of moments of the height function in the Temperleyan and hedgehog cases are the same. As in Section 3.3.3 we give only the sketch of the proof of Corollary 1.1.4. The novel part of the argument is in (3.9), then Lemma 4.3.3 completes the proof.

Due to [41] one can obtain the following result for hedgehog approximations. Let $f_+(z,w) = f_0(z,w) + f_1(z,w)$ and $f_-(z,w) = f_0(z,w) - f_1(z,w)$.

**Proposition 4.3.2.** *Let $\gamma_1, \dots, \gamma_m$ be a collection of pairwise disjoint paths running from the horizontal straight boundary segment of $\Omega$ to $z_1, \dots, z_m$ respectively. Let $h(z_i)$ denote the height function at a point in a hedgehog domain $\Omega^\delta$ lying within $O(\delta)$ of $z_i$. Then*

$$\lim_{\delta \to 0} \mathbb{E}[(h(z_1) - \mathbb{E}[h(z_1)]) \cdot \ldots \cdot (h(z_m) - \mathbb{E}[h(z_m)])] \; = \tag{3.7}$$

$$\sum_{\epsilon_1, \dots, \epsilon_m \in \{-1,1\}} \epsilon_1 \cdots \epsilon_m \int_{\gamma_1} \cdots \int_{\gamma_m} \det_{i,j \in [1,m]} (F_{\epsilon_i, \epsilon_j}(z_i, z_j))\, dz_1^{(\epsilon_1)} \cdots dz_m^{(\epsilon_m)}, \tag{3.8}$$

*where* $dz_j^{(1)} = dz_j$ *and* $dz_j^{(-1)} = d\overline{z_j}$, *and*

$$F_{\epsilon_i,\epsilon_j}(z_i,z_j) = \begin{cases} 0 & i=j \\ f_+(z_i,z_j) & (\epsilon_i,\epsilon_j)=(1,1) \\ f_-(z_i,z_j) & (\epsilon_i,\epsilon_j)=(-1,1) \\ \overline{f_-(z_i,z_j)} & (\epsilon_i,\epsilon_j)=(1,-1) \\ \overline{f_+(z_i,z_j)} & (\epsilon_i,\epsilon_j)=(-1,-1). \end{cases}$$

*Proof.* The function $F^{\delta}_{\text{s-hol}}(\cdot)$ coincides with $\frac{1}{\delta}C_{\Omega^\delta}(\cdot,v_0)$ on the set $\text{Int}\blacklozenge^\delta \cup \partial^\flat_{\text{int}}\blacklozenge^\delta \cup \partial^\sharp_{\text{int}}\blacklozenge^\delta$. Therefore, due to Theorem 4.2.5 and Proposition 4.2.7 one has convergence of the coupling function up to the horizontal straight part of the boundary. The rest of the proof of the proposition mimics the proof of [41, Proposition 20]. □

Recall that in the Temperleyan case [41] one has $f_+(z,w) = \frac{1}{\pi(z-w)}$ and $f_-(z,w) = \frac{1}{\pi(z-\overline{w})}$. In the hedgehog case we have

$$\begin{cases} f_+(z,w) = \frac{1}{\pi(z-w)} \\ f_-(z,w) = i\cdot\frac{1}{\pi(z-\overline{w})}. \end{cases} \tag{3.9}$$

**Lemma 4.3.3.** *The limits of moments of the height function in Temperleyan case and hedgehog case are the same.*

*Proof.* It is easy to check that the determinants in (3.8) are the same for both cases. □

**Remark 4.3.4** (conformal covariance)**.** *Let* $\Omega$ *and* $\Omega'$ *be simply connected domains. Let* $f^\Omega_+(z,w)$ *and* $f^\Omega_-(z,w)$ *be the functions defined as above for the region* $\Omega$. *The function* $f^\Omega_+(z,w)$ *is holomorphic in both variables and the function* $f^\Omega_-(z,w)$ *is holomorphic in* $z$ *and antiholomorphic in* $w$. *Let* $\phi$ *be a conformal mapping of* $\Omega$ *onto* $\Omega'$. *Then*

$$f^\Omega_+(z,w) = f^{\Omega'}_+(\phi(z),\phi(w))\cdot(\phi'(z))^{\frac{1}{2}}\cdot(\phi'(w))^{\frac{1}{2}},$$

$$f^\Omega_-(z,w) = f^{\Omega'}_-(\phi(z),\phi(w))\cdot(\phi'(z))^{\frac{1}{2}}\cdot\overline{(\phi'(w))}^{\frac{1}{2}}.$$

By Lemma 4.3.3 the following proposition holds for hedgehog domains as well. Therefore the rest of the argument of the proof of Corollary 1.1.4 is exactly as in [42, Theorem 1.1].

**Proposition 4.3.5** ([42])**.** *Let* $\Omega$ *be a simply connected domain. Let* $z_1,\dots,z_m$ *(with* $m$ *even) be distinct points of* $\Omega$. *Let* $\Omega^\delta$ *be a hedgehog approximation of* $\Omega$ *and* $h_{\Omega^\delta}$ *be the height function of a uniform domino tiling in the domain* $\Omega^\delta$. *Then*

$$\lim_{\delta\to 0}\mathbb{E}[(h_{\Omega^\delta}(z_1)-\mathbb{E}[h_{\Omega^\delta}(z_1)])\cdot\ldots\cdot(h_{\Omega^\delta}(z_m)-\mathbb{E}[h_{\Omega^\delta}(z_m)])] \;=$$
$$\left(-\frac{16}{\pi}\right)^{m/2}\sum_{pairings\,\alpha} g_D(z_{\alpha(1)},z_{\alpha(2)})\cdot\ldots\cdot g_D(z_{\alpha(m-1)},z_{\alpha(m)}),$$

*where* $g_D$ *is the Green function with Dirichlet boundary conditions on* $\Omega$.

And the following lemma completes the proof of Corollary 1.1.4.

**Lemma 4.3.6** ([6, 42])**.** *A sequence of multidimensional random variables whose moments converge to the moments of a Gaussian, converges itself to a Gaussian.*

In Section 2.2 it was shown that there is a factorization of the gradient of the expectation of the height function in the double-dimer model into a product of two discrete holomorphic functions. In this section we use this factorisation and result of Theorem 4.2.5 to show the convergence of the expectation of the double-dimer height function to the harmonic measure for approximations by hedgehog domains.

### 4.4.1 A factorization of the double-dimer coupling function

Let $F\colon \bar{\blacklozenge} \to \mathbb{C}$ be a function such that $F|_{\partial\blacklozenge} = 0$ and $F$ is discrete holomorphic everywhere in $\lozenge$ except at the face $v_0$ where one has $[\bar{\partial}F](v_0) = \lambda$. Similarly, let $G : \bar{\lozenge} \to \mathbb{C}$ be a function such that $G|_{\partial\lozenge} = 0$ and $G$ is discrete holomorphic everywhere in $\blacklozenge$ except at the face $u_0$ where one has $[\bar{\partial}G](u_0) = i$. Let $u \in \blacklozenge$ and $v \in \lozenge$, then due to [68, Proposition 3.11] $C_{\text{dbl-d},\Omega}(u, v) = \text{const} \cdot F(u)G(v)$, where const $= \frac{1}{4G(v_0)}$.

Note that the function $F$ (resp., G) coincide with the dimer coupling function $C_\Omega(\cdot, v_0)$ (resp., $C_\Omega(u_0, \cdot)$) up to a multiplicative constant.

### 4.4.2 Proof of Theorem 1.1.7

From now onwards, let $u_0$ be a point on a lower horizontal straight part of the boundary of the domain $\Omega$, and $v_0$ be a point on a right vertical straight part of $\partial\Omega$. Let $f_\Omega := f_\Omega^{v_0}$ and $g_\Omega := f_\Omega^{u_0}$, where $f_\Omega^v(z)$ solves boundary value problem (F1)–(F2) described in Lemma 4.1.10. Note that due to Proposition 4.2.7 the function $F^\delta$ converges to $f_\Omega$ and the function $G^\delta$ converges to $g_\Omega$. Now to complete the proof of Theorem 1.1.7 it remains to prove the following:

**Proposition 4.4.1.** *Let $\Omega$ be a bounded simply connected domain in $\mathbb{C}$ with smooth boundary. Let $v_0$ and $u_0$ be the points on the straight part of the boundary of the domain $\Omega$. Assume that the boundary arc $(u_0v_0)$ contains 0. Then the function*

$$\int_0^w \mathrm{Re}[f_\Omega(z)g_\Omega(z)\,dz]$$

*is proportional to the harmonic measure* $\mathrm{hm}_\Omega(w, (v_0u_0))$ *in the domain $\Omega$.*

*Proof.* Let $\phi$ be a conformal mapping of the domain $\Omega$ onto the unit disk $\mathbb{D}$ such that $v_0$ mapped onto $-i$ and $u_0$ mapped onto 1. Note that $\phi'(v_0) > 0$ and $\phi'(u_0) > 0$, since $u_0$ (resp., $v_0$) is a point on a lower horizontal (reps., right vertical) straight part of $\partial\Omega$. Let us consider the product of functions $f_\Omega(z)$ and $g_\Omega(z)$. It equals

$$\begin{aligned} f_\Omega(z)\cdot g_\Omega(z) &= \frac{1}{2\pi}\left(\frac{\mu-\phi(v_0)\bar{\mu}}{\phi(z)-\phi(v_0)}\right)\cdot(\phi'(z))^{\frac{1}{2}}\cdot(\phi'(v_0))^{\frac{1}{2}} \\ &\quad\times\frac{1}{2\pi}\left(\frac{\mu-\phi(u_0)\bar{\mu}}{\phi(z)-\phi(u_0)}\right)\cdot(\phi'(z))^{\frac{1}{2}}\cdot(\phi'(u_0))^{\frac{1}{2}} \\ = \frac{ci\lambda\cdot\phi'(z)}{(\phi(z)-\phi(v_0))(\phi(z)-\phi(u_0))} &= \frac{\bar{\lambda}c}{\phi(v_0)-\phi(u_0)}\cdot\left(\log\frac{(\phi(z)-\phi(v_0))}{(\phi(z)-\phi(u_0))}\right)', \end{aligned}$$

hence $\int \mathrm{Re}[fgdz]$ is proportional to $\frac{1}{\pi}\mathrm{Im}\left[\log\left(\frac{\phi(z)-\phi(v_0)}{\phi(z)-\phi(u_0)}\right)\right]$ which is the harmonic measure of $(v_0u_0)$. □

# Chapter 5

# Dimers and circle patterns

## 5.1 Bipartite graphs and circle patterns

In this section, we establish a correspondence between bipartite graphs with positive face weights and circle patterns with embedded dual. While the construction can be extended to general real weights, certain aspects are nicer in the positive weight case, in particular the embedding property of the dual graph (Theorem 5.1.2 below).

The correspondence holds for several different types of boundary conditions. Although in the intermediate steps we discuss somewhat general boundary conditions, for the final result (Theorem 5.1.2) we will need to consider only the (simplest) case of a circle pattern with outer face of degree 4 (which is necessarily cyclic).

### 5.1.1 Centers of circle patterns

Let $\mathcal{G}$ be a connected embedded bipartite planar graph. Let $\hat{\mathcal{G}}$ be obtained from $\mathcal{G}$ by adding a vertex $v_\infty$ connected to all vertices on $\mathcal{G}$'s outer face. Let $\mathcal{G}^*$ be the planar dual of $\hat{\mathcal{G}}$. We call the vertices of $\mathcal{G}^*$ on its outer face the *outer dual vertices*. There is one outer dual vertex for every edge on the outer face of $\mathcal{G}$. We refer to $\mathcal{G}^*$ as the *augmented dual* of $\mathcal{G}$ to distinguish it from the usual dual.

Suppose $z : V \to \mathbb{C}$ is an embedding of $\mathcal{G}$ with cyclic faces, except perhaps the outer face, which we assume convex. Assume also that each bounded face contains its circumcenter.

The circumcenters then form an embedding $u : F \to \mathbb{C}$ of the graph $\mathcal{G}^*$, except for the outer dual vertices. For each outer dual vertex $v$ of $\mathcal{G}^*$ define $u(v)$ to be a point on the perpendicular bisector of the corresponding edge of $\mathcal{G}$, and external to the convex hull of $\mathcal{G}$. We can think of $u(v)$ as the center of a circle passing through the two vertices of the corresponding outer edge of $\mathcal{G}$.

Since each dual edge connects the centers of two circles with the corresponding primal edge as a common chord, each dual edge is a perpendicular bisector of the primal edge.

Recalling that $\mathcal{G}$ is bipartite, note that the alternating sum of angles around every non-outer dual vertex is zero. Moreover note that the faces of the augemented dual graph are convex: we have a *convex embedding*, that is, an embedding with convex faces, of $\mathcal{G}^*$.

The converse to this construction also holds:

**Proposition 5.1.1.** *Suppose $\mathcal{G} = (V, E, F)$ is a bipartite graph and $u : F \to \mathbb{C}$ is a convex embedding of $\mathcal{G}^*$. Then there exists a circle pattern $z : V \to \mathbb{C}$ with $u$ as centers*

*if and only if the sum of alternate angles around every non-outer dual vertex is* $\pi$.

Note also that we don't require $z$ to be an embedding, only a realization with the property that vertices on each face lie on a circle. It seems difficult to give conditions under which $z$ will be an embedding, although the space of circle pattern embeddings in which each face contains the circumcenter is an open subset of our space of realizations.

*Proof.* It remains to show that given such an embedding $u$, there is a circle pattern with $u$ as centers. We construct such a circle pattern $z$ as follows. Pick a vertex $i$ and assign the vertex to some arbitrary point $z_i$ in the plane. We then define $z_j$ for a neighboring vertex $j$ in such a way that $z_j$ is the image of $z_i$ under reflection across the line connecting the neighboring dual vertices. Because of the angle condition, iteratively defining the $z$ value around a face will return to the initial value. Hence the map $z$ is well defined and independent of the path chosen. □

### 5.1.2 From circle patterns to face weights

Suppose $\mathcal{G}$ is a planar bipartite graph and we have an embedded circle pattern $z : V(\mathcal{G}) \to \mathbb{C}$, in which each bounded face contains its circumcenter, with outer face convex but not necessarily cyclic. Let $u : F \to \mathbb{C}$ be the circle centers (defining $u$ on outer dual vertices as above).

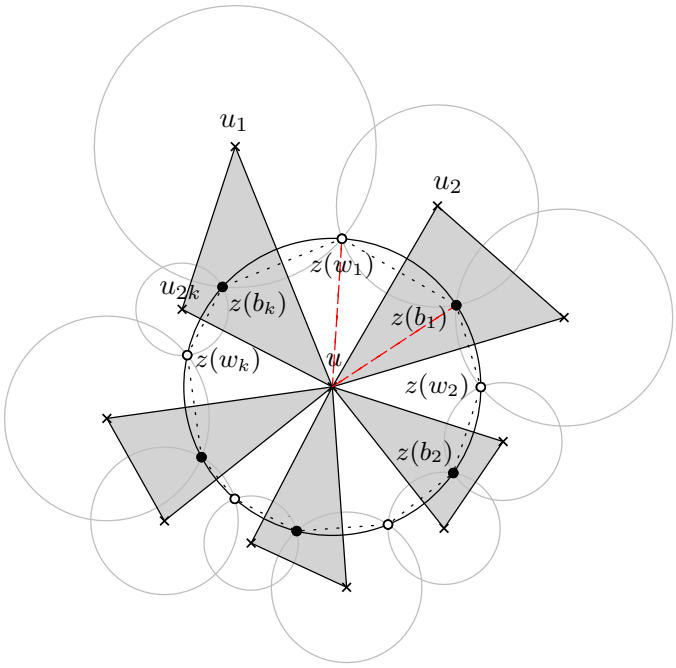


Figure 5.1: Kasteleyn weights on a circle pattern: $K(w_1, b_1) = u_2 - u$. Note that $z(w_1)$ and $z(b_1)$ are symmetric with respect to the line $uu_2$.

Now define a function $\omega(wb) = u_l - u_r$ where $l, r$ denote the left and the right face of the edge $wb$ oriented from $w$ to $b$, see Fig. 5.1. Define a matrix $K$ with rows indexing the white vertices and columns indexing the black vertices by $K(w, b) = \omega(wb)$. We claim that $K$ is a Kasteleyn matrix (with complex signs). To see this, suppose a bounded face $f$

with center $u$ has vertices $w_1 b_1 \dots w_k b_k$ in counterclockwise order. We denote the centers of the neighboring faces as $u_1, u_2, \dots, u_{2k}$. Then

$$\frac{K_{w_1 b_1} K_{w_2 b_2} \dots K_{w_k b_k}}{K_{w_1 b_0} K_{w_2 b_1} \dots K_{w_k b_{k-1}}} = \frac{(u_2 - u)(u_4 - u) \dots (u_{2k} - u)}{(u - u_1)(u - u_3) \dots (u - u_{2k-1})}$$

where $b_0 = b_k$. The angle condition is equivalent to say that the face weight

$$X_f := (-1)^{k+1} \frac{(u_2 - u)(u_4 - u) \dots (u_{2k} - u)}{(u - u_1)(u - u_3) \dots (u - u_{2k-1})} = (-1)^{k+1} \frac{K_{w_1 b_1} K_{w_2 b_2} \dots K_{w_k b_k}}{K_{w_1 b_0} K_{w_2 b_1} \dots K_{w_k b_{k-1}}} \quad (1.1)$$

is positive and $K$ is a Kasteleyn matrix. This associates a positive face-weighted bipartite planar graph to a circle pattern.

We claim, additionally, that if the outer face of $z(\mathcal{G})$ is cyclic (which will be the case if it has degree 4, see below) the graph $\mathcal{G}$ has dimer covers and is nondegenerate (each edge is an element of at least one dimer cover). The existence of dimer covers follows if we can find a *fractional dimer cover* (fractional matching), that is, an element of $[0,1]^E$ summing to 1 at each vertex: recall that the set of dimer covers of a graph is the set of vertices of the polytope of fractional dimer covers [60]. To find a fractional dimer cover, associate to each edge $wb$ the quantity $\frac{\theta_{wb}}{2\pi}$ where $\theta_{wb}$ is the angle at $w$ (or $b$, they are the same) of the quad whose diagonals are the vertices $w, b$ and the two dual vertices of that edge. In the case that one of these dual vertices is an outer dual vertex, define the angle $\theta_{wb}$ at $w$ instead as follows. Let $u_{f_o}$ be the circumcenter of the outer face, and $u$ be the other dual vertex of the edge $wb$. Define $\theta_{wb} = \angle uwb + \angle bwv$ where $v$ is a point lying past $w$ on the ray from $u_{f_o}$ through $w$. Note that the angle obtained at $b$ by the analogous method will equal that at $w$. Since $\sum_b \theta_{wb} = 2\pi = \sum_w \theta_{wb}$, this defines a fractional dimer cover.

The nondegeneracy follows from the fact that the fractional matching is nonzero on each edge.

### 5.1.3 Coulomb gauge for finite planar graphs with outer face of degree 4

In this section let $\mathcal{G}$ be a face-weighted bipartite planar graph, which has dimer covers, is nondegenerate, and has outer face of degree 4. Let $P$ be a convex quadrilateral. We construct a circle pattern for $\mathcal{G}$ with $\mathcal{G}^*$ embedded in $P$. See Figure 5.2 for an example. Our inductive construction will in principle work for graphs with outer face of higher degree, but the initial step of the induction proof is more complicated and is not something we currently can handle.

Let $\mathcal{G}$ have outer boundary vertices $w_1, b_1, w_2, b_2$. Let $X : F \to \mathbb{R}_{>0}$ be a positive real number associated to each bounded face. Let $P \subset \mathbb{R}^2$ be a convex quadrilateral, with edges $W_1, B_1, W_2, B_2 \in \mathbb{C}$ summing to zero.

The graph $\mathcal{G}^*$ has outer face of degree 4; denote the vertices of its outer face by $f_{11}$, $f_{12}$, $f_{21}$ and $f_{22}$, where $f_{ij}$ is adjacent to the edge $(w_i b_j)^*$.

We construct a convex embedding in $P$ of $\mathcal{G}^*$, with the outer vertices of $\mathcal{G}^*$ going to the vertices of $P$, satisfying the property that the vertices of $\mathcal{G}^*$ go to the circle centers of a circle pattern with the combinatorics of $\mathcal{G}$ (in the sense that the angles satisfy

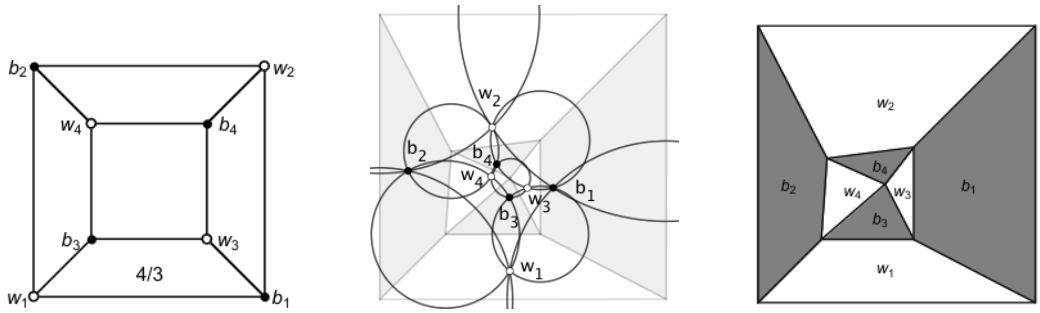


Figure 5.2: The "cube" graph on the left (with all face weights 1 except the one indicated with weight 4/3) is embedded as a circle pattern (middle) with the augmented dual graph $\mathcal{G}^*$ of circle centers having outer boundary a square $P$ (right).

Proposition 5.1.1), and moreover the face variables $X_f$ of $\mathcal{G}$ give the "alternating product of edge lengths" as in (3.2).

Let $K$ be a Kasteleyn matrix associated to $\mathcal{G}$ with face weights $X$. Let $G(w)$ and $F(b)$ be functions on white and black vertices of $\mathcal{G}$ satisfying the properties that: for all internal white vertices $w$, we have

$$\sum_b G(w)K_{wb}F(b) = 0, \tag{1.2}$$

and for all internal black vertices $b$, we have

$$\sum_w G(w)K_{wb}F(b) = 0, \tag{1.3}$$

and for $i = 1, 2$

$$\sum_w G(w)K_{wb_i}F(b_i) = B_i \tag{1.4}$$

$$\sum_b G(w_i)K_{w_ib}F(b) = -W_i. \tag{1.5}$$

Functions $G, F$ satisfying (1.2) and (1.3) are said to give a *Coulomb gauge* for $\mathcal{G}$. The reason for such a name is that the edge weights $G(w)K_{wb}F(b)$ have zero divergence at each internal vertex, which is similar to the case of the Coulomb gauge in electromagnetism, corresponding to the choice of a divergence-free vector potential [38, Section 6.5]. The existence of a Coulomb gauge $G, F$ satisfying the boundary conditions (1.4),(1.5) (for graphs with boundary lengths 4 or more) is discussed in Section 5.1.4 below. As shown there, the equations (1.2)-(1.5) determine $G$ and $F$ up to a finite number of choices: in fact typically two choices for boundary length 4, see below.

Given $G, F$ satisfying the above, define a function $\omega$ on oriented edges by $\omega(wb) = G(w)K_{wb}F(b)$ (and $\omega(bw) = -\omega(wb)$, so that $\omega$ is a flow, or 1-form).

The equations (1.2) and (1.3) imply that $\omega$ is co-closed (divergence free) at internal vertices. Thus $\omega$ can be integrated to define a mapping $\phi$ from the augmented dual graph $\mathcal{G}^*$ into $\mathbb{C}$ by the formula

$$\phi(f_1) - \phi(f_2) = \omega(wb) \tag{1.6}$$

where $f_1, f_2$ are the faces adjacent to edge $wb$, with $f_1$ to the left and $f_2$ to the right when traversing the edge from $w$ to $b$. The mapping $\phi$ is defined up to an additive constant; we choose the constant so that the vertices $f_{11}, f_{12}, f_{22}, f_{21}$ go to the vertices of $P$.

**Theorem 5.1.2.** *Suppose $\mathcal{G}$ has outer face of degree 4. The mapping $\phi$ defines a convex embedding into $P$ of $\mathcal{G}^*$ sending the outer vertices to the corresponding vertices of $P$. The images of the vertices of $\mathcal{G}^*$ are the centers of a circle pattern with the combinatorics of $\mathcal{G}$. Moreover the outer face of $\mathcal{G}$ will also be cyclic.*

Boundary length 4 is special in the sense that if $\mathcal{G}$ has outer face of degree strictly larger than 4, the outer face of the associated circle pattern will not necessarily be cyclic.

*Proof.* We rely on a Theorem of D. Thurston [81, Theorem 6]: any nondegenerate planar bipartite graph with four marked boundary vertices $w_1, b_1, w_2, b_2$ can be built up from the 4-cycle graph with vertices $w_1, b_1, w_2, b_2$ using a sequence of *elementary transformations* (see Figure 1.16); moreover the marked vertices remain in all intermediate graphs.

Therefore to complete the proof it remains to show that, first, the result holds when $\mathcal{G}$ is the simplest graph: a single 4-cycle with only the vertices $w_1, b_1, w_2, b_2$ in that order, and second, if it holds for a graph then it holds for any elementary transformation applied to that graph.

To use this argument we must extend slightly our notion of convex embedding to include the case when $\mathcal{G}$ has degree 2 vertices, and when $\mathcal{G}$ has parallel edges, because these necessarily occur at intermediate stages when we build up the graph $\mathcal{G}$ from the 4-cycle.

When $\mathcal{G}$ has parallel edges connecting two vertices $w$ and $b$, the graph $\mathcal{G}^*$ has one or more degree-2 vertices there; we do not assign a location to these vertices since the circles they correspond to are not defined; rather, we simply embed $\mathcal{G}^*$ as if those parallel edges were joined into a single edge.

When $\mathcal{G}$ has a degree-2 vertex $v$, connected to neighbors $v_1$ and $v_2$, then for the associated Coulomb 1-form $\omega$ we necessarily have $\omega_{vv_1} + \omega_{vv_2} = 0$. This implies that under $\phi$ the duals of these edges get mapped to the same edge. We call this a "near-embedding" since faces of degree 2 in $\mathcal{G}^*$ get collapsed to line segments. Note however that for any such graph $\mathcal{G}$, contracting degree-2 vertices results in a new graph with the same mapping $\phi$, minus those paired edges.

Consequently, among the elementary transformations of Figure 1.16, only the spider move has a nontrivial effect on the embedding.

Now let $\mathcal{H}$ be a graph obtained from $\mathcal{G}$ by applying a spider move. The embedding of $\mathcal{H}$ is obtained from the embedding of $\mathcal{G}$ by a "central move", see (**??**) below. This move gives a convex embedding by convexity of the faces: the new central vertex is necessarily in the convex hull of its neighbors: see Lemma 5.1.3 below.

For the case $\mathcal{G}$ is a 4-cycle, see Lemma 5.1.3 and Figure 5.3.

Finally, the fact that $\phi$ maps the vertices of $\mathcal{G}^*$ to centers of a circle pattern follows from the proof of Proposition 5.1.1 and the fact that the sum of the angles of the corners of the white/black faces around a given vertex of $\phi(\mathcal{G}^*)$ equals $\pi$. The fact that the outer face is cyclic also follows by induction: this is true for the 4-cycle, and the central moves do not move the outer dual vertices, or change their radii. □

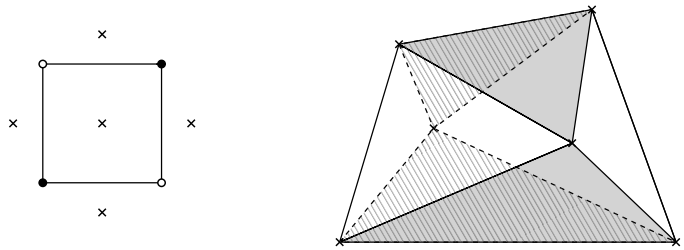

Figure 5.3: For the 4-cycle equation (1.7) defines two solutions, shown for a particular choice of boundary.

We now treat the base case of the induction in the above proof, namely the case of the 4-cycle.

**Lemma 5.1.3.** *Let $Q$ be a convex quadrilateral with vertices $0, 1, z, w$ in counterclockwise order and let $X \in (0, \infty)$. The equation*

$$-\frac{(1-u)(w-u)}{(0-u)(z-u)} = X \tag{1.7}$$

*has two solutions $u$ (counted with multiplicity), both of which lie strictly inside $Q$.*

*Proof.* When $X = 0$ the solutions to (1.7) are $u = 1, u = w$ and when $X = \infty$ the two solutions are $u = 0, u = z$. Notice that no other point on the boundary of $Q$ can be a solution for any $X$ because one of the angle sums $0u1 + zuw$ or $1uz + wu0$ would be larger than $\pi$. So by continuity it suffices to show that for small $X > 0$ there is one solution inside $Q$ near 1 and one solution inside $Q$ near $w$. Solving (1.7) for $u$ and expanding near $X = 0$ gives the solutions

$$u = 1 - \frac{z-1}{w-1}X + O(X^2)$$
$$u = w - w\frac{z-w}{1-w}X + O(X^2).$$

Note that for the first solution, $\arg \frac{w-1}{z-1}$ is less than the angle at 1 of $Q$, so the vector $-\frac{z-1}{w-1}$ points into $Q$ from the point 1; thus this solution is inside $Q$ for small $X > 0$. For the second, $\arg \frac{z-w}{1-w}$ is less than the angle of $Q$ at $w$, so the vector $-w\frac{z-w}{1-w}$ points into the interior of $Q$ from $w$. □

**Remark 5.1.4.** *The* isogonal conjugate *of a point $U$ with respect to a quadrilateral $ABCD$ is constructed by reflecting the lines $UA$, $UB$, $UC$ and $UD$ about the angle bisectors of $A$, $B$, $C$, and $D$ respectively. If these four reflected lines intersect at one point, then this point is called the isogonal conjugate of $U$. Not all points have an isogonal conjugate with respect to a quadrilateral, but only those lying on a certain cubic curve associated with the quadrilateral [3]. One can show that the two solutions to (1.7) are isogonally conjugate with respect to $Q$. Moreover all possible pairs of isogonal conjugate points inside $Q$ can be achieved upon varying $X > 0$.*

### 5.1.4 Existence of Coulomb gauge

In this subsection we consider the case when the outer face of the planar bipartite graph has an arbitrary degree. We prove the existence of at least one Coulomb gauge in this setting.

**Lemma 5.1.5.** *Let $\mathcal{G}$ have outer boundary vertices $w_1, b_1, \ldots, w_k, b_k$. Let $P \subset \mathbb{R}^2$ be a convex polygon, with non-zero edges $W_1, B_1, \ldots, W_k, B_k \in \mathbb{C}$ summing to zero. Suppose that $(\mathcal{G} \setminus \{w_1, b_1, \ldots, w_k, b_k\})$ has a dimer covering and $(\mathcal{G} \setminus \{w_1, b_1, \ldots, w_k, b_k\}) \cup \{b_i, w_j\}$ for any $b_i, w_j$ on the boundary has a dimer covering as well. Then there exists a solution to (1.2)-(1.5) for boundary values $(\vec{B}, \vec{W})$.*

*Proof.* Let $K$ be a Kasteleyn matrix of $\mathcal{G}$. Note that the Kasteleyn matrix is invertible. Let $G(w)$ and $F(b)$ be functions on white and black vertices of $\mathcal{G}$ defined by

$$G(w) = \sum_{i=1}^{k} \alpha_i K^{-1}_{b_i w} \quad \text{and} \quad F(b) = \sum_{j=1}^{k} K^{-1}_{b w_j} \beta_j.$$

for some $\alpha_i, \beta_j \in \mathbb{C}$. Note that for all internal white vertices $w$, we have

$$\sum_b G(w) K_{wb} F(b) = 0,$$

and for all internal black vertices $b$, we have

$$\sum_w G(w) K_{wb} F(b) = 0,$$

and for all $i, j \in \{1, \ldots, k\}$

$$\sum_w G(w) K_{w b_i} F(b_i) = \sum_{j=1}^{k} \alpha_i K^{-1}_{b_i w_j} \beta_j$$
$$\sum_b G(w_j) K_{w_j b} F(b) = \sum_{i=1}^{k} \alpha_i K^{-1}_{b_i w_j} \beta_j.$$

Let $M$ be the $k \times k$ matrix defined by $m_{ij} = K^{-1}_{b_i w_j}$. By the generalized Cramer's rule

$$\det M = \pm \frac{\det(K_{\mathcal{G} \setminus \{w_1, b_1, \ldots, w_k, b_k\}})}{\det K},$$

where $K_{\mathcal{G} \setminus \{w_1, b_1, \ldots, w_k, b_k\}}$ denotes the submatrix of $K$ formed by choosing the rows indexing the white vertices of $\mathcal{G} \setminus \{w_1, b_1, \ldots, w_k, b_k\}$ and columns indexing the black vertices of $\mathcal{G} \setminus \{w_1, b_1, \ldots, w_k, b_k\}$. Note that $K_{\mathcal{G} \setminus \{w_1, b_1, \ldots, w_k, b_k\}}$ is a Kasteleyn matrix of the graph $\mathcal{G} \setminus \{w_1, b_1, \ldots, w_k, b_k\}$, hence

$$|\det(K_{\mathcal{G} \setminus \{w_1, b_1, \ldots, w_k, b_k\}})| = Z_{\mathcal{G} \setminus \{w_1, b_1, \ldots, w_k, b_k\}} = \sum_{m \in M_{\mathcal{G} \setminus \{w_1, b_1, \ldots, w_k, b_k\}}} \nu(m).$$

Therefore the condition that $(\mathcal{G} \setminus \{w_1, b_1, \ldots, w_k, b_k\})$ has a dimer covering implies that $\det M \neq 0$, i.e. the matrix $M$ is invertible. Similarly, since $(\mathcal{G} \setminus \{w_1, b_1, \ldots, w_k, b_k\}) \cup \{b_i, w_j\}$ has a dimer covering for any $b_i, w_j$ on the boundary, all elements of the inverse matrix $M^{-1}$ are non-zero ($m_{ji}^{-1} \neq 0$). We are looking for $k$-tuples $\vec{\alpha} = (\alpha_1, \ldots, \alpha_k)$ and $\vec{\beta} = (\beta_1, \ldots, \beta_k)$ such that

$$\sum_{j=1}^{k} \alpha_i m_{ij} \beta_j = B_i \quad \text{and} \quad \sum_{i=1}^{k} \alpha_i m_{ij} \beta_j = -W_j.$$

That is,

$$\beta_j = \sum_s m_{js}^{-1} \frac{B_s}{\alpha_s} \quad \text{and} \quad \sum_{i,s} \alpha_i m_{ij} m_{js}^{-1} \frac{B_s}{\alpha_s} = -W_j.$$

This last can be written as for each fixed $j = 1, 2, \ldots, k$ as a homogeneous equation

$$\sum_{i,s} \tilde{\alpha}_s \alpha_i m_{ij} m_{js}^{-1} B_s = -W_j \tilde{\alpha}, \tag{1.8}$$

where $\tilde{\alpha} = \prod_{i=1}^{k} \alpha_i$ and $\tilde{\alpha}_s = \prod_{i \neq s} \alpha_i$. Notice that summing over all $k$ equations yields

$$-\sum_j \sum_{i,s} \tilde{\alpha}_s \alpha_i m_{ij} m_{js}^{-1} W_s = \sum_j B_j \tilde{\alpha},$$

which is equivalent to

$$-\sum_i W_i = \sum_j B_j$$

and is one of the assumptions in the lemma. Thus the $k$ equations from (1.8) are redundant and can be reduced to a system of $k-1$ homogeneous equations with $k$ variables, which has a non-trivial solution due to Bézout's theorem.

To finish the proof we need to check that $\alpha_s \neq 0$ for all $s \in \{1, \ldots, k\}$ so that we can recover the coefficients $\beta_j$. Suppose that $\alpha_1 = 0$, then for all $j \in \{1, \ldots, k\}$ we have

$$\sum_{i \geq 2} \alpha_i m_{ij} m_{j1}^{-1} q_1 = 0.$$

Note that $m_{j1}^{-1} \neq 0$ and $q_1 \neq 0$. Therefore for all $j \in \{1, \ldots, k\}$

$$\sum_{i \geq 2} \alpha_i m_{ij} = 0.$$

Hence $\alpha_i = 0$ for all $i \in \{1, \ldots, k\}$. Contradiction. □

**Question:** How many solutions are there? This number is a function only of the graph $\mathcal{G}$, and is invariant under elementary transformations preserving the boundary.

### 5.2 Biperiodic bipartite graphs and circle patterns

In this section we deal with the case of a bipartite graph embedded on a torus, or equivalently a biperiodic bipartite planar graph.

### 5.2.1 Embedding of $\mathcal{G}^*$

Let $\mathcal{G}$ be a bipartite graph embedded on a torus $T$, with complementary regions (faces) which are disks, having dimer covers, and nondegenerate. Let $\nu : E \to \mathbb{R}_{>0}$ be a set of positive edge weights. We fix two cycles $l_1$ and $l_2$ in the dual graph $\mathcal{G}^*$ which together generate the homology $H_1(T, \mathbb{Z})$, and have intersection number $l_1 \wedge l_2 = +1$.

We define new edge weights on $\mathcal{G}$ by multiplying, for $i = 1, 2$, each original edge weight by $\lambda_i$ (resp. $\lambda_i^{-1}$) if the edge crosses $l_i$ with white vertex to its left (respectively right). Define $K(\lambda_1, \lambda_2)$ to be a Kasteleyn matrix of $\mathcal{G}$ with the new edge weights and define a Laurent polynomial $P$ by $P(\lambda_1, \lambda_2) := \det K(\lambda_1, \lambda_2)$. Note that the graph $\mathcal{G}$ with these new edge weights still has the *same face weights* as the original graph. We shall see exactly for which $(\lambda_1, \lambda_2)$ there is a corresponding circle pattern (Theorem 5.2.8 below).

The *spectral curve of the dimer model on* $\mathcal{G}$ is defined to be the zero-locus of $P$ in $(\mathbb{C}^*)^2$. The *amoeba* of $P$ is the image in $\mathbb{R}^2$ of the spectral curve under the mapping $(\lambda_1, \lambda_2) \mapsto (\log|\lambda_1|, \log|\lambda_2|)$. The spectral curve is a *simple Harnack curve* [50]; this has the following consequences (see [62]). Every point $(\lambda_1, \lambda_2)$ of the spectral curve is a simple zero of $P(\lambda_1, \lambda_2)$ or it is a double zero which is then real (a real node). The derivatives $P_{\lambda_1}$ and $P_{\lambda_2}$ vanish only at real points, and vanish simultaneously only at real nodes; The quantity $\zeta := \frac{\lambda_2 P_{\lambda_2}}{\lambda_1 P_{\lambda_1}}$ is the *logarithmic slope* and is real exactly on the boundary of the amoeba (where it equals the slope of the amoeba boundary). At a real node the logarithmic slope $\zeta$ has exactly two limits, which are nonreal and conjugate.

When $(\lambda_1, \lambda_2)$ is a simple zero, $(\bar{\lambda}_1, \bar{\lambda}_2)$ is also a zero of $P(\lambda_1, \lambda_2)$, and in this case it is shown in [49] that $K(\lambda_1, \lambda_2)$ has a kernel which is one-dimensional. Hence there exists a pair of functions $(F, G)$ unique up to scaling, with $F$ defined on black vertices and $G$ defined on white vertices, with $F \in \ker K(\lambda_1, \lambda_2)$ and $G \in \ker K^t(\lambda_1, \lambda_2)$. When $\lambda_1, \lambda_2$ are not both real we call it an *interior* simple zero, it corresponds to a point in the interior of the amoeba, but not at a node.

At a real node, $\lambda_1$ and $\lambda_2$ are both real and the kernel of $K(\lambda_1, \lambda_2)$ is two-dimensional. The kernel is spanned by the limits of the kernels for nearby simple zeros and their conjugates. Let $F, G$ be functions in the kernel of $K(\lambda_1, \lambda_2)$ (resp. of $K^t(\lambda_1, \lambda_2)$) which are limits of those for simple zeros for which $\mathrm{Im}\zeta > 0$.

Let $\tilde{\mathcal{G}}$ be the lift of $\mathcal{G}$ to the plane (the universal cover of the torus). Let $p_1, p_2$ be the horizontal and vertical periods of $\tilde{\mathcal{G}}$ corresponding to $l_1, l_2$ respectively. We extend $F$ and $G$ to $\tilde{\mathcal{G}}$ by, for $i = 1, 2$

$$F(b + p_i) = \lambda_i F(b), \quad G(w + p_i) = \lambda_i^{-1} G(w). \tag{2.9}$$

We define two co-closed 1-forms

$$\omega(wb) = G(w) K_{wb}(\lambda_1, \lambda_2) F(b) \quad \text{and} \quad \hat{\omega}(wb) = \overline{G(w)} K_{wb}(\lambda_1, \lambda_2) F(b) \tag{2.10}$$

and use them to define two mappings $\phi, \hat{\phi} : \tilde{\mathcal{G}}^* \to \mathbb{C}$ using (1.6).

**Remark 5.2.1.** *The mapping $\phi$ is periodic, in the sense that (for $i = 1, 2$) $\phi(v + p_i) = \phi(v) + V_i$ for constant vectors $V_1, V_2$. Indeed,*

$$F(b + p_1) G(w + p_1) = F(b) G(w) \tag{2.11}$$

*and similarly for $p_2$. In the case of a real node, $\lambda_1$ and $\lambda_2$ are real hence (2.11) holds with $G$ replaced with $\bar{G}$ so $\hat{\phi}$ is also periodic.*

As a consequence of Remark 5.2.1, one can project the centers $\{\phi(\tilde{\mathcal{G}}^*)\}$ down to a flat torus and one can give an explicit formula for the aspect ratio of that torus:

**Proposition 5.2.2.** *The periods $V_1$ and $V_2$ of $\phi$ are nonzero as long as $P_{\lambda_1}$ and $P_{\lambda_2}$ are nonzero, and can also be chosen nonzero at a real node by an appropriate scaling. The ratio of the periods is $V_2/V_1 = \zeta = \frac{\lambda_2 P_{\lambda_2}}{\lambda_1 P_{\lambda_1}}$.*

*Proof.* For a matrix $M$ we have the identity $\frac{\partial(\det M)}{\partial M_{i,j}} = M^*_{i,j}$, where $M_{i,j}$ is the $(i,j)$-entry of $M$ and $M^*_{i,j}$ is the corresponding cofactor. Recalling that $P = \det K$, we have

$$\lambda_1 \frac{\partial P}{\partial \lambda_1} = \sum_{\gamma_1} \pm K_{w,b} K^*_{b,w}$$

where the sum is over edges crossing $\gamma_1$ (i.e. those edges of $\mathcal{G}$ with a weight involving $\lambda_1^{\pm 1}$), the sign is given by the corresponding exponent of $\lambda_1$ for that edge, and $K^*$ is the cofactor matrix. When $(\lambda_1, \lambda_2)$ is a simple zero of $P$, we have $K^*K = KK^* = (\det K)\,\mathrm{Id} = 0$ and hence the columns of $K^*$ are multiples of $F$ and the rows are multiples of $G$. In particular, we can write $K^*(b,w) = cF(b)G(w)$ for some scale factor $c$. We find

$$\lambda_1 \frac{\partial P}{\partial \lambda_1} = c \sum_{\gamma_1} \pm K(w,b) F(b) G(w) = cV_1.$$

Similarly

$$\lambda_2 \frac{\partial P}{\partial \lambda_2} = cV_2$$

and we conclude by taking the ratio of these.

If $(\lambda_1, \lambda_2)$ is a node, we can take a limit of nearby simple zeros with, say, $\mathrm{Im}(\zeta) > 0$, and scaling so that $V_1$ is of constant length; since $\zeta$ has a well-defined nonreal limit, $V_2$ will also have a limit of finite length. □

**Theorem 5.2.3.** *If $(\lambda_1, \lambda_2)$ is in the interior of the amoeba of $P$, the realization $\phi$ is a periodic convex embedding of $\tilde{\mathcal{G}}^*$, dual to a circle pattern.*

Note that if $(\lambda_1, \lambda_2)$ is on the *boundary* of the amoeba, then $\zeta$ is real and so by Proposition 5.2.2, $\phi$ cannot define an embedding.

*Proof.* If $(\lambda_1, \lambda_2)$ is an interior simple zero, then we show in Lemma 5.2.7 below that the realization $\phi_1$ defined from $\mathrm{Re}(G(w))K_{wb}F(b)$ is a "T-graph embedding" (see definition in Section 5.2.3), mapping each white face to a convex polygon. (This result is stated in [52] without proof). In particular for $\phi_1$ the sum of the angles of white polygons at vertices of $\tilde{\mathcal{G}}^*$ is $\pi$. This implies that for the realization defined by $\phi$, the sum of angles of the white polygons at vertices of $\tilde{\mathcal{G}}^*$ is also $\pi$, since these polygons are simply scaled copies of those for $\phi_1$. Likewise the realization $\phi_2$ defined from $G(w)K_{wb}\mathrm{Re}(F(b))$ is a T-graph embedding, mapping each black face to a convex polygon. It suffices to show that the orientations of $\phi_1$ and $\phi_2$ agree. Note that the realization defined by $\overline{G(w)}K_{wb}\mathrm{Re}(F(b))$ is also a T-graph embedding with the *reverse* orientation to that of $\phi_2$. Thus the orientations of the white and black faces agree in exactly one of $\phi$ or $\hat{\phi}$. We claim that they agree in $\phi$, not $\hat{\phi}$. This is a consequence of Lemma 5.2.5 below. Thus $\phi$ is a local homeomorphism.

By Remark 5.2.1 and Proposition 5.2.2, $\phi$ is periodic with nonzero periods (at interior simple zeros the $P_{\lambda_i}$ are nonzero) and so $\phi$ is proper, and thus a global embedding (a proper local homeomorphism is a covering map).

If $(\lambda_1, \lambda_2)$ is a real node then one can argue similarly as above; the question of orientation is resolved by taking a limit of simple zeros, since the embeddings depend continuously on $(\lambda_1, \lambda_2)$. □

### 5.2.2 The circles

Let $\phi$ be the embedding of $\mathcal{G}^*$ defined from $\omega$ in (2.10), and $\hat{\phi}$ the realization defined from $\hat{\omega}$. The boundedness of the radii in the circle pattern can be read from the map $\hat{\phi}$:

**Lemma 5.2.4.** *The boundedness of the map $\hat{\phi}$ is equivalent to the boundedness of the radii in any circle pattern.*

*Proof.* Note that $\hat{\phi}(\mathcal{G}^*)$ is defined up to an additive constant. To get $\hat{\phi}(\mathcal{G}^*)$ from $\phi(\mathcal{G}^*)$ one can chose a root face $\phi(b_0)$ and fold the plane along every edge of the embedding. Note that two adjacent vertices of a circle pattern corresponding to $b, w \in \mathcal{G}$ are symmetric with respect to the edge $\phi((wb)^*)$. Therefore they coincide after one folds the plane along $\phi((wb)^*)$. Hence each circle pattern corresponds to a single point under the mapping $\hat{\phi}$, and the radii in the circle pattern are distances from this point to vertices of $\hat{\phi}(\mathcal{G}^*)$. To finish the proof note that the boundedness of these distances is equivalent to the boundedness of the map $\hat{\phi}$. □

We now explain when $\hat{\phi}$ is bounded.

**Lemma 5.2.5.** *If $(\lambda_1, \lambda_2)$ is an interior simple zero, then $\hat{\phi}$ is bounded.*

*Proof.* Assume first that neither of $\lambda_1, \lambda_2$ is real and fix a dual vertex $u \in \tilde{\mathcal{G}}^*$. We have

$$\hat{\phi}(u + 2p_1) - \hat{\phi}(u + p_1) = \lambda_1 \bar{\lambda}_1^{-1}(\hat{\phi}(u + p_1) - \hat{\phi}(u)).$$

Since $|\lambda_1 \bar{\lambda}_1^{-1}| = 1$, the segment $\hat{\phi}(u + p_1)\hat{\phi}(u + 2p_1)$ differs from $\hat{\phi}(u)\hat{\phi}(u + p_1)$ by a rotation around the center of the circle $C_{u,1}$ through $\hat{\phi}(u)\hat{\phi}(u + p_1)\hat{\phi}(u + 2p_1)$ with angle $\arg \lambda_1 \bar{\lambda}_1^{-1} \neq 0$. In particular this implies all the $\hat{\phi}(u + kp_1)$ for $k \in \mathbb{Z}$ lie on $C_{u,1}$. A similar argument holds for $\hat{\phi}(u + kp_2)$. So all the dual vertices $\hat{\phi}(u + k_1p_1 + k_2p_2)$ with $(k_1, k_2) \in \mathbb{Z}^2$ have distance at most the sum of the diameters of these two circles from $\hat{\phi}(u)$ and thus lie in a compact set.

Assume now that $\lambda_1$ is real and $\lambda_2$ is non-real; then $\hat{\phi}$ is periodic in the direction of $p_1$ and almost periodic in the direction of $p_2$. We claim that this is possible only if the period in the direction of $p_1$ is zero: on the one hand the four points $\hat{\phi}(u)$, $\hat{\phi}(u + p_1)$, $\hat{\phi}(u + p_2)$ and $\hat{\phi}(u + p_1 + p_2)$ form a parallelogram (maybe degenerate) because of the periodicity in the direction of $p_1$, and on the other hand, the vectors $\hat{\phi}(u)\hat{\phi}(u + p_1)$ and $\hat{\phi}(u + p_2)\hat{\phi}(u + p_1 + p_2)$ differ by multiplication by $\lambda_2 \bar{\lambda}_2^{-1} \neq 1$, so these vectors must be zero. Therefore $\hat{\phi}$ is also bounded in this case. □

**Lemma 5.2.6.** *For real nodes on the spectral curve, there is a two-parameter family of embeddings $\phi$, up to similarity, but exactly one of them has a bounded $\hat{\phi}$. Moreover, boundedness of $\hat{\phi}$ (in this case) is equivalent to the biperiodicity of the radii in any circle pattern.*

*Proof.* By Remark 5.2.1, $\hat{\phi}$ is biperiodic in the case of a real node. Denote by $a_1, a_2$ the corresponding periods of $\phi$ and by $b_1, b_2$ the periods of the map $\hat{\phi}$. Note that for each $u, v$ in the unit disk $u, v \in \mathbb{D}$ the pair of functions $(F + u\bar{F}, G + v\bar{G})$ also defines, via (1.6), a non-degenerate embedding $\phi_{u,v}$: a black face of $\phi_{u,v}$ is the images of a black face $b$ of $\phi$ under the linear map $z \mapsto z + v\bar{z}$, followed by a homothety with factor $\frac{F(b)+u\bar{F}(b)}{F(b)}$. Similarly the white faces undergo the linear map $z \mapsto z + u\bar{z}$ followed by a homothety; these linear maps have positive determinant when $u, v \in \mathbb{D}$, and so preserve orientation (and convexity).

If we let $a = na_1 + ma_2$ a period of $\phi$ and $b = nb_1 + mb_2$ a period of $\hat{\phi}$, then the corresponding period of $\phi_{u,v}$ is $a + u\bar{b} + vb + uv\bar{a}$. Thus we need

$$a + u\bar{b} + vb + uv\bar{a} \neq 0 \text{ for all } u, v \in \mathbb{D}. \tag{2.12}$$

Note that $a + u\bar{b} + vb + uv\bar{a} = 0$ when $u = -\frac{bv+a}{v\bar{a}+\bar{b}}$. Under what conditions are there no solutions with $u, v \in \mathbb{D}$? The map $v \mapsto -(bv + a)/(\bar{a}v + \bar{b})$ sends the unit circle to itself, and maps the unit disk strictly outside the unit disk if and only if $|a| \geq |b|$. So the above condition (2.12) is equivalent to the condition $|a| \geq |b|$ for all $n, m$. This condition can be further reformulated as follows: the image of $\mathbb{D}$ under the mapping $z \mapsto (a_1 + b_1 z)/(a_2 + b_2 z)$ does not intersect the real line: otherwise, one would have $(a_1 - ta_2) + (b_1 - tb_2)z = 0$ for some real $t$, a contradiction with $|a| \geq |b|$.

Note that $\hat{\phi}$ is biperiodic. To find a bounded $\hat{\phi}$, we need to find $u, \bar{v} \in \mathbb{D}$ such that the periods of $\phi_{u,v}$ are zero:

$$\begin{aligned} b_1 + u\bar{a}_1 + \bar{v}a_1 + u\bar{v}\bar{b}_1 &= 0 \\ b_2 + u\bar{a}_2 + \bar{v}a_2 + u\bar{v}\bar{b}_2 &= 0 \end{aligned}$$

or equivalently,

$$\frac{b_1 + \bar{v}a_1}{\bar{a}_1 + \bar{v}\bar{b}_1} = -u = \frac{b_2 + \bar{v}a_2}{\bar{a}_2 + \bar{v}\bar{b}_2}.$$

Both fractional-linear mappings send the unit disk to itself, since $|a_{1,2}| \geq |b_{1,2}|$. Therefore it is enough to show that this quadratic equation in $\bar{v}$ has a root in $\mathbb{D}$; the corresponding $u$ will lie in $\mathbb{D}$ too.

Clearly, either one of the roots is inside the unit disk and the other outside, or both are on the unit circle. Finally, note that the latter is impossible as one would have

$$\frac{\bar{a}_1 + \bar{v}\bar{b}_1}{\bar{a}_2 + \bar{v}\bar{b}_2} = \frac{b_1 + \bar{v}a_1}{b_2 + \bar{v}a_2} = \frac{a_1 + vb_1}{a_2 + vb_2} \in \mathbb{R}$$

which is contradiction with the fact that the image of $\mathbb{D}$ under the mapping $z \mapsto (a_1 + b_1 z)/(a_2 + b_2 z)$ does not intersect the real line.

The last statement follows because a bounded biperiodic function must have both periods equal to zero. □

### 5.2.3 T-graphs for periodic bipartite graphs

The notion of a T-graph was introduced in [52]. A pairwise disjoint collection $L_1, L_2, \ldots, L_n$ of open line segments in $\mathbb{R}^2$ *forms a T-graph in* $\mathbb{R}^2$ if $\cup_{i=1}^n L_i$ is connected and contains all

of its limit points except for some set $R = \{r_1, ..., r_m\}$, where each $r_i$ lies on the boundary of the infinite component of $\mathbb{R}^2 \setminus \overline{\cup_{i=1}^n L_i}$. Elements in $R$ are called root vertices. Starting from a T-graph one can define a bipartite graph, whose black vertices are the open line segments $L_i$ and whose white vertices are the (necessarily convex) faces of the T-graph. A white vertex is adjacent to a black vertex if the corresponding face contains a portion of the corresponding segment as its boundary. Using a T-graph one can define in a natural geometric way (real) Kasteleyn weights on this bipartite graph: the weights are a sign $\pm$ times the lengths of the corresponding segments, where the sign depends on which side of the black segment the white face is on; changing the choice of which side corresponds to the $+$ sign is a gauge change. Conversely, as described in [52], for a planar bipartite graph with Kasteleyn weights one can construct a T-graph corresponding to this bipartite graph. For infinite bi-periodic bipartite graphs one can similarly construct infinite T-graphs without boundary. For any $(\lambda_1, \lambda_2)$ in the liquid phase (see Section 5.2.4), we consider the realization $\phi_1 : \tilde{\mathcal{G}}^* \to \mathbb{C}$ defined from $\omega(w, b) = \mathrm{Re}(G(w))K(w, b)F(b)$.

**Lemma 5.2.7.** *The realization $\phi_1$ defined above is a T-graph embedding.*

*Proof.* The proof starts along the lines of Theorem 4.6 of [52], which deals with the finite case. The $\phi_1$-image of each black face is a line segment. For a generic direction $u$, consider the inner products $\psi(v) := \phi_1(v) \cdot u$ as $v$ runs over vertices of $\tilde{\mathcal{G}}^*$; we claim that this function $\psi$ satisfies a maximum principle: it has no local maxima or minima. This fact follows from the Kasteleyn matrix orientation: If a face $v$ of $\tilde{\mathcal{G}}$ has vertices $w_1, b_1, \ldots, w_k, b_k$ in counterclockwise order, we denote the neighboring faces as $v_1, v_2, \ldots, v_{2k}$. Then the ratios

$$\frac{\phi_1(v) - \phi_1(v_{2i-1})}{\phi_1(v) - \phi_1(v_{2i})} = \frac{\omega(w_i, b_i)}{-\omega(w_{i+1}, b_i)} = -\frac{\mathrm{Re}(G(w_i))K(w_i, b_i)}{\mathrm{Re}(G(w_{i+1}))K(w_{i+1}, b_i)}$$

(with cyclic indices) cannot be all positive, by the Kasteleyn condition. Thus not all black faces of $\tilde{\mathcal{G}}^*$ adjacent to $v$ have $\phi_1$-image with an endpoint at $v$: at least one has $v$ in its interior and thus there is a neighbor of $v$ with larger value of $\psi$ and a neighbor with smaller value of $\psi$.

It follows from Remark 5.2.1 and Proposition 5.2.2 that $\phi_1$ is a locally finite realization, in the sense that any compact set contains only finitely many points of the form $\phi_1$. Indeed, in the real node case, $2\phi_1 = \phi + \hat{\phi}$ is periodic of nonzero period while in the interior simple zero case, it is the sum of the periodic realization $\phi$ of nonzero period and of the realization $\hat{\phi}$ which is bounded by Lemma 5.2.5.

We claim that the $\phi_1$ image of a white face $w$ is a convex polygon. If not, we could find a vector $u$ and four vertices $v_1, v_2, v_3, v_4$ of $w$ in clockwise order such that both $\psi(v_1), \psi(v_3)$ are larger than either of $\psi(v_2), \psi(v_4)$. By the maximum principle we can then find four disjoint infinite paths starting from $v_1, v_2, v_3, v_4$ respectively on which $\psi(v)$ is respectively increasing, decreasing, increasing, decreasing. We linearly extend $\phi_1$ in order to define it on the edges of $\tilde{\mathcal{G}}^*$. Consider a circle $\mathcal{C}$ such that the disk that it bounds contains $\phi_1(v_i)$ for all $1 \leq i \leq 4$. By the local finiteness property, this disk contains finitely many points of the realization $\phi_1$, hence the four paths must intersect $\mathcal{C}$. Denoting by $A_i$ the point at which the $i$-th path intersects $\mathcal{C}$ for the first time for $1 \leq i \leq 4$, we obtain that $\psi(A_1), \psi(A_3)$ are larger than either of $\psi(A_2), \psi(A_4)$, which contradicts the convexity of $\mathcal{C}$ and completes the proof of the claim that the $\phi_1$-image of each white face is convex.

A similar argument applied to the black segments shows that the set of white faces adjacent to a black segment winds exactly once around the black segment, rather than multiple times, so $\phi_1$ is a local embedding near a black segment.

Since $\phi_1$ is also locally finite, it has to be proper hence it is a global embedding. □

### 5.2.4 Correspondence

Let $\mathcal{G}$ be a bipartite graph on the torus, with an equivalence class of positive edge weights under gauge equivalence. Recall the definition of the spectral curve $P(\lambda_1, \lambda_2) = 0$ defined from this data. We say that $\mathcal{G}$ is in a *liquid phase* if the origin is in the interior of the amoeba of $P$ (this terminology comes from [50] and refers to the polynomial decay of correlations for the corresponding dimer model on $\tilde{\mathcal{G}}$). In this case the roots $(\lambda_1, \lambda_2)$ of $P$ for which $|\lambda_1| = |\lambda_2| = 1$ consist in either a pair of conjugate simple roots $(\lambda_1, \lambda_2), (\bar{\lambda}_1, \bar{\lambda}_2)$ or a real node $(\lambda_1, \lambda_2) = (\pm 1, \pm 1)$.

By Theorem 5.2.3 above, associated to the data of a liquid phase dimer model is a periodic, orientation preserving convex embedding $\phi$ of $\mathcal{G}^*$, well defined up to homothety and translation. The converse is also true, giving us a bijection between these spaces:

**Theorem 5.2.8.** *For toroidal graphs, the correspondence between liquid phase dimer models and periodic circle center embeddings is bijective.*

*Proof.* Given a periodic, orientation-preserving embedding $\phi$ of $\tilde{\mathcal{G}}^*$ satisfying the angle condition (and thus a convex embedding), we define edge weights by associating to each edge $e$ in $\tilde{\mathcal{G}}$ the complex number corresponding to the dual edge $e^*$ dual to $e$, oriented in such a way that the white dual face lies on its left. These edge weights define positive $X$ variables, because the sum of black angles equals the sum of white angles around each dual vertex.

Let $K$ be the associated Kasteleyn matrix, with $K(w, b)$ equal to the corresponding complex edge weight. Then we see that $K$ is in a Coulomb gauge, since the sum of the $K(w, b)$ around each vertex is zero.

It remains to see that the weights are in a liquid phase. Since all face weights are real, $K$ is gauge equivalent to a matrix $K_0(\lambda_1, \lambda_2)$, which has real weights except on the dual curves $\gamma_1, \gamma_2$ where the weights are multiplied by $\lambda_1^{\pm 1}, \lambda_2^{\pm 1}$ as before. Thus $K = GK_0F$ for some functions $G, F$. If at least one of $\lambda_1, \lambda_2$ is nonreal, then $(\lambda_1, \lambda_2)$ is an interior zero of $P$, so we are in a liquid phase. If $\lambda_1, \lambda_2$ are both real, then $K_0$ is real; in this case $K_0$ must have two dimensional kernel: both $\mathrm{Re}(F)$ and $\mathrm{Im}(F)$ are in the kernel, and $\mathrm{Re}(G)$ and $\mathrm{Im}(G)$ are in the left kernel; since the embedding is two-dimensional either $\mathrm{Re}(F)$ and $\mathrm{Im}(F)$ are independent vectors or $\mathrm{Re}(G)$ and $\mathrm{Im}(G)$ are independent vectors. Thus $(\lambda_1, \lambda_2)$ is at a real node of $P$ and again we are in a liquid phase. □

## 5.3 From planar networks to circle patterns

### 5.3.1 Harmonic embeddings of planar networks

A *circular planar network* is an embedded planar graph $\mathcal{G} = (V, E, F)$, with a distinguished subset $B \subset V$ of vertices on the outer face called boundary vertices, and with a conductance function $c : E \to \mathbb{R}_{>0}$ on edges. Associated to this data is a Laplacian

operator $\Delta : \mathbb{C}^V \to \mathbb{C}^V$ defined by

$$\Delta f(v) = \sum_{w \sim v} c_{vw}(f(v) - f(w)).$$

An embedding $f : V \to \mathbb{C}$ is *harmonic* if $\Delta f(v) = 0$ for $v \in V \setminus B$. Harmonic embedding of planar networks arise in various contexts: resistor networks, equilibrium stress configurations, and random walks.

Let $\mathcal{G}$ be a circular planar network, with boundary consisting of vertices $B = \{v_1, \ldots, v_k\}$ on the outer face. The dual $\mathcal{G}^*$ is a graph which is dual to $\mathcal{G}$ in the usual sense except that $\mathcal{G}^*$ has $k$ outer vertices, one between each pair of boundary vertices of $\mathcal{G}$. $\mathcal{G}^*$ is also a circular planar network with boundary $B^*$ consisting of these outer vertices.

Let $P$ be a convex $k$-gon with vertices $z_1, \ldots, z_k$. One can find a function $z : V \to \mathbb{C}$ harmonic on $V \setminus B$ and with values $z_i$ at $v_i$ for $i = 1, \ldots, k$. Then $z$ defines a harmonic embedding of $\mathcal{G}$, also known as the Tutte embedding, see [83].

We can also define a harmonic embedding of the dual graph $\mathcal{G}^*$ (harmonic on $\mathcal{G}^* \setminus B^*$) as follows. If $z_1$ and $z_2$ are two primal vertices and $z_1'$ (resp. $z_2'$) denotes the dual vertex associated with the face to the right (resp. left) of the edge $z_1 z_2$ when traversed from $z_1$ to $z_2$, then we set

$$z_2' - z_1' = i c_{z_1 z_2}(z_2 - z_1).$$

Since the function $z$ is harmonic, this defines a unique embedding of the dual $\mathcal{G}^*$ once one fixes the position of a single dual vertex. This embedding of the dual graph is also harmonic with respect to the inverse conductance (one should take $c_{z_1' z_2'} = c_{z_1 z_2}^{-1}$). Each primal edge is orthogonal to its corresponding dual edge, hence the pair constituted of the harmonic embeddings of the primal and the dual graph form a pair of so-called *reciprocal figures*.

### 5.3.2 From harmonic embeddings to circle patterns

There is a map from a circular planar network $\mathcal{G}$ to a bipartite graph $\mathcal{G}_H$ with face weights, known as Temperley's bijection [51]: To every vertex and every face of $\mathcal{G}$ is associated a black vertex of $\mathcal{G}_H$. To every edge of $\mathcal{G}$ is associated a white vertex of $\mathcal{G}_H$. A white vertex and a black vertex of $\mathcal{G}_H$ are connected if the corresponding edge in $\mathcal{G}$ is adjacent to the corresponding vertex or face in $\mathcal{G}$. Every bounded face of $\mathcal{G}_H$ is a quadrilateral consisting of two white vertices and two black vertices as in the middle of Fig. 5.4. Note that the planar network $\mathcal{G}$ has edge weights $c_e = \ell_{e^*}/\ell_e$ where $\ell_e$ is the distance between the primal vertices and $\ell_{e^*}$ the distance between the dual vertices. In [51], the induced edge weight on an edge of $\mathcal{G}_H$ which is a half-edge of a dual edge of $\mathcal{G}$ is always set to 1 while an edge of $\mathcal{G}_H$ which is a half-edge of a primal edge $e$ of $\mathcal{G}$ has weight $c_e$. Thus the bipartite graph has face weights

$$X_f = c_{e_1}/c_{e_2}$$

where $e_1, e_2$ are two consecutive edges of $\mathcal{G}$ adjacent to face $f$ of $\mathcal{G}_H$. For these weights the partition function of the planar network on $\mathcal{G}$ is equal to the partition function of the dimer model on $\mathcal{G}_H$ up to a multiplicative constant [51].

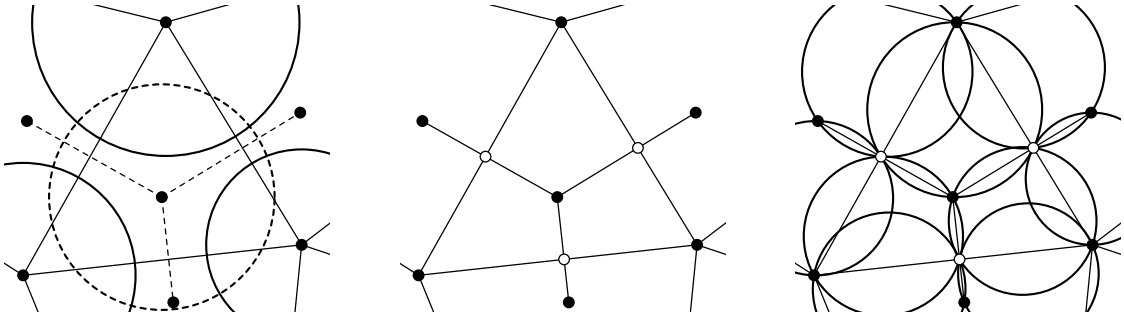

Figure 5.4: From the vertices of reciprocal figures to a circle pattern.

In this section we convert a reciprocal figure into a circle pattern in such a way that the following diagram commutes:

$$\begin{array}{ccc} \text{Planar network } \mathcal{G} & \longrightarrow & \text{Bipartite graph } \mathcal{G}_H \\ \updownarrow & & \updownarrow \\ \text{Reciprocal figure} & \longrightarrow & \text{Circle pattern} \end{array}$$

Let $f : V(\mathcal{G}) \to \mathbb{C}$ be a harmonic embedding of a planar network $\mathcal{G}$ in a convex polygon $P$; let $g : F(\mathcal{G}) \to \mathbb{C}$ be its dual. We define a realization $z : V(\mathcal{G}_H) \to \mathbb{C}$ of the bipartite graph $\mathcal{G}_H$ such that $z = f$ for the black vertices coming from the vertices of $\mathcal{G}$ and $z = g$ for those from the faces of $\mathcal{G}$. On the white vertices, we take $z$ as the intersection of the line through the primal edge and the line through the dual edge under $f$ and $g$. Then $z$ has cyclic faces and thus is a circle pattern with the combinatorics of $\mathcal{G}_H$. The face weights induced on $\mathcal{G}_H$ from the circle pattern coincide with those from Temperley's bijection.

*Proof.* Since every dual edge of $\mathcal{G}$ is perpendicular to its primal edge under the harmonic embeddings, the quadrilateral faces of $\mathcal{G}_H$ have right angles at their white vertices. Hence every face of $z$ is cyclic and hence we obtain a circle pattern. The circumcenter of each cyclic face of $z$ is the midpoint of the two black vertices. By similarity of triangles, the edge weight induced from the distance between circumcenters has the following form: For an edge of $\mathcal{G}_H$ that is a half-edge of a primal edge $e$ of $\mathcal{G}$, it has weight $\ell_{e*}/2$. For an edge of $\mathcal{G}_H$ that is a half-edge of a dual edge $e^*$, it has weight $\ell_e/2$. Thus for every quadrilateral face $\phi$, the face weight is

$$X_\phi = \frac{\ell_{e_1^*}}{\ell_{e_1}} \frac{\ell_{e_2}}{\ell_{e_2^*}} = \frac{c_{e_1}}{c_{e_2}}$$

which coincides with that from Temperley's bijection. □

### 5.3.3 Star-triangle relation

It is a well-known fact [30] that a network can be reduced to the trivial network by performing star-triangle and triangle-star moves, as well as two other types of moves: replacing two parallel edges (sharing the same endpoints) with a single edge, and replacing two edges in series with a single edge (that is, deleting a degree-2 vertex).

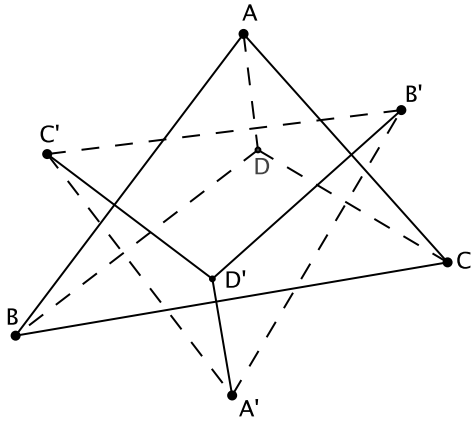


Figure 5.5: Steiner's theorem (see e.g. [2, 4.9.18]) states the perpendicular to $(AB)$ going through $C'$, the perpendicular to $(BC)$ going through $A'$ and the perpendicular to $(AC)$ going through $B'$ are concurrent if and only if the perpendicular to $(A'B')$ going through $C$, the perpendicular to $(B'C')$ going through $A$ and the perpendicular to $(A'C')$ going through $B$ are concurrent.

The star-triangle move has a simple interpretation in terms of reciprocal figures: it corresponds exactly to Steiner's theorem (see Figure 5.5), as was observed in [55]. The star-triangle move corresponds to replacing a vertex which is the intersection of three primal edges by a dual vertex which is the intersection of three dual edges; Steiner's theorem guarantees that these three dual edges intersect at a common point.

In [35] it was observed that a $Y - \Delta$ transformation for planar networks can be decomposed into a composition of four urban renewals for dimer models, upon transforming the planar network into a dimer model via Temperley's bijection. We show that this decomposition can be seen in purely geometric terms, using the correspondences between planar networks and reciprocal figures on the one hand, and between dimer models and circle patterns on the other hand.

The star-triangle move for reciprocal figures can be decomposed into four Miquel moves, upon transforming the reciprocal figures into a circle pattern as described in Theorem 5.3.2.

*Proof.* This decomposition is illustrated in Figure 5.6. We start with a triangle $ABC$ in a harmonic embedding, we denote by $D'$ the dual vertex associated with that triangle and by $A', B'$ and $C'$ the three dual vertices adjacent to $D'$. We construct the circle pattern associated with the reciprocal figures as described in Theorem 5.3.2, denoting by $a', b'$ and $c'$ the intersections of the primal edges and their associated dual edges. We respectively denote by $O_A$, $O_B$ and $O_C$ the centers of the circumcircles of the quadrilaterals $Ac'D'b'$, $Ba'D'c'$ and $Cb'D'a'$. We also respectively denote by $O_{AC'}$, $O_{C'B}$, $O_{BA'}$, $O_{A'C}$ $O_{CB'}$ and $O_{B'A}$ the circumcenters of the triangles $Ac'C'$, $C'c'B$, $Ba'A'$, $A'a'C$, $Cb'B'$ and $B'b'A$. We first apply the Miquel move $M_{O_C}$ to the quadrilateral $D'a'Cb'$ with circumcenter $O_C$. The points $D'$, $a'$, $C$ and $b'$ respectively transform into $c'$, $I_{A'}$, $c$ and $I_{B'}$, which form a cyclic quadrilateral with circumcenter denoted by $O$. Then we apply the Miquel

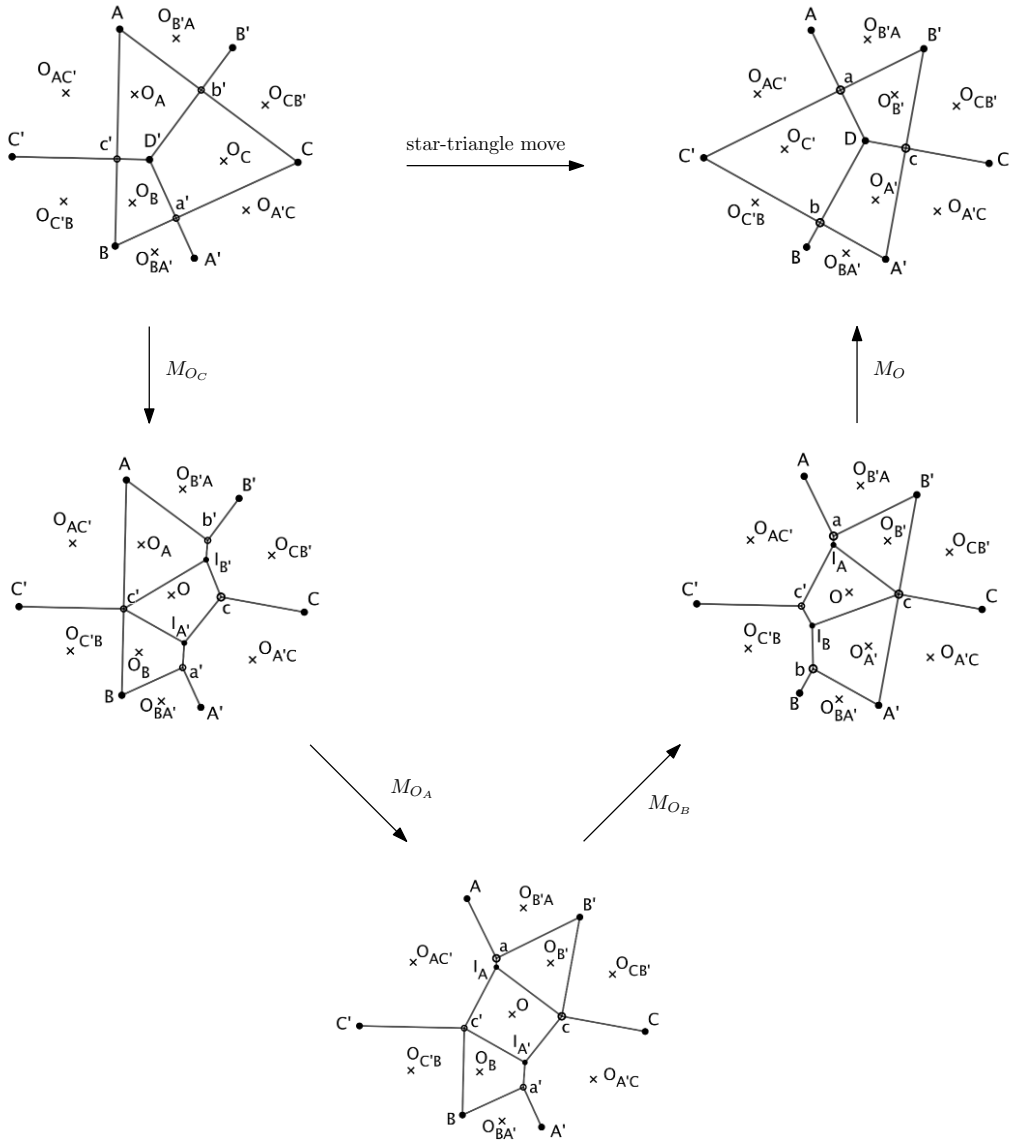


Figure 5.6: Decomposition of a star-triangle move for reciprocal figures into four Miquel moves.

move $M_{O_A}$ to the quadrilateral $Ac'I_{B'}b'$ with circumcenter $O_A$. The points $A$, $c'$, $I_{B'}$ and $b'$ respectively transform into $a$, $I_A$, $c$ and $B'$, which form a cyclic quadrilateral with circumcenter denoted by $O_{B'}$. Next we apply the Miquel move $M_{O_B}$ to the quadrilateral $Ba'I_{A'}c'$ with circumcenter $O_B$. The points $B$, $a'$, $I_{A'}$ and $c'$ respectively transform into $b$, $A'$, $c$ and $I_B$, which form a cyclic quadrilateral with circumcenter denoted by $O_{A'}$. Finally we apply the Miquel move $M_O$ to the quadrilateral $I_Ac'I_Bc$ with circumcenter $O$. The points $I_A$, $c'$, $I_B$ and $c$ respectively transform into $a$, $C'$, $b$ and $D$, which form a cyclic quadrilateral with circumcenter denoted by $O_{C'}$.

We now show that this point $D$ created by a composition of four Miquel moves coincides with the point $\tilde{D}$ created by the star-triangle move applied to the reciprocal figures. First, as observed in the proof of Theorem 5.3.2, in a circle pattern coming from reciprocal figures, the center of each circle is the midpoint of the segment formed by the two black vertices. Since $O_{AC'}$ is the circumcenter of the triangle $AC'a$ and is the midpoint of $[AC']$, this implies that the perpendicular to $(B'C')$ going through $A$ is the line $(Aa)$. Similarly, $(Bb)$ is the perpendicular to $(A'C')$ going through $B$ and $(Cc)$ is the perpendicular to $(A'B')$ going through $C$. Hence the point $\tilde{D}$ created by the star-triangle move is the intersection point of the three lines $(Aa)$, $(Bb)$ and $(Cc)$. Because of the orthogonality property at $a, b$ and $c$, the point $\tilde{D}$ lies on the circumcircles of the three triangles $aC'b$, $bA'c$ and $cB'a$ so $\tilde{D} = D$. □

## 5.4 From Ising s-embeddings to circle patterns

We consider the Ising model on a planar graph $\mathcal{G}$ with edge weights $x_e$, related to the coupling constants $J_e > 0$ by $x_e = \tanh(\beta_c J_e)$, where $\beta_c$ is the inverse critical temperature. Chelkak introduced in [15] an **s-embedding** of $\mathcal{G}$, which is an embedding $s$ defined on each vertex, dual vertex and edge midpoint of $\mathcal{G}$ with the following property: For any edge $e$ in $\mathcal{G}$, if $v_0^\bullet$ and $v_1^\bullet$ (resp. $v_0^\circ$ and $v_1^\circ$) denote the endpoints of $e$ (resp. of the edge dual to $e$) and $v_e$ denotes the midpoint of $e$ as on Figure 5.7, then $s(v_0^\bullet)$, $s(v_0^\circ)$, $s(v_1^\bullet)$ and $s(v_1^\circ)$ form a tangential quadrilateral with incenter $s(v_e)$, meaning that there exists a circle centered at $s(v_e)$ and tangential to the four sides of the quadrilateral.

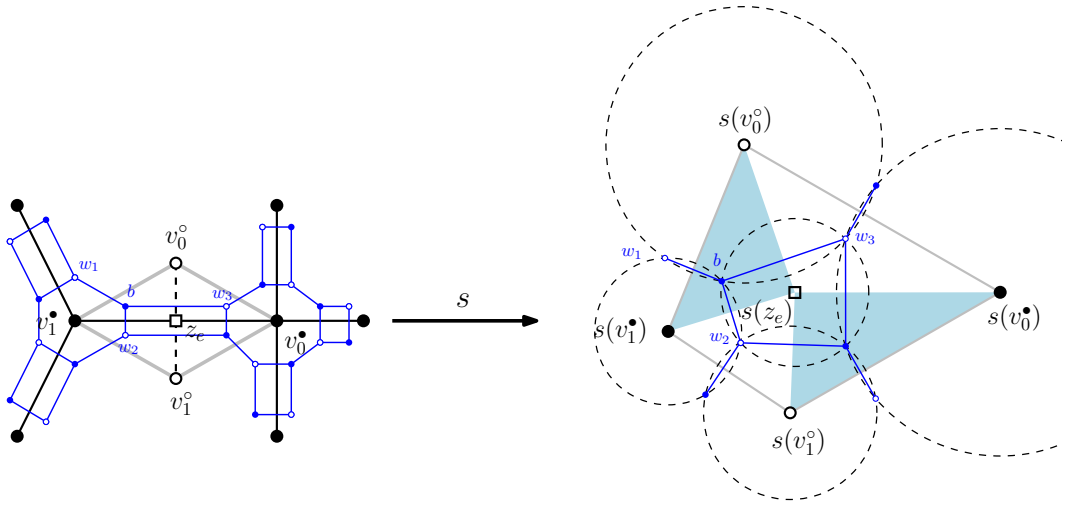


Figure 5.7: Ising graph $\mathcal{G}$ (black vertices); dual graph $\mathcal{G}^*$ (white vertices); dimer graph $\mathcal{G}_D$ (blue).

On the other hand, Dubedat [26] gave a natural map from the double Ising model on $\mathcal{G}$ to a bipartite dimer model $\mathcal{G}_D$, as in Fig. 5.7: Each edge in $\mathcal{G}$ is replaced by a quadrilateral in $\mathcal{G}_D$ and each vertex or face of degree $d$ in $\mathcal{G}$ is replaced by a face of degree $2d$ in $\mathcal{G}_D$. Every face of $\mathcal{G}_D$ corresponds to a vertex, an edge or a face of $\mathcal{G}$. For every edge $e$ of $\mathcal{G}$, define $\theta_e \in (0, \pi)$ by

$$x_e = \tan \frac{\theta_e}{2}.$$

Then we define the edge weights on $\mathcal{G}_D$ by the following formulas (adopting the notation of Figure 5.7):

$$\omega(bw_1) = 1, \quad \omega(bw_2) = \cos\theta_e, \quad \omega(bw_3) = \sin\theta_e.$$

For these weights the partition function of the Ising model on $\mathcal{G}$ is equal (up to a multiplicative constant) to the partition function of the dimer model on $\mathcal{G}_D$, see [26].

The goal of this section is to show that the following diagram commutes:

$$\begin{array}{ccc} \text{Ising model on } \mathcal{G} & \longrightarrow & \text{Bipartite graph } \mathcal{G}_D \\ \updownarrow & & \updownarrow \\ \text{s-embedding} & \longrightarrow & \text{Circle pattern} \end{array}$$

In particular, the s-embedding of the vertices, dual vertices and edge midpoints of $\mathcal{G}$ coincide with the circle centers associated with the bipartite graph $\mathcal{G}_D$. Note that combinatorially this is consistent since each face of $\mathcal{G}_D$ corresponds to either a vertex, a face or an edge of $\mathcal{G}$.

**Theorem 5.4.1.** *An s-embedding of $\mathcal{G}$ provides an embedding of $\mathcal{G}_D^*$ into $\mathbb{C}$ sending each vertex of $\mathcal{G}_D^*$ to the centers of a circle pattern associated with $\mathcal{G}_D$.*

*Proof.* It suffices to prove that, for each face of the bipartite graph $\mathcal{G}_D$, the alternating product of the edge weights $\omega$ induced by $s$ satisfies (1.1), where $X$ is the face weight of $\mathcal{G}_D$.

First, we check the conditions on the faces of $\mathcal{G}_D$ that correspond to vertices or faces of $\mathcal{G}$. By symmetry, it suffices to consider just a face of $\mathcal{G}$. Let $v^*$ be a vertex of the dual graph of $\mathcal{G}_D$ which corresponds to a face of $\mathcal{G}$ of degree $d$ and denote by $v_{e_1}, v_1, v_{e_2}, v_2, \ldots, v_{e_d}, v_d$ the neighbors of $v^*$ in $\mathcal{G}_D^*$ in counterclockwise order, where the vertices of type $v_{e_i}$ correspond to an edge in $\mathcal{G}$ while the vertices of type $v_i$ correspond to a vertex in $\mathcal{G}$. The weight of an edge in $\mathcal{G}_D$ dual to an edge of type $v^*v_{e_i}$ (resp. $v^*v_i$) is of the form $\sin\theta_i$ (resp. is equal to 1). Hence we need to show the following two formulas:

$$\arg \frac{\prod_{i=1}^d s(v_{e_i}) - s(v^*)}{\prod_{i=1}^d s(v_i) - s(v^*)} = \pi \quad \text{and} \quad \frac{\prod_{i=1}^d |s(v_{e_i}) - s(v^*)|}{\prod_{i=1}^d |s(v_i) - s(v^*)|} = \prod_{i=1}^d \sin\theta_i.$$

By splitting each formula into $d$ equations centered around the edges of type $v^*v_{e_i}$, it suffices to prove the following two formulas, where we are using the notation of Figure 5.7:

$$\arg \frac{s(v_e) - s(v_0^\circ)}{s(v_0^\bullet) - s(v_0^\circ)} = \arg \frac{s(v_1^\bullet) - s(v_0^\circ)}{s(v_e) - s(v_0^\circ)}, \tag{4.13}$$

$$\sin^2\theta_e = \frac{|s(v_e) - s(v_0^\circ)|^2}{|s(v_1^\bullet) - s(v_0^\circ)| \cdot |s(v_0^\bullet) - s(v_0^\circ)|}. \tag{4.14}$$

Formula (4.13) follows from the fact that $s(v_e)$ is the center of the incircle of the quadrilateral with vertices $s(v_0^\bullet)$, $s(v_0^\circ)$, $s(v_1^\bullet)$ and $s(v_1^\circ)$. For the other formula, we start from formula (6.3) in [15] which implies that

$$\tan^2\theta_e = \frac{|s(v_0^\circ) - s(v_e)| \cdot |s(v_1^\circ) - s(v_e)|}{|s(v_0^\bullet) - s(v_e)| \cdot |s(v_1^\bullet) - s(v_e)|},$$

hence

$$\frac{1}{\sin^2\theta_e} = \frac{|s(v_0^\circ) - s(v_e)| \cdot |s(v_1^\circ) - s(v_e)| + |s(v_0^\bullet) - s(v_e)| \cdot |s(v_1^\bullet) - s(v_e)|}{|s(v_0^\circ) - s(v_e)| \cdot |s(v_1^\circ) - s(v_e)|}. \tag{4.15}$$

Furthermore, we have the following formula:

$$\begin{aligned} &|s(v_1^\bullet) - s(v_0^\circ)| \cdot |s(v_0^\bullet) - s(v_0^\circ)| = \\ &\frac{|s(v_0^\circ) - s(v_e)|}{|s(v_1^\circ) - s(v_e)|} \left(|s(v_0^\circ) - s(v_e)| \cdot |s(v_1^\circ) - s(v_e)| + |s(v_0^\bullet) - s(v_e)| \cdot |s(v_1^\bullet) - s(v_e)|\right), \end{aligned} \tag{4.16}$$

since $s(v_0^\bullet)$, $s(v_0^\circ)$, $s(v_1^\bullet)$ and $s(v_1^\circ)$ form a tangential quadrilateral of incenter $s(v_e)$.

Next, we check these conditions for faces of $\mathcal{G}_D$ corresponding to edges of $\mathcal{G}$. We need to show the following two formulas:

$$\arg \frac{(s(v_0^\bullet) - s(v_e))(s(v_1^\bullet) - s(v_e))}{(s(v_0^\circ) - s(v_e))(s(v_1^\circ) - s(v_e))} = \pi, \tag{4.17}$$

$$\frac{\cos^2\theta_e}{\sin^2\theta_e} = \frac{|s(v_0^\bullet) - s(v_e)| \cdot |s(v_1^\bullet) - s(v_e)|}{|s(v_0^\circ) - s(v_e)| \cdot |s(v_1^\circ) - s(v_e)|}. \tag{4.18}$$

Formula (4.17) follows from subdividing the quadrilateral with vertices $s(v_0^\bullet)$, $s(v_0^\circ)$, $s(v_1^\bullet)$ and $s(v_1^\circ)$ into four triangles sharing the common vertex $s(v_e)$, taking the alternating sum of four formulas of the type of (4.13). Formula (4.18) follows immediately from formula (6.3) in [15]. □

# Chapter 6

# T-embeddings

In this chapter we introduce the notion of *t-embeddings* for embeddings studied under the name "centers of a circle pattern" in the previous chapter. We also introduce the definition of discrete *t-holomorphicity* on such an embedding. We focus on understanding the link between these functions and actual continuous holomorphic functions to study holomorphic observables of the dimer model.

## 6.1 T-embeddings and circle patterns

### 6.1.1 T-embeddings

In this section we give a definition of a t-embedding and describe how to introduce Kasteleyn weights on the bipartite dual in a natural geometric way.

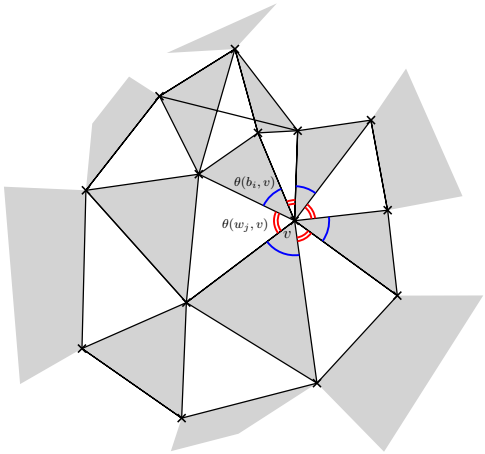


Figure 6.1: A portion of a t-embedding. Angle condition around a vertex: $\sum_{f \text{ white}} \theta(f, v) = \sum_{f \text{ black}} \theta(f, v) = \pi$.

**Definition 6.1.1.** *A t-embedding in the whole plane* is an (embedded) map covering the whole plane with the following properties:

- Proper: All edges are straight segments and they don't overlap. All the faces are convex and have angles in $(0, \pi)$.
- Bipartite dual: The dual graph of the map is bipartite, let us call the bipartite classes white and black.

- Angle condition: For every vertex $v$ we have

$$\sum_{f \text{ white}} \theta(f, v) = \sum_{f \text{ black}} \theta(f, v) = \pi,$$

where $\theta(f, v)$ denotes the angle of a face $f$ at the neighbouring vertex $v$, see Fig. 6.1.

We can extend the definition to finite maps.

**Definition 6.1.2.** *A finite t-embedding* is a finite embedded planar map with the following properties:

- Proper: All edges are straight segments and they don't overlap. All the faces are convex and have angles in $(0, \pi)$.
- Bipartite dual: The dual graph of the map becomes bipartite once the outer vertex is removed, let us call the bipartite classes white and black.
- Angle condition: For every interior vertex $v$ we have

$$\sum_{f \text{ white}} \theta(f, v) = \sum_{f \text{ black}} \theta(f, v) = \pi,$$

where an interior vertex is a vertex which is not adjacent to the outer face.

We call the union of the closed faces in a finite t-embedding the domain of the t-embedding. We say that a vertex of the dual graph $\mathcal{G}$ of a finite t-embedding is an interior vertex if the associated face of the embedding is not adjacent to the outer face. Other vertices are called boundary vertices and we write $\partial B$ and $\partial W$ for the set of boundary black and white vertices.

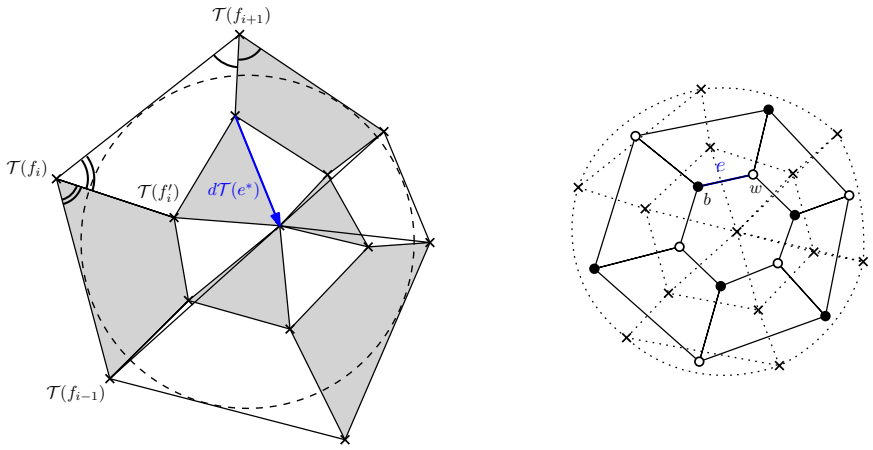


Figure 6.2: **Left:** a perfect t-embedding $\mathcal{T}(\mathcal{G}^*)$. The edge $\mathcal{T}(f_i)\mathcal{T}(f_i')$ lies on the bisector of the angle $\mathcal{T}(f_{i-1})\mathcal{T}(f_i)\mathcal{T}(f_{i+1})$. **Right:** associated graph $\mathcal{G}^*$ (dotted) together with its planar dual bipartite graph $\mathcal{G}$.

**Definition 6.1.3.** We call a finite t-embedding *a perfect t-embedding* if the boundary of the domain of t-embedding forms a convex tangental polygon, all boundary vertices have degree three and all non-boundary edges adjacent to boundary vertices lie on bisectors of the boundary polygon, see Fig. 6.2.

Given a t-embedding, we will call $\mathcal{G}^*$ the associated map seen as an abstract combinatorial object and $\mathcal{G}$ its planar dual (minus the outer face in the case of a finite embedding) also seen abstractly. We will call the set of black and white vertices of $\mathcal{G}$ respectively $B$ and $W$ and typical vertices either $b$ or $w$ depending on their color. Given an oriented edge $(bw)$ of $\mathcal{G}$, we denote by $(bw)^*$ the oriented dual edge which has the first vertex (here $b$) to its right. We let $\mathcal{T}$ denote the map from $\mathcal{G}^*$ to $\mathbb{C}$ giving the position of any dual vertex in the embedding. Given $e^* = (v, v')$ an oriented edge of $\mathcal{G}^*$, we let $d\mathcal{T}(e^*) := \mathcal{T}(v') - \mathcal{T}(v)$. Finally we set for each edge $e$ of $\mathcal{G}$, $\chi(e) = |d\mathcal{T}(e^*)|$ and we note that this defines positive weights on $\mathcal{G}$.

Proposition 5.1.1 implies that a t-embedding can be considered as an embedding of centers of some circle pattern. Thus due to Section 5.1.2 we have the following proposition:

**Proposition 6.1.4.** *Define $K(b, w) = d\mathcal{T}((bw)^*)$ if $b$ and $w$ are neighbours and 0 otherwise, then $K$ is a Kasteleyn matrix for the weights $\chi$.*

### 6.1.2 Folding and circle pattern

Due to the proof of Proposition 5.1.1 the following definition is consistent.

**Definition 6.1.5.** *A circle pattern realisation $\mathcal{C}$ of $\mathcal{G}$ is constructed from $\mathcal{T}$ as follows. Fix an arbitrary white vertex $w_0$ and choose $\mathcal{C}(w_0)$ arbitrarily, then define $\mathcal{C}$ at neighbours of $w_0$ and iteratively everywhere by saying that for any neighbours $b$ and $w$, points $\mathcal{C}(b)$ and $\mathcal{C}(w)$ are symmetric with respect to the line $\mathcal{T}((bw)^*)$.*

This construction produces a two-dimensional family of realisations parametrized by the position of $\mathcal{C}(w_0)$. It is not clear whether $\mathcal{C}$ is a proper embedding. However, for all faces of $\mathcal{G}$, all its vertices lie on a single circle and vertices are intersection points of at least three circles.

As discussed in Section 5.2.2, the above construction can be described as follows: the plane is folded along all the edges of $\mathcal{T}$ (where the angle condition guaranties that this operation makes sense), then pierce an arbitrary point in the folded plane. Finally, unfold and the realisation is given by the position of all the punctures. Let us introduce a formal definition of this folding of the plane in terms of t-embedding $\mathcal{T}$.

**Definition 6.1.6.** A function $\eta : \mathcal{G} \to \mathbb{T}$ is said to be *an origami square root function* if it satisfies

$$\eta_b \bar{\eta}_w = \frac{d\mathcal{T}((bw)^*)}{|d\mathcal{T}((bw)^*)|}$$

for all pairs $(b, w)$ of white and black neighbouring vertices.

**Remark 6.1.7.** *The above definition is inconsistent as $\eta$ has to branch over every face of $\mathcal{G}$, with the values on the two sheets being opposite of each other. By an abuse of notation we will consider $\eta$ as a well defined function and we note that $\eta^2$ is always defined. To get a well defined function, we define $\phi_b, \phi_w$ in $(-\pi/2, \pi/2]$ so that*

$$\phi = \arg \eta \mod \pi.$$

*Note that $\phi$ is a well defined function.*

Now we can formally define the folding of the plane along the edges of the plane in term of $\eta$.

**Definition 6.1.8.** *The origami differential form associated to $\eta$ is:*

$$d\mathcal{O}(z) = \begin{cases} \eta_w^2\, dz & \text{if } z \text{ is in the white face } w \\ \eta_b^2\, d\bar{z} & \text{if } z \text{ is in the black face } b. \end{cases}$$

*Note that $d\mathcal{O}$ is well defined along edges of $\mathcal{T}$ in the direction of the edge.*

$$d\mathcal{O}((bw)^*) = \eta_w^2\, d\mathcal{T}((bw)^*) = \eta_b^2\, \overline{d\mathcal{T}}((bw)^*).$$

*Proof.* We need to check that $\eta_w^2\, d\mathcal{T}((bw)^*) = \eta_b^2\, \overline{d\mathcal{T}}((bw)^*)$. Indeed, note that

$$\frac{d\mathcal{T}((bw)^*)}{\overline{d\mathcal{T}}((bw)^*)} = \frac{\eta_b \bar{\eta}_w}{\bar{\eta}_b \eta_w} = \frac{\eta_b^2}{\eta_w^2},$$

since $\bar{\eta}_b = \eta_b^{-1}$ and similarly for $\eta_w$. □

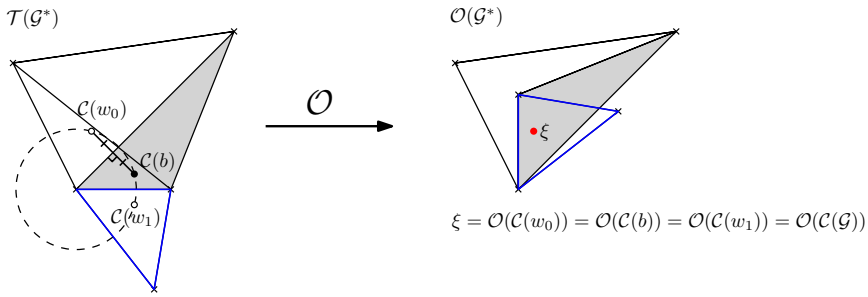


Figure 6.3: To get an origami map $\mathcal{O}(\mathcal{G}^*)$ from $\mathcal{T}(\mathcal{G}^*)$ one can choose a root face $\mathcal{T}(w_0)$ and fold the plane along every edge of the t-embedding.

**Lemma 6.1.9.** *The origami differential form $d\mathcal{O}$ is a closed form (inside the domain of the embedding in the finite case). We denote its primitive by $\mathcal{O}$ and call it the origami map.*

*Proof.* We need to check that the integral around any closed contour vanishes. For closed contours inside a face, there is nothing to prove. For a closed path that crosses a single edge $(bw)^*$, this follows from the fact that the computation of $d\mathcal{O}((bw)^*)$ from the right and left agree as noted in the definition. It remains to check for a small circle around a vertex of $\mathcal{T}$. Let $e^{i\theta_k}$ be the directions of the edges adjacent to a vertex $v$ taken in positive order, with the faces between $e^{i\theta_{2k}}$ and $e^{i\theta_{2k+1}}$ white and the others black. Let $\omega$ be a circle of radius $r$ with the center at $v$. Then

$$\oint_\omega d\mathcal{O} = r \sum_k \eta_{w_k}^2 (e^{i\theta_{2k+1}} - e^{i\theta_{2k}}) + \eta_{b_k}^2 (e^{-i\theta_{2k+2}} - e^{-i\theta_{2k+1}}) =$$

$$r \sum_k \eta_{w_k}^2 \left( \frac{d\mathcal{T}((w_k b_k)^*)}{|d\mathcal{T}((w_k b_k)^*)|} - \frac{d\mathcal{T}((b_{k-1} w_k)^*)}{|d\mathcal{T}((b_{k-1} w_k)^*)|} \right) + \eta_{b_k}^2 \left( \frac{\overline{d\mathcal{T}}((b_k w_{k+1})^*)}{|d\mathcal{T}((b_k w_{k+1})^*)|} - \frac{\overline{d\mathcal{T}}((w_k b_k)^*)}{|d\mathcal{T}((w_k b_k)^*)|} \right)$$

$$= r \sum_k \eta_{w_k}^2 (-\eta_{b_k} \bar{\eta}_{w_k} - \eta_{b_{k-1}} \bar{\eta}_{w_k}) + \eta_{b_k}^2 (\bar{\eta}_{b_k} \eta_{w_{k+1}} + \bar{\eta}_{b_k} \eta_{w_k}) = 0,$$

since $\bar{\eta}_b = \eta_b^{-1}$ and $\bar{\eta}_w = \eta_w^{-1}$. □

It is easy to check that $\mathcal{O}$ maps $z$ to its position after the folding procedure described in the construction of $\mathcal{C}$ so that in a sense $\mathcal{C} = \mathcal{O}^{-1}(\mathcal{C}(w_0))$, see Fig. 6.3. However, this will only hold if for any face $f$ of the t-embedding, $\mathcal{C}(f)$ is inside face $f$, which is not clear in general. Note that $\eta^2$ describe the local rotation after the folding. With a slight abuse of notation (already implicit in definition of the origami differential form), we will allow ourself to also see $\mathcal{O}$ as a map from $\mathcal{G}^*$ to $\mathbb{C}$.

**Remark 6.1.10.** *There is a one dimensional family of origami square root functions, parametrized by the value at one point.*

Let us now remark on the geometry of the function $\eta$:

**Lemma 6.1.11.** *Let $b_1, b_2$ be two black vertices adjacent to a white vertex $w$. Let $v$ be the dual vertex adjacent to $b_1$, $b_2$ and $w$, and we assume that in the positive order around $v$ we get $b_1$, $w$, $b_2$. Then for any origami square root function and associated $\phi$,*

$$\phi_{b_2} - \phi_{b_1} = \theta_{w,v} \mod \pi,$$

*where $\theta_{w,v}$ is the angle of the white face $w$ at the vertex $v$, taken in positive direction.*

*Similarly, for white vertices $w_1, w_2$ adjacent to a black vertex $b$: Assume that $w_1$, $b$, $w_2$ are in a positive order around their common dual vertex $v$, then*

$$\phi_{w_2} - \phi_{w_1} = -\theta_{b,v} \mod \pi.$$

*Proof.* Let $v_i \neq v$ be points on $\mathcal{T}((wb_i)^*)$ for $i \in \{1, 2\}$. Up to sign change, we have

$$\eta_{b_2}\bar{\eta}_{b_1} = \frac{d\mathcal{T}((b_2w)^*)}{|d\mathcal{T}((b_2w)^*)|} \cdot \frac{\overline{d\mathcal{T}((b_1w)^*)}}{|d\mathcal{T}((b_1w)^*)|} = \frac{v - v_2}{|v - v_2|} \cdot \frac{\overline{v_1 - v}}{|v_1 - v|} = -e^{i\theta_{w,v}}.$$

Taking the argument, the global sign change translates to the fact that the equality holds modulo $\pi$ so we obtain the lemma. The second case can be checked similarly. □

In other words, around a vertex of the t-embedding, the directions $\eta_{b_i}$ are in positive order, with the angles given by the white vertices.

### 6.1.3 T-embeddings and T-graphs

In this section we discuss how T-graphs are related to t-embeddings. We introduce a notion of non-proper T-graphs and generalize the result of Lemma 5.2.7.

**Definition 6.1.12.** *A proper T-graph in the whole plane* is a closed subset of $\mathbb{C}$ which can be written as the disjoint union of a countable number of open segments.

*A proper finite T-graph* is a closed subset of $\mathbb{C}$ which can be written as the disjoint union of a finite number of open segments and a finite collection of single points, with the additional constraint that all the points lie on the outer face.

In the case of a finite T-graph, we say that single points in the construction are the boundary vertices of the T-graph.

Note that since the union of the segments form a closed set, the endpoints of any segment have to lie inside another segments or at a boundary point. Furthermore this is the only way two segments can meet so the name T-graph refers to the fact that every vertex looks like a T (or a K in fact) but not like a Y or X.

**Definition 6.1.13.** *In Definition 6.1.12, a union of segments which are not disjoint but satisfy the other conditions is said to be a non-proper T-graph.*

*We also call T-graph with possibly degenerate faces of the whole plane a union of open segments $L_i = (v_i^-, v_i^+)$ such that for any $i$, both limit points $v_i^\pm$ lie either in some $L_j$, or coincides with at least two other limit points. In the second case, we say that there is a degenerate face at $v_i^\pm$. The finite case is defined similarly.*

**Proposition 6.1.14.** *For any $\alpha$ with $|\alpha| = 1$, the set $\mathcal{T} + \alpha\mathcal{O}$ is a T-graph, possibly non proper and with degenerate faces. In this T-graph:*

- *The image of a white face $\Delta_w$ is a translate of $(1 + \alpha\eta_w^2)\Delta_w$ (with its orientation),*
- *The image of a black face $\Delta_b$ is a translate of $2 \cdot \mathrm{Proj}_{\sqrt{\alpha}\eta_b}(\Delta_b)$.*

*Moreover, if $\mathcal{O}$ is bounded and $\mathcal{T}$ is an embedding in the whole plane, then $\mathcal{T} + \alpha\mathcal{O}$ is a proper T-graph (still with possibly degenerate faces). For a generic choice of $\alpha$, no face is degenerate.*

*Proof.* On a white face $w$, we have $d(\mathcal{T} + \alpha\mathcal{O}) = (1 + \alpha\eta_w^2)\, dz$ which proves the first item. The second is identical. The angle property of a t-embedding together with the fact that all white faces preserve the orientation implies that the end of each segment either lies on some other segment or belongs to a degenerate face. Therefore $\mathcal{T} + \alpha\mathcal{O}$ form a T-graph possibly non-proper. Finally, to show that the faces do not overlap in the case of bounded origami map, we use the same proof as in the explicit hexagonal case [52, Theorem 4.6]: every face is mapped with the same orientation so if two faces were to overlap, one could create an arbitrary large path in $\mathcal{T}$ such that its image winds at least twice around a point. This is a contradiction with $\mathcal{O}$ bounded. □

Similarly, $\mathcal{T} + \alpha\bar{\mathcal{O}}$ forms a T-graph with flattened white faces.

**Proposition 6.1.15.** *For any $\alpha$ with $|\alpha| = 1$, the set $\mathcal{T} + \alpha\bar{\mathcal{O}}$ is a T-graph, possibly non-proper and with degenerate faces. In this T-graph:*

- *For any white vertex $w$, $(\mathcal{T} + \alpha\bar{\mathcal{O}})(\Delta_w) = 2\,\mathrm{Proj}_{\sqrt{\alpha}\bar{\eta}_w}(\Delta_w)$.*
- *For any black vertex $b$, $(\mathcal{T} + \alpha\bar{\mathcal{O}})(\Delta_b) = (1 + \alpha\bar{\eta}_b^2)\Delta_b$.*

## 6.2 T-holomorphic functions

In this section, we will work with a fixed t-embedding $\mathcal{T}$ of a finite or infinite *triangulation* and a fixed origami square root function $\eta$. For simplicity of notations for vertices $b$ or $w$ of $\mathcal{G}$, we will write $\mathcal{T}(b)$ or $\mathcal{T}(w)$ to denote the corresponding triangle in the embedding. A large part of the work will be in associating functions defined on black vertices and on white vertices. We will denote by $F^\circ$ the restriction of a function $F$ to white vertices and $F^\bullet$ the restriction to black vertices. We will denote by a subscript $\mathfrak{b}$ or $\mathfrak{w}$ when we "primarily" associate a function to black or white vertices.

### 6.2.1 Definition and basic properties

In this section, we introduce the definition of *t-holomorphicity* for a function and give some basic deterministic facts about such functions.

Let $K$ be a Kasteleyn matrix defined as in Proposition 6.1.4. We start by noting that the kernel of $K$ is related to functions with 0 contour integral. Given a discrete path $\gamma = (e_1, \dots, e_n)$ on $\mathcal{G}^*$ and a function $F$ on edges, we define $\int_\gamma F\, d\mathcal{T} = \sum F(e_i)\, d\mathcal{T}(e_i)$, and we similarly define the contour integrals around sets of primal vertices. We extend functions defined on black or white primal vertices to dual edges by fixing $F^\circ((bw)^*) = F^\circ(w)$ and similarly for black.

**Lemma 6.2.1.** *Let $F^\circ$ be a function from $W$ to $\mathbb{C}$. For any interior black vertex $b$ we have*

$$(KF^\circ)(b) = -\oint_{\partial b} F^\circ\, d\mathcal{T} = \overline{\bar\eta_b^2 (K\eta^2 \bar F^\circ)(b)}$$

*where $K\eta^2\bar F^\circ = \sum_{w\sim b} K(b,w)\eta_w^2 \overline{F^\circ(w)}$. Similarly, for function defined on black vertices and any interior white vertex $w$,*

$$(F^\bullet K)(w) = \oint_{\partial w} F^\bullet\, d\mathcal{T} = \overline{\eta_w^2 (\bar\eta^2 \bar F^\bullet K)(w)}.$$

*Proof.* By definition of $K$

$$(KF^\circ)(b) = \sum_{w\sim b} d\mathcal{T}((bw)^*)\cdot F^\circ(w),$$

note that the right hand side is the definition of the integral of $F^\circ d\mathcal{T}$ in the negative direction around an interior vertex $b$. Taking the complex conjugate and using $\eta_w^2\, d\mathcal{T}((bw)^*) = \eta_b^2\, \overline{d\mathcal{T}((bw)^*)}$, we obtain

$$\sum_{w\sim b} \overline{d\mathcal{T}((bw)^*) F^\circ(w)} = \sum_{w\sim b} \eta_b^{-2}\eta_w^2\, d\mathcal{T}((bw)^*)\overline{F^\circ(w)}$$

which implies the last equality.

For black vertices, note that with our convention $\sum_{b\sim w} F^\bullet(b)\, d\mathcal{T}((bw)^*)$ is the integral around $w$ in the positive direction. As above its complex conjugate can be rewritten as

$$\sum_{b\sim w} F^\circ(b)\eta_b^{-2}\eta_w^2\, d\mathcal{T}((bw)^*),$$

which is the last equality. □

Note that for any white vertex $w$ the equality $\oint_{\partial w} F^\circ\, d\mathcal{T} = 0$ holds since $\mathcal{T}$ is well defined. Therefore $KF^\circ = 0$ over a domain $D$ is equivalent to $\oint F^\circ\, d\mathcal{T} = 0$ for all loops in $D$. Similarly for function on black vertices.

**Definition 6.2.2.** Given a t-embedding $\mathcal{T}$ of a triangulation and an origami square root function $\eta$, a function $F_\mathfrak{b} : B\cup W \to \mathbb{C}$ is said to be *t-black-holomorphic* if

$$\begin{cases} F_\mathfrak{b}^\circ(w) \in \eta_w\mathbb{R} & \text{for all } w\in W,\\ \mathrm{Proj}_{\eta_w}[F_\mathfrak{b}^\bullet(b)] = F_\mathfrak{b}^\circ(w) & \text{for all } b\in B\setminus \partial B,\ \forall w\sim b. \end{cases}$$

Similarly, we say that $F_{\mathfrak{w}}$ is *t-white-holomorphic* if

$$\begin{cases} F^{\bullet}_{\mathfrak{w}}(b) \in \bar{\eta}_b \mathbb{R} & \text{for all } b \in B, \\ \mathrm{Proj}_{\bar{\eta}_b}[F^{\circ}_{\mathfrak{w}}(w)] = F^{\bullet}_{\mathfrak{w}}(b) & \text{for all } w \in W \setminus \partial W, \forall b \sim w. \end{cases}$$

We call a function *t-holomorphic* if it satisfies either of these conditions.

The typical example of t-black-holomorphic function is $w \to K^{-1}(w, b)$ for a fixed black vertex $b$. So, the notation is designed so that in the future $F_{\mathfrak{b}}$ can be seamlessly replaced by $F_b$ for an actual vertex $b$.

**Lemma 6.2.3.** *Given t-embedding $\mathcal{T}$ of a triangulation and an origami square root function $\eta$, let $F^{\bullet}_{\mathfrak{w}}$ be a function on black vertices such that $F^{\bullet}_{\mathfrak{w}}(b) \in \bar{\eta}_b \mathbb{R}$ for all black vertices $b$. There exists an extension of $F^{\bullet}_{\mathfrak{w}}$ into a t-white-holomorphic function $F_{\mathfrak{w}}$ if and only if $F^{\bullet}_{\mathfrak{w}} K = 0$ on $W \setminus \partial W$, i.e $\oint F^{\bullet}_{\mathfrak{w}}\, d\mathcal{T} = 0$.*

*Similarly, a function on white vertices such that $F^{\circ}_{\mathfrak{b}} \in \eta_w \mathbb{R}$ admits an extension as a t-black-holomorphic function if and only if $K F^{\circ}_{\mathfrak{b}} = 0$ on $B \setminus \partial B$.*

*Proof.* Fix an interior white vertex $w$ and let $b_1$, $b_2$, $b_3$ be its adjacent black vertices. The function $F^{\bullet}_{\mathfrak{w}}$ can be extended to $w$ into a t-white-holomorphic function if and only if the three lines perpendicular to respectively $\bar{\eta}_{b_i}\mathbb{R}$ going through $F^{\bullet}_{\mathfrak{w}}(b_i)$ intersect. This corresponds to the system of equations with unknown $F(w)$:

$$F(w) + \bar{\eta}^2_{b_i} \overline{F(w)} = 2 \cdot F^{\bullet}_{\mathfrak{w}}(b_i) \quad \text{for all } i \in \{1, 2, 3\}.$$

Multiplying each equation by $K(b_i, w)$ and using that $\sum K(b_i, w) = \oint d\mathcal{T} = 0$ and $\sum \bar{\eta}^2_{b_i} K(b_i, w) = \sum \bar{\eta}^2_{b_i} d\mathcal{T} = \oint d\bar{\mathcal{O}} = 0$, we obtain that the equations have a solution if and only if $\sum F^{\bullet}_{\mathfrak{w}}(b_i) K(b_i, w) = 0$ as desired.

For a function on white vertices, similarly we want

$$F(b) + \eta^2_w \overline{F(b)} = 2 \cdot F^{\circ}_{\mathfrak{b}}(w_i) \quad \text{for all } i \in \{1, 2, 3\}.$$

which gives the desired solution multiplying by $K(b, w_i)$ and using $\eta^2_w d\mathcal{T} = \eta^2_b\, d\bar{\mathcal{T}} = d\mathcal{O}$ in the other direction. □

**Proposition 6.2.4.** *If $F_{\mathfrak{b}}$ is a t-black-holomorphic function, then*

$$2 \cdot F^{\circ}_{\mathfrak{b}}\, d\mathcal{T} = F^{\bullet}_{\mathfrak{b}}\, d\mathcal{T} + \bar{F}^{\bullet}_{\mathfrak{b}}\, d\mathcal{O}$$

*and it is a closed form away from the boundary. If $F_{\mathfrak{w}}$ is a t-white-holomorphic function then*

$$2 \cdot F^{\bullet}_{\mathfrak{w}}\, d\mathcal{T} = F^{\circ}_{\mathfrak{w}}\, d\mathcal{T} + \bar{F}^{\circ}_{\mathfrak{w}}\, d\bar{\mathcal{O}}$$

*and it is a closed form away from the boundary. By closed away from the boundary, we mean that the sum over any loop using only interior edges vanishes.*

*Proof.* The equalities hold due to the proof of Lemma 6.2.3. Let us show that these forms are closed. We start with the case of a t-black-holomorphic function. Around a black vertex, the statement reduces to the fact that $d\mathcal{T}$ and $d\mathcal{O}$ are closed. Let us compute

the integral around a fixed white vertex $w$ (note that our sign convention naturally corresponds to moving in positive direction around white vertices)

$$\begin{aligned}\oint_{\partial w} F_{\mathfrak{b}}^{\bullet}\, d\mathcal{T} + \bar{F}_{\mathfrak{b}}^{\bullet}\, d\mathcal{O} &= \sum_{b\sim w} F_{\mathfrak{b}}(b)\, d\mathcal{T}(bw)^* + \overline{F_{\mathfrak{b}}(b)}\eta_w^2\, d\mathcal{T}(bw)^* \\ &= \sum_{b\sim w} 2\cdot \mathrm{Proj}_{\eta_w}[F_{\mathfrak{b}}(b)]\, d\mathcal{T}(bw)^* \\ &= 2\cdot F_{\mathfrak{b}}(w)\sum_{b\sim w} d\mathcal{T}(bw)^* = 0.\end{aligned}$$

The other case is identical. □

**Proposition 6.2.5.** *If $F_{\mathfrak{b}}$ and $F_{\mathfrak{w}}$ are respectively a t-black-holomorphic and a t-white-holomorphic functions, then*

$$2\cdot F_{\mathfrak{b}}^{\circ}F_{\mathfrak{w}}^{\bullet}\, d\mathcal{T} = \mathrm{Re}\left(F_{\mathfrak{b}}^{\bullet}F_{\mathfrak{w}}^{\circ}\, d\mathcal{T} + \bar{F}_{\mathfrak{b}}^{\bullet}F_{\mathfrak{w}}^{\circ}\, d\mathcal{O}\right)$$

*is a closed form away from the boundary.*

*Proof.* We check separately the integral around black and white vertices. Around a white vertex, we have

$$\oint_{\partial w} \mathrm{Re}\left(F_{\mathfrak{b}}^{\bullet}F_{\mathfrak{w}}^{\circ}\, d\mathcal{T} + \bar{F}_{\mathfrak{b}}^{\bullet}F_{\mathfrak{w}}^{\circ}\, d\mathcal{O}\right) = \mathrm{Re}\big(F_{\mathfrak{w}}^{\circ}\oint_{\partial w} F_{\mathfrak{b}}^{\bullet}\, d\mathcal{T} + \bar{F}_{\mathfrak{b}}^{\bullet}\, d\mathcal{O}\big) = 0$$

using Proposition 6.2.4. Around a black vertex, replacing the second term by its complex conjugate we get

$$\mathrm{Re}\big(F_{\mathfrak{b}}^{\bullet}\oint_{\partial b} F_{\mathfrak{w}}^{\circ}\, d\mathcal{T} + \bar{F}_{\mathfrak{w}}^{\circ}\, d\bar{\mathcal{O}}\big) = 0.$$

using Proposition 6.2.4. □

### 6.2.2 T-holomorphicity and harmonicity on T-graphs

In this section, we present the relation between t-holomorphicity and a random walk on T-graphs. We show that a t-white-holomorphic function $F_{\mathfrak{w}}$, can be integrated into a real harmonic function on a T-graph.

**Proposition 6.2.6.** *Let $F_{\mathfrak{w}}$ be a t-white-holomorphic function, then $F_{\mathfrak{w}}$ can be seen as the derivative of a real harmonic function on $\mathcal{T}+\mathcal{O}$. More precisely, there exists a real harmonic function $H$ such that along the image of a black vertex $b$ we have $dH = F_{\mathfrak{w}}(b)dz$ and inside the image of a white vertex $w$ we have $dH = \mathrm{Re}(F_{\mathfrak{w}}(w)dz)$.*

*Proof.* Actually the proof is the explicit construction. Let us call $b^+$ and $b^-$ the two endpoints of the segment of $\mathcal{T}+\mathcal{O}$ associated to a black vertex $b$. On edges of $\mathcal{T}+\mathcal{O}$ we define $dH(b^-b^+) = F_{\mathfrak{w}}(b)\cdot(b^+-b^-)$ and note that this defines a real antisymmetric function on oriented segments of $\mathcal{T}+\mathcal{O}$ independent of the choice of $b^+$ and $b^-$. This also naturally extends linearly to the mid point to give an antisymmetric function on edges of $\mathcal{T}+\mathcal{O}$, which we see as usual as a discrete 1-form. Let us now check that this form can be integrated. Let $\Delta_w$ be a white face and let $u_1,u_2,u_3,b_1,b_2,b_3$ be respectively its

vertices and the neighbouring black vertices, all in positive order with $b_i$ between $u_{i+1}$ and $u_i$. We have

$$\begin{aligned}\int_{\Delta_w} dH &= \sum F_{\mathfrak{w}}(b_i)\cdot(u_{i+1}-u_i)\\ &= \sum F_{\mathfrak{w}}(b_i)\cdot(1+\eta_w^2)\,d\mathcal{T}((b_iw)^*)\\ &= (1+\eta_w^2)\cdot F_{\mathfrak{w}}^{\bullet}K = 0\end{aligned}$$

where the last equality comes from Lemma 6.2.3.

To check the derivative in the image of a white face, it is enough to check that the formula agrees with the derivative along vertices. Fix $w$ and $b$ two neighbouring vertices, and let $d\ell$ denote an increment along the segment associated to $b$ (i.e we mean $dz \in \eta_b\mathbb{R}$, $d\ell \in \mathbb{R}$). Along this segment we have

$$\begin{aligned}Re(F_{\mathfrak{w}}(w)\,dz) &= Re(F_{\mathfrak{w}}\eta_b\,d\ell)\\ &= \eta_b \mathrm{Proj}_{\bar{\eta}_b}[F_{\mathfrak{w}}(w)]\,d\ell\\ &= F_{\mathfrak{w}}(b)\,dz\end{aligned}$$

which concludes the proof. □

**Remark 6.2.7.** *In [20] it is shown that* $\mathrm{Re}(F_{\mathfrak{w}})$ *and* $\mathrm{Im}(F_{\mathfrak{w}})$ *itself are harmonic but for the reverse walk on another T-graphs.*

### 6.2.3 A priori regularity

We now consider a sequence $\mathcal{T}^\delta$ of t-embeddings (which we think of as corresponding to a mesh size $\delta$) satisfying the following.

- There exists $\ell$, $L$ such that the length of all edges in $\mathcal{T}^\delta$ are between $\delta\ell$ and $\delta L$.
- There exists $\epsilon > 0$ such that all angles are in $[\epsilon, \pi-\epsilon]$ uniformly in $\delta$.
- There exists $C > 0$ such that $\mathcal{O}^\delta \leq C\delta$ uniformly in $\delta$.
- There is a fixed bounded open set $U$ such that for all $\delta$, $U$ is contained in the union of all interior triangles of $\mathcal{T}^\delta$.

Denote the T-graph $\mathcal{T}^\delta + \mathcal{O}^\delta$ by $T^\delta$. We will use the following proposition proven in [20] using a connection between T-graphs and t-embeddings and results of [4, 5].

**Proposition 6.2.8** (Harnack inequality, [20])**.** *Let $F^\delta$ be a t-holomorphic function on $\mathcal{T}^\delta$, let $H^\delta$ be its primitive (in the sense of Proposition 6.2.6) on a T-graph $T^\delta$. Then there exist positive constants $A$ and $\alpha$ such that the following holds: Let $x$ be a point at distance $R$ from the boundary of $U$, let $r < R$ and $y \in B(x,r)$ then*

$$|F^\delta(x) - F^\delta(y)| \leq A\cdot\left(\frac{r}{R}\right)^{2\alpha}\cdot \max_{B(x,R)\cap\mathcal{T}^\delta}|F^\delta| \qquad \textit{uniformly in } \delta$$

*and*

$$|H^\delta(x) - H^\delta(y)| \leq A\cdot\left(\frac{r}{R}\right)^{2\alpha}\cdot \max_{B(x,R)\cap T^\delta}|H^\delta| \qquad \textit{uniformly in } \delta.$$

Now, let us show how to deduce from the above proposition that the supremum norm of $F^\delta$ is bounded by the supremum norm of $H^\delta$.

**Proposition 6.2.9.** *Let $\mathcal{T}^\delta$ be t-embeddings satisfying the above assumptions. Let $H^\delta$ be a primitive of a t-holomorphic function $F^\delta$. Let $V$ be an open set such that $\overline{V} \subset U$ . Then there exists a constant depending only on $U$ and $V$ and the constants in the assumption on the sequence of t-embeddings such that the following holds*

$$\max_V |F^\delta| \leq \text{const} \cdot \max_U |H^\delta| \quad \textit{uniformly in } \delta.$$

Note that for a t-white-holomorphic function, it is enough to control the norm on white vertices since the values on black vertices are projections and therefore have a smaller norm, and similarly for t-black-holomorphic functions. We also don't need to make a difference between the t-embedding and the associated T-graph because they are at most $O(\delta)$ away from each other.

*Proof.* Rescaling everything, we can also assume that $\max_U H^\delta = 1$. Let $x$ be a point at distance $R$ from the boundary of $U$.

From the Harnack inequality applied to $F^\delta$ and to $H^\delta$, we find that there exist constants $A$ and $\alpha$ such that for all $r < R$

$$\text{osc}_{B(x,r)}(F^\delta) \leq A \cdot \left(\frac{r}{R}\right)^{2\alpha} \cdot \max_{B(R)} |F^\delta|$$

and

$$\text{osc}_{B(x,r)}(H^\delta) \leq A \cdot \left(\frac{r}{R}\right)^{2\alpha},$$

where $\text{osc}_{B(u,r)}(F^\delta) = \max_{x,y \in B(u,r)} |F^\delta(x) - F^\delta(y)|$.

From the second inequality applied to vertices at distance $\delta$ from each other and the fact that $F^\delta$ is the derivative of $H^\delta$, we find that there exist constants $C$ and $\gamma > 0$, such that

$$\max_{B(x,R-\sqrt{\delta})} |F^\delta| \leq C/\delta^{1-\gamma},$$

note that constants can be chosen in such a way that $C = (2A)^{1/\alpha}$.

Suppose that

$$\max_{B(x,r)} |F^\delta| \geq M \quad \text{and} \quad \text{osc}_{B(x,r)}(F^\delta) \leq M/2,$$

then

$$\text{osc}_{B(x,r)}(H^\delta) \geq rM.$$

Note that for $r$ satisfying $r \leq (R - \sqrt{r})$ one has

$$\text{osc}_{B(x,r)}(F^\delta) \leq Ar^\alpha \cdot C/\delta^{1-\gamma} \quad \text{and} \quad \text{osc}_{B(x,r)}(H^\delta) \leq Ar^\alpha.$$

This means that

$$\max_{B(x,r)} |F^\delta| \leq M \quad \text{provided} \quad \begin{cases} Ar^\alpha \cdot C/\delta^{1-\gamma} \leq M/2, \\ Ar^\alpha \leq rM, \end{cases}$$

i.e.

$$\max_{B(x,r)} |F^\delta| \le \max\{2Ar^\alpha \cdot C/\delta^{1-\gamma}, Ar^{\alpha-1}\}.$$

By taking $r = \frac{1}{2C}\delta^{1-\gamma}$ we obtain

$$\max_{B(x,r)} |F^\delta| \le A(2C)^{1-\alpha}/\delta^{(1-\alpha)(1-\gamma)}.$$

Thus, we obtain one step of the procedure

$$\Big(C, 1-\gamma\Big) \quad \longrightarrow \quad \Big(A(2C)^{1-\alpha}, (1-\alpha)(1-\gamma)\Big).$$

Note that $A(2C)^{1-\alpha} \le C$, hence we can leave constant $C$. Keep iterating, and denote $r$ and $\gamma$ obtained after $\ell$ steps by $r_\ell$ and $\gamma_\ell$.

Stop this procedure when

$$1-\gamma_k = \frac{\log c}{\log \delta},$$

with a fixed constant $c \ll 1$. Note that $1/\delta^{1-\gamma_k} = 1/c$. Therefore after $k$ steps we obtain

$$\max_{B(x,\tilde{R})} |F^\delta| \le \frac{(2A)^{1/\alpha}}{c},$$

where $\tilde{R} = R - \sum_{j=1}^k \sqrt{r_j}$. Let us show that $\tilde{R} \ge R/2$. Note that

$$r_k = \frac{1}{2(2A)^{1/\alpha}}\delta^{1-\gamma_k} = \frac{c}{2(2A)^{1/\alpha}} \ll 1,$$

and

$$r_{k-\ell} = \frac{1}{2(2A)^{1/\alpha}}\delta^{1-\gamma_{k-\ell}} = \frac{1}{2(2A)^{1/\alpha}}\delta^{(1-\gamma_k)/(1-\alpha)^\ell} = \frac{c}{2(2A)^{1/\alpha}} \cdot c^{1/(1-\alpha)^\ell - 1}.$$

To finish the proof note that $1/(1-\alpha)^\ell - 1 \ge \alpha\ell$, therefore constant $c$ can be chosen in such a way that $\sum_{j=1}^k \sqrt{r_j} \le R/2$. □

**Corollary 6.2.10.** *Let $\mathcal{T}^\delta$ be a sequence of t-embeddings (of mesh size $\delta$) satisfying the above assumptions. Assume that $F^\delta$ are uniformly bounded on $B(r,0) \cap \mathcal{T}^\delta$. Then*

- *$F^\delta$ is uniformly Hölder on compact subsets of $B(r,0)$;*
- *Integrals $\int F^\delta d\mathcal{T}^\delta$ along closed contours vanish as $\delta \to 0$.*

## 6.3 Open problems and potential applications

### 6.3.1 Existence of t-embeddings

Due to results of Chapter 5 we have the following theorem:

**Theorem 6.3.1.** *T-embeddings of the dual graph $\mathcal{G}^*$ exist at least in the following cases:*

- *If $\mathcal{G}$ is nondegenerate bipartite finite graph with outer face of degree 4, with an equivalence class of real Kasteleyn edge weights under gauge equivalence.*

- *If $\mathcal{G}$ is doubly periodic bipartite graph, with an equivalence class of doubly periodic real Kasteleyn edge weights under gauge equivalence which corresponds to a liquid phase. We can in this case add the additional condition that $\mathcal{O}$ is bounded, then such biperiodic t-embedding is unique.*

*In the second case, t-embeddings with bounded $\mathcal{O}$ are in bijection with the interior of the amoeba and the corresponding t-embeddings will always be periodic.*

Recall that Lemma 5.2.4 states that boundedness of the map $\mathcal{O}$ is equivalent to the boundedness of the radii in any circle pattern.

In Section 5.1.4 we discussed the existence of a Coulomb gauge that corresponds to the finite t-embedding realisation with convex boundary conditions where all boundary vertices have degree three. In addition, in a perfect t-embedding the outgoing dual edges are bisectors of the corresponding corners of the outer face and all these bisectors intersect at a single point.

**Open question ([20]).** The existence of perfect t-embeddings.

In terms of the functions $F$ and $G$, the bisectors condition can be written as

$$\arg \frac{(K_\partial F)(w)}{G(w)} = \arg \frac{F(b)}{(K_\partial^\top G)(b)},$$

for each pair of neighboring $b$ and $w$ at the boundary (above, the matrix $K_\partial$ acts on functions defined on boundary vertices in the following way: take $F$ at the boundary, find all values in the bulk by solving the boundary value problem, compute $KF$ at boundary vertices of the other color).

Assume that $(K_\partial F)(w) = \lambda_w G(w)$ and $(K_\partial^\top G)(b) = \lambda_b F(b)$ for some $\lambda_b, \lambda_w \in \mathbb{R}_+$. To handle the intersection of all bisectors at a point, compute the height of the triangle based on a given side of the outer face, say on $[K_\partial F](w)G(w) = \lambda_w (G(w))^2$. Direct computation shows that the height is

$$\lambda_w \cdot \frac{\mathrm{Im}[G(w)\overline{F(b_1)}] \cdot \mathrm{Im}[G(w)\overline{F(b_2)}]}{\mathrm{Im}[F(b_1)\overline{F(b_2)}]} \;=\; \lambda_w^{-1} \cdot \frac{\mathrm{Im}[(K_\partial F)(w)\overline{F(b_1)}] \cdot \mathrm{Im}[(K_\partial F)(w)\overline{F(b_2)}]}{\mathrm{Im}[F(b_1)\overline{F(b_2)}]},$$

where $b_1$ and $b_2$ are two neighbors of $w$ along the boundary. All these quantities (as well as their counterparts for the boundary vertices of the opposite color) must be the same. Thus, one arrives at the following algebraic formulation of the fact that a given t-embedding is perfect:

$$G(w) = \mathrm{cst} \cdot \frac{\mathrm{Im}[F(b_1)\overline{F(b_2)}]}{\mathrm{Im}[(K_\partial F)(w)\overline{F(b_1)}] \cdot \mathrm{Im}[(K_\partial F)(w)\overline{F(b_2)}]} \cdot (K_\partial F)(w)$$

and similarly for $F(b)$. Clearly, these equations survive under the simultaneous real-linear change $F \mapsto F + k\overline{F}$, $G \mapsto G + k\overline{G}$.

**Conjecture ([20]).** A prefect t-embedding is always unique up to such transforms.

**Observation ([20]).** Provided the outer face has a big degree and uniformly small edges, the condition of convexity implies $k = o(1)$ and thus essentially fixes the embedding.

**Proposition 6.3.2.** *A perfect t-embedding form a convex embedding of the dual graph.*

*Proof.* Let $\mathcal{T}(f_{i-1}), \mathcal{T}(f_i), \mathcal{T}(f_{i+1})$ be three consecutive boundary vertices of a perfect t-embedding and let $\mathcal{T}(f_i')$ be the non-boundary vertex adjacent to $\mathcal{T}(f_i)$, see Fig. 6.2. Note that if one folds the plane along the edge $\mathcal{T}(f_i)\mathcal{T}(f_i')$ then the images of $\mathcal{T}(f_{i-1})$, $\mathcal{T}(f_i)$ and $\mathcal{T}(f_{i+1})$ lie on a line. Therefore all the images of the outer face of a perfect t-embedding $\mathcal{T}$ under the origami mapping $\mathcal{O}$ are located on a line. Let us assume that this is the real line $\mathbb{R}$ and consider the family of T-graphs $\mathcal{T}+\alpha\mathcal{O}$, with $|\alpha|=1$. Clearly, the projections of the outer dual vertices of a T-graph $\mathcal{T}+\alpha\mathcal{O}$ onto the line $i\alpha\mathbb{R}$ are cyclically ordered. Denote $\mathcal{T}+\alpha\mathcal{O}$ by $T_\alpha$.

To show that all white faces of $\mathcal{T}$ are convex polygons, let us prove that the projections of the vertices of the face $(\mathcal{T}+\mathcal{O})(w)$ onto the direction $i\mu$ are cyclically ordered, for any $\mu\in\mathbb{C}, |\mu|=1$. Suppose that $(1+\eta_w^2)\neq 0$. On a white face $w$, we have $dT_\alpha = d(\mathcal{T}+\alpha\mathcal{O}) = dz+\alpha\eta_w^2 dz$. It is enough to show that for some $\alpha$ the projections of the vertices of the face $(\mathcal{T}+\alpha\mathcal{O})(w)$ onto the direction $i\mu\frac{1+\alpha\eta_w^2}{1+\eta_w^2}$ are cyclically ordered. Set $\alpha=\frac{\mu}{\bar\mu}$, then $\mu\frac{1+\alpha\eta_w^2}{1+\eta_w^2}\,||\,\alpha$. Indeed, for $\alpha=\frac{\mu}{\bar\mu}$ one has $\mu(1+\eta_w^2)+\bar\alpha\mu(1+\bar\eta_w^2)\in\mathbb{R}$. Therefore $\bar\alpha\mu(1+\alpha\eta_w^2)(1+\bar\eta_w^2)\in\mathbb{R}$, and hence $\bar\alpha\mu\frac{1+\alpha\eta_w^2}{1+\eta_w^2}\in\mathbb{R}$.

Due to the proof of [52, Theorem 4.6], for any vector $\xi\in\mathbb{C}$, the function $\mathrm{Proj}_\xi[T_\alpha]$ satisfies the maximal principle, i.e., $\mathrm{Proj}_\xi[T_\alpha(\cdot)]$ has no local maxima or minima at interior faces of $\mathcal{G}$. Set $\xi=i\alpha$, since the projections of the outer vertices onto the direction $i\alpha$ are cyclically ordered the maximal principle implies that the projections of the vertices of the face $(\mathcal{T}+\alpha\mathcal{O})(w)$ onto the direction $i\alpha$ are cyclically ordered. Similarly one can show that all black faces of $\mathcal{T}$ are convex polygons.

Let us show that all white faces of a perfect t-embedding have the same orientation. Note that on a black face $b$, we have $dT_\alpha = d(\mathcal{T}+\alpha\mathcal{O}) = dz+\alpha\eta_b^2\,d\bar z$. Then for $\alpha=\eta_b^2$ the image of $b$ under $T+\alpha\mathcal{O}$ is orthogonal to $i\alpha$. Let $b$ be an interior black vertex and let $\Delta_b$ be the associated convex polygon in $\mathcal{T}$. Suppose that the image of $b$ under $T_\alpha$ is orthogonal to $i\alpha$. Note that $T_\alpha(b)=\mathrm{Proj}_{\sqrt{\alpha}\eta_b}(\Delta_b)$. Since $\Delta_b$ is a convex polygon the boundary of this polygon can be naturally divided into two arks $\mathrm{arc}_{\mathcal{T}(f_1)\mathcal{T}(f_n)}$ and $\mathrm{arc}_{\mathcal{T}(f_n)\mathcal{T}(f_1)}$. Such that each arc maps one–to–one to the segment $T_\alpha(f_1)T_\alpha(f_k)$ and the vertices of $T_\alpha(b)$ are cyclically ordered. For consistency of notation denote $f_1$ by $f_1^2$.

Consider two white faces $\mathcal{T}(w_0)=\Delta_{w_0}$, $\mathcal{T}(w_k)=\Delta_{w_k}$ adjacent to the face $\Delta_b$ such that the face $\Delta_{w_0}$ is adjacent to $\mathcal{T}(f_1^2)$ and shares with $\Delta_b$ an edge of $\mathrm{arc}_{\mathcal{T}(f_n)\mathcal{T}(f_1)}$ while $\Delta_{w_k}$ shares with $\Delta_b$ an edge of $\mathrm{arc}_{\mathcal{T}(f_1)\mathcal{T}(f_n)}$, see Fig. 6.4. Let us show that $\Delta_{w_0}$ and $\Delta_{w_k}$ have the same orientation. To prove that these two convex polygons are oriented in the same way in the t-embedding it is enough to prove that they are oriented in the same way in some of the aforementioned T-graphs. Let $f_0f_1^k$ and $f_kf_{k+1}^4$ be edges of $\Delta_b$ adjacent to $\Delta_{w_0}$ and $\Delta_{w_k}$ respectively. Let $f_0^1$ and $f_k^3$ be some vertices of faces $\Delta_{w_0}$ and $\Delta_{w_k}$ not adjacent to $\Delta_b$, see Fig. 6.4. Suppose that $T_\alpha(w_0)$ and $T_\alpha(w_k)$ have opposite orientations. Then $T_\alpha(f_0^1)$ and $T_\alpha(f_k^3)$ are on the same side of the line $T_\alpha(f_1^2)T_\alpha(f_n)$, see Figure 6.4. Since the projections of the outer vertices onto the direction $i\alpha$ are cyclically ordered the maximal principle for $\mathrm{Proj}_{i\alpha}(T_\alpha)$ implies that the projections of $T_\alpha(f_0^1)$, $T_\alpha(f_1^2)$, $T_\alpha(f_k^3)$, $T_\alpha(f_{k+1}^4)$ are cyclically ordered as well. Hence $T_\alpha(f_0^1)$ and $T_\alpha(f_k^3)$ are on different sides of the line $T_\alpha(f_1^2)T_\alpha(f_{k+1}^4)$. Therefore for any $k\in\{1,\dots,n-1\}$ faces $T_\alpha(w_0)$ and $T_\alpha(w_k)$ have the same orientation. It is easy to conclude that then all white faces of $\mathcal{T}$ adjacent to $\Delta_b$ have the same orientation.

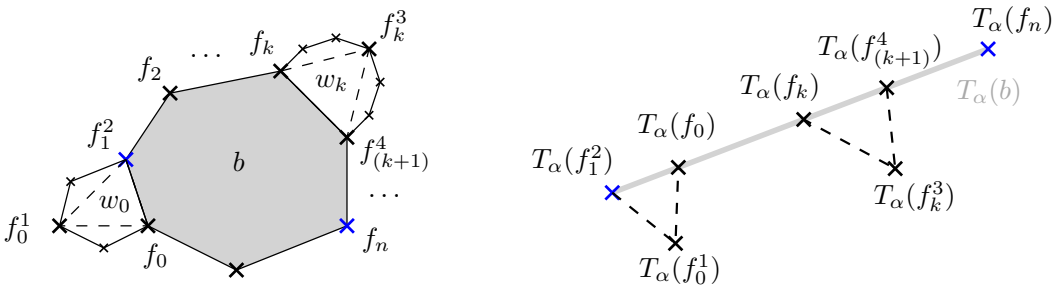


Figure 6.4

Hence all white faces of $\mathcal{T}$ are convex polygons with a common orientation. Similarly one can show that all black faces of $\mathcal{T}$ have a common orientation. Since all boundary quads in a perfect t-embedding have a common orientation, one can conclude that all faces have a common orientation.

The fact that no two faces overlap follows from an argument similar to the one used in [52] for T-graphs. Note that the boundary of $\mathcal{T}(G^*)$ is a convex polygon, we glue the black and white faces starting from the boundary and because they all have the same orientation, they cannot start overlapping. □

**Corollary 6.3.3.** *The origami map of a perfect t-embedding at the boundary is bounded above by the doubled maximal side of the outer face.*

*Proof.* Note that each side of the boundary tangental polygon of a perfect t-embedding can be decomposed naturally into two pieces of tangents from corresponding vertices of the boundary polygon. Note also that tangent segments from one vertex have the same length. To finish the proof recall from the proof of the previous proposition that the image of the outer polygon under a folding of the plane lies on a line and the images of two adjacent sides have opposite directions. □

The above corollary implies that for a perfect t-embedding $\mathcal{T}^\delta$ of mesh size $\delta$ an origami map $\mathcal{O}^\delta$ is of order $\delta$ at least on the boundary. Therefore due to Section 6.2.3 perfect t-embeddings seems to be "correct" finite t-embeddings to study the scaling limit of the dimer model.

### 6.3.2 Potential applications

We will now discuss informally why we are interested in t-holomorphic functions. For this, we will give the main steps that we think can be followed to understand the height fluctuations in the dimer model using the notion of t-holomorphicity and the a priori regularity estimate proved in the above section. Let us already point out that the very significant issue of boundary conditions will not be addressed in this sketch. Indeed we are still far from having a good understanding of the effect of general boundary conditions even in simple lattices.

More precisely, let us consider the following toy problem: given a sequence of perfect t-embeddings $\mathcal{T}^\delta$ satisfying assumptions of Section 6.2.3 and two points $x$ and $x'$ compute $\mathrm{Cov}(H^\delta(x), H^\delta(x'))$ where $H^\delta$ is the dimer model height function. The standard approach is to pick two paths $\gamma$ and $\gamma'$, running from the boundary to $x$ and $x'$ respectively, and

to write each term as the sum of its increments along either $\gamma$ or $\gamma'$. Developing the expression for the sum, this gives

$$\mathrm{Cov}(H^\delta(x), H^\delta(x')) = \sum_{u_i \text{ along } \gamma} \sum_{v_j \text{ along } \gamma'} \mathrm{Cov}(H^\delta(u_{i+1}) - H^\delta(u_i), H^\delta(v_{j+1}) - H^\delta(v_j)).$$

It is well known [41] that the covariance above can be written in term of the inverse of the Kasteleyn matrix, so if we write $b_i, w_i$ and $b'_j, w'_j$ the endpoints of the edge crossed along $\gamma$ and $\gamma'$, we get the expression

$$\mathrm{Cov}(H^\delta(x), H^\delta(x')) = \sum_{(b_i w_i)\in\gamma} \sum_{(b'_j w'_j)\in\gamma'} K(b_i, w_i)K(b'_j, w'_j)K^{-1}(b_i, w'_j)K^{-1}(b'_j, w_i).$$

Now we want to understand how the above depends on $x'$ when $x$ is fixed. We can rewrite $K^{-1}(b'_i, .) = F_{b'_i}$, $K^{-1}(., w'_i) = F_{w'_i}$ and the sum along $\gamma'$ as an integral $d\mathcal{T}$ so we get

$$\begin{aligned}\mathrm{Cov}(H^\delta(x), H^\delta(x')) &= \sum_{(b_i w_i)\in\gamma} K(b_i, w_i) \int_{\gamma'} F^\circ_{b_i} F^\bullet_{w_i} d\mathcal{T} \\ &= \sum_{(b_i w_i)\in\gamma} K(b_i, w_i) \mathrm{Re}\left( \int_{\gamma'} F^\bullet_{b_i} F^\circ_{w_i} d\mathcal{T} + \bar{F}^\bullet_{b_i} F^\circ_{w_i} d\mathcal{O} \right).\end{aligned}$$

Now suppose that we can take a subsequential scaling limit for $F^\bullet_{b_i} F^\circ_{w_i}$, then the integral $d\mathcal{O}$ becomes negligible because $\mathcal{O} = O(\delta)$ which means that $F^\bullet_{b_i} F^\circ_{w_i}$ becomes holomorphic in the limit and therefore $\mathrm{Cov}(H^\delta(x), H^\delta(x'))$ becomes harmonic in $x'$ in the limit.

On the other hand, we know that $\mathrm{Cov}(H^\delta(x), H^\delta(x')) \geq 0$. Indeed in the double dimer case it follows from the expression of the height function in terms of loops: the loops surrounding both points contribute positively and the others have no contribution. In the single dimer case, it is known that the height function satisfies the Fortuin-Kasteleyn-Ginibre inequality (it is easy to check it for example by considering flip around faces). We can also hope to find soft probabilistic arguments showing that $\mathrm{Cov}(H^\delta(x), H^\delta(x'))$ goes to 0 when either point comes close to the boundary. This means that in the limit, $\mathrm{Cov}(H^\delta(x), H^\delta(x'))$ is a positive harmonic function with 0 boundary condition and this identifies it uniquely as a multiple of the green function, as it should be for a convergence to the Gaussian free field.

From the above sketch, we see that a key step is to be able to take a sub-sequential scaling limit of $K^{-1}(b_i, w'_j)K^{-1}(b'_j, w_i)$, which means proving boundedness and equicontinuity. Due to [20], see Section 6.2.3, t-holomorphic functions together with its primitive satisfy Harnack inequality with constants independent of $\delta$ which gives uniform Hölder estimates and implies that t-holomorphic functions cannot be much larger than their primitive which should help to obtain boundedness.

# Appendix A

# Appendix. Piecewise Temperleyan domains on isoradial graphs

In this section we will discuss the result of Theorem 3.2.5 for the dimer model on isoradial graphs. The notion of a rhombic lattice (or isoradial graph) was introduced by Duffin [29] as a large family of graphs, where discretizations of Laplace and Cauchy-Riemann operators can be defined similarly to the case of the square lattice. The class of isoradial graphs forms a large class of graphs where classical complex analysis results have discrete analogs, see [21]. A lot of planar graphs admit isoradial embeddings [53]. Discrete complex analysis allows to obtain results for two-dimensional lattice models on isoradial graphs, notably the Ising [61, 22] and dimer [46, 25, 27, 58] models.

Let $\Gamma$ be an isoradial graph, i.e. a planar graph in which each face is inscribed into a circle of a common radius $\delta$. Also one can thing about $\delta$ as a mesh size of the isoradial graph. Suppose that all circle centers are inside the corresponding faces, then the dual graph $\Gamma^*$ is also isoradial with the same radius. The rhombic lattice is the graph on the union $\Lambda$ of the two vertex sets $\Gamma$ and $\Gamma^*$ (see Fig. A.1). We will use the following assumption (see [21])

(♠) the rhombi angles are uniformly bounded from 0 and $\pi$.

The dimer model on isoradial graphs was introduced by Kenyon [46]. A dimer configuration in this setup is a perfect matching of the bipartite graph $\Omega^\delta$ defined as follows. The vertex set of $\Omega^\delta$ consists of a union of $\Lambda$ (two types of black vertices) and rhombi centers (white vertices), and there is an edge between black and white vertices if the black vertex and corresponding rhombi are adjacent (see Fig. A.1). Note that $\Omega^\delta$ is an isoradial graph, where each face is inscribed into a circle of radius $\frac{\delta}{2}$, for more details see [27].

We will call a white vertex on the boundary of $\Omega^\delta$ a *corner* if it is adjacent to two boundary black vertices of different types. We can define as before the notion of *convex* and *concave* white corners, see Fig. A.1. Note that Lemma 3.1.1 holds also in the isoradial case. An isoradial graph $\Omega^\delta$ is called a *$2n$-black-piecewise Temperleyan graph* if it has $n+1$ convex white corners and $n-1$ concave white corners, see Fig. A.1. Now we can formulate the similar result for isoradial graphs analogous to Theorem 3.2.5.

**Theorem A.1.** *Let $\Omega^\delta$ be a sequence of isoradial $2k$-black-piecewise Temperleyan graphs approximating a continuous domain $\Omega$. Assume that each $\Omega^\delta$ admits a perfect matching.*

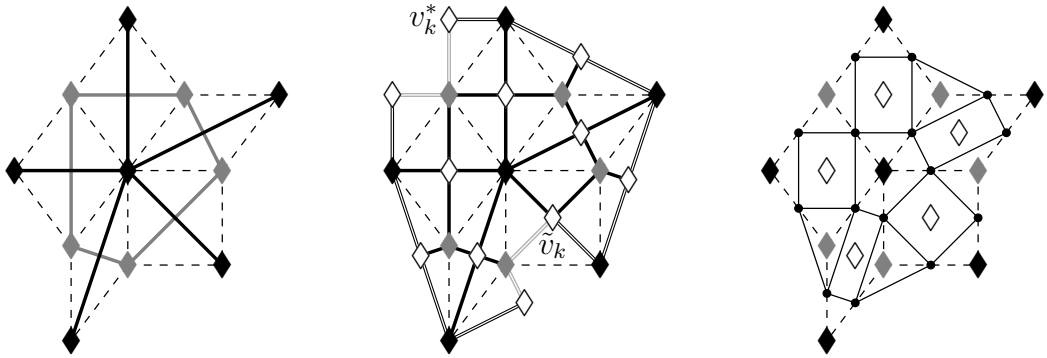


Figure A.1: Left: isoradial graph $\Gamma$ (black), its dual graph $\Gamma^*$ (gray) and the corresponding rhombic lattice (dashed). Center: isoradial $2n$-black-piecewise Temperleyan graph with $n = 2$; the set of rhombic centers (white), the bipartite graph (vertices: white, gray and black; edges: solid lines), the elements of the sets of white corners $\{v_k^*\}_{k=1}^{n+1}$ and $\{\tilde{v}_k\}_{k=1}^{n-1}$. Right: the set of midedges of the rhombic lattice, the set $\mathcal{V}$ (circles).

*Let the sets of white boundary vertex $\{v_k^{*\delta}\}_{k=1}^{n+1}$ and $\{\tilde{v}_k^{\delta}\}_{k=1}^{n-1}$ approximate the sets of boundary points $\{v_k^*\}_{k=1}^{n+1}$ and $\{\tilde{v}_k\}_{k=1}^{n-1}$ correspondingly, and let $v_0^{\delta}$ approximate a point boundary point $v_0$ which lies on a straight segment of the boundary of $\Omega$. Then $F_{\text{iso}}^{\delta}$ converges uniformly on compact subsets of $\Omega$ to a continuous holomorphic function $f_\Omega$, where $f_\Omega$ is defined as in Proposition* 3.1.4.

*Proof.* The proof mimics the proof of Theorem 3.2.5 using the toolbox described in [21, Definition 2.1, Proposition 2.7, Definition 2.12, Proposition 2.14, Theorem 2.21]. □

# Bibliography


[1] V. E. Adler, A. I. Bobenko, and Y. B. Suris, *Classification of integrable discrete equations of octahedron type*, Int. Math. Res. Not., (2012), pp. 1822–1889.

[2] A. V. Akopyan, *Geometry in figures*, Createspace, 2011.

[3] A. V. Akopyan and A. A. Zaslavsky, *Different views on the isogonal conjugation*, Matematicheskoe prosveshenie, 3 (2007), pp. 61–78.

[4] N. Berestycki, B. Laslier, G.Ray, *A note on dimers and T-graphs*, arXiv:1610.07994

[5] N. Berestycki, B. Laslier, G.Ray, *Universality of fluctuations in the dimer model*, arXiv:1603.09740.

[6] P. Billingsley, *Probability and measure*, Wiley, New York 1979.

[7] A. Borodin, P. Ferrari, *Anisotropic Growth of Random Surfaces in 2 + 1 Dimensions*. (2008). Communications in Mathematical Physics. 10.1007/s00220-013-1823-x.

[8] A. Borodin, P. Ferrari, *Random tilings and Markov chains for interlacing particles*, Preprint (2015), http://arxiv.org/pdf/1506.03910v1.pdf.

[9] A. Borodin, V. Gorin, *Shuffling algorithm for boxed plane partitions*. (2009). Advances in Mathematics. 220. 1739-1770. 10.1016/j.aim.2008.11.008.

[10] A. Borodin, L. Petrov *Integrable probability: From representation theory to Macdonald processes*. (2013). Probability Surveys [electronic only]. 11. 10.1214/13-PS225.

[11] A. Bufetov, V. Gorin, *Fourier transform on high-dimensional unitary groups with applications to random tilings*, arXiv:1712.09925.

[12] A. Bufetov, V. Gorin, *Representations of classical Lie groups and quantized free convolution* Geom. Funct. Anal. (2015) 25: 763. https://doi.org/10.1007/s00039-015-0323-x

[13] A. Bufetov, A. Knizel, *Asymptotics of random domino tilings of rectangular Aztec diamonds*, Ann. Inst. H. Poincaré Probab. Statist. 54 (2018), no. 3, 1250–1290. doi:10.1214/17-AIHP838.

[14] R. Burton, R. Pemantle, *Local characteristics, entropy and limit theorems for spanning trees and domino tilings via transfer-impedances*, Annals of Probability, 21(3): 1329–1371, 1993.

[15] D. Chelkak, *Planar Ising model at criticality: state-of-the-art and perspectives*, Preprint, (2017). http://arxiv.org/abs/1712.04192.

[16] D. Chelkak, H. Duminil-Copin, C. Hongler, A. Kemppainen, and S. Smirnov. *Convergence of Ising interfaces to Schramm's SLE curves.* C. R. Math. Acad. Sci. Paris, 352(2):157–161, 2014.

[17] D. Chelkak, A. Glazman, S. Smirnov, *Discrete stress-energy tensor in the loop O(n) model*, ArXiv e-prints 1604.06339 (2016).

[18] D. Chelkak, C. Hongler, K. Izyurov, *Conformal invariance of spin correlations in the planar Ising model*, Ann. of Math. (2), 181 (2015), 1087–1138.

[19] D. Chelkak, K. Izyurov, *Holomorphic spinor observables in the critical Ising model*, Comm. Math. Phys. 322. (2013), no.2, 303–332.

[20] D. Chelkak, B. Laslier, and M. Russkikh, *Holomorphic functions on t-embeddings of planar graphs.* In preparation.

[21] D. Chelkak and S. Smirnov, *Discrete complex analysis on isoradial graphs*, Adv. Math. 228 (2011), 1590–1630.

[22] D. Chelkak and S. Smirnov, *Universality in the 2D Ising model and conformal invariance of fermionic observables*, Invent. Math., 189 (2012), no. 3, 515–580.

[23] H. Cohn, N. Elkies, and J. Propp, *Local statistics for random domino tilings of the Aztec diamond*, Duke Math. J. 85 (1996), 117–166.

[24] H. Cohn, R. Kenyon, J. Propp, *A variational principle for domino tilings*, J. Amer. Math. Soc. 14 (2001), no. 2, 297–346.

[25] B. de Tilière, *Scaling limit of isoradial dimer models and the case of triangular quadri-tilings*, Ann. Inst. H. Poincaré, Prob. et Stat. 43 (2007), no. 6, 729–750

[26] J. Dubédat, *Exact bosonization of the Ising model* , arXiv:1112.4399v1.

[27] J. Dubédat, *Dimers and families of Cauchy-Riemann operators I* , J. Amer. Math. Soc. 28 (2015), 1063–1167.

[28] J. Dubédat, *Double dimers, conformal loop ensembles and isomonodromic deformations*, arXiv:1403.6076.

[29] R. Duffin, *Potential theory on a rhombic lattice*, J. Combinatorial Theory 5 (1968), 258–272.

[30] G. V. Epifanov, *Reduction of a plane graph to an edge by star-triangle transformations*, Dokl. Akad. Nauk SSSR, 166 (1966), pp. 19–22.

[31] M. E. Fisher, *On the dimer solution of planar Ising models*, Journal of Mathematical Physics 7 (1966), no. 10, 1776–1781.

[32] M. E. Fisher and H. N. V. Temperley, *Dimer problem in statistical mechanics-an exact result*, Philos. Mag., 6(68):1061–1063, 1961.

[33] V. Fock and A. Goncharov, *Moduli spaces of local systems and higher Teichmuller theory*, Publ. Math. Inst. Hautes E tudes Sci., (2006), pp. 1–211.

[34] S. Fomin and A. Zelevinsky, *The Laurent phenomenon*, Adv. in Appl. Math., 28 (2002), pp. 119–144.

[35] A. B. Goncharov and R. Kenyon, *Dimers and cluster integrable systems*, Ann. Sci. E c. Norm. Supér. (4), 46 (2013), pp. 747–813.

[36] C. Hongler and S. Smirnov, *The energy density in the planar Ising model*, Acta Math. 211 (2013), 191–225.

[37] Y. Ikhlef, R. Weston, M. Wheeler, P. Zinn-Justin *Discrete holomorphicity and quantized affine algebras.* Journal of Physics A: Mathematical and Theoretical. 2013 ; Vol. 46, No. 26. pp. 1-34

[38] J. D. Jackson, *Classical electrodynamics*, John Wiley Sons, Inc., New York-London-Sydney, second ed., 1975.

[39] K. Johansson, *Non-intersecting paths, random tilings and random matrices*, Probability Theory and Related Fields, 123, 225–280, 2002

[40] P. W. Kasteleyn, *The statistics of dimers on a lattice. I. The number of dimer arrangements on a quadratic lattice*, Physica 27 (1961), 1209–1225.

[41] R. Kenyon, *Conformal invariance of domino tiling* , Ann. Probab. 28 (2000), 759–795.

[42] R. Kenyon, *Dominos and the Gaussian free field*, Ann. Probab. 29 (2001), 1128-1137.

[43] R. Kenyon, *Height fluctuations in the honeycomb dimer model*, Communications in Mathematical Physics, 281(3):675–709, 2008.

[44] R. Kenyon, *Local statistics of lattice dimers*, Ann. Inst. H. Poincaré, Prob. et Stat. 33 (1997), 591–618.

[45] R. Kenyon, *Conformal invariance of loops in the double-dimer model*, Comm. Math. Phys. 326 (2014), no. 2, 477–497.

[46] R. Kenyon, *The Laplacian and Dirac operators on critical planar graphs*, Invent. Math. 150 (2002), no 2, 409–439.

[47] R. Kenyon, W. Lam, S. Ramassamy, M. Russkikh *Dimers and circles*, arXiv:1810.05616.

[48] R. Kenyon and A. Okounkov, *Limit shapes and the complex Burgers equation*, Acta Math. 199 (2007), no. 2, 263–302.

[49] R. Kenyon and A. Okounkov, *Planar dimers and Harnack curves*, Duke Math. J., 131 (2006), pp. 499–524.

[50] R. Kenyon, A. Okounkov, S. Sheffield *Dimers and Amoebae*, Ann. Math. 163 (2006), 1019–1056

[51] R.Kenyon, J.Propp, D.Wilson, *Trees and matchings*, Electr.J.Combin.7(2000), research paper 25.

[52] R. Kenyon and S. Sheffield *Dimers, tilings and trees*, J. Combin. Theory Ser. B, 92 (2004), pp. 295–317.

[53] R. Kenyon, J.-M. Schlenker *Rhombic embeddings of planar quad-graphs*, Trans. AMS, 357:3443–3458, 2004.

[54] B. G. Konopelchenko and W. K. Schief, *Menelaus' theorem, Clifford configurations and inversive geometry of the Schwarzian KP hierarchy*, J. Phys. A, 35 (2002), pp. 6125–6144.

[55] B. G. Konopelchenko and W. K. Schief *Reciprocal figures, graphical statics, and inversive geometry of the Schwarzian BKP hierarchy*, Stud. Appl. Math., 109 (2002), pp. 89–124.

[56] B. Laslier, *Central limit theorem for T-graphs*, arXiv preprint arXiv:1312.3177, 2013.

[57] G. Lawler, O. Schramm, and W. Werner, *Conformal invariance of planar loop-erased random walks and uniform spanning trees*. Ann. Probab., 32(1B):939–995, 2004.

[58] Z. Li *Conformal invariance of isoradial dimers*, arXiv preprint arXiv:1309.0151.

[59] M. Lis, *Circle patterns and critical Ising models*, Preprint, (2017). http://arxiv.org/abs/1712.08736.

[60] L. Lovasz and M. D. Plummer, *Matching theory*, AMS Chelsea Publishing, Providence, RI, 2009. Corrected reprint of the 1986 original [MR0859549].

[61] Ch. Mercat *Discrete Riemann Surfaces and the Ising Model*, Comm. Math. Phys., 218(1):177–216, 2001.

[62] G. Mikhalkin, *Real algebraic curves, the moment map and amoebas*, Ann. of Math. (2), 151 (2000), pp. 309–326.

[63] A. Miquel, *Theoremes sur les intersections des cercles et des spheres*, J. Math. Pures Appl., (1838), pp. 517–522.

[64] J. K. Percus, *One more technique for the dimer problem*, J. Mathematical Phys., 10:1881–1888, 1969.

[65] L. Petrov, *Asymptotics of Uniformly Random Lozenge Tilings of Polygons. Gaussian Free Field*, arXiv:1206.5123.

[66] L. Petrov, *Asymptotics of Random Lozenge Tilings via Gelfand-Tsetlin Schemes, Probability Theory and Related Fields*, 160 (2014), no. 3, 429–487

[67] J. Propp, *Lattice structure for orientations of graphs*, October 1, 1993, arXiv:math/0209005.

[68] M. Russkikh, *Dimers in piecewise Temperleyan domain*, M. Commun. Math. Phys. (2018). 10.1007/s00220-018-3113-0.

[69] M. Russkikh, *Dominos in hedgehog domains*, arXiv:1803.10012

[70] O. Schramm, *Circle patterns with the combinatorics of the square grid*, Duke Math. J., 86 (1997), pp. 347–389.

[71] O. Schramm, *Conformally invariant scaling limits, an overview and a collection of problems*, in Proceedings of the ICM 2006, Madrid. 2006.

[72] O. Schramm, *Scaling limits of loop-erased random walks and uniform spanning trees*, Selected works of Oded Schramm. Volume 1, 2, 791–858, Sel. Works Probab. Stat., Springer, New York, 2011.

[73] O. Schramm, S. Sheffield *Contour lines of the two-dimensional discrete Gaussian free field*, Acta Math., 202 (2009), 21–137.

[74] S. Sheffield, *Exploration trees and conformal loop ensembles*, Duke Math. J. 147 (2009), no. 1, 79–129.

[75] S. Sheffield, *Gaussian free fields for mathematicians*, Probab. Theory Related Fields 139 (2007), no. 3-4, 521–541.

[76] S. Sheffield, W. Werner *Conformal loop ensembles: the Markovian characterization and the loop-soup construction*, Ann. of Math. (2) 176 (2012), no. 3, 1827–1917.

[77] S. Smirnov, *Towards conformal invariance of 2D lattice models*, proceedings of the international congress of mathematicians (ICM), Madrid, Spain, August 22–30, 2006. Vol. II: Invited lectures, 1421–1451. Zurich: European Mathematical Society (EMS), 2006.

[78] S. Smirnov, *Conformal invariance in random cluster models. I. Holomorphic fermions in the Ising model*, Ann. of Math. (2), (172) 1435–1467, 2010.

[79] S. Smirnov, *Critical percolation in the plane: conformal invariance, Cardy's formula, scaling limits*. C. R. Acad. Sci. Paris S er. I Math., 333(3):239–244, 2001.

[80] H. Temperley, *Combinatorics: Proceedings of the British Combinatorial Conference 1973*, London Math. Soc. Lecture Notes Series #13, (1974), 202–204.

[81] D. P. Thurston, *From dominoes to hexagons*, in Proceedings of the 2014 Maui and 2015 Qinhuangdao conferences in honour of Vaughan F. R. Jones' 60th birthday, vol. 46 of Proc. Centre Math. Appl. Austral. Nat. Univ., Austral. Nat. Univ., Canberra, 2017, pp. 399–414.

[82] William P. Thurston, *Conway's tiling groups*, The American Mathematical Monthly, Vol. 97, No. 8, Special Geometry Issue (Oct.,1990), pp. 757-773.

[83] W. T. Tutte, *How to draw a graph*, Proc. London Math. Soc. (3), 13 (1963), pp. 743–767.

[84] M. Wang, H. Wu *Level Lines of Gaussian Free Field I: Zero-Boundary GFF*, SPA 127 (2017) 1045-1124.